Wax Based Emulsions For Use In Lipstick Application

By

Akash Beri

A thesis submitted to
The University of Birmingham
for the degree of
DOCTOR OF ENGINEERING

School of Chemical Engineering
College of Physical and Engineering Sciences
The University of Birmingham

February 2015

Abstract

Water-in-oil emulsions have the potential to eradicate drying of the lips caused by constant lipstick application by improving moisturising properties and delivering hydrophilic molecules to the lips.

To conduct this research, a food microstructure approach was utilisied developing emulsion structures' using either a batch or continuous process and monitoring the affect these structures had on physical and material properties. The lubricating properties of emulsions structures were then compared to a trained sensory panel. Finally the release behaviour of a moisturising agent was investigated.

It was shown that the ingredients used to produce the microstructure are pivotal in indicating the melting profile, droplet size and material properties of the final structure. Specifically, when an aqueous phase is incorporated within a hard shell the elastic modulus increases as the aqueous phase become part of the wax network. The effect of lubrication showed that friction coefficient of a solid emulsion could be related to how smooth a lipstick would be perceived based on the Kokani Model. Finally, it was shown that the release of a moisturising agent is governed by the droplet size and the amount of destruction caused to the wax network.

Acknowledgements

Firstly I would like to thank my academic supervisor Prof. Ian Norton for all his help and guidance throughout the EngD scheme, in particular the constant motivation he provided. I would also like to thank Dr Richard Greenwood for his constant encouragement, especially during the write up stage.

Within Alliance Boots, I would like to thank both Sonja Clarke and William O'Leary for their devotion to this project, constant support and useful discussion in developing a cosmetic product. I would also like to thank Angela Morgan and the sensory team for their support in running a trained sensory panel and conducting the sensory analysis for this thesis.

Within the University of Birmingham, I would like to thank the entire Microstructure group for their constant guidance and support, in particular Dr Roman Pichot, Dr Jennifer Norton, Dr Thomas Mills and Dr Ben Le Reverend. I would also like to thank Dr Richard Watson for proof reading my thesis and for helpful suggestions. Finally I would like to thank all the support staff, particularly John Hooper, Lynn Draper, Kathleen Haynes and Bob Sharp.

My gratitude goes to the EPSRC for this funding opportunity which has allowed this work to be conducted.

I would like to thank all my friends from the University of Birmingham for all the great memories that we have generated in our times together.

Last but not least, I would thank my wonderful family, Ashok, Sumita, Sanjeev, Chaya and Joanne Beri for all their encouragement throughout the EngD. Without your support this would not have been possible.

Table of Contents

List of Figures

List of Tables

Nomenclature

Nuclear Magnetic Resonance

d	droplet diameter
$d_{3,2}$	Surface weighted mean droplet diameter
$d_{3,3}$	Volume weighted mean droplet diameter
G	Gradient strength
M_g/E	Echo attenuation
Δ	Length of time between two starting points of field gradient pulses
δ	Length of time for each field gradient pulse
σ	Standard deviation of the logarithm of the droplet diameter
τ	time

Differential Scanning Calorimetry

M	Mass
Q	Heat energy transferred
T_c	Crystallisation Temperature
T_{end}	End temperature for Melting profile
T_g	Glass transition temperature
T_j	Jacket temperature
T_m	Melting temperature
T_{onset}	Onset temperature for Melting profile
T_{peak}	Peak temperature during Melting profile
ΔH_c	Latent heat of crystallisation

Rheology/Compression

A	Cross Sectional Area
D	Fractal dimension
F	Applied load/ Compression Force
G’	Elastic Modulus
G’’	Viscous Modulus

H	Initial Height
H_O	Height of each sample as recorded during compression
k	Characteristic of the spring
L_o	Original Length
M	Mass
M	Modulus of elasticity
R	Radius
x	Backbone fractural dimension
ΔL	Elongation of the spring
ε_E	Engineering strain
ε_H	True strain
σ_E	Engineering stress
σ_H	True Stress
τ	Shear Stress
Φ	Particle volume fraction
$\dot{\gamma}$	Shear rate

Tribology

F	Frictional Force
C_p	Specific heat capacity
k	Viscosity
m	mass
N	Avogadro's number
Q	Energy dissipated
R	Gas Constant
r	radius
V	Velocity
W	Applied normal force
μ	Coefficient of friction

Release

A	Area under curve

c	Concentration
D	Diffusivity
G_c	Glycerol concentration
t	Time

Other

ΔP_L	Laplace Pressure
A_i	Area of interface
E_r	Emulsifier required
S_c	Surface coverage
α	Alpha
β	Beta
β'	Beta prime
γ	Surface tension
τ_{coag}	Coagulation time
τ_{enc}	Encounter time
τ_{FD}	Film disruption time
τ_{ft}	Film thinning time

Abbreviations

ANOVA	Analysis of variance
CW	Carnauba wax
D.F.B	Difference from bench
DSC	Differential scanning calorimetry
EM	Electron microscope
FT IR	Fourier transformer infra red
HLB	Hydro lipophilic balance
IFT	Interfacial tension
IV	Impeller velocity
L.S.D	Least significant difference
LVR	Linear viscoelastic region

MW	Microcrystalline wax
NMR	Nuclear magnetic resonance
O/W	Oil-in-water
PDMS	Polydimethyl siloxane
PGPR	Polyglycerol polyricinoleate
PS	Pin stirrer
RT	Residence time
SEM	Scanning electron microscope
SPI	Soy protein isolate
SSHE	Scraped surface heat exchanger
SSPS	Soy soluble polysaccharides
TAG	Triacylglycerol
W/O	Water-in-oil

Chapter 1. Introduction

1.1 Background

The microstructure approach (Figure 1.1) has been used in the food industry to produce innovative products that meet consumer demands. It states that the properties of a product are dependent on its microstructure. The microstructure is a function of the ingredients and the processing conditions (Norton and Norton, 2010). Using this approach, it is possible to design new products that meet consumer demands within the cosmetic industry. To the author's knowledge, this approach has not been implemented in the design process for developing novel lipstick formulations.

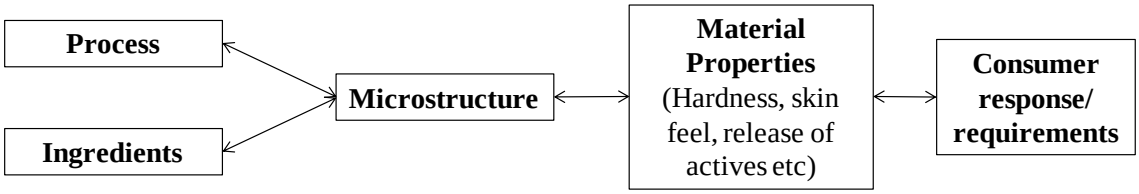

Figure 1.1 – Schematic for Microstructural approach (adapted from Norton and Norton (2010).

Lipsticks are a solid fatty based hydrophobic product comprised of waxes (5 – 25 wt %), oils (30 – 80 wt %) and pigments (1 – 10 wt %) (Harry, 1973). The oil provides a base for the waxes and allows the pigments to disperse throughout the lipstick. Castor, mineral, jojoba and vegetable oil are the main oils used in lipstick production. It is important to note that the oils are normally treated with an antioxidant in order to improve shelf life. Castor oil is predominately used as it has the ability to dissolve the pigments used in lipsticks (bromoacid dyes), due to its polar nature. It is comprised of mainly triglyceride fatty acids with ricinoleic acid (Harry, 1973). Waxes are used to give structure to the formulation, thus allowing the formulation to be moulded and used as a lipstick (solid at room temperature and spreadable at lip temperature (32 °C)). Currently a variety of different waxes (carnauba wax, beeswax, candelilla wax, paraffin

wax, microcrystalline wax, performalene etc.) are used as a blend to provide a structure that delivers said properties.

The excess use of hydrophobic lipsticks can lead to lip dryness due to an accumulation of hydrophobic layers on the lip, which prevents natural lubrication from saliva and water vapour (in the atmosphere). Currently, to improve wearers comfort, emollients (alcohols or polysaccharides) are added by manufactures (Decker *et al.*, 1997). An alternative method to improving lubrication of a lipstick would be to create water-in-oil (W/O) emulsion based lipsticks. This will allow the delivery of moisture directly to the lip.

Water, despite its natural attribute as a moisturiser, is not used in the formulation of commercially available lipstick. However, there are a few examples of W/O emulsion based lipsticks in the literature. Lombardi and Voccaro (1993) provided a list of ingredients which were used to produce an emulsion lipstick without providing a detailed formulation. Dunphy *et al.* (1992) formulated an emulsion based lipstick using phospholipids to stabilise the water droplets. These two studies highlighted that the incorporation of water within a lipstick is possible. However, the authors did not discuss emulsion stabilisation mechanisms, the chemistry between ingredients, the material properties of the emulsion lipsticks or how emulsion lipsticks were produced. Wang and Lee (1997) published the first work on the strength of emulsion based lipsticks. The authors used compression testing to show that emulsifiers (lipophilic or hydrophilic) had no effect on the strength of the lipstick. They also showed that water inclusion increased the strength of emulsions. These results were challenged by Le Réverend *et al.* (2011b) who showed that higher water content (up to 40 wt %) weakened the lipstick structure.

Production of lipsticks has also received little attention in the literature. Traditionally, lipsticks are manufactured using a 4 stage batch process which utilises varying types of roller mills (ball, sand, roller and corundum) (Daley, 1968). These methods do not allow control of the crystallisation of waxes during the process which leads to inhomogeneous structures being formed (Dweck and Burnham, 1980).

In order to fully utilise the microstructural approach for designing emulsion based lipsticks, one must consider the impact an emulsion structure has on consumer response. An example can be found in the cosmetic industry where experimental data has been related to consumer response. Kusakari *et al.* (2003) related friction from a tribological technique to 'spreading' and 'stickiness' scores. However, there is no evidence in the literature of solid wax based structures being analysed experimentally in a tribometer.

Finally it should be noted that the inclusion of water allows the encapsulation of active hydrophilic agents into the microstructure. To the author's knowledge there is no literature investigating the release of active agents in lipstick formulations. The use of active agents (such as glycerol) could allow direct delivery of moisturising agents to the lips, thus prevent drying of the lips.

1.2 Objectives

Given the aforementioned gaps in the knowledge required for designing emulsion based lipsticks, the aim of this thesis is to advance the understanding of designing emulsion based lipsticks by utilising the microstructure approach.

Specifically, to achieve this objective, emulsion based lipsticks were produced using either a batch or continuous process and a variety of ingredients (emulsifiers, waxes and

different aqueous phase volumes). Their final structure and properties were assessed using a variety of techniques to understand how the structure related to both material properties and consumer acceptance.

1.3 Relevance to Alliance Boots

Alliance Boots, the industrial funder to this study, is a multinational organisation that has multiple avenues of business. Alliance Boots controls 16 % of the European market share for colour cosmetics (Figure 1.2). The total European cosmetic market is worth approximately £1.5 billion of which lipsticks take up an appropriate £200 million (Mintel, 2012). Lipstick form an intrinsic part of the company and to maintain/improve their market share it must develop new and innovative products that meet consumer demands.

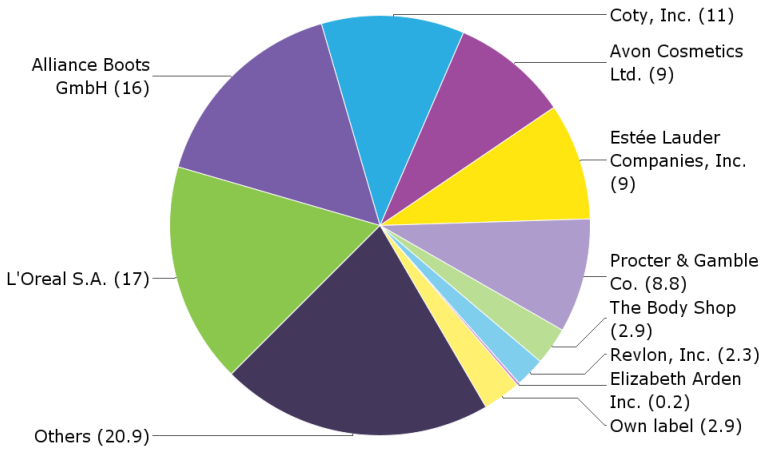

Figure 1.2 – Pie chart of the UK colour cosmetics market divided into company retail market share (%)(taken from Mintel, 2012)

Alliance Boots consumers have identified that commercially available lipsticks dry their lips. As a result there has been a drive to produce a lipstick that can deliver moisture to the lips.

As discussed in the previous section, W/O emulsions have the potential to produce microstructures that are suitable for lipstick application that deliver moisture directly to the lip. Furthermore, the ability to monitor the release of an active agent would allow Alliance Boots to add additional claims for their lipsticks which would improve the marketability of the product. Finally, the use of a tribological technique to predict consumer response could reduce the amount of formulations being analysed by a sensory panel. This would be extremely beneficial for Alliance Boots who operate using a trained sensory panel which is extremely expensive.

1.4 Thesis Layout

The following chapter (Chapter 2) provides a review of the relevant literature on four major topics: emulsions, crystallisation, tribology and release. Chapter 3 then describes the materials used and methodology for all of the different experimental techniques used throughout the study.

Chapters 4 – 7 are the results chapters for this thesis. Chapter 4 discusses the design of an emulsion based lipstick. This begins with a discussion on the influence of a batch process (in particular the effect of emulsifiers and aqueous phase volume) and a continuous process (in particular processing parameters). The melting behavior of emulsion based lipsticks is then discussed as this is crucial in a lipstick being used for its primary function (solid at room temperature but spreadable at lip temperature). The final part of this chapter discusses the stability of emulsion based lipsticks.

Chapter 5 discusses the material properties of emulsion based lipsticks. For this, different waxes and wax blends were initially discussed followed by a discussion on the effect of water inclusion and water content. The material properties were then manipulated by using a continuous process to control the amount of crystallisation

during processing. The material properties were assessed using either uni axial compression and/or oscillatory rheology.

Chapter 6 probes the use of a pin-on-disk tribometer in examining the lubricating properties of solid wax based emulsion. In particular the role of different waxes, water content, dispersed phase viscosities and droplet size. The second part of this chapter utilises a trained sensory panel (supplied by Alliance Boots) in order to compare tribological data with sensory attributes.

Chapter 7, the final results chapter, discusses the development of a technique to monitor the release of a moisturising agent (glycerol) from a wax based structure. Initially the release of glycerol is discussed in quiescent conditions. The release behavior is then discussed by using a COMSOL model. Following this, the release of glycerol during structural breakdown is discussed, in terms of compression and droplet size.

The conclusions of this research are summarised (0) along with recommendations for future work. A full list of the references and appendices used though out this thesis are then shown.

Chapter 2. Literature Review

2.1 Introduction

The aim of this chapter is to review the relevant literature, related to this study. This includes an overview of emulsions and how they can be formed. Then, the formation of crystal structures will be discussed. The fundamentals of tribology are then discussed. In particular, how tribology has been used in both the cosmetic and food industries to compare friction with sensory perception. Finally the releases from colloidal structures are then examined in terms of release *via* diffusion and release during application.

2.2 Emulsions

Emulsions are a common form of material found in the food, cosmetic and pharmaceutical industry (Braisch *et al.*, 2009).As previously stated (section 1.1) emulsions could help deliver moisture to lips. Emulsions are traditionally defined as a dispersion of droplets of one liquid in another, the two being immiscible (commonly oil and water) (Dickinson and Stainsby, 1982). However emulsions are thermodynamically unstable, which will lead to phase separation (Hodge and Rousseau, 2003), in order to minimise the contact area between the two phases (Rousseau, 2000). To overcome this instability an emulsifier (discussed in section 2.4.4) is added, these are surface active molecules that adsorb to the interface to stabilise emulsions (Rousseau and Hodge, 2005). The type of emulsifier can dictate whether one produces a water-in-oil (W/O) emulsion (such as, margarine) or an oil-in-water (O/W) emulsion (such as moisturizers, mayonnaise and milk). Fat crystals or particles can also be used to stabilse emulsions (discussed further in section 2.4.3).

2.2.1 Emulsification

In order to produce an emulsion, one must first supply enough energy into the two immiscible liquids to provide mechanical agitation (Walstra, 1993) which results in the dispersion of one liquid into the other. It is important to note that these will immediately

begin to phase separate (process discussed further in section 2.3). Emulsion formation (and the size of droplets produced) is controlled by droplet break up, emulsifier adsorption and droplet coalescence.

2.2.1.1 Droplet Break up

Droplet break up is a function of both disruptive and interfacial forces. The interfacial forces are controlled by the Laplace pressure (Δp_l) (Equation 1.1) and are responsible for keeping the droplet spherical (McClements, 2005).

$$\Delta p_l = \frac{4\gamma}{d} \qquad \textbf{Equation 2.1}$$

Where γ is the interfacial tension between the water and oil, and d is the droplet diameter.

In order to break up a droplet a disruptive force (that is greater than the interfacial forces) is required (Stone, 1994). The disruptive force can be generated by a number of different homogenisation techniques (Walstra, 1983a). For the purpose of this thesis only two techniques were investigated; a Silverson high shear mixer (batch process) and a scraped surface heat exchanger (SSHE) and pin stirrer (PS) (continuous process). A high shear mixer operates in a batch mode, whereby the two phases are placed in vessel and mechanically agitated by a mixing head that can rotate at high speeds. This causes disruption between the interfaces between both phases resulting in larger droplets breaking into smaller droplets. Increasing the head speed increases the disruptive forces thus resulting in even smaller droplets. The SSHE and PS is a continuous process that is commonly used in the food industry to produce margarine. In this technique both emulsification and crystallisation can occur in the same process. The SSHE has scraper blades on a rotating axis. These blades provide the disruptive forces to break up the

droplets into smaller ones. The SSHE also has a temperature control allowing fat crystals (in the case of margarine) to be formed around water droplets causing Pickering stabilisation (see section 2.4.3)

2.2.1.2 The role of the emulsifier

As interfacial tension decreases the ease at which a droplet can be disrupted increases (Equation 2.1). Therefore it should be possible to create greater disruption in the presence of an emulsifier (see section 2.4.4) as an emulsifier reduces the interfacial tension (Walstra, 1993). It is important to note that the rate at which an emulsifier adheres to the interface will affect the efficiency of the process. For example if there is a low concentration of emulsifier at the interface, greater disruptive forces will be required to produce smaller droplets. Whereas at high concentrations (a lower interfacial tension), smaller disruptive forces are required for droplet disruption (Walstra, 1983b).

2.2.1.3 Droplet Coalescence

During emulsification, droplet-droplet collision is extremely probable. Therefore if the droplets are not protected they will come together and coalesce (process explained in section 2.3.4). Immediately after disruption, there is a greater surface area of interface; if there is not sufficient emulsifier present to cover this interface, coalescence will occur. In order to prevent immediate coalescence, it would be necessary to form an emulsifier barrier around the newly formed droplet before it has the opportunity to collide with another droplet (Walstra, 1993).

2.3 Emulsion Instability

As previous stated emulsions are thermodynamically unstable and therefore as soon as they form they begin to phase separate. Within the emulsions all the droplets undergo Brownian motion and therefore collide on a regular basis. The instability of emulsions

is a result of these collisions. There are two basic interactions; attraction and repulsion. If attraction dominates the droplets adhere together and phase separation begins, however, if repulsion dominates the emulsion will be stable and remain dispersed.

Phase separation is a result of an emulsion attempting to minimise contact area of the two phases and therefore lowering the overall energy of the system. There are four main mechanisms that contribute to emulsion instability including creaming/sedimentation, flocculation, Ostwald ripening and coalescence (Rousseau, 2000).

2.3.1 Creaming/Sedimentation

Creaming/ sedimentation (Figure 2.1) is caused by a difference in density between the two different phases under the influence of gravity that can lead to phase separation. For example Beydonun e*t al.* (1998) investigated the phenomena of settling. This was done by studying the effect of having a multiphase continuous medium on the settling velocity of spherical particles. The research showed that by increasing the emulsion viscosity, the settling velocity decreased (Beydoun *et al.*, 1998). The study worked well in illustrating the effect on varying emulsion viscosity; however it did not investigate the effect of varying droplet sizes within the emulsion as this will cause pressure differences between droplets leading to coalescence.

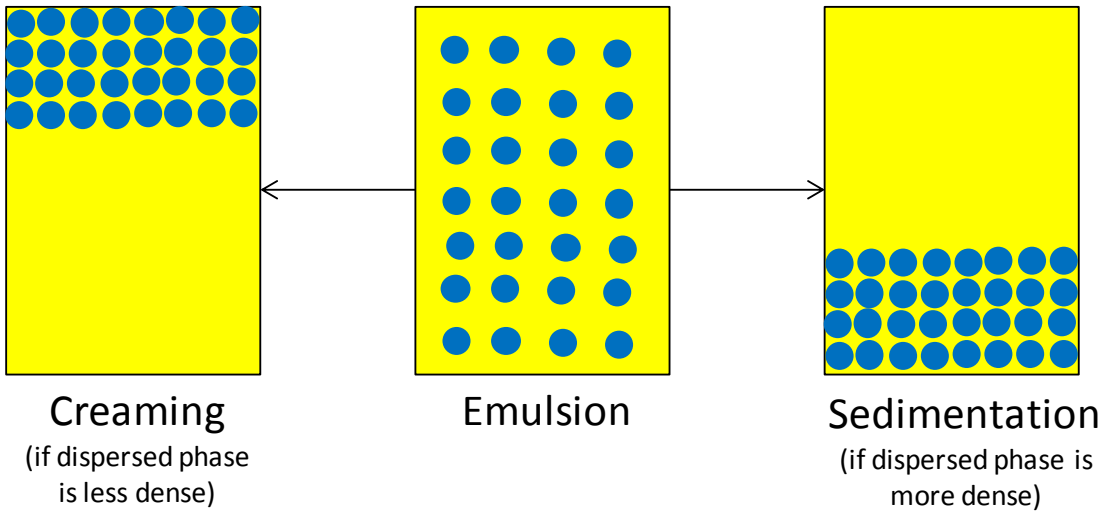

Figure 2.1 – Schematic representing both creaming and sedimentation

2.3.2 Flocculation

Flocculation can simply be described as aggregation of particles due to weak attractive force between droplets (Figure 2.2). This phenomena depends on the interaction energy between two droplets as a function of inter droplet distance. The interaction energy is a combination of both repulsive and attractive forces. In emulsions the repulsive forces are governed by the emulsifier used and the attractive forces are controlled by London-van-der-Waals forces. It is important to remember that during flocculation droplets maintain their structural integrity and therefore this phenomena is reversible (Rousseau, 2000).

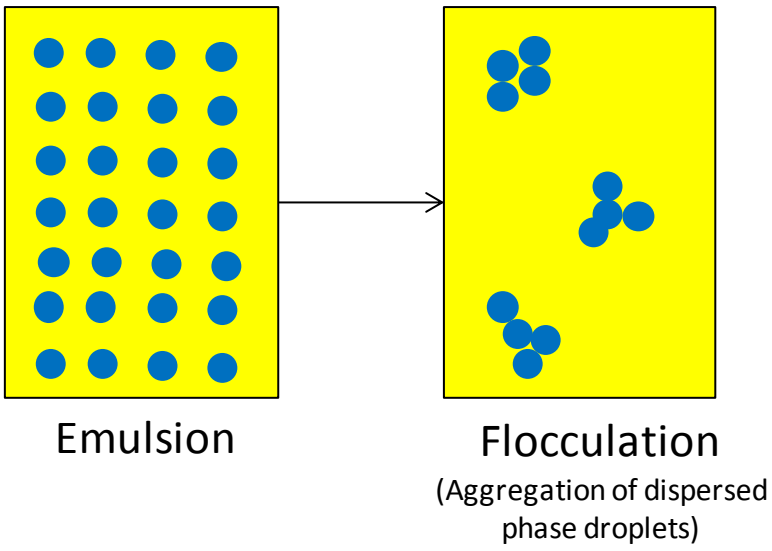

Figure 2.2 – Schematic representing flocculation

2.3.3 Ostwald Ripening

Ostwald ripening (Figure 2.3) is a phenomenon where larger droplets grow at the expense of smaller ones as a result of a solubility gradient being formed between small and large droplets (Dickinson *et al.*, 1999).

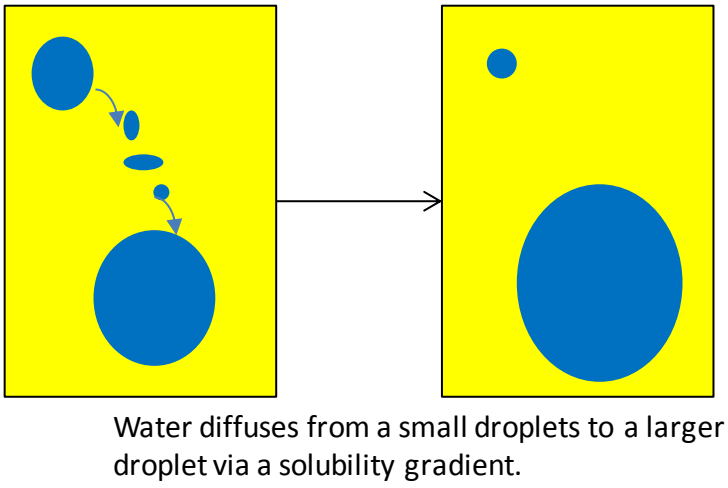

Figure 2.3 - Schematic representation of Ostwald Ripening

The rate at which the larger droplet grows depends on the solubility of the continuous phase as this affects the rate of molecular diffusion and the difference in partial pressures between the dispersed phase droplets (known as the Laplace pressure difference).

With the emulsions being considered for this research Ostwald ripening is of little importance as there is limited solubility between the aqueous and oil phases.

2.3.4 Coalescence

Coalescence is where two droplets combine to form a larger droplet after collision (Figure 2.4) (Kabalnov, 1998). As two droplets approach one another, a thin film (section 2.3.4.1) of continuous phase is formed between the two droplets (Ivanov *et al.*, 1999). For coalescence to occur this film must rupture (section 2.3.4.2), allowing the fluid in the droplets to merge together (Kabalnov, 1998). This mechanism is driven by the fact that the emulsion wants to move to its most thermodynamically stable state, where there is the least contact between both phases (McClements, 2005).

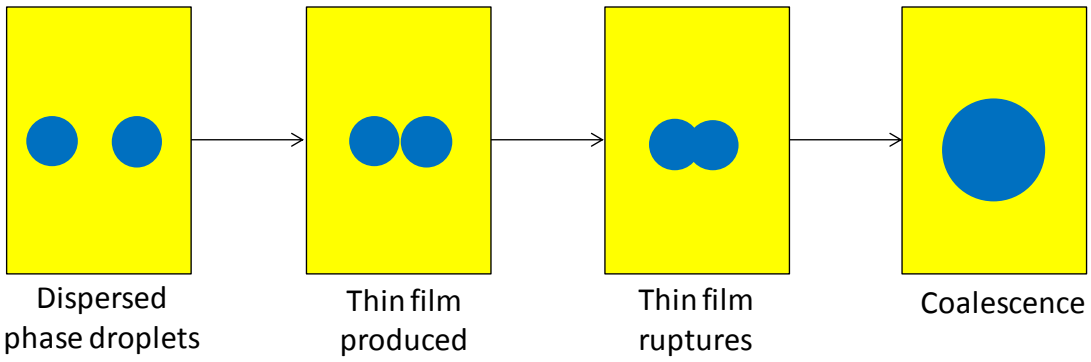

Figure 2.4 - Schematic of Coalescence

2.3.4.1 Thin Film

A thin film is produced as two droplets come into close proximity. As the fluid flows out of the thin film, a hydrodynamic resistance is formed due to the friction generated from the fluid flow. Before these droplets can get any closer, the remaining fluid needs to be pushed out. The film will continue to thin resulting in a number of events occurring. The droplets can either; move away from each other (known as no aggregation), remain in a state of secondary medium (known as weak flocculation), remain in a state of primary medium (known as coagulation) or the droplets come together and coalesce. The outcome of droplet-droplet interaction depends on the colloidal and hydrodynamic interactions (Figure 2.5)

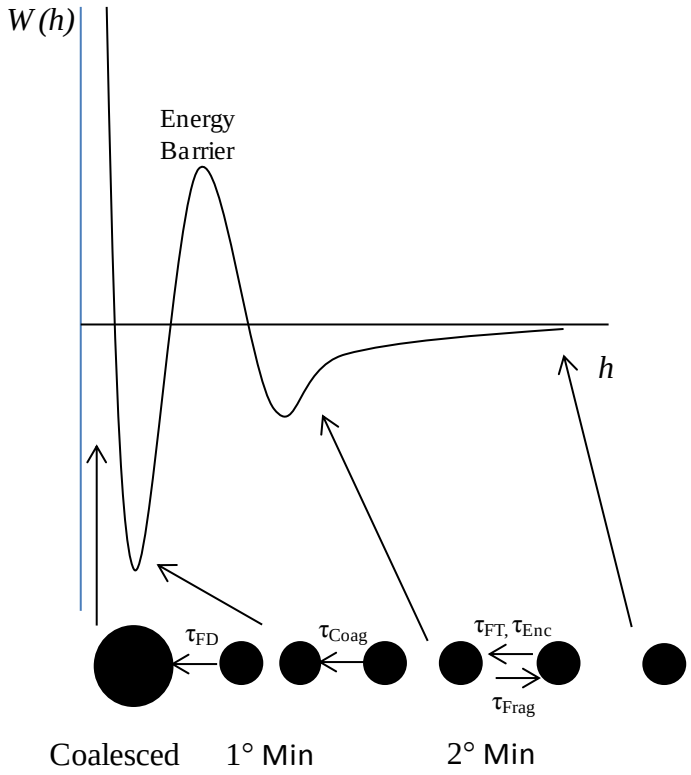

Figure 2.5 – Schematic representation of physiochemical processes involved when two droplets approach one another. Where τ_{FD} – film disruption time, τ_{Coag} – coagulation time, τ_{FT} – film thinning time and τ_{Enc} – encounter time (Image adapted from McClements (2005)).

No aggregation – After the droplets collide, if there is a high energy barrier and if the secondary minimum is low, the droplets will move apart.

Weak Flocculation – When there is a large energy barrier and a deep secondary minimum, the droplets tend to weakly flocculate. This results in a thick film being produced (in the order of nm) between the droplets.

Coagulation – When the energy barrier is low and there is strong short range repulsion between droplets then the droplets can fall into primary minimum.

2.3.4.2 Film Rupture

Coalescence occurs when the thin film of liquid between the droplets is ruptured. It is important to note that if there is no short range repulsion between droplets, then rapid coalescence will occur after the droplets fall into primary medium. There are a variety of different mechanisms that can lead to coalescence. This is determined by the characteristics of the continuous phase which separates the droplets (*e.g.* the viscosity, interfacial tension and thickness). The mechanisms that control coalescence depend on whether there is emulsifier present in the system. If there is no emulsifier present in the system then the following mechanisms lead to film rupture and coalescence.

Capillary Wave Formation – Capillary waves are a result of thermal motion within the system and are formed spontaneously. When the amplitude of the thermal variations is half that of the film thickness then a point of contact will occur between the two droplets. This leads to the formation of a hole, which allows the fluid between two droplets to combine.

Spontaneous Hole Formation – Tiny holes can form spontaneously in the thin film due to thermal motion of the system. Kalbanov (1998) stated that if these holes are

below a critical value then they will collapse, however if they are above this value they will grow resulting in film rupture.

In the majority of emulsion systems the droplets are coated by a layer of emulsifier. Therefore alternative factors may be responsible for film rupture (McClements, 2005).

Insufficient Emulsifier – If there is a lack of emulsifier within the system, it could lead to incomplete coverage of the W/O interface. This then leads to gaps on the interface, therefore when two droplets come into close proximity coalescence can occur *via* either capillary wave formation or spontaneous hole formation. It should be noted that this type of coalescence is more likely to occur during homgenisation due to new interfacial surfaces constantly being created.

Film Stretching – Film stretching occurs if a large stress is applied to the interface. This causes some of the emulsifier to be dragged across the interface, thus leaving some areas with a depletion of emulsifier. If two depleted regions of different droplets approach one another, coalescence could then occur.

Film Tearing – Van Aken (2004) stated that in situations where large stresses are applied to the interface (when this is comprised of highly cohesive emulsifier molecules *i.e.* proteins), a tear can occur in the interfacial membrane. This leads to emulsifier depleted reaches resulting in coalescence.

Coalescence is a major problem with emulsions and there are various ways in which the process of coalescence can be reduced. These methods will be discussed in section 2.4.

2.4 Emulsion Stabilisation

Creaming, flocculation, coalescence and Ostwald ripening are constantly working to minimise the energy within the emulsion, causing the emulsion to ruin. As previously discussed this is caused when droplets collide, therefore the basis of stabilisation is determined by these collisions. Since there are always strong, long-range attractive forces between similar droplets, it is necessary to provide long range repulsion between the droplets to impart stability. This repulsion should be at least as strong as the attractive force and comparable in range of the attractive interaction (McClements, 2005).

Stability can be obtained by surrounding the droplets: with an electrical double layer (electrostatic stabilisation), with adsorbed or chemically attached polymeric molecules (steric stabilisation) or with free polymer in the dispersion medium (depletion stabilisation) (McClements, 2005). It can also be achieved by increasing the viscosity of the continuous phase which lowers the mobility of the dispersed phase resulting in fewer collisions.

2.4.1 Electrostatic Stabilisation

Electrostatic stabilisation is an effective way to counterbalance the London van der Waals attraction between droplets. Ionic groups can be adsorbed to the surface of the droplet to form a charged layer. To maintain electroneutrality, an equal number of counter-ions with the opposite charge will surround the droplets and give rise overall charge neutral double layers (McClements, 2005). This layered droplet will then repel other similar droplets preventing coalescence. For example Tran and Rousseau (2013) were able to prevent the destabilisation of soy protein isolate (SPI) dispersions by using soy soluble polysaccharides (SSPS) under acidic conditions. Figure 2.6 shows a

possible interaction mechanism between SPI + SSPS complexes in the presence of NaCl. It shows that electrostatic stabilisation can occur at a certain pH (Tran and Rousseau, 2013).

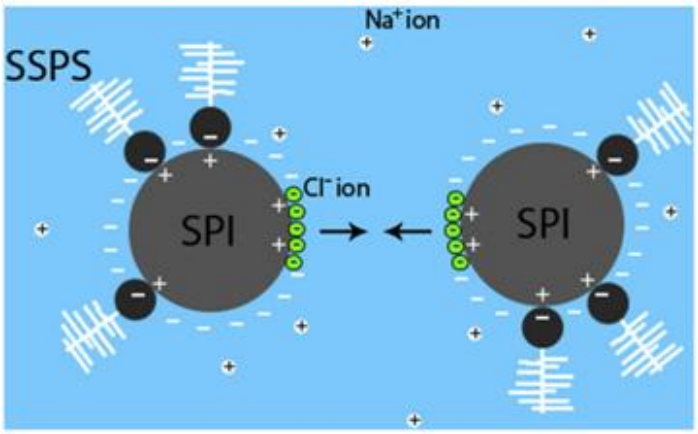

Figure 2.6 - Suggested interaction mechanism between SPI + SSPS complexes in the prescense of NaCl (taken from Tran and Rousseau, 2013)

2.4.2 Polymeric Stabilisation

Polymers, including natural polymers such as proteins and gums can be used to stabilise emulsions. Any polymer with molecular weights >10,000 D are comparable or in excess of the range of van der Waals attraction. Therefore as long as the polymer generates repulsion then it will help form a stable emulsion (Napper, 1983).

There are two different mechanisms accepted for polymeric stabilisation of emulsions: (1) steric stabilisation and (2) depletion stabilisation.

(1) Steric stabilisation of emulsions is achieved by attaching macromolecules to the surface of droplets *via* chemisorption. These macromolecules cause steric hindrance between droplets preventing them from coalescing as shown in Figure 2.7.

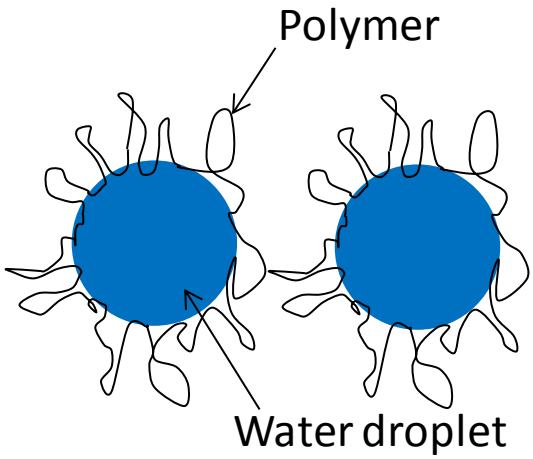

Figure 2.7 - Schematic of Steric Stabilisation

An example of steric stabilisation was shown in 2002 Chanamai and McClements compared Gum Arabic and modified starch as emulsifiers. The influence of pH, $CaCl_2$ and temperature were investigated to monitor whether steric or electrostatic stabilisation were the predominant mechanisms for stabilisation (Chanamai and McClements, 2002). Results showed that steric repulsion has greater significance than electrostatic repulsion when using either gum Arabic or modified starch stabilised emulsions.

(2) Depletion stabilisation of emulsions is achieved by adding macromolecules that are free in solution (as shown in Figure 2.8). This creates repulsive forces between approaching droplets preventing coalescence from occurring.

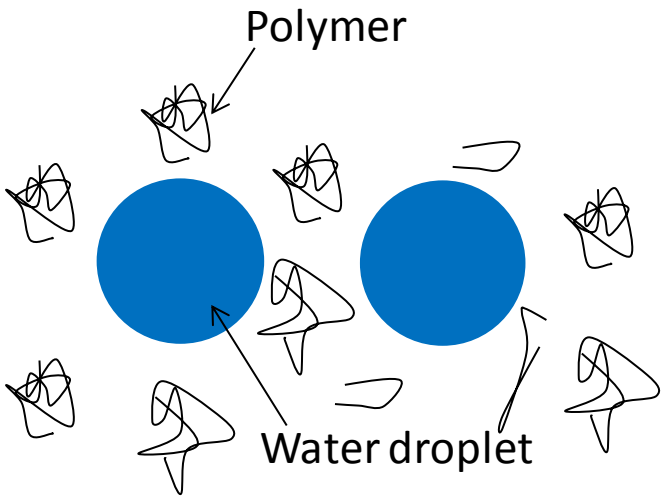

Figure 2.8 - Schematic of Depletion Stabilisation

2.4.3 Fat Particles in Emulsion Stability

For fat crystals to assist in the stabilisation of emulsions they must collect at the emulsion droplet interface which will then provide a physical barrier to coalescence (Figure 2.9) (Rousseau, 2000). This type of emulsion is referred to as a Pickering emulsion (Dickinson, 2010).

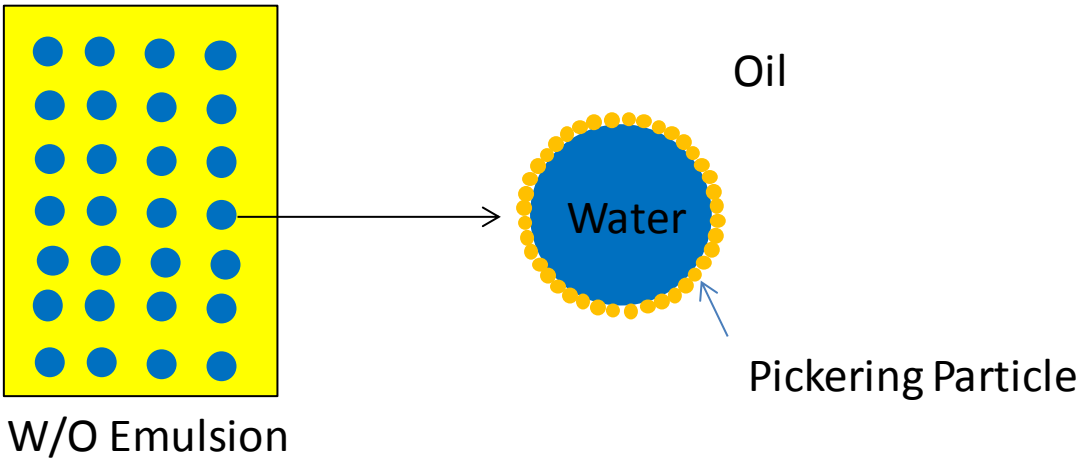

Figure 2.9 - Schematic of Pickering stabilisation

Pickering (1907) was the first to study the formation and stability of colloidal stabilisation of emulsions. This was done by investigating the use of different metal sulphates on the stability of emulsions (Pickering, 1907). In the 1960's Lucassen-Reynders investigated the role of colloidal particles in food emulsions. It became known that the addition of solid particles are necessary for product stabilisation *via* a steric mechanism (Dickinson, 2010, Rousseau, 2000). For example, ice crystals are used to stabilise ice cream, fat particles stabilise whipped cream and egg yolk particles stabilise mayonnaise (Rousseau, 2000).

The use of fat crystals in W/O emulsions can impart stability in two ways, (1) Pickering stabilisation and (2) the presence of a fat crystal network in the continuous phase prevents droplet movement therefore preventing coalescence, hence long term emulsion stability (Frasch-Melnik *et al.*, 2010, Hodge and Rousseau, 2003).

Frasch-Melnik *et al.* (2010) and more recently Norton and Fryer (2012) have utilised Pickering particles in stabilising W/O emulsions. The latter also used a continuous fat network which would result in long term stability. Frasch-Melnik *et al.* (2010) investigated the use of both mono and triglycerides as Pickering particles without the use of other emulsifiers. Results show that sintered shells were formed around the water droplets. Norton and Fryer (2012) investigated cocoa butter W/O emulsions; results showed that water droplets were coated with sintered crystals indicating Pickering stabilisation.

2.4.4 Emulsifiers

An emulsifier is a surface active molecule that is both hydrophilic ('water loving') and hydrophobic ('water hating') allowing it to adsorb to a W/O interface which can prevent droplet aggregations and coalescence during formation and storage (Coupland

and McClements, 1996, McClements, 2002). Emulsifiers operate by lowering the interfacial tension between the dispersed and continuous phase (Rousseau, 2000).

The concentration of emulsifier used is crucial in producing stable emulsions. It needs to be high enough to cover the droplet surface (which increases as the droplet size decreases). If there is not enough emulsifier to cover in the entire droplet surface coalescence could occur if the droplets come into close proximity. When excess emulsifier is used the droplet size formed depends on the emulsification process involved.

2.5 Crystal Networks

Crystal networks are comprised of different levels of structures, each of which contribute to the macroscopic properties of the overall network (Figure 2.10). This includes the spreadability of spreads, butters and margarines or the snap of chocolate or the strength of a lipstick (Narine and Marangoni, 1999a).

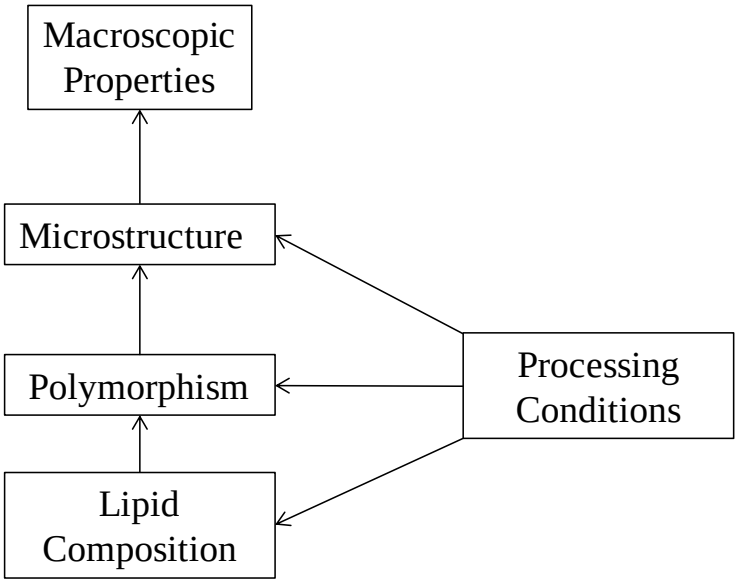

Figure 2.10 - Factors affecting macroscopic properties of fat networks (Image adapted from Narine and Marangoni (1999a)).

2.5.1 Lipid Composition

Lipids predominately consist of triacylglycerols (TAG's) and in order for them to be a fundamental component in a crystal network they must initially crystallise.

Crystallisation is achieved in when a solution (containing crystal particles e.g TAG's) is cooled below the melting point of the crystal particles. Jensen and Mabis (1966) showed that when a triacylglycerol (TAG) molecule crystallises it adopts a tuning fork configuration, otherwise known as a chair conformation. Several of these 'chains' then align side by side in order to maximise the van der Waal interactions. As

shown in Figure 2.11, the chains generally consist of two, three or four chain lengths of fatty acids constituents of TAG.

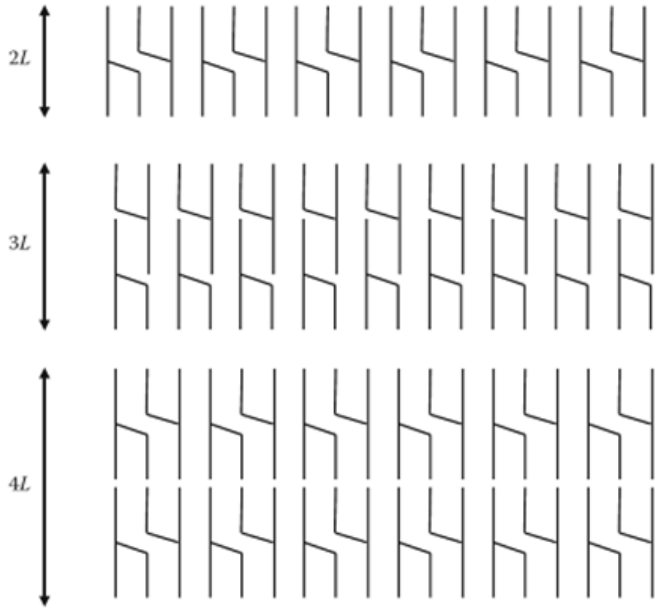

Figure 2.11 – Stacking Possiblities for triacylgylcerol in fat crystals where the letter L represents fatty acid chain length (Image adapted from Marangoni and Wesdrop (2012))

Van den Tempel (1961) developed an early mechanical model which suggested that fat networks comprised of an assembly of chains which individually consisted of particles that were packed closely together *via* van der Waal interactions. These particles are a result of a nucleation step which allows crystals to be produced.

2.5.1.1 Nucleation

There are two mechanisms by which nucleation can occur. (1) Homogeneous nucleation (otherwise known as primary nucleation) – this is where crystals are formed spontaneously or (2) heterogeneous nucleation - this is where crystal formation occurs around impurities. The rate at which nucleation occurs is determined by two factors. The first is the energy required to fabricate a new surface area and the second is the energy gained when the metastable liquid crystal transfers to its thermodynamically

more stable solid state. The second of these factors drives nucleation allowing a nucleus to be formed. A nucleus is an aggregation of crystalline structures that is large enough to lead to a decrease in Gibbs energy (Kloek *et al.*, 2000). It has been found that in the majority of cases, crystal nucleation starts as a result of impurities. As they provide an interface that can act as templates for nucleation (Campbell *et al.*, 2002). Walstra (1998) showed that for most applied systems, bulk fats crystallise *via* a heterogeneous mechanism due to the presence of dust or foreign particles (which act as the surface template for nucleation). Heterogeneous crystallisation is more favourable than homogenisation crystallisation as the energy required for homogeneous nucleation is a lot higher (Campbell *et al.*, 2002, Kloek *et al.*, 2000).

2.5.2 Processing Conditions

One of the other major influences on crystal networks are the processing conditions involved in producing crystal networks (including cooling rate). Campos *et al*. (Campos *et al.*, 2002) investigated the effect of cooling rate on the structure and mechanical properties of milk fat and lard. Results showed that when a cooling rate of > 5 °C / min were used a higher crystallisation rate was observed. This was due to the formulation being rapidly cooled causing lots of nucleation sites in shorter time period. Whereas when a slower rate of cooling is used (< 0.1 °C / min) the frequency at which nucleation sites occur is reduced. Therefore leading to less crystals being formed (Campos *et al.*, 2002). The cooling rate can dictate the size of the fat crystals being formed.

Foley and Bradley (1984) investigated temperature induced effects on crystallisation behaviour. Results showed that when a formulation was cooled slowly large crystal aggregates were formed. When a slow cooling rate is use, a long induction time is required to form nuclei. These nuclei then grow to form larger crystals within a

solution. Crystal growth is favoured over new nuclei formation as the time taken for nuclei formation is longer than the time taken for mass transfer and diffusion onto a newly formed crystal. On the other hand when samples are cooled rapidly, the induction time is short. This results in a large number of crystals being formed which are evenly distributed throughout the solution. Crystal growth is inhibited as the viscosity of the solution increases due to the rapid formation of many nuclei (Foley and Brady, 1984, Campos *et al.*, 2002).

Another processing condition that can affect crystallisation is shear. Shear can distribute newly formed crystals throughout a sample. For example when using SSHE which has a jacketed vessel. Initially nucleation occurs at the jacket wall (as this is the location with the greatest cooling) this can be brought into the bulk solution (by a scraper), causing seeding of new crystals (Campbell *et al.*, 2002). This phenomena is known as secondary nucleation.

2.5.3 Crystal Structures

TAG's can exist in one of three main polymorphic forms; alpha (α), beta prime (β') or beta (β) (Larsson, 1966). Jensin and Mabis (1966) have been attributed with determining the first full crystal structure. They determined that tricaprin was in a β-form structure. The alpha form is the least stable and has a hexagonal subcell, β' is slightly more stable and has a orthorhombic subcells and β is the most stable with a triclinic subcells (Figure 2.12) (Sato, 2001). The different subcell structures control the arrangement of the crystals in the crystal lattice (Sato, 2001).

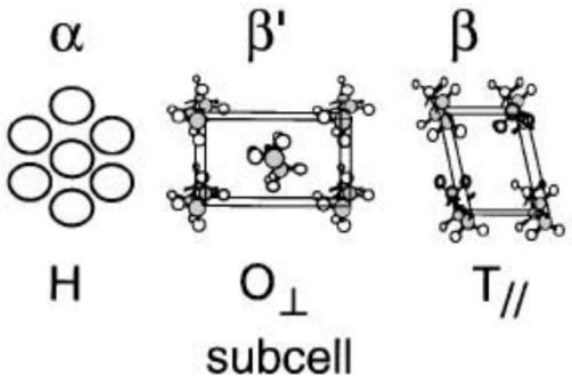

Figure 2.12 - Examples of the structure of different polymorphs in triacylglycerols (taken from Sato 2001)

Crystal form can be determined using a technique known as differential scanning calorimetry (DSC). Norton *et al*. (1985) investigated the melting behaviour of triglycerides (tripalmitin and tristearin) with triolein. Results showed that when a fast cooling rate (1 K / hr) was used α crystals (least stable) were favoured. Whereas when a slow cooling rate was utilised (0.1 K / min) β crystals were more favoured (most stable). They also found that at faster cooling rates the crystallisation temperature increased (Norton *et al.*, 1985).

When a solution containing fat crystals is cooled below the crystallisation temperature, α-form crystals are the first to form. This is due to the low activation energy of nucleation (Figure 2.13), as a result many α-form crystals from in a short period of time.

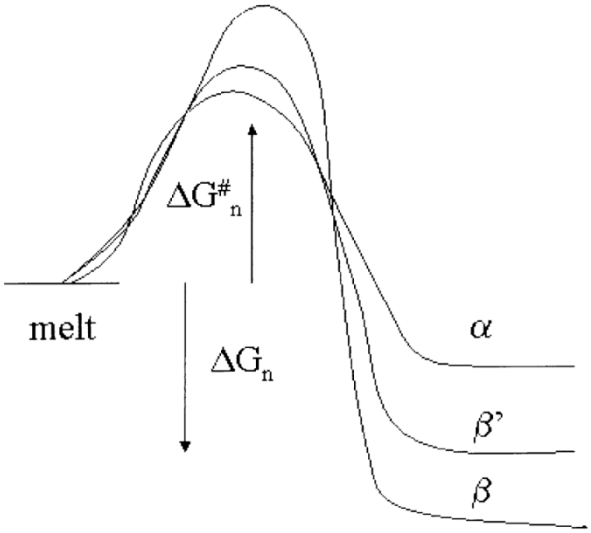

Figure 2.13 – Free Energy of activation Vs free energy of formation for the nucleation of different polymorphic forms of fat (taken from Marangoni, 2002)

Fat crystals exhibit polymorphic forms due to their high glyceride content. However, waxes are defined as simple esters of fatty acids with alcohols. As a result the polymorphism in waxes is reduced, with the orthorhombic subcell prevailing (Jenning and Gohla, 2000).

When TAG's present in the melt begin to crystallise into varying polymorphic states a fat crystal network begins to develop/form. These crystals then aggregate into larger microstructures *via* both a mass and heat transfer process (Narine and Marangoni, 1999a). In this microstructural level (Figure 2.10), the solid network can be defined as an amorphous solid whereas the intramicrostructural level is deemed fractural in nature (Narine and Marangoni, 1999b). The fractural geometries within the microstructure are extremely important in determining the macroscopic properties (material properties) of the fat crystal network and range from 1 – 140 μm (Narine and Marangoni, 1999b).

2.5.4 Links between Crystal Network and Macroscopic Properties

Van den Tempel (1961) suggested there was a linear link between the elastic modulus and solid volume fraction. This was later shown to be untrue by Nederveen (1963) and Papenhuijzen (1971). Nederveen (1963) investigated the mechanical properties of pure glyceryl tristearate crystals in oil. The author concluded that the modulus did not follow a linear relationship as was suggested by Van den Tempel (1961) but required further investigations in order to understand the mechanical behavior of the crystals in suspension. It was later noted by Edwards and Oakeshott (1989) that fat crystal networks are mathematically similar to flocculated colloids, which showed that the elastic properties of polymer gels can be explained using scaling theory. Brown and Ball (1985) were responsible for the early development of the scaling theory in terms of colloidal gels. They suggested that aggregates should behave as mass fractals on a scale that is big enough to be compared to the primary particle size. From this they produced a power law relationship linking elastic modulus to the solid volume fraction. This was later confirmed by Shih *et al*. (1990) who identified two different regimes (strong-link and weak link regime) depending on the concentration of the colloidal gel. However, before we can discuss the different regimes it is important to consider the meaning behind fractal systems.

2.5.4.1 Fractal Systems

As previously stated the microstructure is composed of fractal aggregates, where each aggregate is comprised of fractal objects that are self similar, with different levels of scales. Jullien and Botet (1987) related the radius (R) to the mass (M) of the aggregates;

$$M(r) \alpha R^{D} \qquad \text{Equation 2.2}$$

Where D is a fractal dimension.

Rousseau, Marangoni and Jeffery (1998) showed that the elastic modulus of a network is controlled by the following relationship;

$$G' \sim \phi^{m} \qquad \text{Equation 2.3}$$

Where ϕ is the particle volume fraction. The elastic behavior of the network depends on the on the concentration of the particles, and can be categorised into either strong link or weak link regimes.

2.5.4.1.1 Strong-link Regime

In this regime, the crystals (gel particles) grow large. This results in each crystal acting as a weak spring, causing the elastic constant of the network to be dominated by the elastic constant of the flocs (Shih *et al.*, 1990), Shih 1990 represented this using the following relationship:

$$G' \sim \phi^{[(d+x)/(d-D)]} \qquad \text{Equation 2.4}$$

Where D is the fractional dimension, x is the backbone fractural dimension and ϕ particle concentration,

2.5.4.1.2 Weak - Link Regime

In this regime, the elastic constant of the network is dominated by the links formed between different fractural geometries and occurs at high particle concentration. De Gennes (1979) showed that in a semi dilute polymer solutions the elastic constant increases as a function of ϕ in a power law manner.

2.6 Material Properties

In the previous section, we introduced how a crystal network affects the materials properties of a final structure. Therefore it is important to consider the fundamentals of deformation and material testing.

2.6.1 Hooke's law

Hooke's law provides the bases for characterizing the properties of solids. It states that elongation of a spring (ΔL) is directly proportional to the applied load;

$$\mathbf{F = k\Delta L} \qquad \textbf{Equation 2.5}$$

Where k is a characteristic of the spring.

The range at which Hooke's law is obeyed is refered to as the elastic region. In this region, when the applied load is removed from a spring, the spring will return to its original position resulting in reversible deformation. Whereas when an applied load is greater than the elastic limit, irreversible deformation takes place. At this point Hooke's law is no longer obeyed. If the load is applied beyond the limit of elasticity, the spring will reach a breaking point.

Hooke's law can be applied to semi solid materials, as long as the deformations on the material remain within the elastic region. In semi solid materials, a material may also behavior in a plastic manner. This is where the material deforms considerably without breaking even when passed beyond the limit of elasticity.

2.6.2 Stress-strain Relationships

As previously stated a material will deform when a load is applied, however the amount of deformation will also be dependent on the dimensions of the material. Therefore the

constant k (equation 2.5), can be modified to incorporate the dimensions of a material;

$$\frac{F}{A} = M\frac{\Delta L}{L_O} \qquad \textbf{Equation 2.6}$$

Where A is the cross sectional area, Lo is the original length of the sample, ΔL is the change in length of the sample and M is the modulus of elasticity.

The applied stress (σ) and resulting strain (ϵ_E) can be defined as;

$$\sigma = \frac{F}{A} \textbf{ and } \varepsilon_E = \frac{\Delta L}{L_O} \qquad \textbf{Equation 2.7}$$

Therefore;

$$\sigma = M\,\varepsilon_E \qquad \textbf{Equation 2.8}$$

The applied stress is proportional to the strain and the elastic modulus is a constant that provides information on the elastic properties of the material.

2.6.2.1 Different types of stresses and Moduli

There are three different types of stresses (tensile, compressive and shear) that can arise when a material is exposed to a load. If a material is stretched or compressed in one dimension it results in tensile or compressive stresses respectively. If however opposite forces are applied on opposite faces of the material, shear stresses are produced. The moduli that results from these stresses can provide information regarding material properties. Traditionally, these stresses are either applied using a texture analyser (for more information see section 3.4.6) or rheometer.

Le Reverend *et al*. (2011b) utilised texture analysis (with a penetration depth analysis probe) to investigate the effect of water content on material properties. They related the force required to penetrate the material to hardness. Results showed that as

the water content increased the penetration depth also increased resulting in a softer product. Wang and Lee (1997) also utilised texture analysis, however, they used compression to assess material properties of emulsion lipsticks. They related the force required to cause fracture to the hardness of a lipstick. Results showed that the introduction of water in the form of droplets initially softens a formulation (313 ± 30 to 223 ± 22 g), however when the amount of water was increased from 5 wt % to 15 wt % the hardness also increased (140 ± 13 to 270 ± 28 g). Wang and Lee offered no explanation for this phenomenon. They simply stated that the water was not in sufficient quantity to make a contribution to the hardness.

More recently, texture analysis has been used in the world of polymer gels to understand the mechanical properties of different gel systems. It has been noted by Norton *et al.* (2011) that when a True stress- True strain curve is plotted (Figure 2.14) there are two regions of linearity before the material fractures. The first is indicative of Young's modulus which is a measure of stiffness. The second region was termed bulk modulus and was representative of the materials ability to withstand compression. Other mechanical properties such as point of fracture and work of failure (area under the curve) can also be assessed from this curve (Norton *et al.*, 2011).

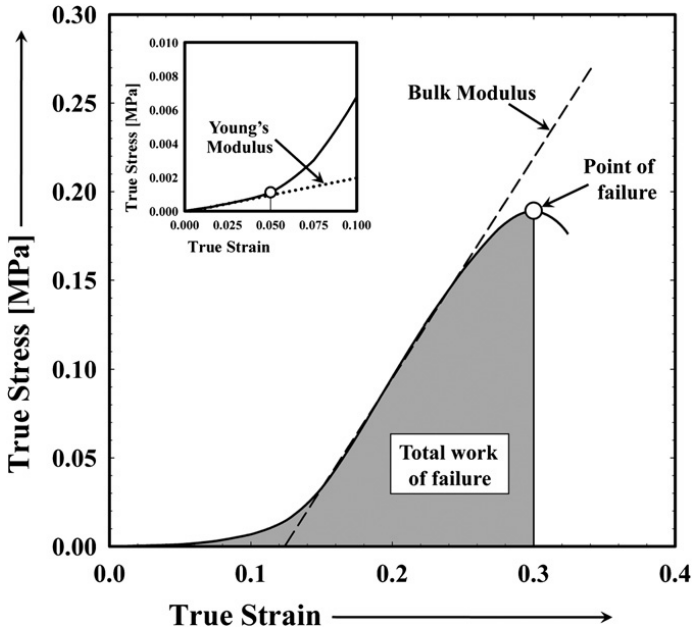

Figure 2.14 Schematic of a typical true stress/true strain curve obtained during uni axial compression (taken from (Norton *et al.*, 2011).

Shear stresses can be obtained using rheological techniques which provides information on the elastic behavior of a material. Shear stress (τ) and can be calculated when dividing the force required to cause deformation (F) by the cross sectional area of the material (A). The strain is the distance moved divided by the original length of the material. The rate at which the material deforms is known as the shear rate ($\dot{\gamma}$). The viscosity of a sample is then τ divided by the $\dot{\gamma}$.

When analysing the rheological properties of materials they can be classed by the two extremes; Hookean solids or Newtonian liquid. For elastic solids the energy generated (elastic modulus) when the material is deformed is stored resulting in the material returning to its original form (recovering) once the force causing deformation is removed (Hooke's Law). For liquids the energy generated when the material is sheared is loss in heat and therefore the material never returns to its original state. The majority of materials exhibit both these properties and are known as viscoelastic materials

(Bohlin-Instruments, 1994). Oscillation rheometry can give information regarding the viscoelastic properties and will be discussed in the next section.

Oscillation rheometry

Oscillatory rheometry allows a sinusoidal stress to be applied to the material. Therefore the resulting strain response will be sinosoidal. The key for oscillation rheometry is to not destroy the sample during the experiment; this can occur if the sample is over strained resulting in the destruction of the elastic structure. To prevent this from happening it is important to measure the linear viscoelastic region (LVR). This is done by running an experiment where the stress is increased and the frequency is kept constant resulting in a graph where the elastic (G') and viscous (G'') modulus cross or it is the point whereby G' and G'' stop being independent of stress (This is shown in Figure 2.15). At this point the material is no longer behaving as a solid and is more viscous like. From this curve a value of strain can be obtained that is within the LVR, this can be input into a controlled stress experiment where the frequency is varied allowing information regarding the materials viscoelastic properties to be obtained (Bohlin-Instruments, 1994). G' is a measure of the deformation energy which is stored within the sample during shear, thus showing the elastic (solid-like) behaviour. G'' is the deformation energy that is dissipated as heat during in shear, and indicates the viscous (liquid-like) behaviour (Tabilo-Munizaga and Barbosa-Cánovas, 2005).

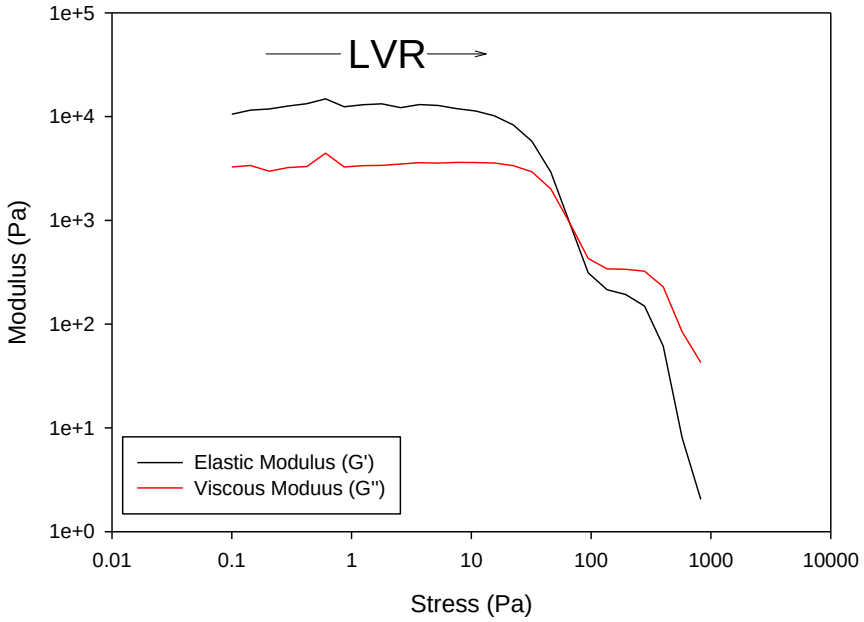

Figure 2.15 – Typical amplitude sweep (stress from 0.1 – 1000 Pa) curve at a frequency of 1 Hz

Operating within the LVR allows a greater understanding of the interactions between fat crystals (*i.e.* the weak link regime) and therefore gives an insight into different levels of structure within the microstructure. Rye *et al.* (2005) used oscillation rheology within the LVR to show that G' was proportional to the yield point (previously described as point of fracture) of milk fat.

2.7 Tribology

Tribology is the science and technology of interacting surfaces that are in relative motion. It involves the study of friction, wear and lubrication during application. Traditionally tribology has been used in the mechanical engineering sector to study/ improve the performance of machine components (such as gears, bearings and brakes). The performance is governed by the behaviour in the contact between the two surfaces in relation to the resistance to wear and friction generation (Bhushan and Hsu, 2001, Barwell, 1974, Nakada, 1994). In these applications, lubricants are added to the surfaces to reduce friction and wear, which can improve both the lifetime of equipment and the equipment efficiency.

Friction is a result of the movement of one surface to another and is defined by the following equation;

$$\boldsymbol{F = \mu W} \qquad \textbf{Equation 2.9}$$

Where F is the frictional force (N), μ is the coefficient of friction and W is the applied (perpendicular to the direction of friction) normal force (N).

For any given system, friction is dependent on a number factors which include, surface roughness, type of lubricant relative speeds of surfaces and temperature. Friction between two surfaces can be assessed using a tribometer, where either both surfaces can rotate or where one remains fixed and the other.

Traditionally, different lubricants are used to investigate their affect on reducing wear within metal contacts. As a result modern day tribometers are able to detect wear changes in surfaces. This could prove to be valuable when assessing solid wax surfaces for use in lipstick application, as a lipstick would have to wear to transfer to the lip.

2.7.1 Analysing Friction

As previously stated, tribology is the study of friction. Friction can be obtained using a variety of tribological techniques. Luengo *et al.* (1997) used a sliding stage technique (Figure 2.16) to analyse the tribology of chocolate. In this technique a load is dragged across a sample in a horizontal manner which the friction coefficient is being recorded.

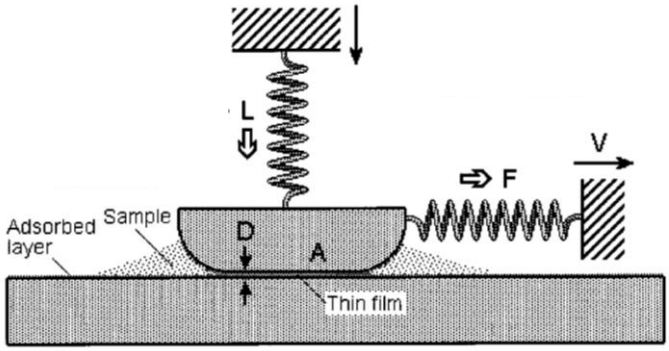

Figure 2.16 Schematic representation of sliding stage (adapted from Luengo *et al.* (1997))

More recently a tribometer (Figure 3.23) has been used in both the cosmetic (Lodén and Wessman, 2001) and food industry (de Wijk and Prinz, 2005) in order to relate friction to how a formulation will behave on the skin or in the mouth respectively. In the cosmetic industry a pin-on-disk set up is normally utilised as the stationary surface can be likened to skin and the rotating surface can be related to the application. Timm *et al.* (2011) utilised a pin-on-disk set up to show that the addition of cosmetic polymer particles reduced the friction of the overall system. This reduction was dependent on the particle size.

Whereas in the food industry, both surfaces rotate in order to mimic the complex nature of consuming foods. Dresselhuis *et al.* (2008, 2007) utilised two rotating surfaces in a tribometer to show the effect of O/W emulsions in mouth like conditions. It should be noted that to the author's knowledge there is limited work conducted on W/O liquid emulsions and non on solid W/O emulsions in a tribometer. Therefore the latter will be investigated as part of this thesis.

2.7.1.1.1 Tribopair

The surfaces used for tribology along with the lubricant, help determine friction. In a tribometer there are two surfaces, traditionally a stainless steel ball and a stainless steel disk. However this is of little relevance to both the food and cosmetic industry as the surfaces do not deform which does not represent either a skin or mouth feel (Dresselhuis *et al.*, 2008). Tribological studies in the cosmetics and food industry tend to use either two soft surfaces; elastomer disk with a (polydimethyl siloxane (PDMS)) ball or an elastomer disk with a steel ball (Dresselhuis *et al.*, 2007, Timm *et al.*, 2011). Garrec and Norton (2013) showed that an elastomer-steel ball combination produced the lowest margin of error when investigating hydrocolloid solutions. Consequently this tribopair was used for the work presented in this thesis.

2.7.2 Sensory Perception and Tribology

Verhagen and Engelen (2006) stated that there are multiple factors that affect the mouthfeel of food products. This makes it difficult for industries to correctly predict how a consumer may respond to new innovative products without using sensory panels. Tribological measurements have been shown to relate lubrication properties with both mouthfeel (Malone *et al.*, 2003) and skinfeel (Kusakari *et al.*, 2003). Malone (2003) related the frictional values of varying fat contents (measured in a tribometer) with 'fattiness' scores obtained from a sensory panel. Similarly in the cosmetic industry,

Kusakari *et al.* (2003) utilised a tribological technique to relate frictional values of different moisturisers with 'spreading and 'stickiness' scores obtained from a sensory panel. However is should be noted that in both systems utilise solids suspended in a liquid. To the authors knowledge there is no evidence of sensory perception for solid waxes (lipsticks) being related to frictional values. Therefore there is a need to investigate the possibility of using a tribometer in assessing how a formulation will be perceived by a consumer.

2.8 Controlled Release from Colloidal Structures

Release from colloidal structures has been observed in the pharmaceutical and food industry (Pothakamury and Barbosa-Cánovas, 1995). Controlled release is defined as a method by which active agents/ ingredients are made available to a desired site and time at a specific rate (Pothakamury and Barbosa-Cánovas, 1995). Traditionally, controlled release is achieved using a microencapsulation technique whereby the desired component is sealed in capsules and is released upon the influence of stimuli (such as temperature or pH). The controlled release of the active agent is governed by diffusion, biodegradation, swelling or osmotic pressure (Pothakamury and Barbosa-Cánovas, 1995). For the purpose of this thesis release by diffusion will be discussed.

2.8.1 Release via Diffusion

There are two main systems (reservoir and matrix) by which controlled release occurs *via* diffusion.

2.8.1.1 Reservoir Systems

In a reservoir system the active is surrounded by a rate-controlling barrier. The barrier can be non porous, macroporous or microporous (Langer and Peppas, 1983b), with the release rate dependent on the thickness, area and permeability of the membrane (Baker, 1987). There are 4 steps involved with the release of an active from a reservoir system (Himmelsten, 1991);

1. Diffusion of the active through the reservoir

2. Dissolution or partitioning of the active agent between the reservoir fluid and the barrier.

3. Diffusion through the barrier

4. Transport away from the barrier.

Barrier controlled release has been reported in the literature. Frasch-Melnik *et al.* (2010) used fat crystals as Pickering particles to create a barrier which prevented the release of salt from the reservoir. They also showed that melting the fat crystals resulted in the barrier being destroyed which allowed the release of the active.

2.8.1.2 Matrix Systems

In a matrix system, an active agent is dissolved throughout a polymer mass (*i.e.* a gel structure). The release behaviour depends on the type of carrier material, the geometry of the system and the amount of active agent (Pothakamury and Barbosa-Cánovas, 1995). There are three steps involved with release of an active from a matrix system (Himmelsten, 1991);

1. Diffusion of the active of the active to the matrix surface

2. Partition of the active between the matrix and the surrounding environment.

3. Transport away from the matrix surface.

The release of volatiles from matrix (gel) structures were investigated by both Boland *et al (2006)* and Juteau *et al*. (2004). Boland *et al (2006)* showed that the use of pectin lowered the partition coefficient with slowed the release of hydrophobic compounds (methyl anthranilate). Juteau *et al.* (2004) showed the use of a polysaccharide (iota-carrageenan) reduced the amount of ethyl hexanoate released as the mass transfer coefficient and the partition coefficient is reduced.

2.8.2 Release in Application

In recent years, there has been a drive towards understanding the release of food actives during application/use.

Koliandris *et al* (2008) used a texture analyser (with a two compression repeat model) to investigate the effect of structural breakdown on the release of sodium ions trapped in varying gel structures. They showed that the differences in salt concentrations were related to the strain at rupture and to the extent of fracture during compression. Mills *et al.* (2011) took this idea further by using a seven stage compression model (to mimic chewing) to monitor release of salt from gels. Results showed that when structural breakdown occurred (after point of fracture), salt was released from the structure whereas minimal release occurred before fracture (Mills *et al.*, 2011).

Chapter 3. Materials and Methodology

3.1 Introduction

This chapter provides detailed information on the materials used and the methods utilised for sample formation and instrumental analysis. It also includes some theory behind the analytical techniques.

3.2 Materials

3.2.1 Waxes and Emulsifiers

All materials (castor oil, carnauba wax, microcrystalline wax, hard paraffin, performalene, Eutanol G, Butylated Hydroxytoluene BP, Multiwax X145 AH, Ocytl Palmitate, Indopol H-100, Softisan and Parsol MCX) used to produce the continuous phase of emulsions were supplied by Alliance Boots PLC (UK). These were used in combination with double distilled water and various emulsifiers: polyglycerol polyricinoleate (PGPR (HLB 1.5)) (Palsgaard, Denmark), sorbitan olivate (HLB 4.3) (Aston Chemicals, UK), monoolein (HLB 3.6) (Cargill, Spain) or monostearate (HLB 3.2) (Cargill, Spain) to produce emulsions.

3.2.2 Tribometer Surfaces

Two surfaces were used in tribology studies conducted within this thesis: elastomer discs and stainless steel balls. The elastomer discs (4 mm White Silicon Sheet, Samco Silicon Products) were cut from large sheets and used as supplied. The stainless steel balls were ¾ inch diameter AISI 400 stainless steel (PCS Instruments, London).

3.3 Sample Formation

This section discusses the methods used to form the various wax/oil blends, which were then used as the continuous phase when producing an emulsion

3.3.1 Wax/Oil Blends

All wax/oil blends were prepared by first weighing the exact weight percentage of each component and melting until molten (~90 °C) using a hot plate and magnetic stirrer (This took approximately 30 minutes depending on batch size). Once molten wax/oil blends were poured into a variety of moulds (explained in individual analytical method sections later (section 3.4)). Moulds were then cooled quiescently by placing into a freezer for approximately 20 minutes (cooling rate 2.4 ± 0.2 °C/min) to allow for the wax/oil blend to crystallise.

For all studies (unless otherwise stated), that compared wax/oil blends with emulsions, 2 wt % PGPR was added to the wax/oil blend in order to monitor the effect of incorporating water into the microstructure.

3.3.2 Emulsions

Emulsions in this thesis were produced using two techniques; a batch process and a continuous process.

3.3.2.1 Batch Process

A continuous phase formulation containing castor oil (40 - 95 wt %), carnauba wax (0 - 20 wt %), microcrystalline wax (0 – 20 wt %) and paraffin (5 wt %) or performalene (5 wt %) was melted with either PGPR, sorbitan olivate, monoolein or monostearate (0.2 - 5 wt %) and the aqueous phase (distilled water, 10 – 40 wt %) in varying quantities until molten (~90 °C). The pre-mixture was emulsified for 5 minutes using a Silverson L4RT (Silverson Machines Ltd, UK) high shear mixer at ~75 °C,

fitted with a fine emulsifier screen (pores ~1 mm) at ~10,000 rpm. Following emulsification, the emulsion was poured into moulds and cooled quiescently by placing in a freezer for 20 minutes (cooling rate: 2.4 ± 0.2 °C / min) to allow for the continuous phase to crystallise.

3.3.2.2 Continuous Process

Emulsions were prepared using a bench-scale process commonly used in the food industry called a "margarine line" composed by a Scrapped Surface Heat Exchanger (SSHE) and a Pin Stirrer (PS). This unit was chosen as it can both emulsify and can control crystallisation during the process.

The SSHE unit (volume ~40 mL) includes a shaft, onto which two series of seven blades are diametrically attached, rotating in a fixed jacketed envelope (Figure 3.1a). The PS unit (volume ~150 mL) includes a shaft, onto which four series of pins are attached in "cross" shape, rotating in a fixed jacketed envelope (Figure 3.1b).

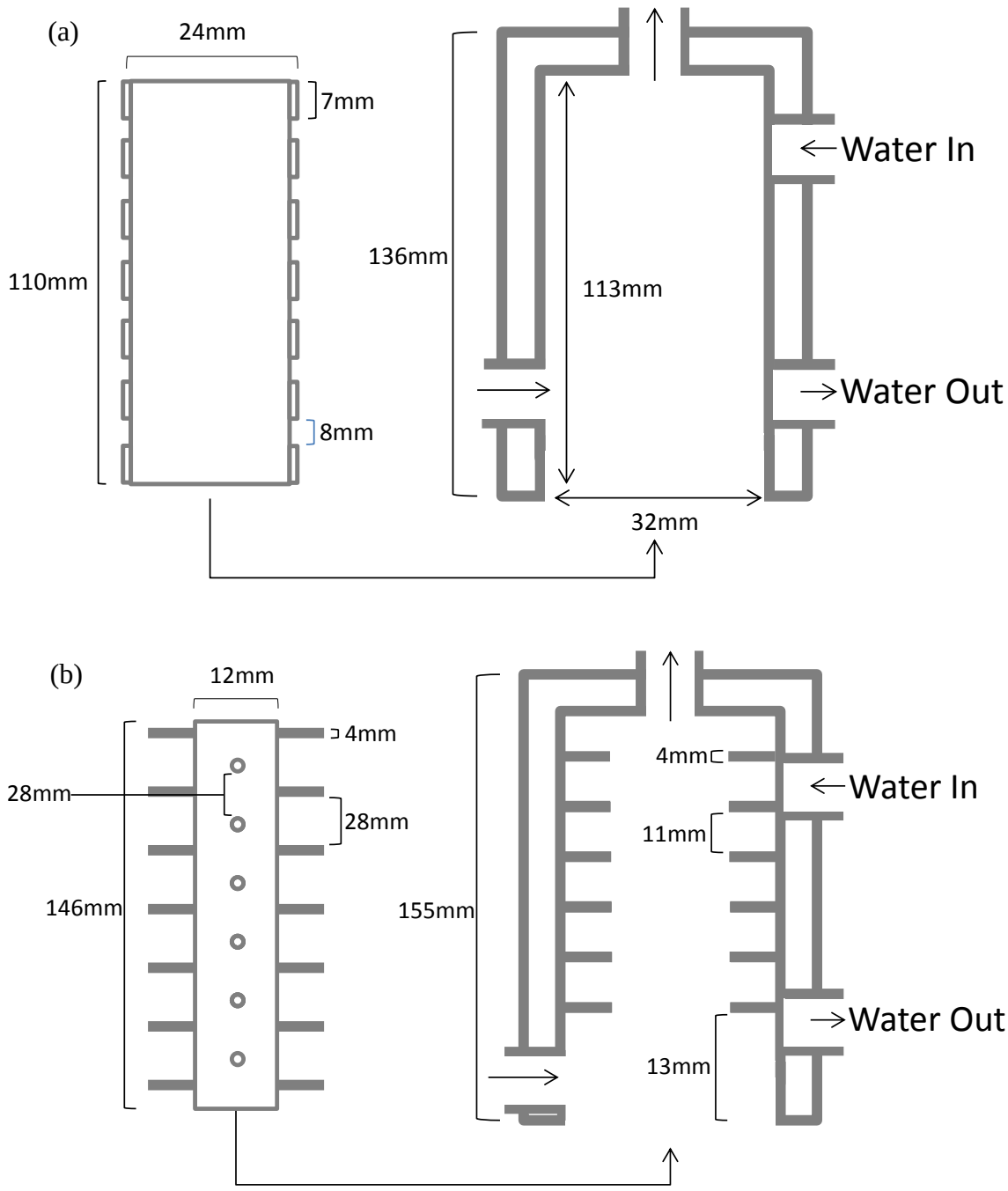

Figure 3.1– Schematic representation of (a) the scraped surface heat exchanger (SSHE) and (b) the pin stirrer (PS). Key dimensions are labeled. This Figure shows the inlets and outlets (represented with arrows) of both the cavity and jacket.

A pre-emulsion was formed at ~ 90 °C using an overhead stirrer fitted with an anchor shaped impeller until homogeneous for 5 min, and then passed through either the SSHE unit only or the SSHE unit combined with the PS unit. The margarine line offers the possibility to adjust 3 different parameters: the flow rate through the unit(s), the unit

jacket temperature and impeller rotational velocity (IV)) of both units. In this thesis, these parameters were varied as follow; 3 flow rates (30, 60 and 90 mL/min), 4 temperatures (55, 60, 65 and 80 °C) and 2 IV for the SSHE unit (500 and 1500 rpm) and 3 IV for the PS unit (500, 1000 and 1500 rpm). A schematic representation of both the SSHE and PS set up is shown in Figure 3.2.

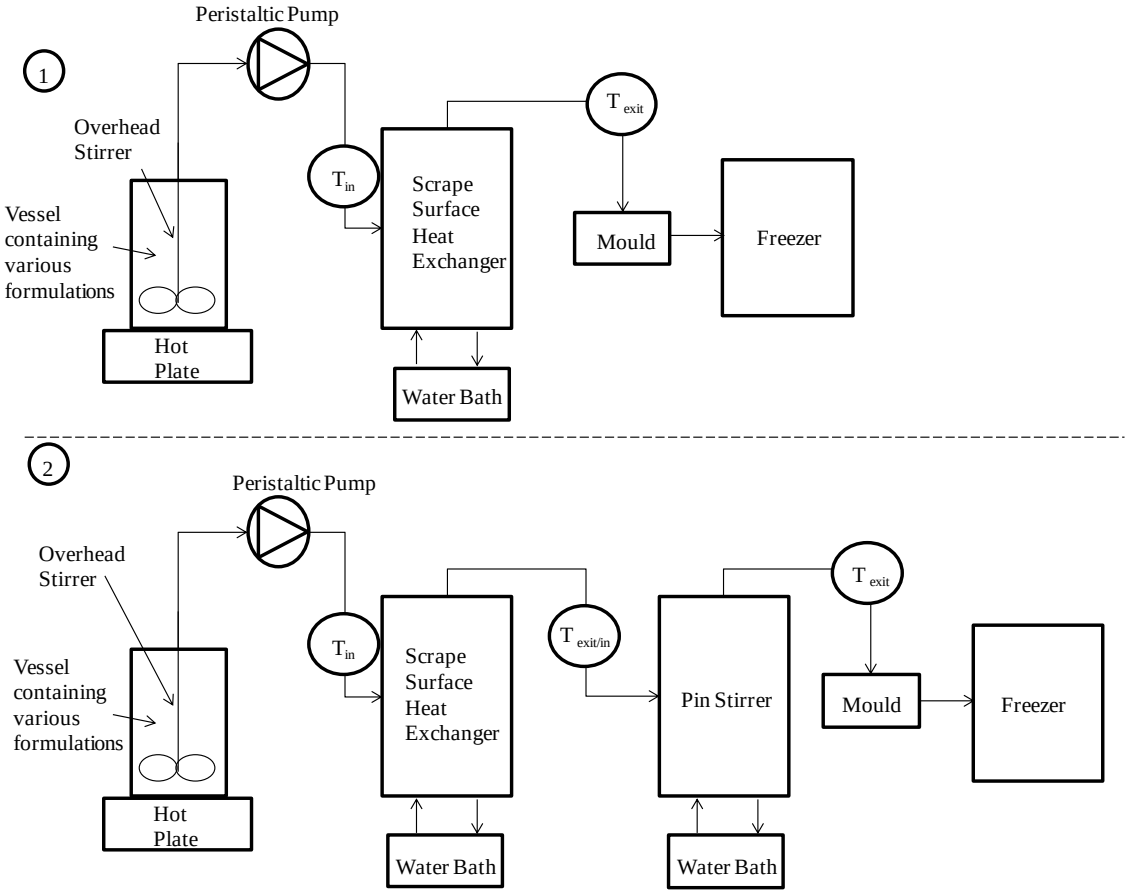

Figure 3.2 – Schematic representation of experimental set-up used for continuous process experiments where (1) is scrape surface heat exchanger (SSHE) and (2) SSHE and pin stirrer.

The chosen temperatures were selected specifically based on the crystallisation of the continuous phase (this will be discussed in Chapter 4). Thermocouples, placed before and after both units, were used to measure the temperature in order to obtain an insight into the crystallisation occurring in the process. It is important to note that for

experiments with set up 1, an additional two temperatures (70 and 75 °C) were investigated as results indicated a trend that required further investigation. Following emulsification, the emulsion was placed in a freezer for 20 minutes (cooling rate: 2.4 ± 0.2 °C / min) to allow for the continuous phase to fully crystallise.

The composition of the continuous phase used throughout the continuous process study was 85 wt % castor oil (CO), 5 wt % carnauba wax (CW) and 10 wt % microcrystalline wax (MW). This composition was chosen as results in this work have shown that this provided a melting profile suitable for lipstick application (discussed later in Chapter 4). Emulsions passed through the SSHE unit only were composed of 88 wt % oil (continuous) phase, 10 wt % water (dispersed phase) and 2 wt % PGPR. For emulsions passed through both units the continuous phase was altered to contain 80 wt % CO, 5 wt % CW, 10% wt MW and 5 wt % paraffin (keeping the amount of water and PGPR the same. The addition of paraffin to the composition strengthens the emulsion (Le Révérend *et al.*, 2011a) which renders the material property analysis possible; attempts were made to characterise material properties of emulsion passed through the whole unit and containing no paraffin, but the formulation was too soft to perform any measurement. Oil phase with added paraffin when required and PGPR was heated up to 90 °C and gently stirred for about 1h. Water was also heated up to 90 °C and added to the oil phase to form the pre-emulsion as mentioned above.

3.3.3 Tribology Set-Up

3.3.3.1 Pin and Disc

A mini traction machine (MTM PCS Instruments, London) was used to investigate the lubricating properties of both waxes and emulsions. The machine consists of a ball loaded onto an elastomer disc. In a pin and disc set up, the ball remains stationary and

the disc rotates. This results in a contact zone between the two surfaces being produced, where the material is assessed.

3.3.3.1.1 Sample Preparation

Waxes and emulsions were moulded in a specific manner, so they could be assessed using a tribological technique. Initially, an elastomer disc was cut out from supplied sheets and cleaned by sonicating in ethanol (5 min) and then water (5 min). Once clean, the elastomer disc was placed into a mould (similar design to the cutter) which had a raised aluminum frame (3 mm). Molten wax or emulsion was then poured into the mould and placed into the freezer for 20 minutes. Once fully crystallised the top of the mould was scraped using a flat stainless steel blade to allow a flat surface to be analysed. Each disc (with 3 mm of material) was analysed once with five repeats of each material. Secondly, a stainless steel ball was cleaned by sonicating in ethanol (5 min) and water (5 min). It is important to note that these were reused following the same cleaning procedure.

3.3.4 Release Experiments (Chapter 7)

Experiments were conducted using two different experimental set ups. For quiescent release, a vessel (Figure 3.3) was used to study the release of glycerol at three different temperatures (20 °C (room temperature), 32 °C (lip temperature) and 80 °C (above melting temperature of continuous phase). For release under compression, a cylindrical vessel (Figure 3.3) was placed on a heated plate (lip temperature), beneath a 40 mm diameter texture analyser (Stable Micro Systems, TA XT2) probe to investigate the effect of cyclic compression (compression every 3 minutes) on release. This method was similar to that shown by Mills *et al* (2011). In both systems, 0.5 ml of solution were taken at regular intervals and analysed via FT-IR to calculate the amount of glycerol

released. An overhead stirrer (25 mm diameter propeller) was used in compression testing.

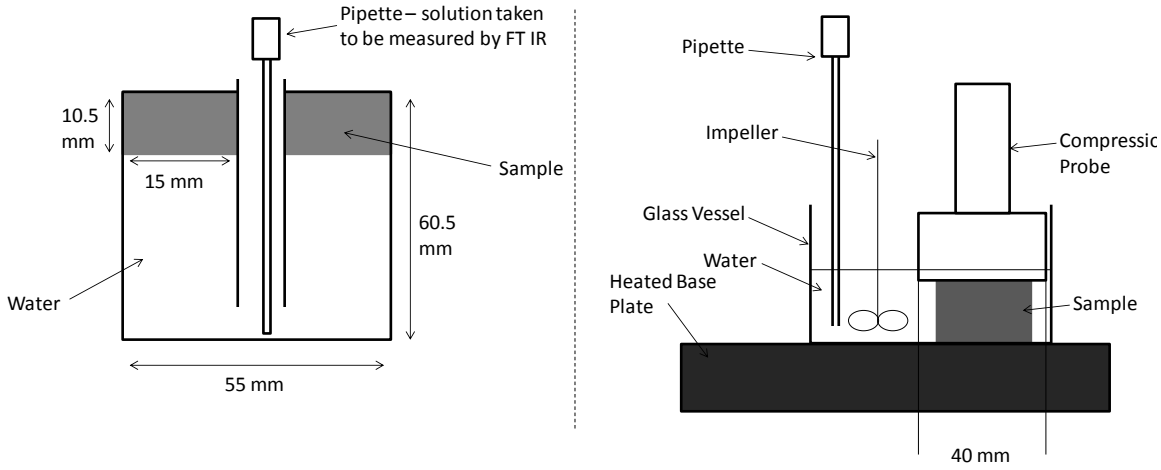

Figure 3.3 – Schematic representation of the two experimental set ups used in this study.

3.3.4.1 Glycerol Release in Quiescent Conditions

Each of the emulsions (30 wt % aq phase (50:50 water:glycerol)), 68 or 69 wt % continuous phase (100 wt % castor oil or 5 wt % and 10 % microcrystalline wax in castor oil or 15 wt % paraffin wax in castor oil and 1 or 2 wt % PGPR) was tested to study the release of glycerol from the emulsion structure to a surrounding volume of water. Samples were initially emulsified using a Silverson high shear mixer (10,000 rpm for 5 min), they were then poured directly onto the volume of water (200 ml) until 30 g was measured. Samples were then placed in an oven and the temperature (20, 32 and 80 °C) was kept constant over a period of up to 12 days. 0.5 ml of the surrounding water solution was then removed with a pipette and analysed using FT-IR. Aliquots were taken at intervals to obtain a release profile for a given temperature.

In order to employ FT-IR spectroscopy as a technique for measuring glycerol release from an emulsion structure, it is important to construct a calibration curve of known glycerol concentrations. Therefore 25 fold dilutions (assuming that a mix of 50 % water and 50 % glycerol represents a 100 % stock solution) were produced by diluting the stock solution. This was done by removing 10 ml of the stock (taken for testing) and adding 10ml of distilled water to the remaining solution, thus allowing a range of dilutions to be produced with a molarity of 7.2 – 326 nM. Each dilution was then measured with an FT-IR between 1400 – 800 cm^{-1}. Figure 3.4 shows the peaks obtained for 0, 24, 48 and 100 % glycerol solutions. From these curves, it is clear that 2 main peaks were observed at ~1110 and 1045 cm^{-1}. This broad peak is indicative of the C-O bond for glycerol (Higson and Amus, 2004). It is important to note that the FT-IR can detect the O-H bond present in glycerol (at ~3350 ± 50 cm^{-1}). However this peak would overlap with the O-H bond in water and therefore were not considered for analysis. Niewoudt *et al* (2004) utilised FT-IR to investigate the release of glycerol from both red and white wine. Their results also detected a peak between 1100 – 1075 cm^{-1}.

The area under these curves was calculated using the trapezium rule (Allison *et al.*, 1995) and related to the percentage of glycerol (Figure 3.5) From Figure 3.5 it is observed that a linear fit which passes through the origin (R^2 of 0.993) is obtained, resulting in the equation;

$$\boldsymbol{A = 0.0083\ G_c} \qquad \textbf{Equation 3.1}$$

Where A is the area under the curve and G_c is the glycerol concentration (wt %).

This equation was then utilised to calculate the amount of glycerol released for each sample that was being assessed.

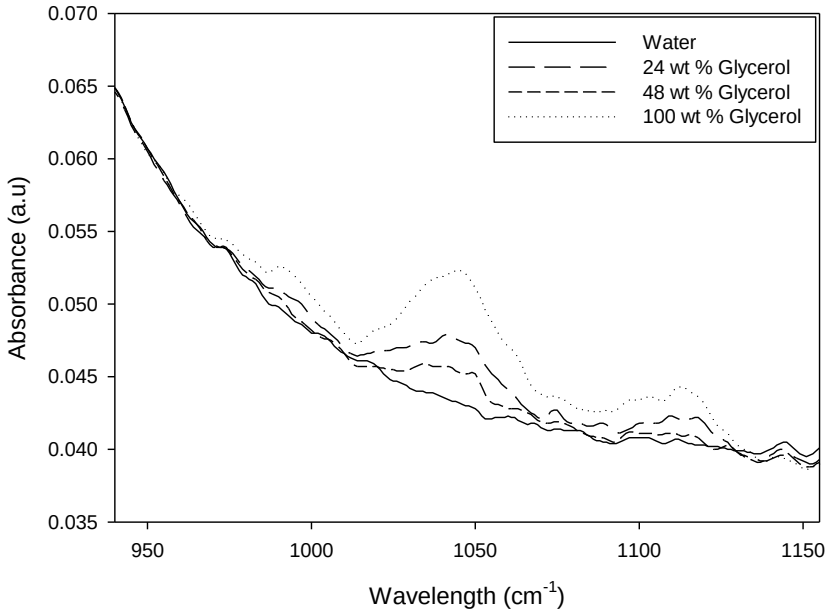

Figure 3.4 - FT-IR spectra (940-1160 cm^{-1}) of varying glycerol concentrations.

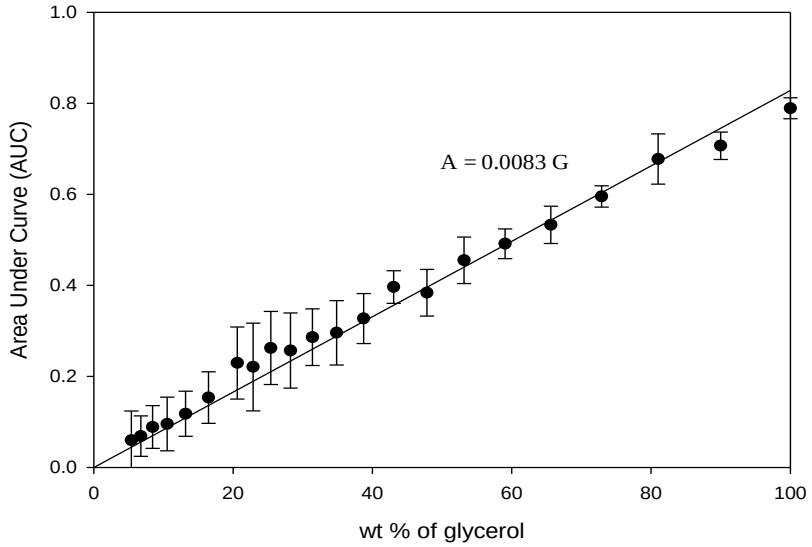

Figure 3.5 - Calibration Curve for all glycerol concentrations

3.3.4.2 Mathematical Modelling

The effective diffusivities of each system were obtained using the diffusion model in COMSOL multiphysics (COMSOL Inc. Burlington), MA, USA), for a comparison to

the experimental data, this followed a modeling technique shown by Mills *et.al.* (2011).The experimental arrangement was drawn in three dimension using the transient diffusion model showing the emulsion sitting on the body of water. The diffusion equation was used to calculate the effective diffusivities.

$$\frac{dc}{dt} + \nabla(-D\nabla c) = 0 \qquad \textbf{Equation 3.2}$$

Where c is the concentration of glycerol, *D* is diffusivity and t is time. The diffusivity of the water was set to 10 m^2s^{-1} assuming instantaneous mixing once glycerol has been released from the emulsion structure. The external boundaries of the water were set to insulate and the temperature was set to 20, 32 and 80 °C. COMSOL was linked to MATLAB (Mathworks, Cambridge) and run to calculate the diffusivities for comparison to the average experimental data for each experiment. To improve the accuracy for the values of diffusivities three iterations were conducted to minimise the sum of squares between the experimental and theoretically predicted data.

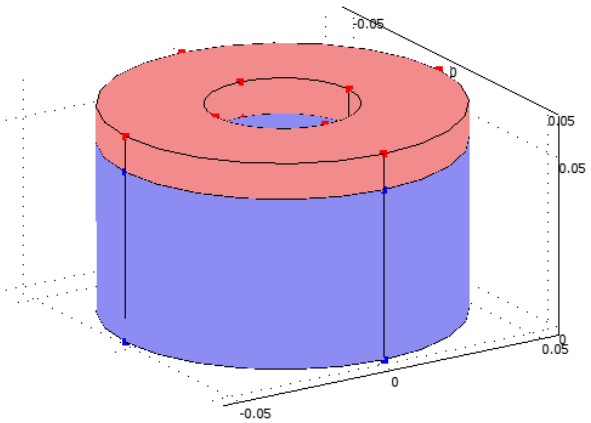

Figure 3.6 – 3D geometry used with COMSOL. Dimensions match those used in experimental work. Sample is located at the top and is equivalent to 30 g. Water (200 ml) is located on the bottom.

3.3.4.3 Glycerol Release Under Uni Axial Compression

The effect of cyclic (every 3 minutes) uniaxial compression on the release of glycerol from an emulsion structure was investigated. Samples were initially compressed in order to determine which strains should be used for testing (Figure 3.7). From this test three different strains were chosen; 7 % (no destruction of sample), 20 % (after the point of fracture of sample) and 90 % (full compression of sample). Samples were held fixed within the testing vessel by lowering the compression arm into contact with the sample. 200 ml of water was then added to the vessel and cyclic compressions (7 compressions in total) were conducted every 3 minutes for a total of 20 minutes (with the first compression occurring at 0 minutes). All measurements were conducted at 32 °C to mimic release at lip temperature.

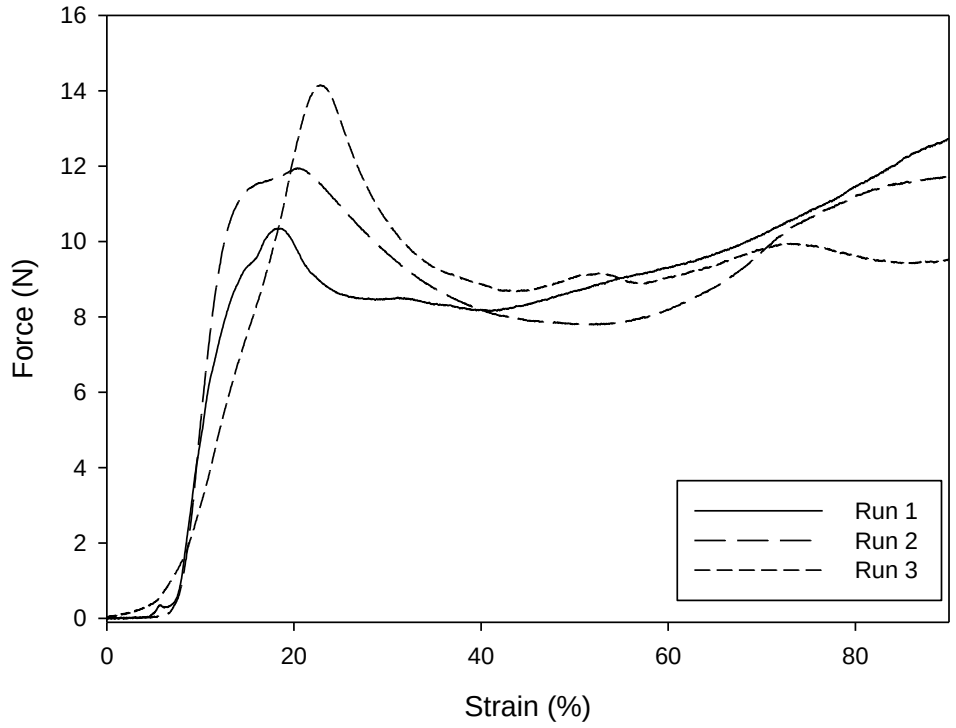

Figure 3.7 – Stress strain curves for an emulsion containing 30 % aqueous phase (50:50 mix of glycerol: water). Tests were performed at a constant rate of 1 mm/s to a strain of 90 %.

3.4 Analytical Method

Throughout this thesis, a variety of different analytical techniques and tools were used. This section outlines the analytical procedures that were followed for each technique.

3.4.1 DSC (Chapter 4)

The melting properties of continuous phase formulations and emulsions were investigated using a Differential Scanning Calorimeter (Perkin Elmer DSC Series 7, UK), equipped with thermal analysis software (Pyris). DSC is a thermo analytical technique which is frequently used to study thermal changes in foods (Fava, 1968, Yildiz and Unluturk, 2009). The principle of power compensation DSC is highlighted in the schematic diagram below (Figure 3.8). The reference pan contains only air whereas the sample pan will contain the sample. The key to this technique is that both pans are kept at the same temperature during an isothermal or temperature ramp experiment (Yildiz and Unluturk, 2009). This can be done at various rates of temperature increase (*e.g.* 5°C per minute or 10°C per minute).

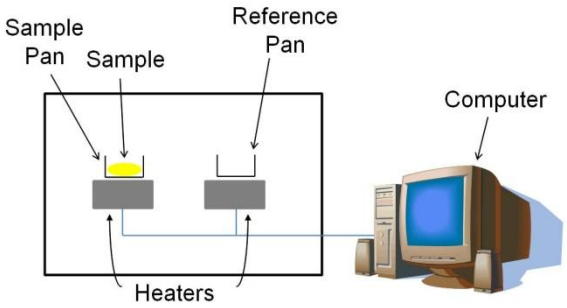

Figure 3.8 - Schematic of Power compensated DSC

The computer controls the temperature of both pans which have individual heaters and keeps the rate of heating constant. More energy is required to heat the sample pan,

therefore the heater heating this pan has to work harder than the heater for the reference pan. The machine then measures how much more heat is required to keep the pans at the same temperature and this is plotted as a graph of heat flow against temperature (Figure 3.9) . Figure 3.9 shows the three different peaks that can be obtained from a DSC measurement. T_g is the glass transition temperature, this only occurs with polymers and is not applicable for this thesis. T_c is the crystallisation temperature; this is the temperature at which the molecules in the sample start to arrange and phase transition occurs from a liquid to a solid. This releases heat, as a result the heater which heats the pan no longer has to, and therefore a dip in curve is observed (the T_c is the temperature at the lowest part of the peak). From this curve we can determine the latent heat of crystallisation which is the energy required to accomplish a phase change from a liquid to a solid at a constant temperature. This can be calculated from the following equation;

$$\boldsymbol{Q = \Delta H_C\, M} \qquad \textbf{Equation 3.3}$$

Where, Q – heat energy transferred (J), M – mass (g) and ΔH_C – latent heat of crystallisation (J g^{-1})

Once the crystallisation temperature is known it can help improve the procedure of making certain emulsions, as the crystallisation of the waxes is crucial to the microstructure of the product.

The rate of crystallisation is also important as it has been found that the rate can be related to the size of crystals formed. As wax crystals stabilise the W/O interface, the smaller the crystals, result in a higher proportion of interface being stabilised which is essential for emulsions.

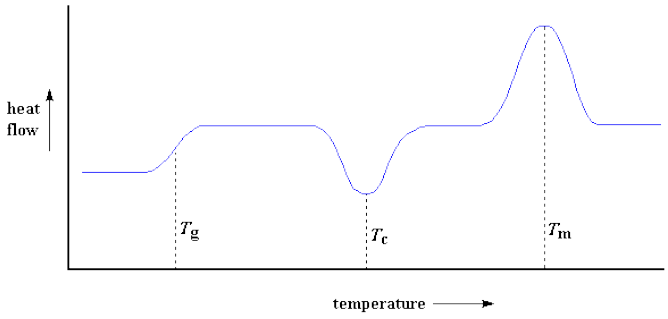

Figure 3.9 - Graph of Heat Flow Vs Temperature (where Tg - glass transition temperatue, Tc - crystillisation temperature and Tm - melting temperature)

The melting temperature (T_m) is the temperature at which most of the molecules in the sample melt resulting in a phase transition from solid to a liquid. This is the opposite to crystallisation, therefore the sample absorbs heat, which means the heater has to heat the sample pan to keep it at the same temperature as the reference pan, hence a peak is observed (Figure 3.9).

By using the equation previously mentioned the latent heat of melting can be calculated, which is the energy required for a phase transition from solid state to liquid state.

In reality the melting of the sample starts at the start of the peak (T_{onset}) and ends at the end of the peak (T_{end}). This temperature range is crucial for the product as it is critical for the products performance. This is due to the fact that the consumer requires the product to be solid at room temperature and for it to be able to spread when it comes into contact with the lips (~32°C).

Throughout this thesis the instrument was calibrated for temperature using indium and tin, with an empty aluminum pan as a reference. Samples were loaded into 50 µL

capacity aluminum pans, and sealed with aluminum covers. Pans were heated at a rate of 10 °C/min, from a range of 10 ° C to 120 ° C.

The expected melting enthalpies of continuous phase formulations were calculated from pure samples of both carnauba wax (Figure 3.10a) and microcrystalline wax (Figure 3.10b). For example, for a formulation containing 5 wt % carnauba wax (in castor oil) the expected melting enthalpy wax calculated as 5 % of the melting enthalpy for a 100 % pure carnauba wax sample.

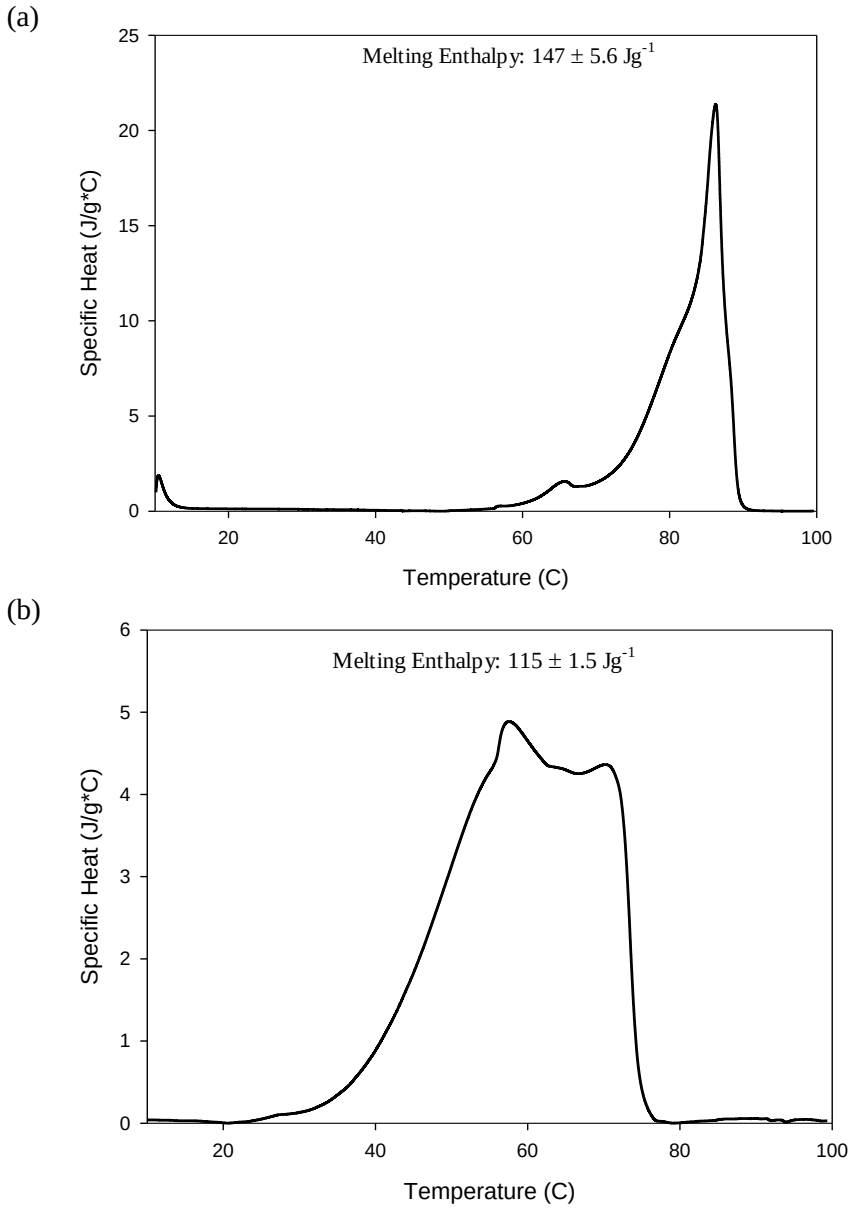

Figure 3.10 – Melting Profile curve for (a) 100 wt % carnauba wax and (b) 100 wt % microcrystalline wax. The samples were heated at a rate of 10 °C/min.

3.4.2 NMR (Chapter 4, 5, 6 and 7)

Droplet size measurements were performed using a pulsed field gradient NMR equipped with a water droplet size application (restricted diffusion) (Minispec mq series, Bruker Optics, UK) at ~5 ℃ in order to measure the volume-weighted mean droplet diameter ($d_{3,3}$).

The use of NMR for droplet size determination in W/O emulsions has been well documented by both Brucker (2001) and van Duynhoven *et al*. (2002a). It should be noted that, not only is this technique fast and non destructive, but it can be used to give micro structural parameters which can be linked to shelf life and mouth feel (Bruker, 2001, van Duynhoven *et al.*, 2002b, van Duynhoven *et al.*, 2002a). The theory behind NMR measurements will now be discussed.

3.4.2.1 Theory of NMR measurements

The movement of protons within a sample is measured using a low field NMR. Initially a magnetic field is applied. Once applied the protons align with the magnetic field, rotating around an axis parallel to the field lines, and showing a net magnetisation which is in the direction of the magnetic field (along the z-axis). This is known as vector M.

Different radio frequencies (90° and 180° pulses) are applied to the rotating frame. At a 90° pulse along the x' axis, vector M rotates 90° clockwise in the y'z' plane, resulting in vector M pointing in the y' direction (open position) (Figure 3.11). At a 180 pulse, vector M rotates 180 resulting in vector M pointing in the z' direction (close position) (Figure 3.11) (Bruker, 2001).

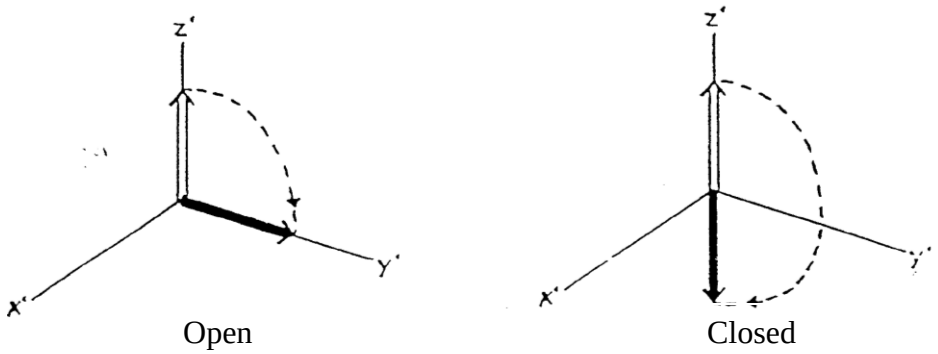

Figure 3.11 – Examples of effect of radio frequencies pulses on rotating frame in the direction of vector M where (a) open position after a 90° pulse and (b) closed position after a 180° pulse (Image taken from Bruker Minispec mq Droplet size manual).

When different radio frequencies are applied in a specific order it is known as the Hahn spin echo sequence. This is the sequence used to monitor the movement of protons. The sequence consists of switching between the open and close states of vector M after a given time, τ. As a sample contains many protons and vector M is composed of many magnetic moments each of which have different velocities. After the 90° pulse the protons move at different velocities and 'fan out' (Figure 3.12a and Figure 3.12b). Once the 180° pulse is applied the magnetic moments are transposed through the y axis (Figure 3.12c). The movement of protons is now reversed and the 'fan' is closed (Figure 3.12d). At time 2 τ, the signal is refocused as a single vector M, resulting in a sharp echo-signal being received on the oscilloscope. After 2 τ the fanning out begins again, and the signal height decreases (Bruker, 2001).

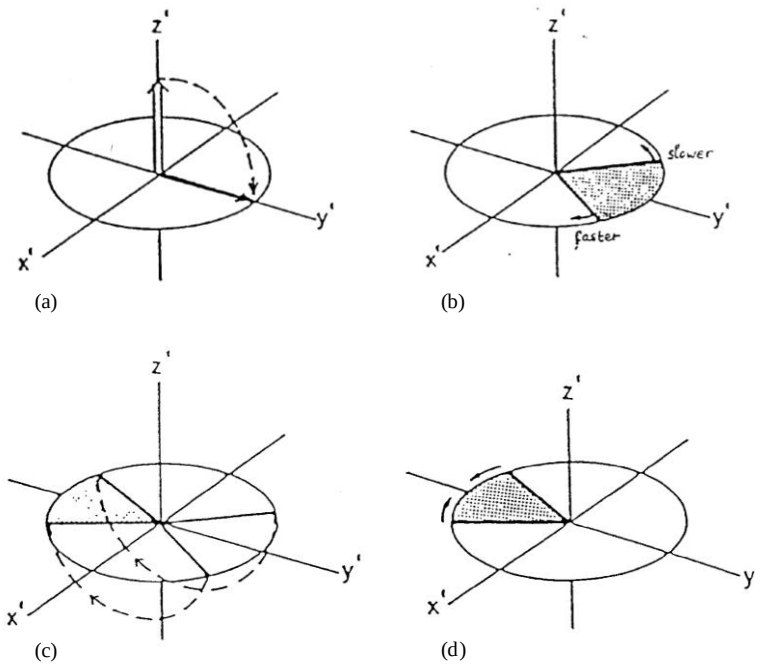

Figure 3.12 – Schematic of the movement of protons after Hahn spin echo sequence is applied where (a) is a 90 pulse (b) protons start to fan out after a magnetic field is applied (c) all signals rotate 180° after a 180° pulse and (d) the protons refocus and the fan closes (Image taken from Bruker Minispec mq Droplet size manual).

.

Field gradient pulses are then applied for short times in conjunction with the Hahn Spin-Echo sequence (Figure 3.13). This is done to measure the diffusion of protons within a sample. Diffusion coefficients are determined by applying field gradient pulses which move vector M within the xy plane over a specific angle. When a pulse (90°) is applied the fanning out of Vector M begins, after which a field gradient pulse is applied resulting in any particular magnetic moment experiencing a different field gradient strength. This causes that particular magnetic moment to be displaced at different angles. Then a 180° pulse is applied with the second field gradient pulse. If there was no diffusion the 'fan' would close and the same signal will be given, however as there is diffusion of the protons which are displaced from different locations within the xy plane, resulting in a loss of signal and small signal (known as an attenuated echo) to become present at 2τ (Bruker, 2001).

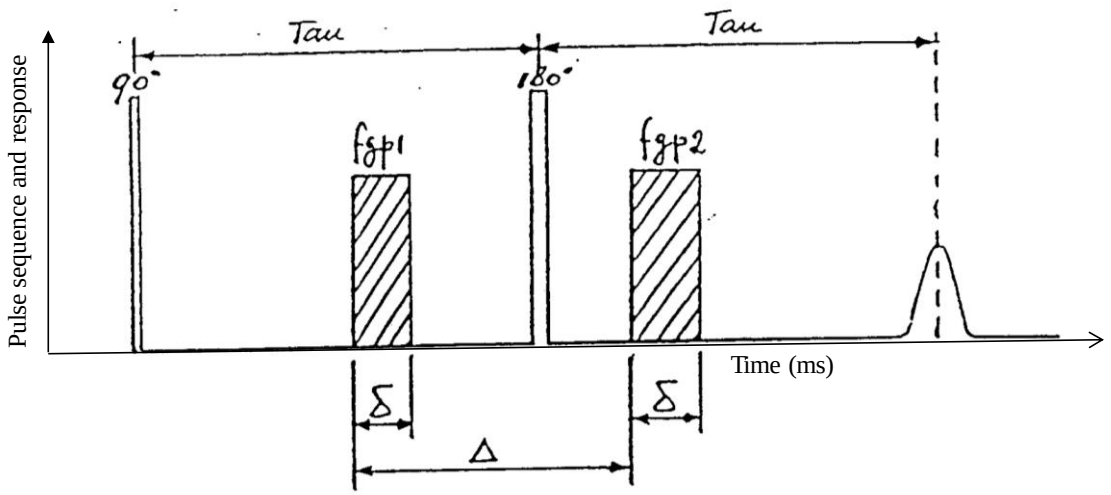

Figure 3.13 – Hahn Spin Echo sequence with field gradient pulses (adapted from Bruker Minispec mq Droplet size manual).

The 'R-Value' can be obtained from the relationship between echo attenuation (M_g) with the peak obtained without the application of field gradient pulse (M_o) in the form of a ratio; M_g / M_o. In a system where there is unrestricted diffusion of the protons (Figure 3.14a), the diffusion rate can be calculated by plotting a graph of R value vs the length of time between the two starting points of field gradient pulses Δ. The slope of this line provides details about the rate of diffusion. The greater the gradient, the higher the rate of diffusion. However when analysing W/O emulsions, the movement of the water protons behave in a restricted regime. The regime is restricted as the protons will be able to move but only within the limits of the droplet. This limit can be seen in Figure 3.14b as Δ is increased the R value becomes constant (Bruker, 2001).

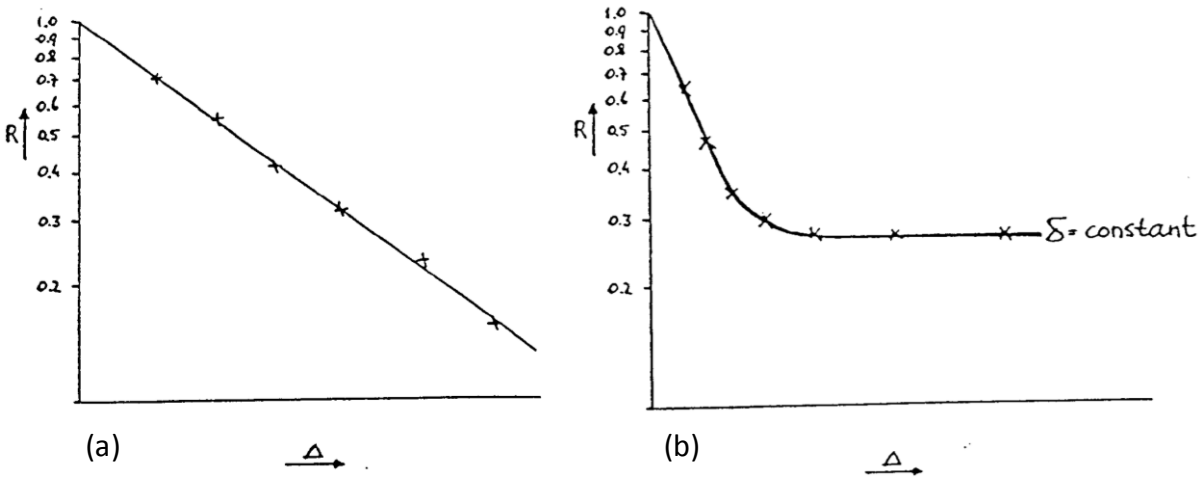

Figure 3.14 – Graph of R (M_g/M_o) Vs time between field gradient pulses (Δ) for (a) unrestricted and (b) restricted diffusion (Image taken from Bruker Minispec mq Droplet size manual).

In order to determine the droplet size distribution a series of measurements are carried out. First an experiment is carried out where δ (the length of time for each field gradient pulse) is fixed and Δ is varied followed by fixing Δ and varying δ. Packer and Rees utilised these experiments in 1971 to give information for an emulsion sample (Packer and Rees, 1971). The Hahn spin echo experiment is slightly varied when working out droplet size distribution as the time of measurement (Δ) required to gain a signal is too long. Therefore the second field gradient pulse is split into two 90° pulses (Bruker, 2001).

One of the major issues when analysing W/O emulsions is that there are also protons within the oil phase. Therefore it is crucial to nullify the magnetisation of the protons within the oil phase after the first 90° pulse. The two different types of protons (oil and water) have different relaxation times, the oil protons relaxes at a quicker rate and therefore if a 180° pulse is used before the modified Hahn Spin-Echo sequence (Figure 3.15 (van Duynhoven *et al.*, 2007)) the oil proton magnetisation is 0 and only

the water protons have magnetisation, which results in the oil proton signal being repressed (Van Den Enden *et al.*, 1990, Goudappel *et al.*, 2001, van Duynhoven *et al.*, 2002a) (Bruker, 2001).

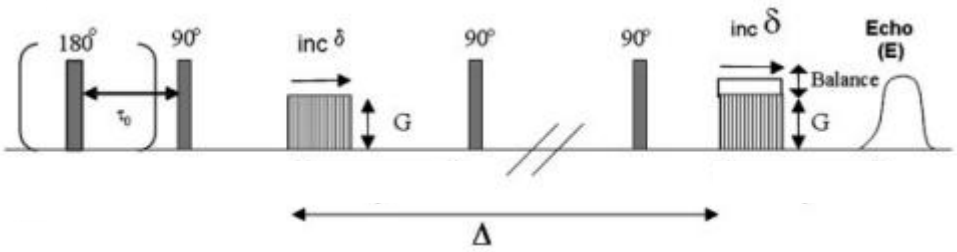

Figure 3.15 – Schematic of a modified Hahn spin echo sequence for measuring W/O emulsions. Where the 180 pulse- τo sequence (prevents the oil proton signal being received), G - Gradient strength, δ – gradient duration, Δ - time between gradient pulses and E –the echo (otherwise known as M_g) (Image modified from Van Duynhoven et Al., 2007)

Before using the acquired data to calculate the droplet size a couple of assumptions need to be made. Firstly, that the droplets within the emulsion are spherical (Hindmarsh *et al.*, 2005) and secondly, that the distribution is log normal (Bruker, 2001).

The Bruker Minispec then generates values of volume weighted mean droplet diameter ($d_{3,3}$) and the standard deviation of the logarithm of the droplet diameter (σ). $d_{3,3}$ represents the midpoint of the frequency distribution of droplet sizes.

Overall NMR is a valuable tool for predicting droplet size, however there is one flaw. This is that all data is fitted to a log normal shape curve. This can be an issue if a W/O emulsion has a bimodal distribution. Therefore the NMR generates a number (known as 'free water') for any proportion of water droplets greater than 100 μm in

diameter. The free water is not included in the droplet size calculation but is recorded separately as a percentage of the total water content.

Throughout this thesis samples were poured into 10 mm NMR tubes and filled to a height of 10 mm. Samples were then placed into a freezer for 20 minutes. All samples were stored at room temperature prior to analysis. All NMR analysis was conducted either on day 0, 1, 7, 10 and 180 after manufacture (where day 0 is day of manufacture).

The mean droplet size ($d_{3,2}$) was then calculated using Equation 1.2 (van Duynhoven *et al.*, 2002a):

$$\boldsymbol{d_{3,2} = d_{3,3} \times e^{-0.5\sigma^2}} \qquad \textbf{Equation 3.4}$$

where, $d_{3,2}$ is the surface-weighted mean droplet diameter, $d_{3,3}$ is the volume-weighted mean droplet diameter, and σ is the standard deviation of the logarithm of the droplet diameter.

3.4.3 Interfacial Tension (Chapter 4)

Interfacial tension measurements of emulsifiers (in castor oil) were carried out in order to assess their surface active properties. Emulsifiers (PGPR, monoolein, monostearate and Sorbitan olivate were prepared at the concentrations used for emulsification (2 wt %).

The interfacial tension between castor oil (containing 2 wt % of emulsifiers) and water was assessed using Kruss K100 tensiometer. Measurements were conducted using a Wilhelmy plate (standard plate – platinium, width – 19.9 mm, height - 10 mm and a depth - 0.2 mm) method. Sample vessel (diameter 70 mm, capacity of 121.5 ml) was used for all measurements, with ~45 ml of castor oil (2% emulsifier) and 25 ml of

double distilled water. Measurements were taken over 2,000 seconds with a surface detection speed of 15 mm/min. Measurements were performed in triplicate.

3.4.4 Microscopy (Chapter 4, 5 and 6)

Cyro-scanning electron microscopy (SEM) and polarised microscopy were used in this research to visualise the microstructure.

3.4.4.1 SEM

Electron microscopes (EMs) are valuable tools in determining the microstructure of products in the range of nanometers (nm) to micrometers (μm). EMs were invented to overcome the magnification limitations of light microscopy, thus allowing 10,000 x magnification of microstructures (Bettina Voutou and Stefanaki, 2008). The first EMs was reported by Marton in 1934 who utilised the technology to view biological images (Heidenreich, 1964). EMs operate in a similar manner to light microscopy, however instead of using light for imaging, a highly focused beam of electrons is used. SEM is conducted under high vacuum which can cause an issue for samples containing water. However this issue can be overcome by using cryo SEM. In this technique a sample is frozen cryogenically by submersing the sample in liquid nitrogen. The internal structure of the sample is then revealed by fracturing the frozen sample. The sample is then etched, by increasing the temperature to ~95 °C which causes the surface ice that has been formed to disappear revealing a stronger image.

Freeze fracture cryo SEM has been used to image a variety of different emulsions which contain a water content (Ge *et al.*, 2006, Norton *et al.*, 2009, Frasch-Melnik *et al.*, 2010, Wang *et al.*, 2012). Ge *et al*.(2006) utilised cryo SEM to investigate the fracture behaviour of colloidal polymer particles in fast frozen suspensions. Figure 3.16 gives an example of an image that was obtained.

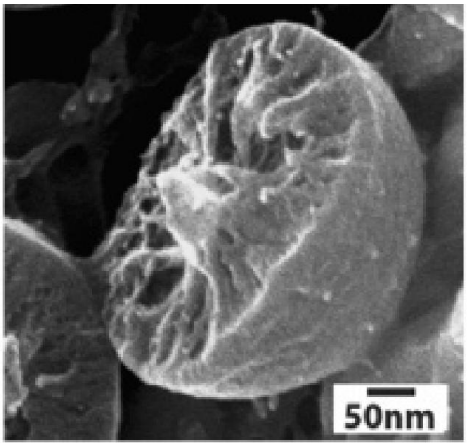

Figure 3.16 – Cryo SEM image of an acrylic latex particle (taken from Ge et al., 2006)

Throughout this research a XL-30ESEM (Philips, the Netherlands) SEM was used for analysis. The structure of the sample was preserved using cryogenic temperatures (below -150 ° C). The sample was attached onto a sample holder and rapidly frozen by immersion into a liquid nitrogen bath for approximately 2 minutes. The sample was then transferred to the high vacuum cryo-unit chamber and freeze-fractured. A thin layer of platinum was sputtered onto the surface. The sample was then moved into the observation chamber, and observations were carried out at 3 - 5 kV at temperature between -100 and -180 °C.

In samples examined in Chapter 7, a variety of etching times (0 – 15 min) were used to examine the effect of waxes at the interface. In the etching process, samples were heated from – 180 °C to – 85 °C following immersion into liquid nitrogen. Samples were then transferred to the high vacuum and followed the previous procedure.

3.4.4.2 Polarised Microscopy

Polarised Micrographs were obtained with a Brunel SP300F digital camera (Canon 1000D, Bruneleus Microscopes Ltd., UK) fitted with an optical light microscope (Brunel Microscopes Ltd., Wiltshire, UK).

3.4.5 Gravimetric Analysis (Chapter 4)

Gravimetric analysis was carried out using a standard bench top balance (Denver Instruments, Model: SI-234, UK). Samples were molded into bullets using a standard lipstick mould (supplied by Alliance Boots) and placed into three different storage conditions 20 ℃ (Room temperature to mimic storage conditions), 30 ℃ (to mimic lip temperature) and cyclic conditions (-10 – 40 ℃ every 4 hours to test how robust the product was) in order to investigate water loss over a products life cycle. The weight of each sample was recorded on day 0, 1 month and 3 months. All tests were performed in triplicate. Each sample was weighed without the holder lid in order to allow any moisture that has been released during storage to be accounted for.

3.4.6 Texture Analysis (Chapter 5, 7)

Texture analysis is a destructive technique that measures the mechanical properties of a given material. The technique monitors a force over time as the material is deformed. As a result a variety of parameters can be determined which gives an insight into how a material will behave. To obtain this force a variety of different tests (which utilise different geometries) can be used. These include penetration depth, 3 point bend and compression testing (Schematics shown in Figure 3.17).

- Penetration depth testing involves using a needle to penetrate the material until a given force is observed (Figure 3.17a). The distance penetrated then gives an indication into how hard a material behaves. For example the harder

the material the less distance the needle will travel and vice versa for a softer material.

- The 3 point bend test has 3 points of contacts with the material being tested. A load is then placed in the centre of the material and moved downwards (Figure 3.17b). This can measure a variety of parameters.
- In compression testing the material is compressed at a specific rate (Figure 3.17c), allowing analysis of a variety of parameters. Initially the material will fracture under load and then spread.

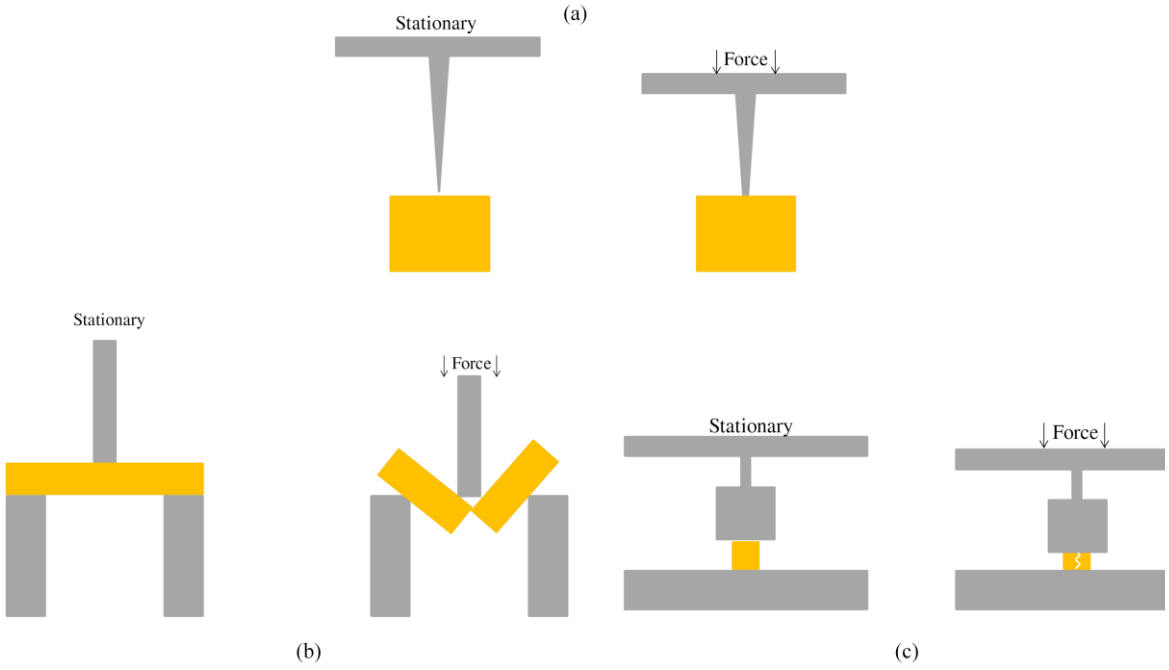

Figure 3.17 – Schematic representation of (a) penetration depth, (b) 3 point bend test and (c) compression testing.

Throughout this thesis the mechanical properties of both continuous phase formulations and emulsions were determined by compression. This was conducted using a TaXT+ (Stable Microsystems, UK) texture analyser. Compression testing was chosen as it is a quantitative method that could be comparable to a qualitative technique currently used in Alliance Boots. Currently Alliance Boots use a trained expert to compress a lipstick between thumb and forefinger in order to determine a relative strength.

The measurements in this thesis involved using a standard compression plate (SMS P/40) with a 40 mm diameter cylindrical aluminum probe. All samples had a diameter of 20 mm and their length was kept at ~20 mm. All measurements were carried out in quadruplet with a compression speed of 1 mms^{-1}.

The data (force/distance) obtained from the texture analyser was converted into true stress and true strain using Equations 3.5, 3.6, 3.7 and 3.8 (obtained from Moresi & Bruno, 2007 (Moresi and Bruno, 2007));

$$\boldsymbol{\varepsilon_E = \frac{H_o - h}{H_o}} \qquad \textbf{Equation 3.5}$$

$$\boldsymbol{\varepsilon_H = \ln(1 + \varepsilon_E)} \qquad \textbf{Equation 3.6}$$

$$\boldsymbol{\sigma_E = \frac{F}{A_o}} \qquad \textbf{Equation 3.7}$$

$$\boldsymbol{\sigma_H = \sigma_E (1 + \varepsilon_H)} \qquad \textbf{Equation 3.8}$$

where, ε_E and ε_H are the engineering and true strain respectively, H_o and h are initial height and height of each sample as recorded during the compression test, σ_E and σ_H are

the engineering and true stress respectively, and F and A_o are compression force applied and initial cross sectional area of sample respectively.

From the true stress/true strain curves (typical curves shown in Figure 3.18) the Young's modulus (as shown by Norton *et al.,* 2011) was taken (the slope of the first linear region of the stress-strain curve) and plotted against either percentage of wax or percentage of water to give an insight into the material properties of the formulations.

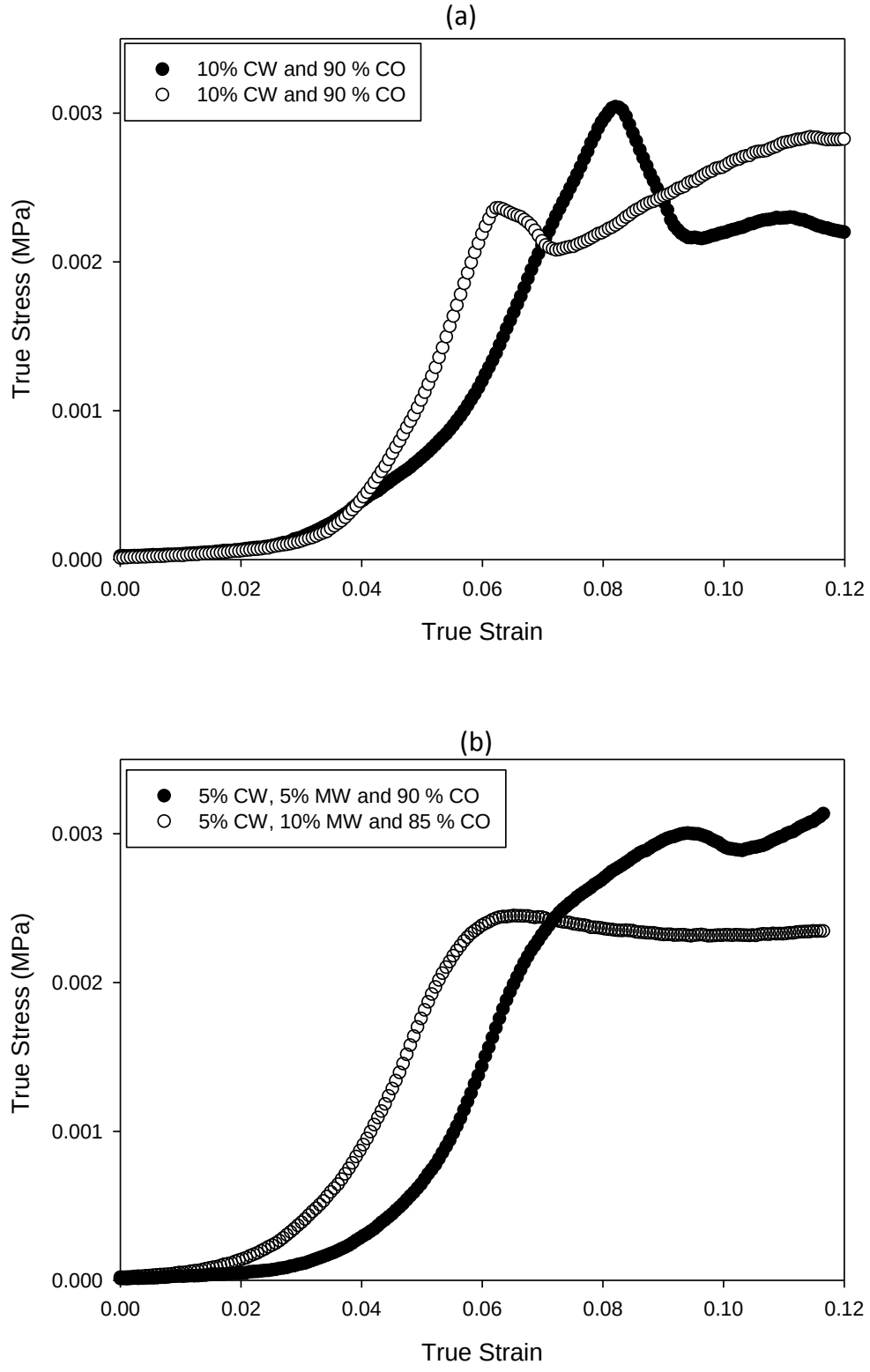

Figure 3.18 - Typical True Stress (MPa) vs True strain curves for bulk oil formulations, where (a) is 10 % carnauba wax (CW) in castor oil (CO), for measurement 1 (●) and measurement 2 (○), and (b) is 5 % microcrystalline wax (MW) and 5 % CW was in CO (●) and 10 % MW and 5 % CW was in CO (○). All samples were melted and stirred using a magnetic stirrer until molten (~ 30-40 minutes) and then

cooled quiescently in the freezer till solid then measured at a compression rate of 1 mm/s at 32 °C.

3.4.7 Rheology (Chapter 5 and 6)

Throughout this thesis a variety of different rheological techniques were utilised. This section provides the methodology for all of the different techniques used.

3.4.7.1 Oscillation Rheology

The elastic modulus (G') and viscous modulus (G") can be determined using a variety of geometries, each of which have different advantages and disadvantages and will be discussed individually.

3.4.7.1.1 Cone and Plate

The cone and plate geometry (Figure 3.19) can be an ideal measuring system as it is very clean and requires only a small amount of material. More often than not the cones are truncated and are positioned so that the missing tip would have touched the lower plate. By removing the tip, a more robust geometry is formed (Bohlin-Instruments, 1994).

Adams and Lodge (1964) showed that by increasing the cone angle the variation in shear rate across the gap increased. This variation is one of the disadvantages of using the cone and plate method.

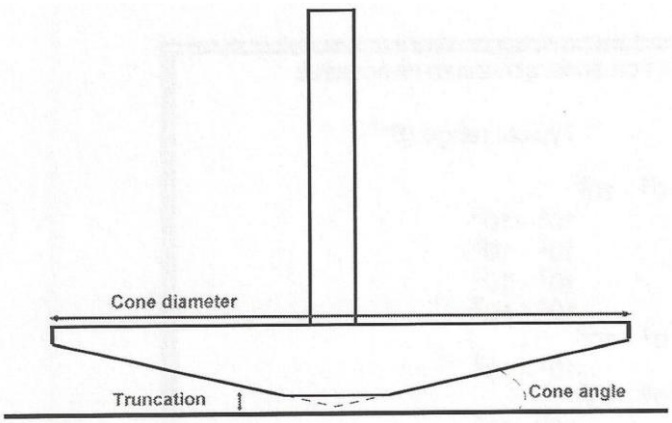

Figure 3.19 – Schematic of cone and plate geometry (taken from Bohlin-Instruments , 1994)

The use of cone and plate is not ideal when running temperature sweeps as it is not possible to guarantees accurate heat transfer due to the gap. Also the cone and plate is an inadequate technique when analysing material that contains particles. As if the particles are not 5-10 times smaller than the gap the particles can jam at the cone apex. Finally if the material contains a high amount of solid material; there can be an issue at high shear rates as the material can be expelled from the gap.

3.4.7.1.2 Parallel Plate

The parallel geometry (Figure 3.20) is also easy to clean and only requires a small amount of material. This geometry is not as sensitive to gap setting which makes it the ideal geometry for use in experiments involving temperature gradients. Like all geometries parallel plates also have disadvantages. The main disadvantage is that the shear rate produced varies across the material being tested, as a result the software on a rheometer uses an average value for the shear rate.

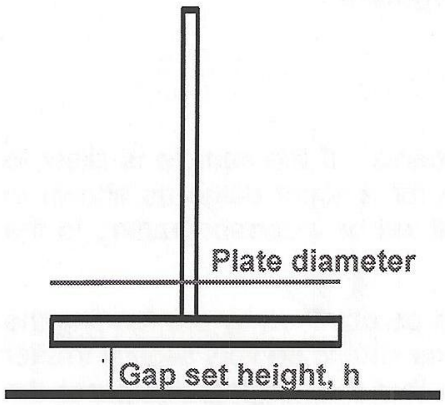

Figure 3.20 – Schematic of parallel plate geometry (taken from Bohlin-Instruments , 1994)

3.4.7.1.3 Cup and Bob

There are a variety of different cup and bob geometries (Figure 3.21). For all types a large volume of material is required and it harder to clean cup and bob geometries. Due to the high volume of material, issues can arise when performing high frequency experiments as the material will exhibit large inertia. The advantage of cup and bob geometries arises when working with low viscosity materials. The large surface area improves sensitivity allowing data to be obtained at low shear rates and viscosities.

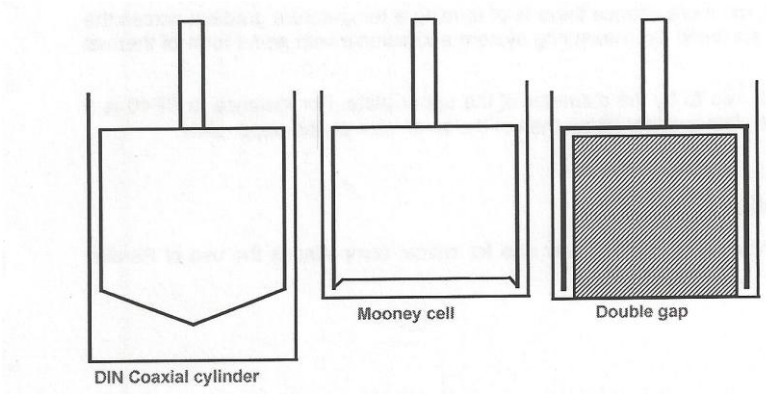

Figure 3.21 – Schematic of cup and bob geometries (taken from Bohlin-Instruments , 1994)

Pal (2000) utilised both parallel plates and cone and plate geometry to investigate the effect of oscillatory rheology on O/W emulsions. Results showed that at high shear stresses, the viscosities measured for both geometries were in agreement, whereas, with low shear stresses, the cone and plate geometry measured lower viscosities than when a parallel plate. This is believed to be due to slippage at the fluid/wall interface.

Throughout this thesis in order to investigate the effect of waxes on the viscoelastic properties of an emulsion, G' and G" were measured using a Bohlin Gemini Nano Rheometer (Malvern, UK), and a 20 mm parallel plate (1 mm gap width) geometry. This geometry was chosen as it is the exact diameter of the mould used, thus allowing thin slices of sample to be used which limits the amount of destruction caused to the wax network during loading.

Initially an amplitude sweep experiment was conducted to calculate the appropriate stress to use for a frequency sweep experiment. This allows the rheological properties of the sample to be measured without destroying the microstructure. For amplitude sweep experiments, the stress was varied (0.1 – 1000 Pa) with a frequency of 1 Hz. A typical example of this was shown previously in Figure 2.15. A stress was then chosen that lies within the linear viscoelastic region, which was then used in the frequency sweep (0.1 – 100 Hz) experiment. Figure 3.22 shows a typical frequency sweep curve. G' and G'' values were taken at a frequency of 5 Hz and plotted against varying parameters for analysis. All experiments were run at 32 °C (lip temperature). All samples were prepared immediately after production by pouring molten solutions into cylindrical moulds (24 mm diameter and 75 mm length) and cooled in a freezer for 20 minutes. Thin slices (~1mm in thickness and 20 mm in diameter) were placed in a parallel plate geometry for testing.

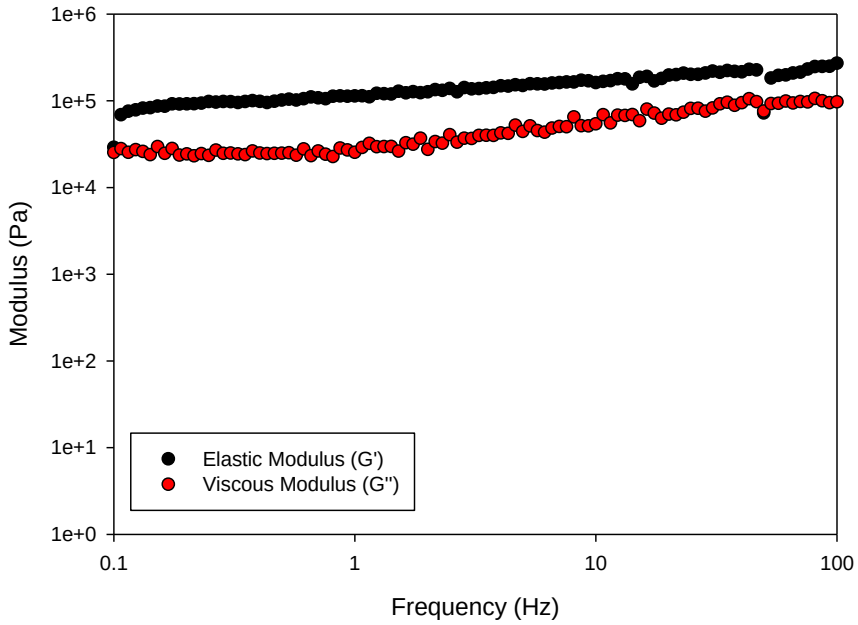

Figure 3.22 – Typical frequency sweep (0.1 – 100 Hz) curve at a controlled stress (within the linear viscoelastic region).

3.4.7.2 Viscosity Measurements

As part of this research, two different viscosity measurements were conducted in chapter 4 and 5.

3.4.7.2.1 Chapter 4

In this chapter the viscosity of the continuous phase was investigated as a function of temperature (50 to 85 °C) in order to determine the effect of wax crystals on viscosity. Effective viscosity was measured using a Bohlin Gemini Nano Rheometer (Malvern, UK), and a 40 mm cone & plate geometry (0.15 mm gap width). All measurements were conducted in triplicate.

3.4.7.2.2 Chapter 5

In this chapter the viscosity of the dispersed phase was calculated at 32 °C. The dispersed phase viscosity was altered by adding varying amounts of glycerol (0, 20, 30,

40 and 50 wt % of glycerol in distilled water). The effective viscosity was then measured using Bohlin Gemini Nano Rheometer (Malvern, UK), and a 40 mm acrylic cone & plate geometry (0.15 mm gap width). All measurements were conducted in triplicate.

3.4.8 Tribometer (Chapter 6)

A mini traction machine was set up following the procedure shown in section 3.3.3 (Figure 3.23). Timed tribological experiments were conducted (30 minutes to 8 hours depending on the time taken to wear a sample to a thin film) at varying loads (0.3, 0.5, 1 and 3N) with one of six disk speeds (1, 3, 5, 10, 30 and 50 mms^{-1}). At the start of test the ball is loaded against the sample, at a defined normal load (*W*). The ball remained stationary and the disk rotates whilst the frictional force is measured (in the contact) by force transducers. The machine also measures the height of the ball in relation to the elastomer disk thus allowing the wear to be calculated over time.

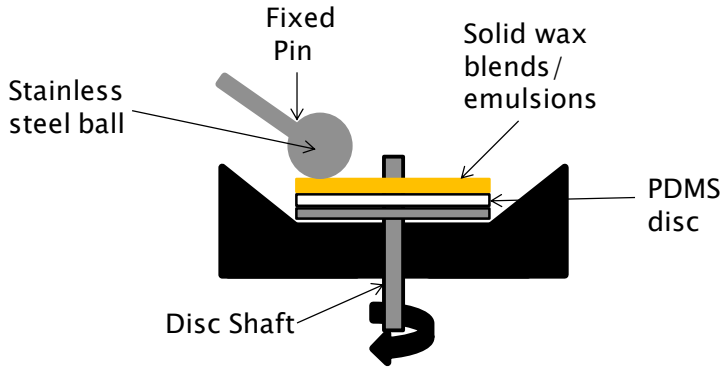

Figure 3.23 – Schematic representation of a tribological set up, with a stainless steel ball and an elastomer disk (with a solid wax/emulsion disk attached).

3.4.9 Sensory Evaluation – Quantitative descriptive analysis (QDA) (Chapter 6)

A trained panel (consisting of 21 women aged 35 - 73) evaluated sensory attributes of a wax blend (bench sample) and emulsions (with different aqueous phase volumes and droplet sizes). Due to the limited number of samples (four) that could be assessed by QDA panelists;

- Bench mark sample (containing 5 wt % carnauba wax, 10 wt % microcrystalline wax and 5 wt % paraffin in castor oil),
- 5 wt % aq phase W/O emulsion,
- 20 wt % aq phase W/O emulsion ($d_{3,2}$ – 3 μm)
- 20 wt % aq phase W/O emulsion with large droplets ($d_{3,2}$ > 100 μm).

All emulsions contained 93, 78 or 79.8 wt % wax blend as the continuous phase. 5 wt % and 20 wt % emulsions contained 2 % PGPR where as 20 wt % emulsion (large droplets) contained 0.2 wt % PGPR.

The panel was trained to score two different attributes (application and sticky/tacky feel) on both the hand and the lip (see Table 3.1). Table 1.1 also highlights how each panelist applied the samples for testing. Testing occurred over a three week (2 days per week) period.

Week 1: Panelists were given a language generation session, whereby they learnt the meaning of each attribute and were trained on the bench sample. At the end of the session all panelists agreed on the bench samples scores which were used to compare against the emulsions

Week 2 and Week 3: In these sessions, the emulsions were presented to the panelists and compared to bench. These were presented unmarked and in a random sequence (generated by the computer software). Panelists assigned a score on line from 0 – 10 for each attribute. All testing was conducted at 23.5 ± 1.4 °C. It is also important to note that after each test, panelists washed either their lips or hands with warm water to remove the sample being tested.

Table 3.1 – Definitions and application procedure provided to each panelist

Attribute	Anchor	Definition	Instructions
Application on hand	0 Drags 10 Glides	Drags – Dry and difficult application with resistance Glides – No resistance felt on application	1. Apply 2 strokes of lipstick onto back of hand with 2 forward strokes and assess. 2. Keep lipstick on back of hand for next attribute
Sticky/Tacky feel on hand	0- nil 10 - high	High – A resistance when fingers are parted Nil – No resistance	1. Apply 2 strokes of lipstick onto index fingertip of opposite hand. 2. Tap index finger with product on over product on back of hand twice. Make decision immediately. 3. Wipe fingers with azo wipes and tissue, keep lipstick on back of hand for next attribute.
Application of lipstick on lips for half lip assessment	0 Drags 10 Glides	Drags – Dry and difficult application with resistance Glides – No resistance felt on application	1. Apply 1 lipstick to half of the top lip from middle to outer and apply to half of the bottom lip with 1 stroke. 2. Repeat with second stroke. 3. Apply the second lipstick to the other half of the lips in the same way.
Sticky/Tacky feel on lip	0- nil 10 - high	High – A resistance when fingers are parted Nil – No resistance	1. Apply 1 lipstick to half of the top lip from middle to outer and apply to half of the bottom lip with 1 stroke. 2. Repeat with second stroke. 3. Apply the second lipstick to the other half of the lips in the same way.

3.4.9.1 Statistical Analysis

Analysis of variance (ANOVA) with post hoc analysis (least significant difference (L.S.D) was done using Compusence (Ontario, Canada). All analysis was conducted using a 95 % confidence interval.

3.4.10 Fourier Transformer Infra Red (FT-IR) Spectroscopy (Chapter 7)

FT-IR (Perkin Elmer spectrometer 100, Cambridge, UK) was used to analyse samples for both glycerol standards (25 dilutions (assuming that a mix of 50 wt % and 50 wt % glycerol represented a 100 % stock solution)) and aliquots taken from release experiments. FT-IR spectra were acquired by placing 0.5 ml aliquots of either glycerol standards or samples from release experiments onto the spectra cell. For all spectra collections, a resolution of 8 cm^{-1} was used. 12 scans in the range of 1400 – 800 cm^{-1} were performed. All analysis was performed in triplicate.

Chapter 4. Designing Wax Based Emulsions for use in Lipstick Application

4.1 Introduction

As described in Chapter 1, lipsticks form an intrinsic part of most cosmetic companies product range and consist mainly of hydrophobic ingredients (waxes, pigments and oils). The excessive use of hydrophobic ingredients can result in dryness of the lips as layering the lip with a hydrophobic layer prevents natural lubrication. Emulsions could be used to deliver moisture to the lips. However, it is critical that an emulsion based lipstick behaves in the same manner as a conventional lipstick. The aim of the work reported in this chapter was to advance the understanding of emulsions designed for lipstick application. This was done in three stages; (1) the effect of producing emulsions *via* either a batch process (in particular the effect of emulsifiers and aqueous phase volume) or a continuous process (in particular processing parameters) on the final droplet size. This will allow delivery of moisture to the lips which is one of the main aims of the project. (2) The melting behavior of different waxes was investigated as this will allow an understanding of a lipstick remaining a solid at room temperature, but spreadable at lip temperature which is of extreme importance for consumer acceptance of the product. (3) The stability of emulsion based lipsticks was investigated.

4.2 Results and Discussion

4.2.1 Emulsions

In order to produce an emulsion based lipstick it is important to consider the impact of incorporating water into the structure. Therefore, a base formulation (taken from the literature (Le Révérend *et al.*, 2011b)) was used as the continuous phase to produce a water-in-oil (W/O) emulsion.

4.2.1.1 Emulsion Design Using a Batch Process

4.2.1.1.1 Emulsion design using emulsifier type and concentration

As described in section 2.4.4, emulsifiers reduce the interfacial tension between two surfaces. Therefore, a series of experiments were conducted to investigate the effect of both emulsifier type and concentration on droplet size in wax based formulations. It is important to note that emulsification was carried out at temperatures (~75 °C) where the waxes remain molten. This prevents wax crystals (*i.e.* Pickering particles) acting as the main stabilising mechanism in the emulsion. The difference between a saturated and unsaturated chain of an emulsifier was investigated by comparing monoolein with monostearate (Kulkarni *et al.*, 2011, Mackles, 1987) as it is hypothesised that the unsaturated nature (double bond) in monoolein could create steric hindrance thus affecting packing of the emulsifier at the interface. Sorbitan olivate was then used to explore the effect of a head group size. These were compared to a polymeric emulsifier (polyglycerol polyricinoleate (PGPR)) as PGPR has been shown to produce small droplets in the food industry (Norton *et al.*, 2009). Figure 4.1 shows the droplet size ($d_{3,2}$, μm) as a function of emulsifier type and concentration. Emulsions formed using either of the monoglycerides (monoolein and monostearate) resulted in droplets being formed in the range of 20 – 28 μm. This was independent of the emulsifier concentration used. Thus suggesting that using either a saturated or unsaturated monoglyceride has no significant effect on the resulting droplet size. Sorbitan olivate is an emulsifier currently used in many Boots formulations (mainly in sun creams), it is a combination of both sorbitan monoolein and sorbitan monostearate. Sorbitan has a head group size that is more than twice that of monoglycerides (head group of ~ 13.9 Å compared to 5 Å, obtained from ChemDraw 12.0). Results showed (Figure 4.1) that the droplet size is ~25 μm which is similar to that obtained for the monoglycerides.

Figure 4.1 also reveals that there is no difference in droplet size when emulsifier concentration is greater than 1 %. However at lower percentages (0.2-1 %), the NMR was unable to measure a droplet size. This suggests that at these percentages the droplets were greater than 100 μm (upper size limit for NMR restricted diffusion). The difference in the amount of Sorbitan olivate required could be caused by a number of reasons; 1) insufficient amount of emulsifier for surface coverage, 2) the ability of the emulsifier to get to the interface during emulsification and 3) the affinity of the emulsifier for the interface. These three hypotheses were investigated individually.

Firstly the amount of emulsifier required for complete surface coverage (assuming a monolayer of emulsifier and spherical droplets) was calculated by using the following equation;

$$\boldsymbol{E_r = A_i / S_c} \qquad \textbf{Equation 4-1}$$

Where E_r is the emulsifier required for surface coverage, A_i is the total area of interface and S_c is the surface coverage value for a specific emulsifier.

The theoretical value calculated using equation 4.1 was compared to actual amount added in reality (shown in Table 4.1). From this it is clear that all emulsifiers were in excess and therefore the difference in concentration of emulsifier required is either due to the emulsifier's ability to get to the interface or its affinity for the interface.

The movement of emulsifier in processing could be dictated by the molecular weight of the emulsifier. Sorbitan olivate has a molecular weight of ~430 g/mol where as the monoglycerides have a molecular weight of 356 g/mol. Therefore in theory Sorbitan olivate should take longer to diffuse to the interface. If this theory was to be true, one would expect PGPR (~500 g/mol) to produce the largest droplets. However, Figure 4.1 illustrates that even at low concentrations of PGPR, droplets are formed in

the range of 4 – 7 μm. This is due to PGPR's ability to produce a thick elastic interface ((Le Révérend *et al.*, 2011b)) preventing coalescence of droplets, by stopping either capillary wave formation or spontaneous holes being formed (as described in section 2.3.4)

The horizontal nature of all the points displayed in Figure 4.1 is a result of the droplet surface being saturated by emulsifier, as suggested by the calculations displayed in Table 4.1.

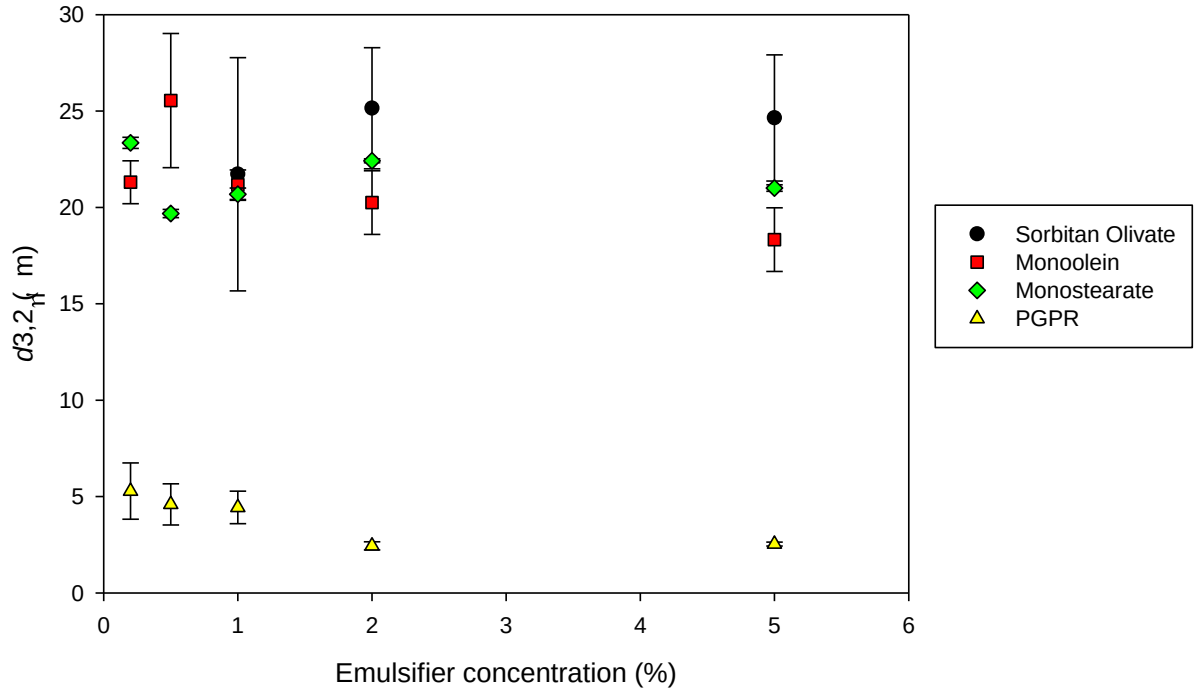

Figure 4.1 Mean droplet diameter ($d_{3,2}$, μm) of 10% water W/O emulsions, as measured by NMR restricted diffusion on day of emulsification, as a function of emulsifier concentration for sorbitan olivate (●), monoolein (■), monostearate (◆) and PGPR (△).

Table 4.1 - Theoretical surface coverage values (m^2/g) for emulsifiers used, calculated using mean droplet size measured by NMR restricted diffusion (values of 23 µm, 25 µm and 5 µm were used for monoglycerides, sorbitan olivate and PGPR, respectively), and head group size of the emulsifiers taken from (a) Choi, Lee, Kim and Kim (2007), (b) calculated using ChemDraw (CambridgeSoft, UK) and (c) calculated from hydronamic radii of PGPR taken from (Gunes *et al.*, 2010). Amount of emulsifier required was then calculated by dividing the total surface area (based on 30 % Water phase) by the surface coverage.

Emulsifier	Surface Coverage (m^2/g)	Amount Required (mg)	Amount added (mg)
Monoglycerides[a]	500	1.57	600
Sorbitan Olivate[b]	8207	0.09	600
PGPR[c]	37800	0.9	600

The reduction in droplet size observed in Figure 4.1 must therefore be due to the affinity of the emulsifier for the interface. This was investigated using interfacial tension (IFT) measurements. In order to determine the IFT of the various emulsifiers, a model system was used where no waxes were incorporated in the continuous phase, thus allowing a liquid system to be analysed.

Figure 4.2 monitors the IFT over a period of 2000 seconds. It clearly shows that the introduction of an emulsifier reduces the surface tension. Both monoglycerides and sorbitan olivate reduce the IFT by approximately 2 mNm^{-1} (from 14.5 – 12.5 mNm^{-1}). In comparison PGPR reduces surface tension by 10 mNm^{-1}. The reduction in IFT results in less mechanical work required to break up the dispersed phase resulting in smaller droplets being formed (Rosen, 1988). This agrees with work shown by Oh and Shah who investigated the effect of different ionic emulsifiers on interfacial tension. They found that as the interfacial tension was reduced from 12.55 to 5.0 mNm^{-1} for lithium dodecyl sulfate and for cesium dodecyl sulfate, the droplet size reduced from 7 to 2.5 µm respectively (Oh *et al.*, 1993).

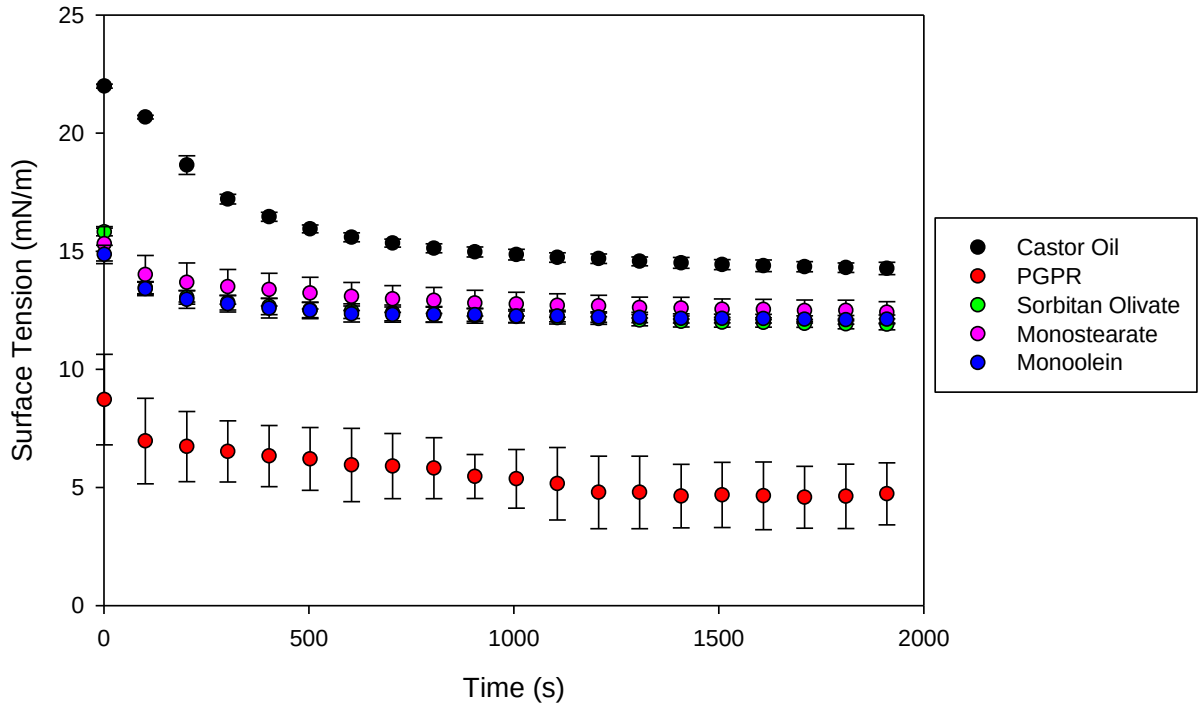

Figure 4.2 – Interfacial tension measurements for different emulsifiers in a model system (no wax). All samples contained 2% emulsifier.

4.2.1.1.2 Effect of Aqueous phase volume and emulsifier concentration on emulsion design

The effect of PGRR on aqueous phase volumes has previously been investigated by Le Reverend *et al* (2011). At the PGPR concentration stated (1 wt %) they showed that with increasing aqueous phase volumes (10 – 40 wt %) all emulsions contained droplets with a $d_{3,3}$ of 7 μm. This leaves the question of whether by changing the emulsifier concentration (0.2, 0.5, 2 and 5 %), there will be an effect on the droplet size measured using NMR restricted diffusion (Chapter 3).

Table 4.2 shows that for all aqueous phase volumes, the droplet size decreases as PGPR concentration increases. At higher aqueous phase volumes (30 % and 40 %), the lower concentrations of PGPR (0.2 and 0.5 wt%) are unable to form emulsions with

droplets under 100 μm. This is a result of there being a greater surface area, and insufficient time for the emulsifier to diffuse to the interface. To test this hypothesis, the processing time for an emulsion (40% aqueous phase and 0.5% PGPR) was doubled from 5 minutes to 10 minutes. This resulted in a reduction in droplet size from >100 μm to 7.4 ± 0.9 μm. Table 4.2 also shows that the droplet size does not reduce after 2% PGPR, due to the limitation of the process to produce smaller droplets.

The SEM micrographs (Figure 4.3) show droplets embedded within a continuous network, which has been previously described in the literature (Ghosh and Rousseau, 2011). The network stabilisation explains the stability against coalescence as the wax crystals provide a physical barrier, preventing movement. From the image it is unclear whether the wax particles are in the interface (displacing emulsifier during crystallisation) or at the interface (moving towards the interface during crystallisation). These images are similar to those previously published by Norton *et al.* (2009) for chocolate. The droplet size observed in the micrographs are comparable to those obtained by the NMR.

Table 4.2 Mean droplet diameter ($d_{3,2}$, µm) measured by NMR restricted diffusion on day of formation as a function of aqueous phase volume and PGPR concentration. Standard deviation is of triplicate measurements.

Aq Phase (%)	PGPR Concentration (%)	d3,2 (µm)	Standard deviation	Aq Phase (%)	PGPR Concentration (%)	d3,2 (µm)	Standard deviation
10	0.2	5.3	1.5	20	0.2	>100	-
	0.5	4.6	1.1		0.5	5.8	1.8
	1	4.4	0.8		1	3.4	0.2
	2	2.4	0.2		2	2.8	0.1
	5	2.5	0.1		5	2.3	0.1
Aq Phase (%)	PGPR Concentration (%)	d3,2 (µm)	Standard deviation	Aq Phase (%)	PGPR Concentration (%)	d3,2 (µm)	Standard deviation
30	0.2	>100	-	40	0.2	>100	-
	0.5	14.2	3.3		0.5	>100	-
	1	6.4	0.6		1	3.4	0.0
	2	2.9	0.3		2	2.7	0.4
	5	2.6	0.1		5	2.8	0.1

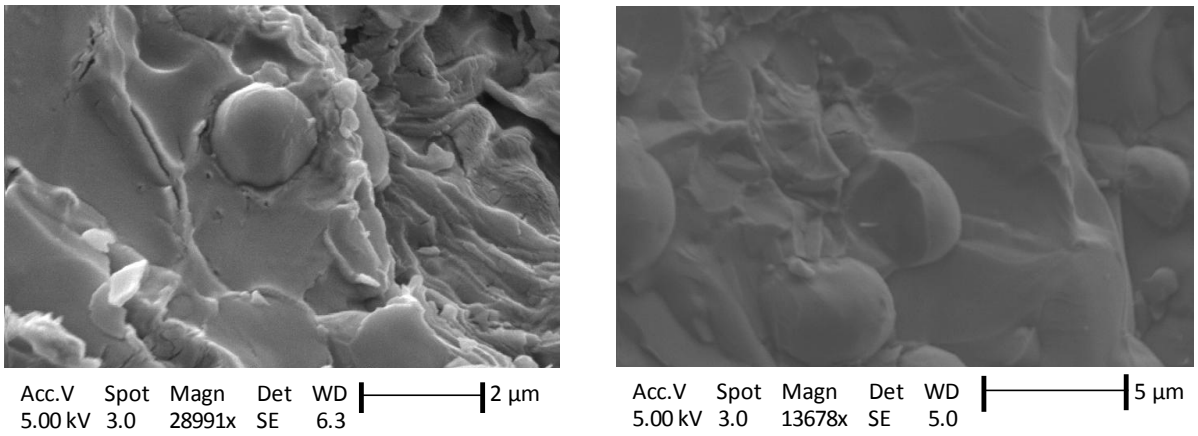

Figure 4.3 - Cyro-SEM micrographs of water droplets surrounded by a hydrophobic continuous phase where (a) is 10 % aqueous phase with 2 % PGPR and (b) 40 % aqueous phase with 2 % PGPR.

4.2.1.2 Effect of a Continuous Process on Emulsion Design

In the food industry, a scraped surface heat exchanger (SSHE) and pin stirrer (PS) has been used to manipulate emulsion droplet size (Norton and Fryer, 2012), as the continuous process allows for greater control of the crystallisation process and therefore greater control of the emulsion microstructure. Also from an industrial point of view the use of a continuous process allows for a more efficient process as there is less down time between batches, resulting in a greater production rate. In this section the effect of droplet size produced *via* a continuous process for an emulsion based lipstick was investigated. Specifically, the effect of different processing parameters (flow rates, jacket temperatures and impeller rotational velocities (IV)) on droplet size were investigated. As described in section 3.3.2.2, the use of a continuous process allows variation of the jacket temperature for both units (SSHE and PS). Therefore in order to determine which jacket temperatures to study, the melting and crystallisation of the continuous phase was investigated. Figure 4.4 shows that the crystallisation starts at ~ 60 °C and continues to ~ 20 °C. As a result jacket temperatures were chosen (55, 60, 65 and 80 °C) that would deliver different levels of crystallisation in the process. At 80 °C there is no crystallisation in the process, whereas at temperatures below 65 °C, crystallisation can occur in the process. Different cooling rates will result in different crystal sizes being produced (Campos *et al.*, 2002). This may affect the viscosity of the continuous phase which in turn has an impact on emulsion droplet size (Norton and Fryer, 2012, van Duynhoven *et al.*, 2002b). It is important to note that at jacket temperatures below 55 °C the formulation fully crystallises which results in blockages of the pipes.

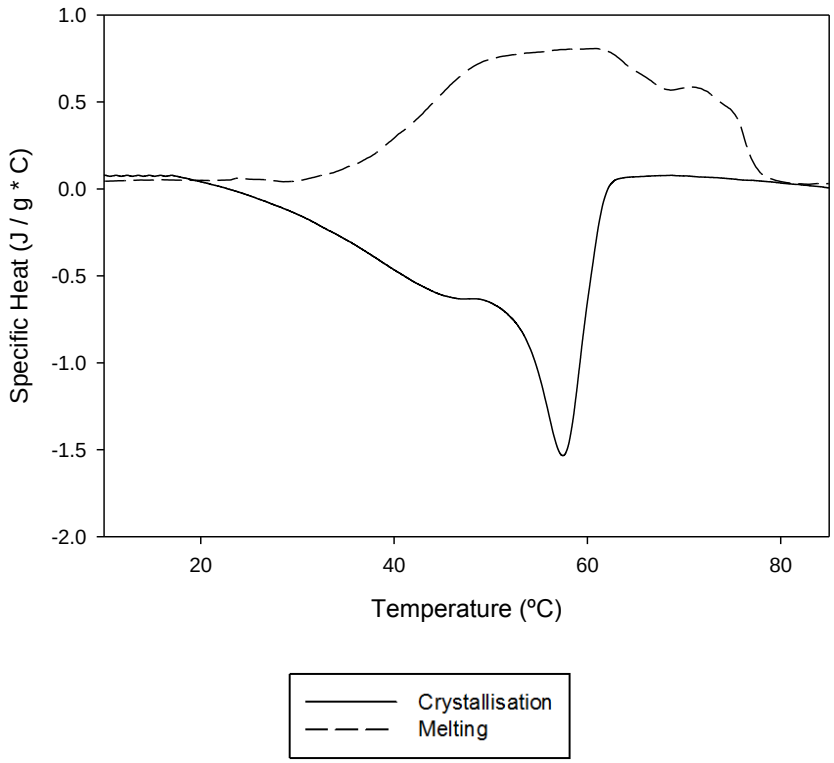

Figure 4.4 - Crystallisation and melting curve for an solution containing 5 % CW and 10 % MW in 85% castor oil obtained via Differential Scanning Calorimeter (Perkin Elmer DSC Series 7, UK), equipped with thermal analysis software (Pyris) at a scan rate of 10 °C/min from 120°C to 10 °C.

4.2.1.2.1 Effect of SSHE on Emulsion Structure

Initially, the effect of SSHE on emulsion droplet size and structure was investigated. It is important to note that the exit temperature varied from the jacket temperatures, therefore, all results will be compared to the exit temperatures. Figure 4.5 shows that smaller droplets are formed at lower temperatures, regardless of the flow rate and IV; for example, at an IV of 1,500 rpm and residence time (RT) of 81.5 s, emulsions produced at an exit temperature ~ 51 °C were ~ 2 μm, whereas those of emulsions produced with an exit temperature ~ 75 °C were ~ 8 μm.

This reduction in droplet size caused by lowering the temperature is thought to be due to a change in the viscosity of the continuous phase. The literature shows that increasing the viscosity of the continuous phase results in a decrease of the emulsion droplet size (Pal, 1996). This is due to higher disruptive shear forces resulting in a more

efficient droplet break-up (Walstra, 1983b), and to a reduction in droplet collision, decreasing droplet re-coalescence (see section 2.3.4 for more details). On the other hand, a higher viscosity lowers the emulsifier adsorption rate, which can lead to droplet re-coalescence.

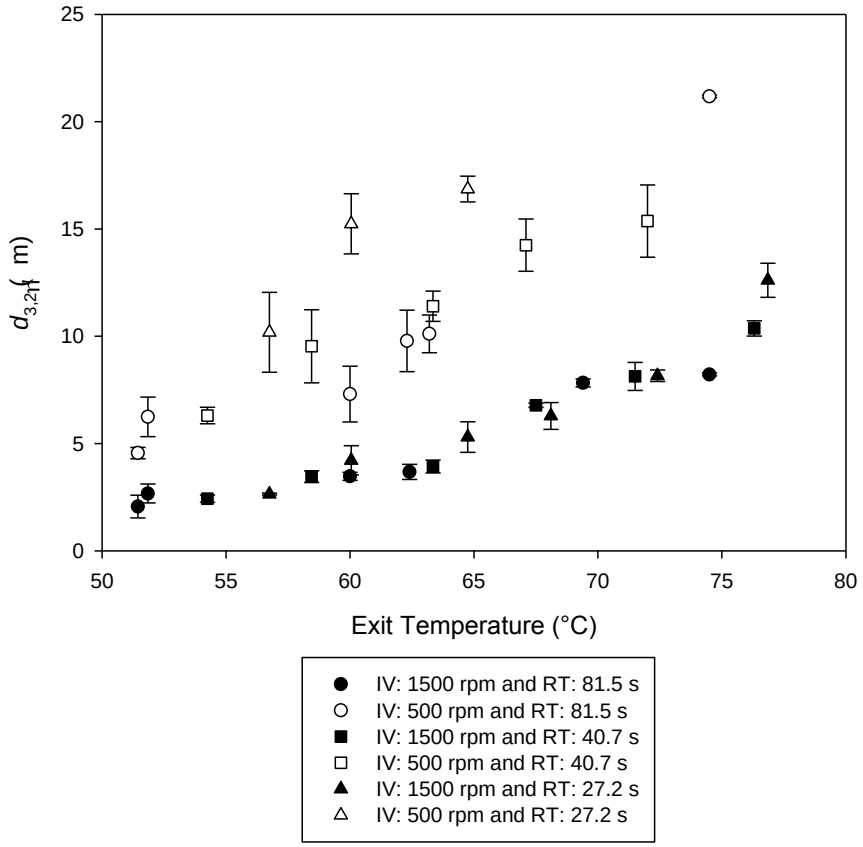

Figure 4.5 - Average droplet size ($d_{3,2}$) measured by NMR on the day of emulsion formation (10 % W/O where the continuous phase consists of 5 wt % CW, 10 wt % MW in castor oil) using SSHE unit as a function of exit temperature under varying processing conditions: Residence time (RT) of ● 81.5 s , ■ 40.7 s and ▲ 27.2 s; Impeller rotational velocity of 500 rpm (open symbols) and 1500 rpm (full symbols).

The viscosity of the oil continuous phase, measured at a fixed shear rate (100 s^{-1}), increases from 0.05 to 0.65 Pa.s by decreasing the temperature from 75 to 50 °C, respectively (Table 4.3). The change in the continuous phase viscosity is due to formation of wax crystals during cooling. The mixture of CW and MW used in the oil solution crystallises between ~ 65 and 55 °C. Above 70°C, no or only a few crystals are

present in the oil phase, resulting in no changes in the viscosity. Lowering the temperature below 70°C results in an increased number of crystals formed, hence a higher viscosity at lower temperatures. At room temperature, the oil phase presents a soft solid structure. Water droplet mobility within the oil phase is reduced at higher viscosity, reducing the risk of droplet collision. The presence of wax crystals does not only contribute to thicken the continuous phase, but also favors the stabilisation of the water droplets. It was shown that MW and CW crystals adsorb at the oil/water interface to a form steric barrier around the emulsion droplets and prevent their coalescence (Le Révérend *et al.*, 2011a).

Table 4.3 - Effective viscosity of the oil continuous phase containing 5% CW and 10% MW in castor oil as a function of the temperature, measured with a constant shear rate of 100 s^{-1} using a cone and plate geometry.

Temperature (°C)	50	55	60	65	70	75	80	85
Effective Viscosity (Pa s)	0.65 ±0.007	0.4 ±0.003	0.24 ±0.004	0.12 ±0.0008	0.07 ±0.0009	0.05 ±0.0008	0.05 ±0.0005	0.04 ±0.0004

It is assumed here that not all wax crystals adsorb at the interface, thus some remain in the bulk phase. Those crystals form a network that results in a soft solid emulsion structure. They also contribute to emulsion stability as they form physical barriers between the droplets, thus trapping the water droplets in a wax network. This stops coalescence by inhibiting the occurrence of droplet collisions. Emulsion droplet size was measured at 5°C, after complete crystallisation. Crystal formation occurs either post-production (jacket temperature T_j ~80°C) or both during emulsification and post-production (T_j ≤65°C). Emulsions formed at a temperature below 65°C contain at the end of emulsification more crystals in the bulk phase than those produced at higher temperature, and would be then expected to have smaller droplets (due to the lower viscosity of the continuous phase at lower temperatures). This was supported by the

results shown Figure 4.5. The reduction in emulsion droplet size observed at lower temperature is then due to both Pickering (crystals at the interface) and network (crystals in the continuous phase) stabilisation. The emulsion size reduction was observed by polarised microscopy. Micrographs of emulsions produced with different processing conditions are shown Figure 4.6. It is clear that at a temperature of 80°C, big droplets are formed. The structure of the continuous phase also seems to be altered by the processing conditions. At 55 °C (Figure 4.6a), the droplets have a shell like structure with crystals 'sitting' around a droplet. This is caused by more nucleation sites being produced (due to the greater temperature difference) during the process allowing small crystals to form which can move towards the interface. When crystals are produced in both the process and post production (Figure 4.6b) a greater network is observed and the droplets are integrated into the wax network. However, when crystals are produced in post production (Figure 4.6c) they do not move towards the W/O interface, this results in droplets acting as defects which will affect the material properties of the emulsion (discussed in Chapter 5).

Given these observations an important consideration is the time the sample is within the process. Figure 4.5 shows that smaller droplets are obtained at higher RT's. For example, at 60 °C and 500 rpm, the droplet size increases from ~7 μm to ~17 μm, by decreasing the RT from 81.5 to 27.2 s, respectively. Emulsions produced at high RT's result in smaller droplet sizes as there is longer for droplet disruption to occur. This effect of RT is reduced at higher IV (1,500 rpm) as droplet break-up occurs faster due to higher shear forces (see section 2.2.1.1).

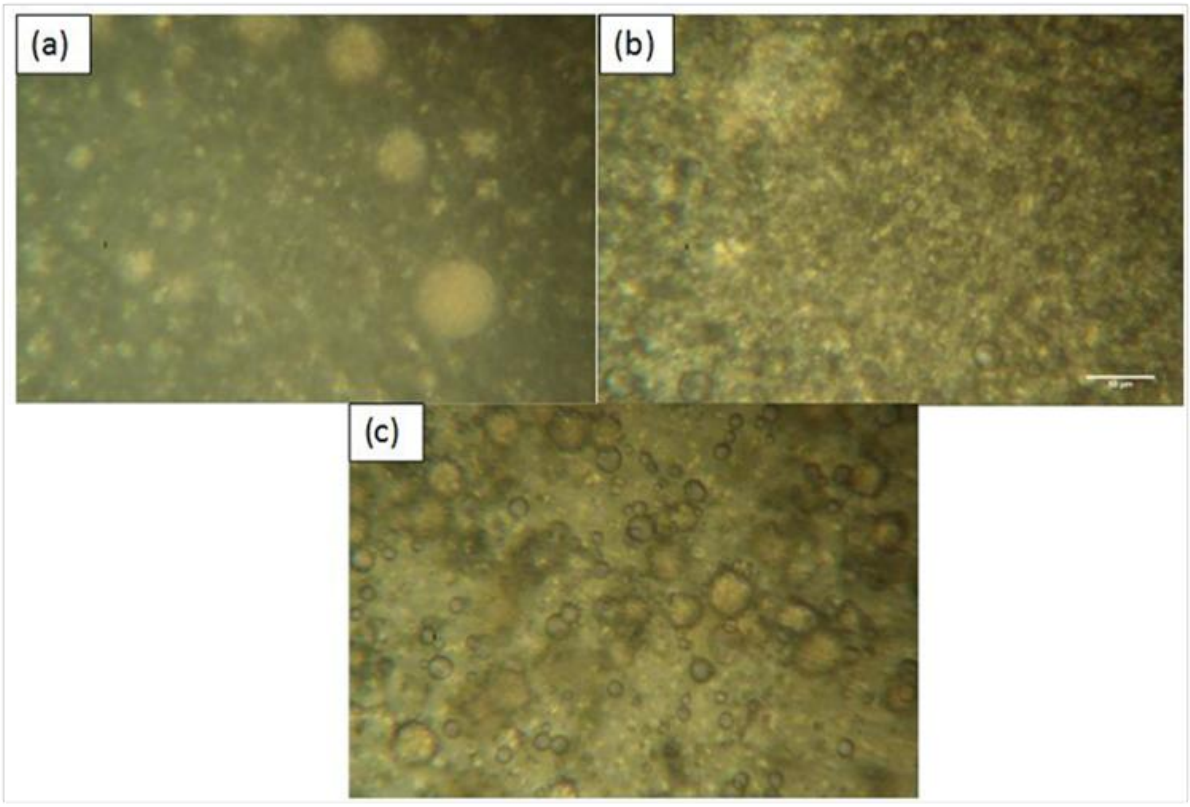

Figure 4.6 - Polarised Microscopy of W/O emulsions formed using a SSHE at an IV of 1500rpm and (a) T_j = 55°C and FR = 30 mL/min, (b) T_j = 65°C and FR = 90 mL/min and (c) T_j = 80°C and FR = 90 mL/min. The bar represents 50 μm.

4.2.1.2.2 Control of Emulsion Structure using a PS

The effect of the addition of a PS unit to the SSHE unit to form part of a "margarine line" on the emulsion droplet size and structure was investigated. 5% of paraffin was added to the initial formulation to strengthen the formulation in order to be analysed using a texture analyser. Nonetheless, droplet sizes of emulsions produced with the SSHE unit were very similar with or without paraffin ($d_{3,2}$ ~ 5 μm). In order to limit the number of parameters to set up for both units, the flow rate was kept constant to 60 mL/min throughout the whole unit, as well as the jacket temperature of the SSHE unit (65°C). These parameters were chosen as it is important that an emulsion that already has a crystal network is passed through the PS, thus allowing the effects of the PS to be examined. Also at low jacket temperatures (55 °C), the heat loss between the units,

caused a blockage in the pipes which prevented the emulsion passing through the PS. The IV of the SSHE unit was adjusted to be either 500 or 1,500 rpm. The IV of the PS unit was adjusted to be 3 different velocities (500, 1,000 and 1,500 rpm) and the jacket temperature was varied from 55 to 80°C.

When the IV of the SSHE unit is set up at 1,500 rpm, droplets that entered the PS unit were ~ 5 μm and no change in droplet size is observed, regardless of the temperature or the IV in the PS unit (Figure 4.7). However, when the IV of the SSHE unit is set to 500 rpm the temperature and IV in the PS unit both have an effect on the final droplet size (Figure 4.8). Firstly the effect of pin stirrer IV is discussed. When the emulsion enters the PS it has a droplet size of ~ 14 μm (Figure 4.8), no change in droplet size is observed at 500 rpm. However the droplet size does decrease at 1,000 rpm (~ 10 μm) and 1,500 rpm (~ 5 – 7 μm). It was also observed that, for this particular system and regardless of the SSHE IV, the smallest droplet diameter ($d_{3,2}$) obtained was ~ 5 μm. Also, in order to reduce the droplet size further using the PS unit, it is necessary to work at a IV of the PS higher than the one of the SSHE. When equivalent IV are used in both units, the final droplet size is driven by disruptive forces in the SSHE unit. This represents a limitation of the process (*i.e* the maximum IV was used), but could be expected as the PS unit was originally designed only to adjust the emulsion material properties (Zhang *et al.*, 2005).

The extent of the decrease in droplet size through the PS unit depends on jacket temperature (T_j) (Figure 4.8). At 1,500 rpm for example, the size decreases from 15 μm to 6 μm at T_j = 55°C, but does not change at T_j = 80°C. Emulsions exiting the SSHE chamber at ~ 63°C are likely to contain liquid wax which has not crystallised. It is argued here that wax crystallisation continues in the PS unit adjusted at a temperature

below 65°C, which as mentioned in section 4.2.1.2.1, contributes (i) to enhance droplet disruption by increasing the continuous phase viscosity, and (ii) to stabilise of water droplets newly formed in the PS chamber by either network or Pickering mechanisms. At T_j = 80°C, no crystals are formed in the PS chamber, resulting in no change in the droplet size.

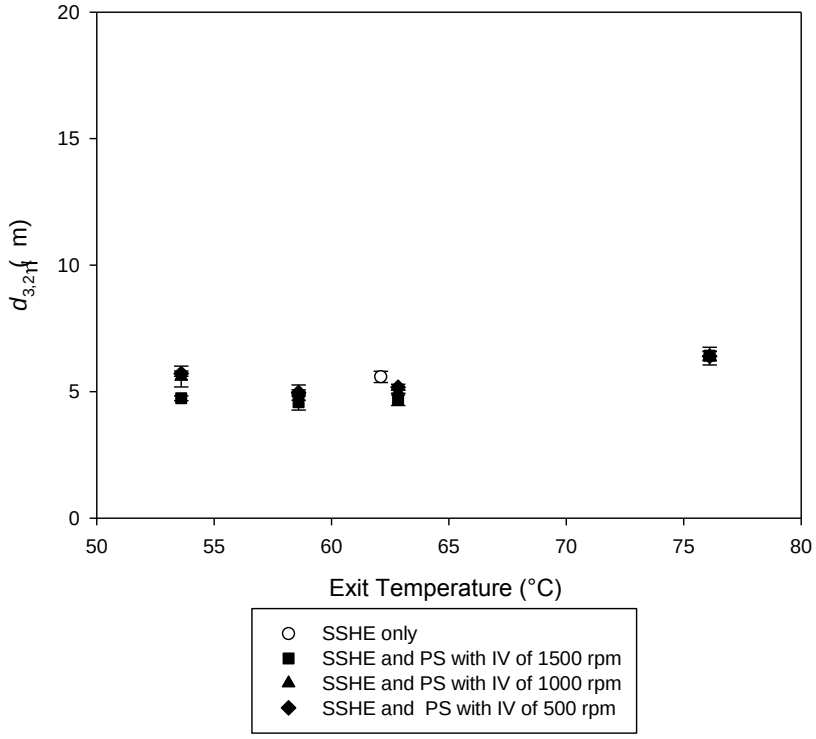

Figure 4.7 - Droplet size ($d_{3,2}$) measured by NMR on the day of emulsion formation (10 % W/O where the continuous phase consists of 5 wt % CW, 10 wt % MW in castor oil) using SSHE and PS units as a function of exit temperature. Processing conditions for the PS unit; ◆ IV = 500 rpm, ▲ IV = 1000 rpm and ■ IV = 1500 rpm. All emulsions were first passed through a SSHE (○) at a Jacket temperature of 65 °C and an IV of 1500 rpm. The overall flow rate though both units was 60 mL/min.

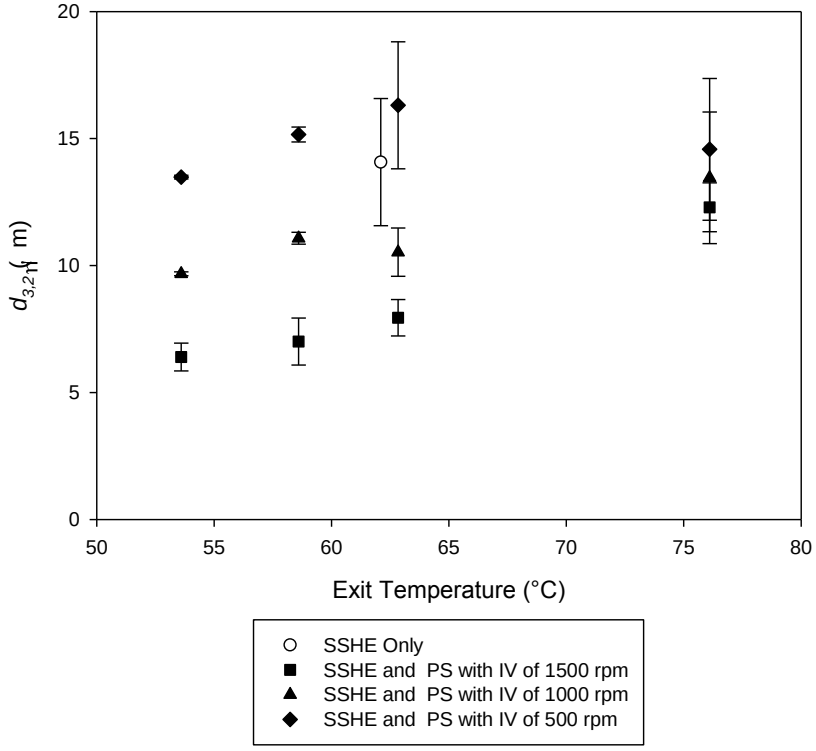

Figure 4.8 - Droplet size ($d_{3,2}$) measured by NMR on the day of emulsion formation (10 % W/O where the continuous phase consists of 5 wt % CW, 10 wt % MW in castor oil) using SSHE and PS units as a function of exit temperature. Processing conditions for the PS unit; ◆ IV = 500 rpm, ▲ IV = 1000 rpm and ■ IV = 1500 rpm. All emulsions were first passed through a SSHE (○) at a Jacket temperature of 65 °C and an IV of 500 rpm. The overall flow rate though both units was 60 mL/min.

4.2.2 Designing Melting Profiles for Lipstick Application

The melting behavior of wax based emulsions is of extreme importance for lipstick application as a lipstick needs to remain solid at room temperature but start to melt at lip temperature (32 °C). However before an emulsion lipstick is considered it is important to investigate the impact of individual waxes on the melting profiles. Both carnauba wax (CW) and microcrystalline wax (MW) were selected to produce the base for an emulsion based lipstick. CW was chosen as it constitutes a large amount of a current lipstick formulation and it has the highest melting enthalpy (193 J/g) which will provide a rigid base structure for a cosmetic lipstick (Taylor, 2011). A rigid structure is required for two reasons; 1) for consumer acceptance and 2) for ease of removal in the molding process. MW was chosen as McKetta (1993) stated that a prerequisite for a good lipstick is that it contains at least one wax that has a melting profile in the region of 55 - 75 °C (McKetta, 1993). The effect of varying concentrations on the melting behavior of both waxes was investigated individually and as blends.

4.2.2.1 Carnauba Wax

The melting profiles of different CW concentrations in castor oil were investigated and the melting enthalpy was compared to a pure sample (Figure 3.10) of CW. Results are shown in both Figure 4.9 and Table 4.4. From Figure 4.9 it can be seen that for all concentrations an endothermic peak is observed with varying melting enthalpies (area under the curves). The melting enthalpies were calculated using the trapezium rule and are shown in Table 4.4 (Allison *et al.*, 1995). The experimental melting enthalpies increase from 8.5 – 33.2 J/g, these results are similar to the expected melting enthalpies which were calculated from a pure sample of CW (Table 4.4). The expected enthalpies were calculated by dividing the concentration of CW in the formulation by the total melting enthalpy of a pure sample of CW.

There is no significant difference between the estimated melting enthalpies and the experimental melting enthalpy. This indicates that the castor oil does not influence the melting behavior of CW. This was shown by assessing the melting and crystallisation behavior of a 100 % castor oil. Figure 4.10 shows that for a temperature range -30 – 50 °C there is no melting or crystallisation behavior, thus, confirming that the melting behavior is governed by the CW concentration and not the influence of castor oil.

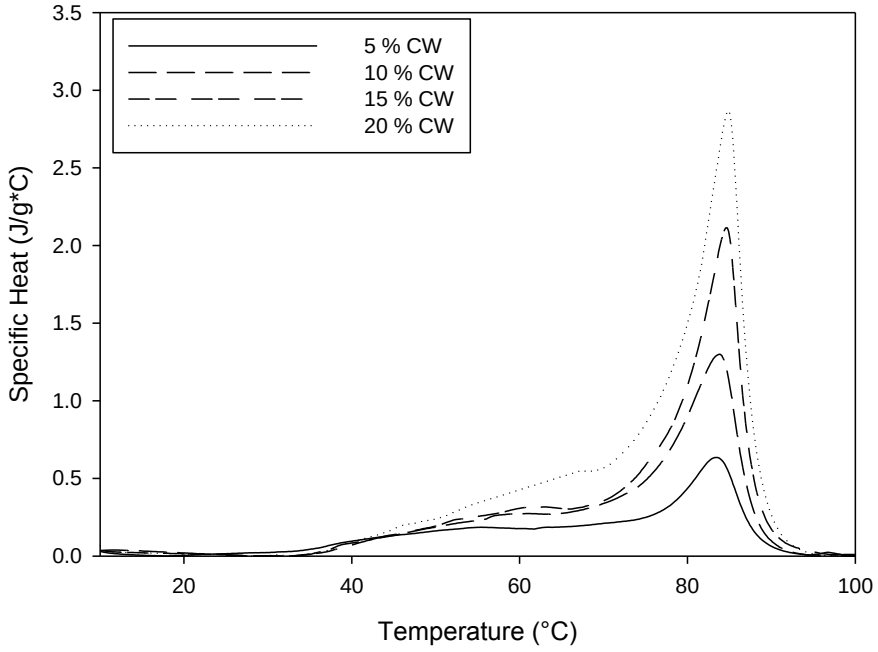

Figure 4.9 – Melting profiles curves for oil phase formulations containing various ratios of carnauba wax (CW) in castor oil (CO). The sample was heated at a rate of 10 °C/ min.

Table 4.4 – Melting range, theoretical and experimental melting enthalpies as a function of carnauba wax concentrations.

Sample	Melting Range (°C)	Expected Melting Enthalpy (J g^{-1})	Experimental Melting Enthalpy (J g^{-1})
5 % CW	37.7-87.5	7.4	8.5 ± 2.1
10 % CW	37.7-94.1	14.8	18.8 ± 1.4
15 % CW	37.9-95.9	22.1	23.5 ± 2.0
20 % CW	37.3-94.3	29.5	33.2 ± 2.9

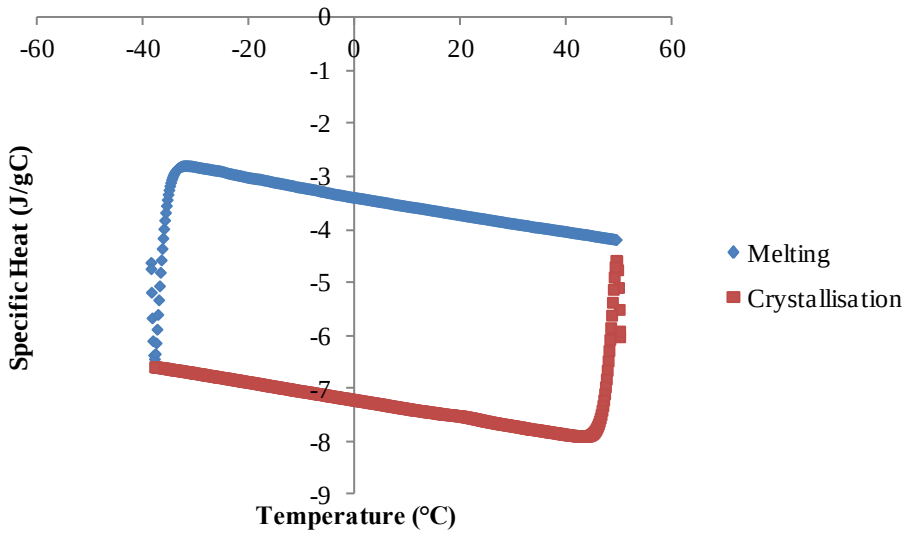

Figure 4.10 - DSC curves for castor oil. The sample was heated at a rate of 10 °C/ min.

4.2.2.2 Microcrystalline Wax

The melting profile of different MW concentrations was investigated and compared to a pure sample (Figure 3.10) of MW, in order to determine the possibility of using MW in lipstick formulations. Results are shown in both Figure 4.11 and Table 4.5. From Figure 4.11 it can be seen that for all MW concentrations an endothermic peak is observed with 2 peaks at ~56 and ~78 °C with varying melting enthalpies. MW consists of iso-alkanes and cycloalkanes of different molecular weight. The broad peak obtained for MW is indicative that the wax is a mixture of different molecular weights that melt at different temperatures. Peterson (2008) *et al* investigated the behavior of Vaseline and a MW. They found that the peaks are due to MW containing multiple components which melt at different temperatures. They also found that if stored at different conditions, the melting behavior can be altered. Their results showed that at different storage temperatures the MW was able to restructure into a more stable crystalline form (Petersson *et al.*, 2008). The experimental melting enthalpies increase from 5.0 – 25.7

J/g, these results are similar to the expected melting enthalpies which were calculated from a pure sample of MW (Table 4.5). This confirms that the melt is due to wax interactions and not impacted by the presence of castor oil.

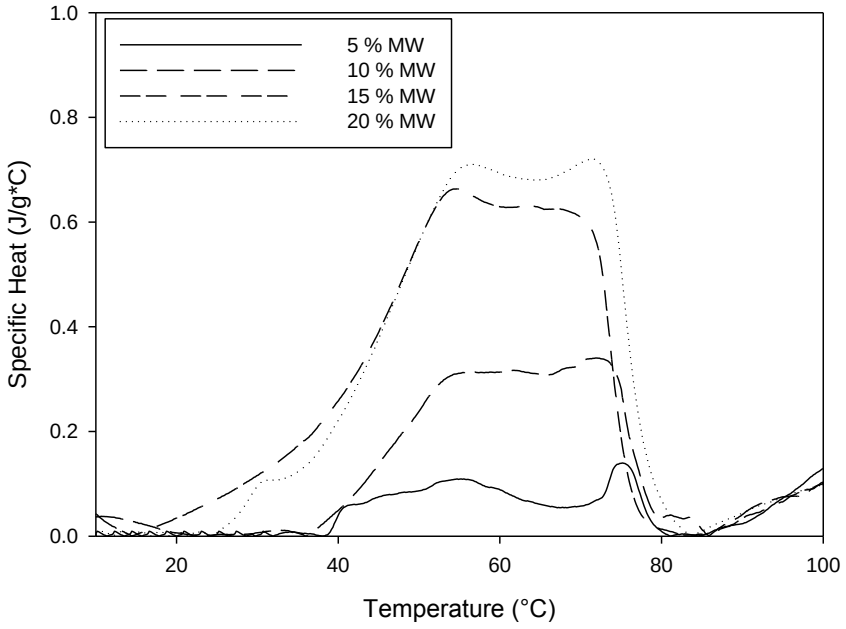

Figure 4.11 - Melting profiles curves for oil phase formulations containing various ratios of microcrystalline wax (MW) in castor oil (CO) . The sample was heated at a rate of 10 °C/ min.

Table 4.5 - Melting range, theoretical and experimental melting enthalpies as a function of microcrystalline wax concentrations.

Sample	Melting Range (°C)	Expected Melting Enthalpy (J g^{-1})	Experimental Melting Enthalpy (J g^{-1})
5 % MW	28.8-80.1	5.8	5.0 ± 1.7
10% MW	27.8-78.0	11.5	9.7 ± 2.2
15% MW	28.9-80.3	17.3	16.2 ± 2.7
20% MW	26.6-78.5	23.1	25.7 ± 2.7

As described in section 1.1, cosmetic lipsticks are a combination of multiple ingredients which provide a lipstick with the ability to be a solid (rigid solid) at room temperature but spreadable (plastic solid) at lip temperature. Figure 4.12 shows the melting profile of a standard commercially available lipstick. From Figure 4.12, a broad endothermic peak is observed from ~ 30 – 90 °C. When this is compared to the melting

profiles shown in both Figure 4.9 and Figure 4.11 it becomes clear that an individual wax will not provide the melting profile required for lipstick application for two reasons. (1) CW has a high melting point with the majority of wax crystals melting at ~85 °C, this would be unsuitable for lipstick application as wax crystals would have to start to melt at lip temperature (32 °C) and (2) MW is too soft to produce lipstick bullets even though it does have the desired melting profile (It is important to note that the softness of the material was observed by attempting to mould the sample and will be quantitatively analysed in Chapter 5). Therefore a combination of MW and CW was investigated for their possible use as the continuous phase of an emulsion based lipstick.

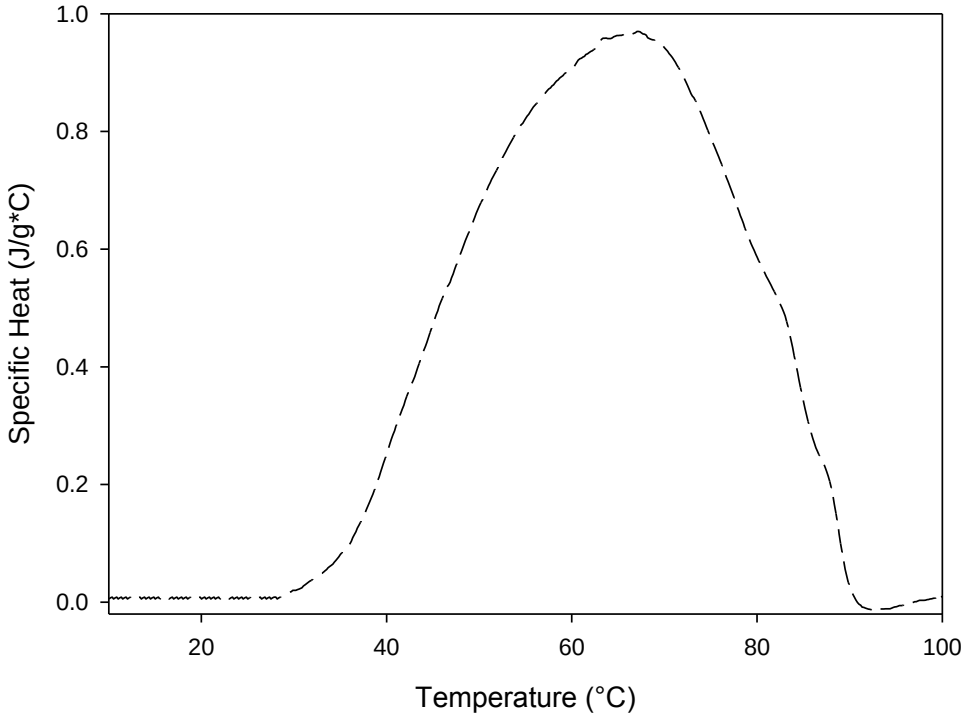

Figure 4.12 - Melting profiles curve for a commercially available moisturising lipstick from the Boots range. The sample was heated at a rate of 10 °C/ min.

4.2.2.3 Blends of Microcrystalline Wax and Carnauba Wax

The melting profiles of formulations containing 5% CW and varying amounts of MW (5 – 20%) were investigated for their use in cosmetic lipsticks. Results are shown in Figure 4.13 and Table 4.6. For all formulations a broad endothermic melting profile is observed in the range of 23.5 – 80 °C. There are two distinct peaks at ~60 and ~75 °C which are due the different components in the formulation. Table 4.6 shows that as the concentration of MW increases from 5% - 20% the onset temperature shifts from 33.8 – 23.5 °C. The shift in onset is due to MW forming irregular sized crystals which disrupts the wax crystal network (the effect of waxes on material properties is discussed in Chapter 5).

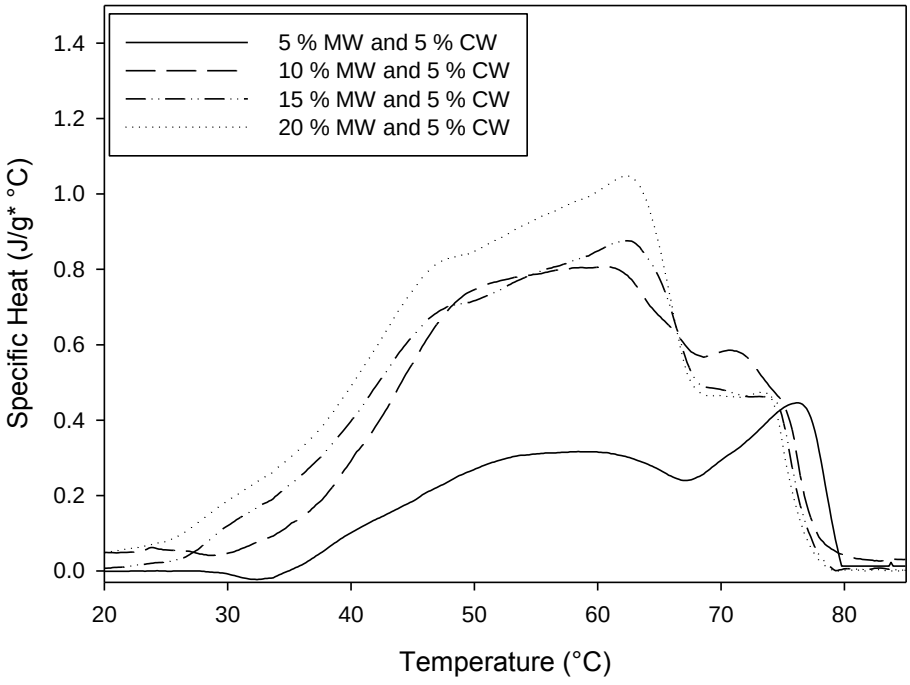

Figure 4.13 – Melting profiles for oil phase formulations containing various ratios of microcrystalline wax (MW) in castor oil (CO) with 5 % carnauba wax (CW). All samples were measured using a DSC scan range from 10 to 120 °C at a rate of 10 °C / min.

Table 4.6 - Onset (T_{onset}), peak (T_{peak}^1 and T_{peak}^2), and end (T_{end}) temperatures as a function of microcrystalline wax concentration

Microcrystalline Wax (%)	T_{onset} (°C)	$T_{peak\,1}$ (°C)	$T_{peak\,2}$ (°C)	T_{end} (°C)
5%	33.8 ± 0.8	60.2 ± 0.7	75.8 ± 0.3	80 ± 0.4
10%	30.5 ± 0.7	61.7 ± 0.4	72.6 ± 0.5	78.7 ± 0.6
15%	26.5 ± 0.7	62.8 ± 0.2	73.2 ± 0.3	78.9 ± 0.4
20%	23.5 ± 2.1	62.5 ± 0.3	72.3 ± 0.5	78.5 ± 1

4.2.2.4 Effect of Aqueous Phases on Melting Profiles

As shown in the previous section, water can be incorporated into the formulation to produce an emulsion. For it to be suitable to be used in a cosmetic lipstick it will need to have a similar melting profile to a conventional lipstick. Therefore a control experiment was conducted in order to determine if the incorporation of water into a wax structure affected the overall melting profile. A formulation containing 5 % CW and 10 % MW was made into an emulsion with varying aqueous phase volumes (10% - 40%) and were analysed *via* DSC. The melting range for a formulation containing no water is approx 30 – 80 °C (previously shown in Figure 4.13). When this is compared to the melting range of emulsions (Figure 4.14) it can be observed that the melting range remains in the same region (~ 30 – 80 °C). From this it can be concluded the melt of the emulsion is governed by the wax blend and not the aqueous phase volume. This agrees with work shown in the food and cosmetic industry show by Norton *et al* and Le Reverend *et al* respectively (Norton *et al.*, 2009, Le Révérend *et al.*, 2011a).

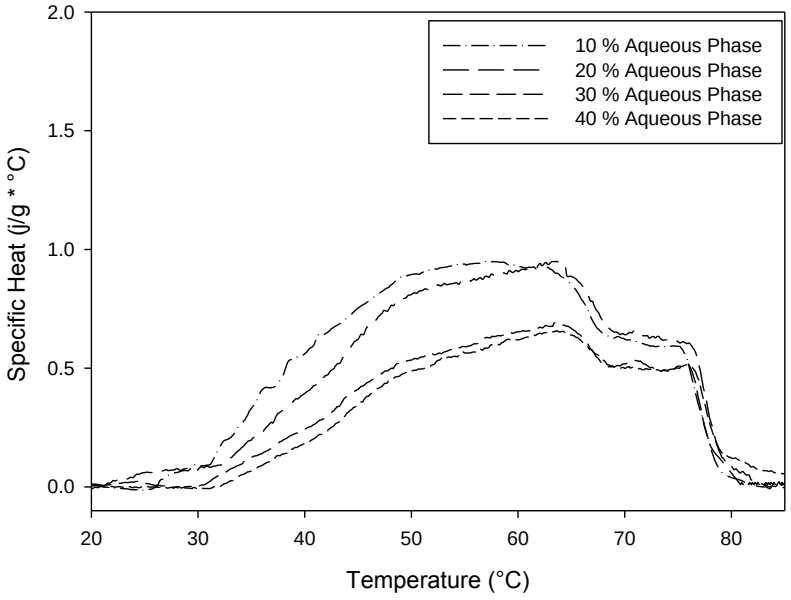

Figure 4.14 - Melting profiles for emulsions containing various aqueous phase volumes where the continuous phase in castor oil (CO) with 5 % carnauba wax (CW). All samples were measured using a DSC scan range from 10 to 120°C at a rate of 10°C / min.

4.2.3 Long term Stability of Emulsions for Lipstick Application

As previously described (section 2.2), emulsions are thermodynamically unstable and therefore will phase separate over time. Therefore in this section the long term stability was investigated using two techniques: droplet size NMR and gravimetric analysis. Initially, a formulation with varying PGPR concentrations (0.5 – 5 %) was turned into an emulsion with varying aqueous phase volumes (10, 20, 30 and 40 %). Table 4.7 shows the results for 30 % aqueous phase. Results indicate that once an emulsion is formed the droplet size does not vary over a 6 month period. For example when 2 % PGPR is used the droplet size on day 0 is 2.9 ± 0.3 μm and the droplet size at the end of 6 months is 2.8 ± 0.4 μm. This suggests that the wax crystal network creates network stabilisation which prevents coalescence from occurring. These results are also true for 10, 20 and 40 % aqueous phase volumes and are shown in Appendix 1.

Table 4.7 Mean droplet diameter ($d_{3,2}$, μm) measured by NMR restricted diffusion from day 0 to day 180 for emulsions produced with varying PGPR concentrations (0.5, 1, 2 and 5wt%). All emulsions contain 30 % water.

	Day 0		Day 1		Day 7		Day 10		D ay 180	
PGPR Concentration (%)	d3,2 (μm)	SD (σ)	d3,2 (μm)	SD (σ)	d3,2 (μm)	SD (σ)	d3,2 (μm)	SD (σ)	d3,2 (μm)	SD (σ)
0.5	14.2	3.3	14.0	3.2	14.2	3.2	14.1	3.4	13.8	3.2
1	6.4	0.6	6.1	0.6	6.1	0.6	6.1	0.6	5.8	0.6
2	2.9	0.3	2.9	0.3	2.8	0.3	2.8	0.3	2.8	0.4
5	2.6	0.1	2.5	0.3	2.5	0.0	2.3	0.1	2.2	0.2

The ability for an emulsion based lipstick to retain its water content in different conditions is of extreme importance. As during its life cycle it will experience a variety of conditions. Therefore a formulation with varying amounts of MW (10, 15 and 20 %) was made into an emulsion of varying aqueous phase volumes (10 – 40 %) and placed in three different storage facilities. These formulations were chosen as they showed they

had a melting profile that was suitable for use in a cosmetic lipstick (Figure 4.13). Three different storage conditions were chosen to mimic typical conditions a cosmetic lipstick would experience during its lifetime; 1) room temperature to represent on the shelf conditions, 2) 30 °C to represent application temperature and 3) cycling (-10 – 40 °C)) conditions to investigate if an emulsion lipstick can withstand temperature fluctuations. The amount of water loss was monitored over a period of 3 months and the percentage water loss is shown in Table 4.8.

Results show that as the amount of aqueous phase increases the amount of water loss increases over a period of 3 months. For example, when 10 % aqueous phase is stored in room temperature conditions the average water loss increases from 0.07 – 0.4 %. It is also important to note that regardless of the storage conditions the amount of water loss remains the same. The amount of water loss is also the same regardless of the amount of MW in the formulation. In general the water loss for all formulations is less than 1 %, thus indicating the majority of the water is trapped within the emulsion's structure. It is suggested here that the 1% water loss is only due to water remaining on the surface of the emulsion, which evaporates over a period of time.

Table 4.8 - Average water loss of emulsions (with 10 – 40 % aq phase volumes and varying amounts of microcrystalline wax (MW) stored in three different storage conditions (room temperature, 30 °C and cyclic (-10 – 40 °C) conditions. All samples also contain 5 % carnauba wax as part of the continuous phase. All emulsions were made using a high shear mixer at 10,000 rpm for 5 min.

		Room Temperature		30 °C		Cyclic (-10 – 40 °C)	
Aq Phase	MW Conc	1 Month (%)	3 Month (%)	1 Month (%)	3 Month (%)	1 Month (%)	3 Month (%)
10	10	0.07	0.40	0.15	0.49	0.20	0.53
20	10	0.19	0.88	0.25	0.84	0.30	0.89
30	10	0.18	0.59	0.37	1.12	0.49	1.35
40	10	0.29	1.24	0.43	1.36	0.35	1.18
10	15	0.04	0.78	0.12	0.41	0.16	0.52
20	15	0.15	1.17	0.36	1.02	0.30	0.93
30	15	0.24	1.40	0.43	1.32	0.39	1.11
40	15	0.22	1.01	0.4	1.28	0.43	1.38
10	20	0.09	0.33	0.19	0.57	0.21	0.65
20	20	0.07	0.91	0.20	0.64	0.25	0.72
30	20	0.20	1.17	0.34	1.22	0.39	1.14
40	20	0.24	0.99	0.38	1.34	0.39	1.22

4.3 Concluding Remarks

In this chapter the use of different emulsifiers allowed the production of emulsions with varying droplet sizes. Results showed that the saturated nature of the emulsifier had very little effect on the droplet size, neither did the use of an emulsifier with a larger head group (all droplets in region of ~18 – 25 μm). PGPR resulted in emulsions with the smallest droplets (~3-5 μm), probably as a result of a thick elastic interface (Le Révérend *et al.*, 2011b).

A lab-scale scraped surface heat exchanger and pin stirrer were shown to be efficient to (1) produce water containing lipstick and (2) control emulsion properties (*e.g.* droplet size). They also allow greater control of crystallisation process which determines the viscosity of the continuous phase, leading to greater experimental design of the final droplet size. The greater control of the crystallisation process will also affect the material properties of emulsion structure. Therefore future work should involve investigating the material properties of emulsions formulated with different crystal sizes (see Chapter 5).

The melting behavior of wax based emulsion systems was investigated. It has been shown that a combination of 5 % CW and 10 % MW provided a melting range of 30 – 80 °C, which is similar to currently available lipsticks (30 – 90 °C). Furthermore the incorporation of water into the formulation does not alter the overall melting profile of the sample.

Chapter 5. Manipulating material properties of wax based emulsion systems for use in lipstick application

5.1 Introduction

As described previously in Chapter 4, varying either the formulation or the processing conditions (batch or continuous) effects the microstructure of the final emulsion formed. This variation in microstructure, will affect the material properties (as previously explained in section 1.1)). The aim of this chapter was to investigate the material properties of wax based emulsions suitable for lipstick application produced *via* either a batch process or a continuous process. In order to achieve this the chapter was split into three stages; (1) the effect of different waxes and wax blends on the overall material properties was investigated, which provides a better understanding of the individual waxes involved. (2) The effect of water inclusion into the formulation (an emulsion) and water content on the material properties. This is important as Muller *et al.* (2009) has shown that introducing additional components into a formed network can affect the material properties. (3) The effect of a continuous process to control the amount of crystallisation during processing was investigated. Different rates of cooling fats/wax have been shown to produce different sizes of fat crystals (Campos *et al.*, 2002). It is hypothesised here that varying crystal size will affect material properties of wax based emulsion systems as it effects the microstructure of the final emulsion.

5.2 Results and Discussion

The introduction of water droplets into a wax network will affect the overall material properties, as it will introduce soft particles into an existing network which could act as defects. In order to examine the effect of water droplets it is important to first consider the wax network the water droplets will become part of. Therefore the material properties of different wax blends will be investigated before a wax blend is turned into an emulsion.

5.2.1 Effect of Wax concentrations on Material Properties

The effect of both CW and MW concentrations on material properties was investigated. Four samples for each continuous phase blend (containing castor oil (40 – 95 wt %), CW (0 – 20 wt %) and MW (0 – 20 wt %).) were compressed using a texture analyser. The force/distance data was then converted into true stress and true strain (see section 3.4.6). The bulk modulus, Young's Modulus and point of fracture were then determined using the method described by Norton *et al*. (2011).

5.2.1.1 Effect of Carnauba Wax

Figure 5.1 shows the relationship between CW concentration and bulk modulus, Young's Modulus and point of fracture. For all three parameters, as the percentage of CW increases from 5 % to 20 %; Young's modulus, bulk modulus and point of fracture increase from 0.001 – 0.040, 0.01 – 0.22 and 0.001 – 0.018 M Pa respectively.

The increase in Young's modulus is similar to the relationship observed by Li (2002) for polymer gels. Li showed power law dependencies ($10^{3.03}$) of methylcellulose in water as the concentration of methylcellulose increased above 1 wt %. This indicated greater links forming between the methylcellulose molecules. In order to determine the cross linked nature within the wax crystal network a log plot of Young's modulus

versus concentration of wax was plotted. Figure 5.2 shows that the Young's modulus increases as a function of wax concentration. This follows a power law relationship (~3), which is indicative of a stronger wax network being formed as greater connections between wax crystals can occur (see section 2.5.4.1.2), these findings are similar to the work published for polymer gels. Nakayama *et al*. (2004) showed that by increasing the amount of cross-linking, the modulus increases, indicating a critically-crosslinked network. This behaviour has also been observed in fat crystal networks, with various studies showing that the hardness of a fat crystal network follows a power law relationship in regard to the solid fat content (Narine and Marangoni, 1999b, Haighton, 1976, Narine and Marangoni, 1999a). CW consists of a complex mixture of high molecular weight esters of acids and hydroxyacids (Lacerda *et al.*, 2011). Thus, by increasing the CW concentration the intrinsic bonding (*e.g.* hydrogen bonding and Van der Waals interactions) between crystals can increase, providing greater connections, which strengthens the network.

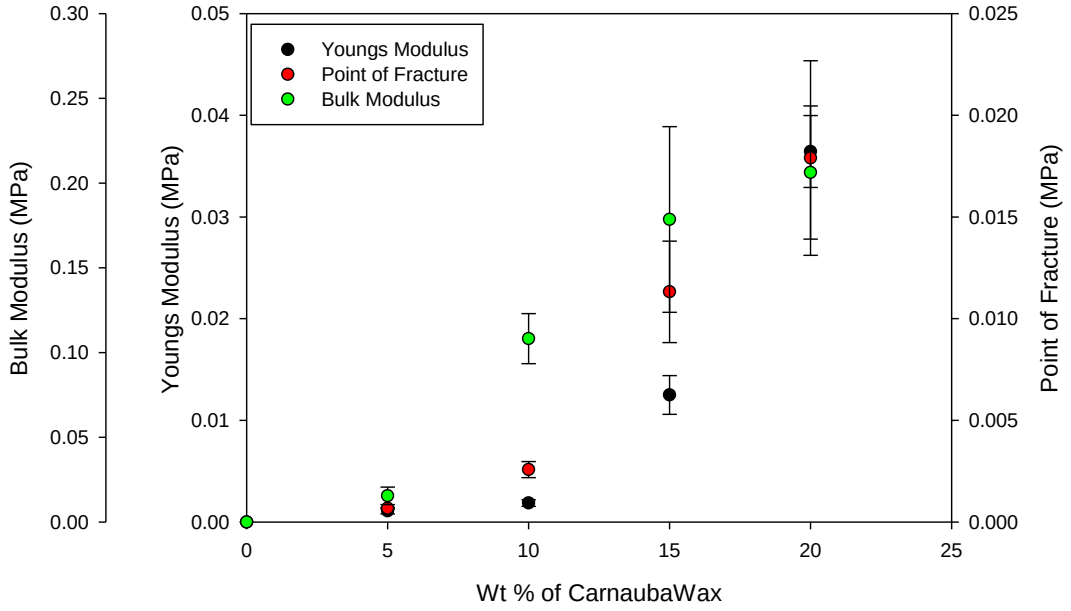

Figure 5.1 – Bulk Modulus, Young's Modulus (MPa) and Point of Fracture (MPa) of varying carnauba wax concentrations in castor oil. All samples were melted and stirred using a magnetic stirrer until molten (~ 30-40 minutes) and cooled quiescently in the freezer until solid then measured at a compression rate of 1 mm/s at 32 °C.

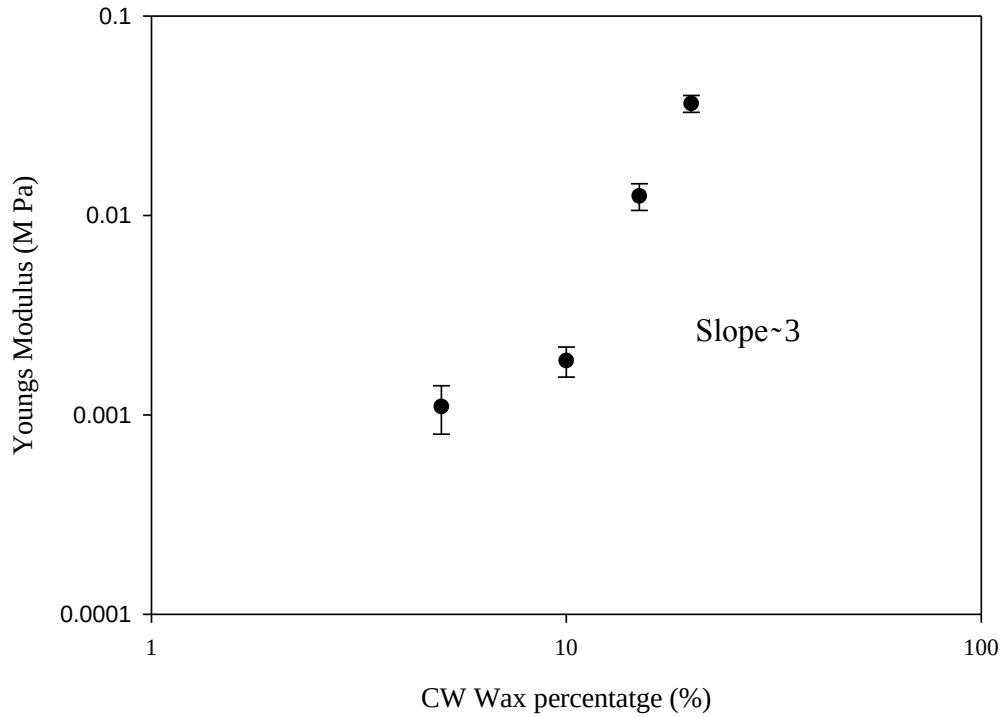

Figure 5.2 - Dependence of Young's Modulus on carnauba wax (CW) concentration (wt %). The solid line is a fit to represent the power law dependence.

5.2.1.2 Effect of Microcrystalline Wax

During the moulding process, samples prepared with only MW were too soft to be removed from the mould required to conduct the experiment. Therefore, 5 wt % CW was added to 5 – 20 wt % MW to investigate the effect of MW on material properties. Figure 5.3 shows a negative correlation with increasing the MW content from 5 wt % to 20 wt % for Young's modulus (0.005 – 0.001 MPa, R^2 = 0.97), point of fracture (0.005 – 0.002 MPa, R^2 = 0.97) and bulk modulus (0.14 – 0.05 MPa, R^2 = 0.95) (lines emitted from Figure for clarity).

MW is a compound of a mixture of linear, branched and cyclic alkanes (Petersson *et al.*, 2008). Petersson *et al.* (2008) stated that due to the large amount of branched and naphthenic hydrocarbons in MW's, they mainly form small irregular crystals during crystallisation. These irregular crystals were shown to disrupt the strength of the crystal network resulting in a weaker structure (Petersson *et al.*, 2008). This disruption of the crystal network can also be observed by a shift in the onset temperature for melting which is reported in (Table 4.6). As MW concentration increases from 5 wt % - 20 wt % the melting onset temperature shifts from 33 – 23 °C. This behaviour agrees with work conducted on dental waxes which shows that MW weakens the crystal network structure (McCabe and Wallis, 2008). It should be noted that when samples containing 5 % CW are compared to ones with 5 % CW and 5 % MW, the bulk modulus increases from 0.002 to 0.004 MPa. This is attributed to an increase in solid wax being added to the system.

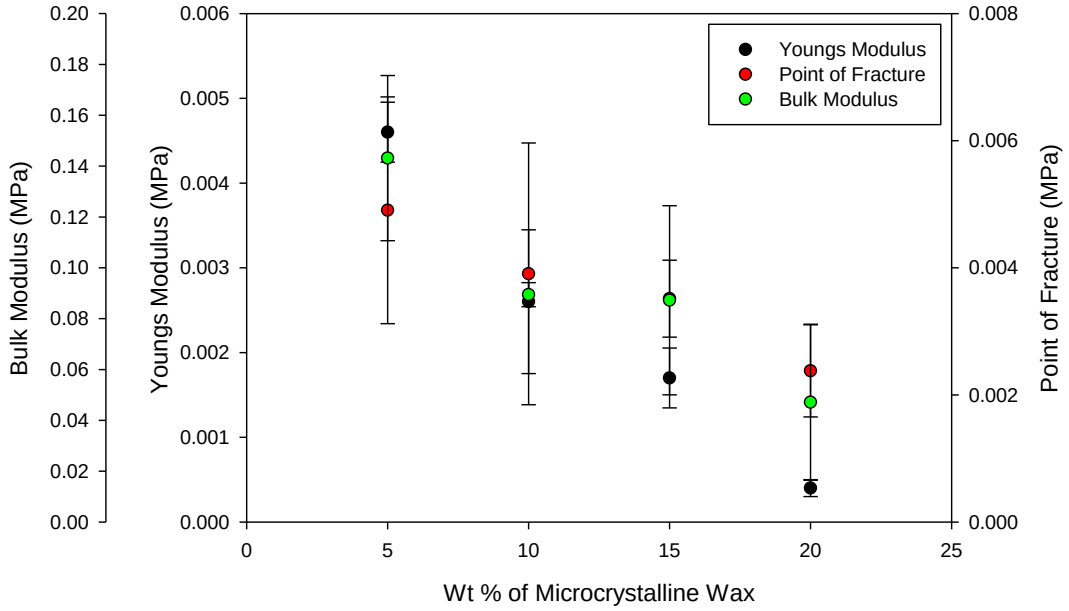

Figure 5.3 - Young's Modulus (MPa), point of Fracture (MPa) and Bulk modulus (MPa) of wax blends containing 5 – 20 % microcrystalline wax and 5 % carnauba wax in castor oil. All samples were melted and stirred using a magnetic stirrer until molten (~ 30-40 minutes) and cooled quiescently in the freezer until solid then measured at a compression rate of 1 mm/s at 32 °C.

5.2.2 Effect of Incorporating Water on Material Properties

In order to produce an emulsion based lipstick it is important to consider the effect that incorporating water into the microstructure has on the material properties.

Figure 5.4 shows that the introduction of water droplets into the formulation reduces the Young's modulus from 0.03 – 0.0015 MPa, decreases the point of fracture from 0.003 to 0.001 MPa and decreases the bulk modulus from 0.09 – 0.03 MPa. The reductions observed for these parameters could be due to several factors; (1) variation in water droplet size as the aqueous phase volume increases, (2) an increase in water droplets (soft filler particles) resulting in greater defects within the microstructure, (3) wax crystals moving to the W/O interface as the amount of interface increases and (4) an overall reduction in the solid wax content.

Pal (1996) investigated the effect of droplet size on the rheology on both W/O and O/W emulsions. Pal showed that by increasing the droplet size of the aqueous phase

volume (4 – 30 μm) in a W/O emulsion, the storage moduli decreases from ~ 0.003 - ~ 0.0002 MPa (Pal, 1996). Pal's findings are to be expected, as larger droplets can act as bigger defects which will affect the overall material properties. In order to determine whether the reduction in Young's modulus (shown in Figure 5.4) is caused by a variation in droplet size, the average droplet size ($d_{3,2}$) was calculated using restricted NMR diffusion. These results have been previously shown in Table 4.2, where the average $d_{3,2}$ was ~ 2.7 μm. Therefore the reduction observed in Young's modulus must be caused by increasing the amount water (soft filler particles) into the microstructure, wax crystals moving from the continuous network to the W/O interface and/or an overall reduction in the solid wax content.

Soft fillers have been shown in the literature to affect the material properties of pre existing colloidal mixtures. Shrinivas *et al. (2009)* investigated the effect of using a soft filler particle (soy bean oil) on the material properties (storage moduli) of a gel formed using 1 % agarose and 10 % gelatin. Results showed that as the concentration of soy bean oil increased from 0 – 30 % the moduli decreased from 0.006 – 0.003 MPa (Shrinivas *et al.,* 2009). Shrinivas's results support the findings in this work that show the reduction in Young's modulus (0.0026 to 0.0014 M Pa) is a result of water droplets being added to the microstructure. However Figure 5.4 shows that by increasing the aqueous phase volume the Young's modulus does not drastically change. This indicates that there is limited change within the microstructure as the aqueous phase volume increases. It should be noted that the Young's modulus is the first linear region on a true stress- true strain curve, this is a very small region when the material is compressed using uni axial compression. Therefore the effect of increasing phase volume was investigated further using oscillation rheology (to provide a greater insight into the link

between the dispersed phase and the continuous phase). This will be discussed in section 5.2.2.2.

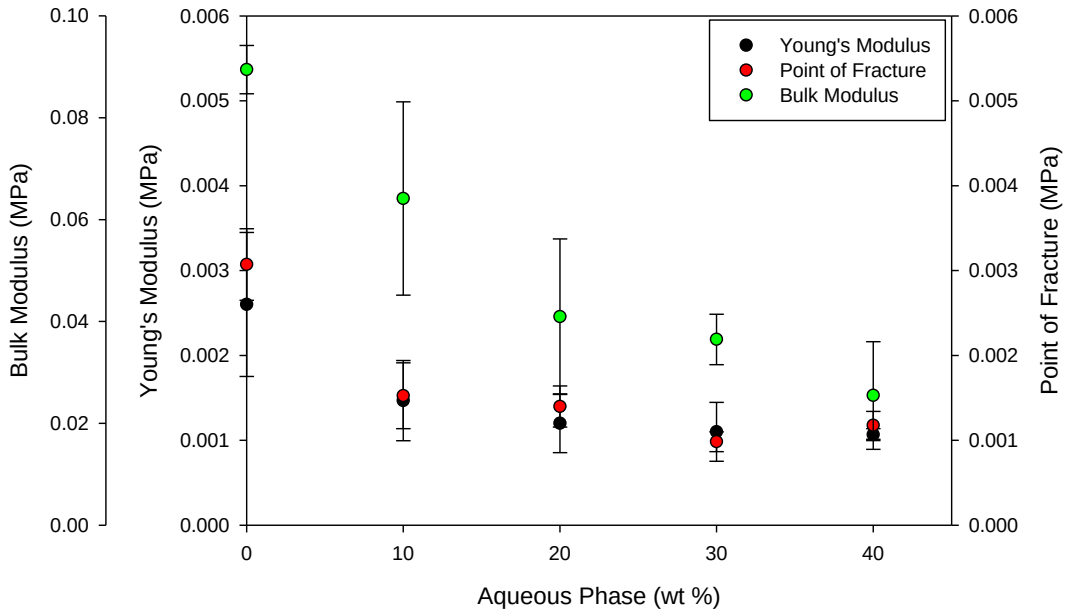

Figure 5.4 - Young's Modulus, Point of Fracture and Bulk modulus (MPa) of emulsions containing 2 wt % PGPR (overall weight %) as a function of aqueous phase volume (10 – 40 wt %), where the continuous phase contains 5 % carnauba wax and 10 % microcrystalline wax in castor oil. All emulsions were produced using a Silverson high shear mixer (for 5 minutes and at ~10,000 rpm) and cooled quiescently in the freezer until solid and measured with a compression rate of 1 mm/s at 32 °C.

5.2.2.1 Effect of adding paraffin wax and performalene to the continuous phase

Two further waxes, paraffin and performalene were added to the continuous phase formulation to investigate their effect on the overall mechanical properties of the emulsion. Performalene is a polyethylene based molecule that forms small crystals (Harris and Butterworth, 2013), which may allow an increase in the number of interactions in the wax network. Hard paraffin is a straight chain hydrocarbon (Wang *et al.*, 2008) and was selected as previous literature has shown that paraffin increases the strength of emulsions, by producing large crystals which will not travel to the W/O interface, resulting in a stronger continuous wax network (Le Révérend *et al.*, 2011b).

When Figure 5.4 (emulsions containing CW and MW's) is compared to Figure 5.5 (emulsions containing CW, MW and paraffin or performalene), it shows an increase in Young's modulus, point of fracture and bulk modulus with the addition of solid wax (particularly performalene (Figure 5.5a)). For emulsions containing 10 wt % aqueous phase the addition of performalene increases the Young's Modulus from ~ 0.003 to ~ 0.005 MPa, the point of fracture from ~ 0.001 to ~ 0.005 MPa and the bulk modulus from 0.09 – 0.13 MPa, indicating a stiffer and stronger emulsion. It should be noted that the emulsions containing 10 wt % aqueous phase and performalene are stronger than the control without performalene (*i.e.* the non-emulsified bulk wax system): the Young's moduli are ~0.005 and ~0.0038 MPa, respectively, the points of fractures are ~0.005 and ~0.003 MPa, respectively and the bulk moduli's ~0.13 and ~0.09 MPa respectively. The samples containing 20 and 30 wt % aqueous phase and performalene are more similar to the control formulation (containing 5 % CW and 10 % MW in castor oil) in terms of Young's Modulus, point of fracture and bulk modulus, but there is some weakening of the structure for samples containing 40 wt % water when compared to the control formulation (Figure 5.4)

The droplet size for all emulsions produced (regardless of wax ratios) were similar (in the range of 2 - 4 μm), therefore, it is thought that performalene produces a greater number of interactions in the wax network resulting in an emulsion that is more resistant to compression, up to a point where the number of droplets (*i.e.* 'defects') increases and reduces the mechanical strength of the crystal network structure.

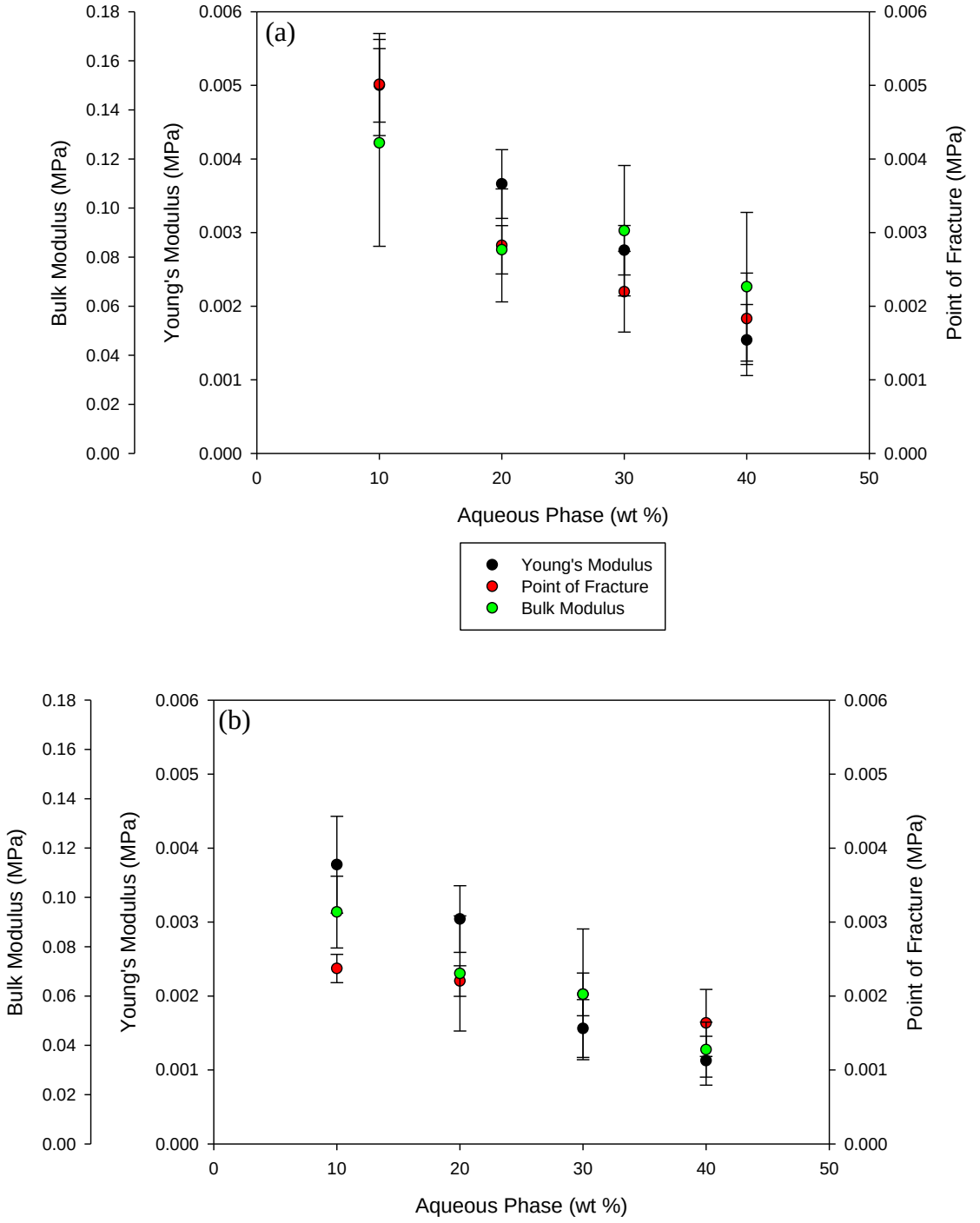

Figure 5.5 - Young's modulus, Point of Fracture and Bulk modulus (MPa) of emulsions containing 2 wt % PGPR (overall weight %) as a function of aqueous phase volume (10 – 40 wt %) where the continuous phase contains 5 % carnauba wax and 10 % microcrystalline wax, and either (a) 5 % performalene or (b) 5 % paraffin. All emulsions were produced using a Silverson high shear mixer and cooled quiescently in the freezer until solid then measured at a compression rate of 1 mm/s at 32 °C.

Overall, these results show that the introduction of water lowers Young's Modulus, point of fracture and bulk modulus resulting in a weaker structure. This observation concurs with previously reported data on lipsticks and foods, which showed that the introduction of water droplets decreases strength (Wang and Lee, 1997, Vereecken *et al.*, 2010). However, Wang and Lee reported that when the water content was increased from 5 to 15 wt % the strength increased (Wang and Lee, 1997). The results obtained in this research (Figure 5.4) show that the Young's Modulus does not increase as water content increases from 10 – 40 wt %. As previously stated (section 5.2.2) the Young's modulus is the first linear region of a true stress- true strain curve, this is a very small region when the material is compressed using uni axial compression. Thus limiting the possibility of analysing the interaction between crystals (weak link regime (see section 2.5.4.1.2)). Therefore in order to assess the interaction between wax crystals within the network, the rheological properties of the emulsion will now be discussed.

5.2.2.2 Rheology of Emulsions

Oscillatory rheology was conducted on emulsions with varying aqueous phase volumes (10 – 40 %) and with differing continuous phase formulations (5 % CW, 10 % MW and with the addition of either 5 % performalene or 5 % paraffin). Previous results (Figure 5.4) have shown increasing the aqueous phase volume did not affect the Young's modulus. Both the elastic modulus (G') and the viscous modulus (G") were investigated directly after the emulsion was chilled in freezer. The literature has shown that by increasing the number of crystals, a more rigid network is produced (Le Révérend *et al.*, 2011a). Therefore, G' (*i.e.* solid-like behaviour) should increase with the addition of crystalline material (paraffin and performalene). Figure 5.6 shows that there is a negative correlation between aqueous phase volume and G' for all the waxes investigated. This is due to the solid wax content decreasing as aqueous phase volume

increases, resulting in fewer interactions between wax moieties. The addition of either paraffin or performalene increases G' (from 0.4 to 0.8 and 1.3 MPa respectively for 10 wt % aqueous phase) with performalene increasing G' by a greater amount for all aqueous phase volumes. This could be attributed to its ability to create interactions in the crystal network, therefore increasing the strength of the crystal network. The reduction in G' at greater aqueous phase volumes is caused by the surface area of the W/O interface increasing with increasing aqueous phase volume, resulting in crystals from the continuous network moving to the interface during cooling (Le Révérend *et al.*, 2011b). As a result a rigid crystal network cannot be formed. When Figure 5.7 is compared to Figure 5.6 it shows that for all emulsions tested, G' is greater than G'' indicating that the emulsion behaves more like a solid. On further analysis of both G' and G'', the phase angle (δ) can be calculated. Figure 5.8 shows that as the aqueous phase volume increases (from 10 – 40 wt %), δ increases from 5 to 15°**.** It is known that if the phase angle is between 0 – 90° then the material can be classified as viscoelastic (Tabilo-Munizaga and Barbosa-Cánovas, 2005). From Figure 5.8 we can conclude that for all aqueous phases studied the emulsion behaves viscoelastically, however, at higher aqueous phase volumes the emulsion behaves slightly more viscously. This can be attributed to the fact that the extent of the continuous phase crystal network decreases as water content increases. This is likely to be caused by a combination of 1) an increase in the number of droplets (and thus the area of the W/O interface) with increasing aqueous phase volume, creating an greater number of defects in the structure and 2) movement of crystals from the bulk to the interface, weakening the network.

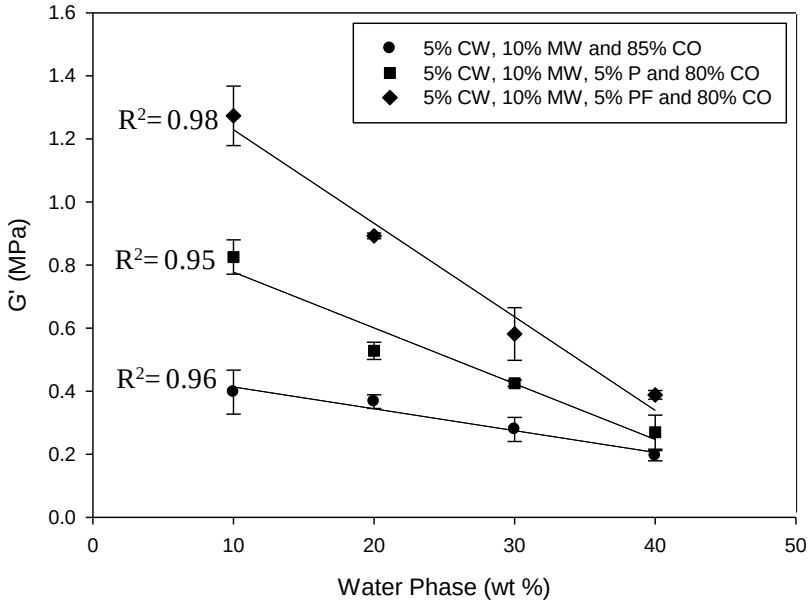

Figure 5.6 - G' (MPa)) as a function of aqueous phase volume for emulsions containing 2wt% PGPR, where the continuous phase contains 5 % carnauba wax (CW) and 10 % microcrystalline wax (MW) (●), and either 5 % paraffin (P) (■) or 5 % performalene (PF) (◆) in castor oil. All emulsions were produced using a Silverson high shear mixer and cooled quiescently in the freezer until solid and measured *via* oscillation rheology. G' value taken at a strain of 1.4 x 10^-5 and a frequency of 5 Hz.

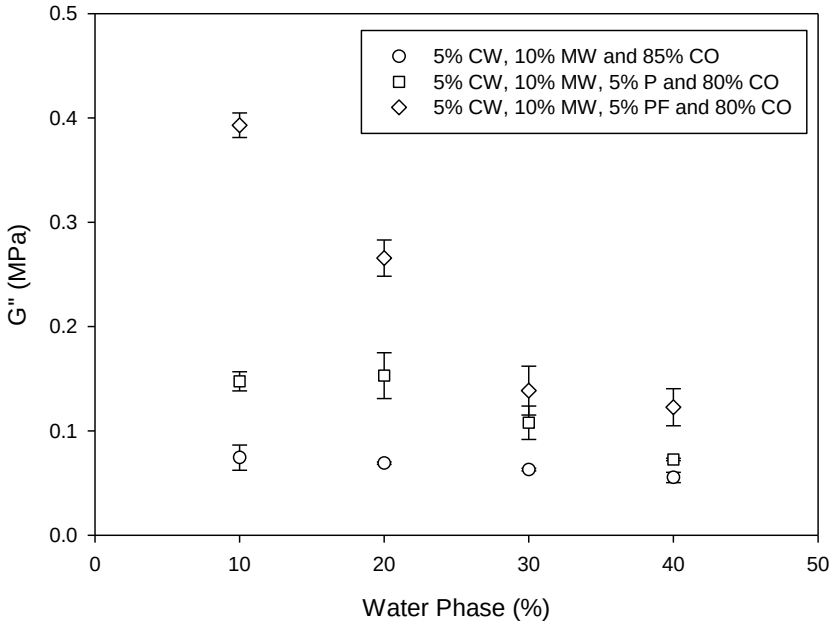

Figure 5.7 - G'' as a function of aqueous phase volume for emulsions containing 2wt% PGPR, where the continuous phase contains 5 % carnauba wax (CW) and 10 % microcrystalline wax (MW) (○), and either 5 % paraffin (P) (□) or 5 % performalene (PF) (◇) in castor oil. All emulsions were produced using a Silverson high shear mixer and cooled quiescently in the freezer until solid and measured *via* oscillation rheology. G' value taken at a strain of 1.4 x 10^{-5} and a frequency of 5 Hz.

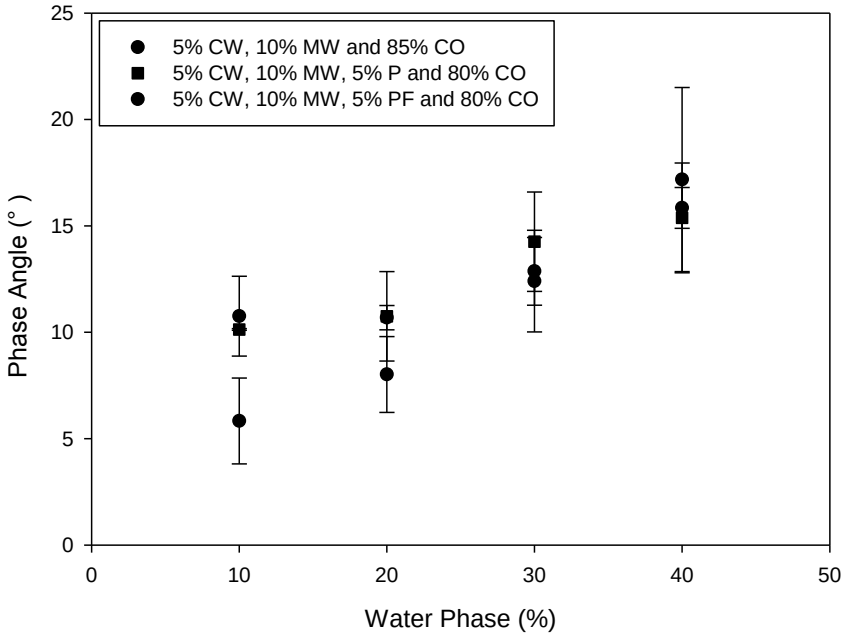

Figure 5.8 - Phase angle As a function of aqueous phase volume for emulsions containing 2wt% PGPR, where the continuous phase contains 5 % carnauba wax (CW) and 10 % microcrystalline wax (MW) (●), and either 5 % paraffin (P) (■) or 5 % performalene (PF) (◆) in castor oil. All emulsions were produced using a Silverson high shear mixer and cooled quiescently in the freezer until solid and measured *via* oscillation rheology.

5.2.3 Effect of a continuous process

For the final part of this chapter, the effect of a continuous production process on the material properties of an emulsion based lipstick was investigated. In previous sections of this chapter, all emulsions were produced using a batch process (Silverson high shear mixer) where the operating temperature was greater than the crystallisation temperature of the continuous phase formulation. In this section the use of a scraped surface heat exchanger (SSHE) and pin stirrer (PS) (as described in 3.3.2.2) were investigated as they allow for greater control of the crystallisation process. Specifically, the effect of processing conditions, including flow rates, jacket temperatures and impeller rotational velocities (IV) on material properties was investigated. The melting and crystallistion behavior of the continuous phase was shown in Figure 4.4, which demonstrated that crystallisation starts at ~ 60 °C and continues until ~20 °C. As a result

temperatures were chosen (55, 60, 65 and 80 °C) that would deliver different levels of crystallisation in the process. At 80 °C there is no crystallisation in the process, whereas at temperatures below 65 °C, crystallisation can occur during processing. It is important to note that at temperatures below 55 °C the formulation solidifies during processing which results in pipe blockages preventing manufacture of emulsions. The material properties of the emulsion were initially assessed by measuring the bulk modulus and point of fracture under uniaxial compression. Uniaxial compression was chosen, as a current test at Alliance Boots for measuring the rigidity of a new lipstick involves simple compression between the thumb and forefinger. Therefore, the use of uniaxial compression technique allows quantitative assessments of samples. Secondly, the elastic modulus of emulsions produced using various processing parameters were assessed using oscillatory rheology. Material testing was conducted for emulsions which passed either through the SSHE only or both the SSHE and PS.

5.2.3.1 Uniaxial Compression

Pre-emulsions containing 10 % aqueous phase, 88 % continuous phase (5 % CW and 10 % MW in castor oil) and 2 % PGPR were passed through a SSHE or a SSHE and PS (these also included 5 % paraffin in the continuous phase) to form an emulsion based lipstick. These were then analysed *via* uniaxial compression to measure both the bulk modulus and the point of fracture. In work done by Wang and Lee (1997), the hardness of a lipstick was linked to the force required to fracture the lipstick (Wang and Lee, 1997). Therefore the point of fracture was measured for lipstick emulsions to understand the effect of processing parameters on the hardness of the emulsions.

Figure 5.9 shows all results as a function of exit temperature. Figure 5.9a and b show that for emulsions produced with the SSHE only, there is little or no change in the bulk modulus (~0.020 - 0.025 MPa) and point of fracture (~0.002 - 0.0025 MPa) as the

temperature increases from ~ 60 to 75°C, regardless of the IV**.** It is important to note that the emulsions formed at 55°C were too soft to be analysed with the texture analyser. This could be due to smaller wax crystals being produced at lower temperatures resulting in more nucleation sites and consequently less crystal growth (the viscoelastic properties of all samples will be discussed later). As previously shown section 4.2.1.2, varying the temperature between 60 and 75°C modifies the emulsion droplet size in the range of ~ 2 – 20 μm. One would expect these changes to affect the material properties, however, these changes in droplet size do not seem to affect either the bulk modulus or point of fracture of emulsions produced through only the SSHE unit. More surprisingly, both parameters are not affected by any modification in the wax network formed in the continuous phase by wax crystals. Crystals formed within a SSHE unit are more likely to be smaller than the ones produced in post production, due to (i) the mechanical action of the scraping blades and (ii) a higher cooling rate in the SSHE unit (Campos *et al.*, 2002). It is expected that different crystal sizes within the continuous phase of emulsions form under different processing conditions, which would allow a variety of network structures within the continuous phase. One would think that these structural differences would impart different material properties on the emulsions. However, no evidence was found regarding this hypothesis through compression testing. This could be a result of uniaxial compression testing being too destructive to show differences in crystal interaction (intrinsic bonding between crystals). Once again oscillatory rheology (within the linear viscoelastic region) was undertaken to investigate the differences in wax networks produced under different processing conditions (see section 5.2.3.2)

Emulsions formed with both units display different mechanical properties (Figure 5.9 c and d). It is observed that for high IV and low exit temperatures, the PS reduces

the bulk modulus (from ~ 0.2 – 0.05 MPa) and point of fracture (From 0.008 – 0.003 MPa). With these conditions the interactions between crystals are broken resulting in a weaker network. At higher temperatures (~80 °C), interactions between crystals will be broken and melted and then reform during post-production crystallisation.

For the range of temperatures studied, the bulk modulus does not seem to depend on the shaft speed of the PS unit (this was also observed when the shaft speed of the SSHE was set up to 1,500 rpm – see Appendix 2). It was previously shown (Figure 4.8) that for a given jacket temperature, emulsion droplet size decreases by increasing PS shaft speed. I conclude here that in this range of droplet sizes (5 – 17 μm), the bulk modulus does not depend on the size of the droplets formed in the process. This is supported by the observation made for the SSHE unit; even though the droplet size depends on the shaft speed of the SSHE unit (section 4.2.1.2.1), no difference is observed in the emulsion point of fracture or bulk modulus.

One would then think that the point of fracture and bulk modulus is a function of the crystals size formed during emulsification and post production cooling. This seems to differ with the results found for the SSHE unit only (Figure 5.9a and b). However, the point of fracture and bulk modulus are measures of the bulk properties, whereas the difference in wax crystal network could be based on the intrinsic connections between crystals. Therefore once again oscillatory rheology was conducted to investigate the wax network properties. It is important to note this information could be calculated from the existing curves of True stress/True strain (Norton *et al.,* 2011). However the first region of linearity (Young's modulus) was extremely difficult to measure from these curves.

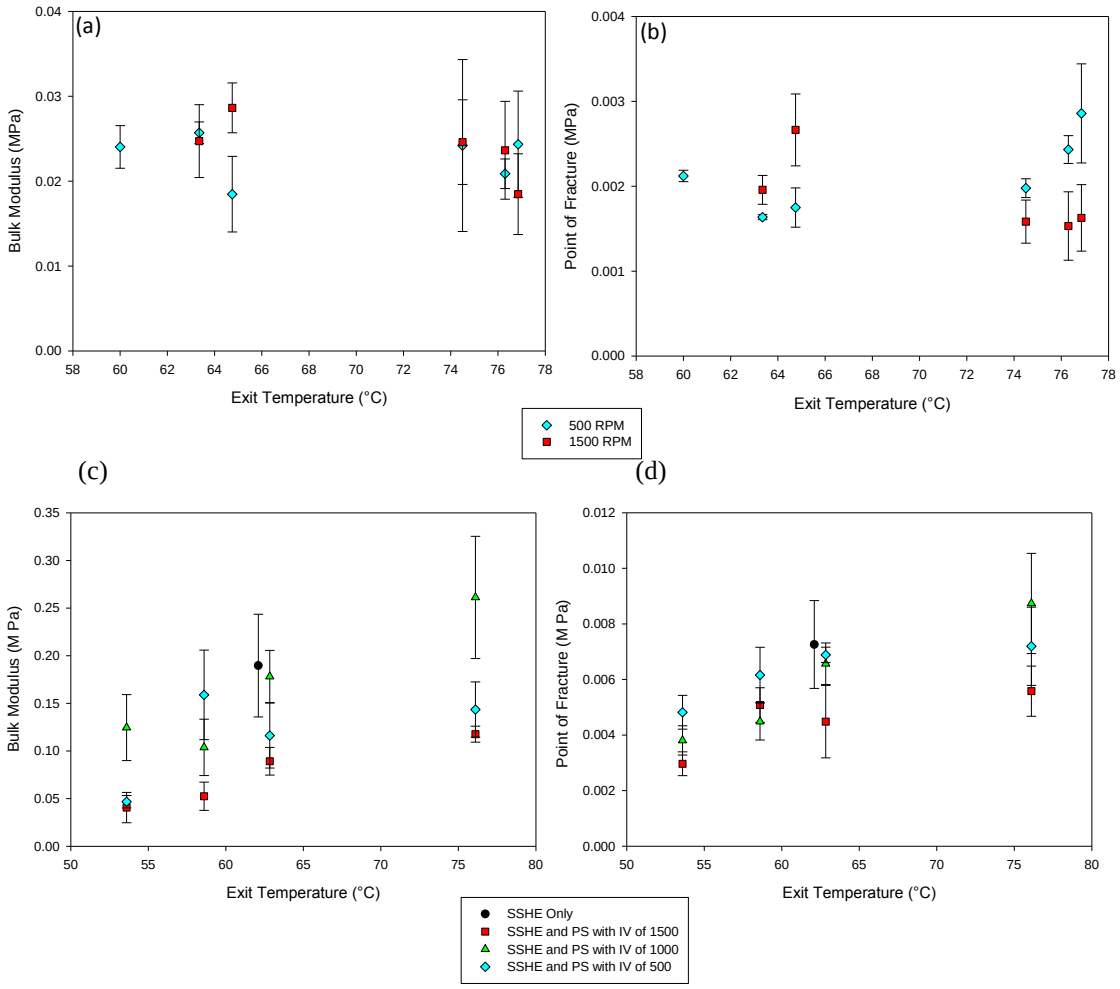

Figure 5.9 - Bulk modulus and point of fracture as a function of exit temperature for 10 % W/O emulsions (where the continuous phase consisted of 5% CW and 10% MW and 5% P in castor oil) passed through the SSHE only ((a) and (b)) and both the SSHE (IV = 500 rpm) and PS ((c) and (d)), at various shaft speeds. Flow rate was fixed at 60 mL/min. All samples were cooled quiescently in a freezer until solid then tested with a compression rate of 1 mm/s at 32°C.

5.2.3.2 Characterisation of the elastic properties of emulsion-based lipstick

5.2.3.2.1 Effect of SSHE on Elastic Modulus

As previously mentioned it was expected that a SSHE would affect the material properties of the resulting products. Previous results in this work have shown no significant difference when determining the bulk modulus and point of fracture (Figure 5.9 a and b). Therefore the viscoelastic properties were assessed by measuring the

elastic modulus *via* oscillation rheology. Once again an initial amplitude sweep was conducted in order to determine the linear viscoelastic region.

Results for SSHE only at various impeller rotational velocities (500 and 1,500 rpm) are shown in Figure 5.10, where the elastic modulus is plotted as a function of the exit temperature (It is important to note that additional jacket temperatures were measured as initial findings showed a trend which required further investigation). As observed for the point of fracture and bulk modulus, there is no effect of the impeller rotational velocities on the elastic modulus. Nonetheless, the elastic modulus of the emulsion, hence emulsion elasticity (Norton *et al.*, 2011), demonstrated a strong dependence on the exit temperature; the elastic modulus showed a maximum at 68°C (~ 0.12 MPa) and is lowest (~ 0.02 MPa) at either 55°C or 75°C. As previously stated, varying the temperature affects both the emulsion droplet size and the formation of crystals. Evidence has been found in the literature regarding the effect of emulsion droplet size on the elastic modulus (Pal, 1996); Pal showed that a decrease in droplet size resulted in a dramatic increase in the elastic modulus. In order to investigate this reported behaviour, the elastic modulus was plotted as a function of emulsion droplet size (Figure 5.11). In general, G' seems to slightly increase with the droplet size, which opposes Pal's findings. But more interestingly, for a given droplet, the elastic modulus varies. For example, at 5 μm, elastic modulus varies from ~ 0.01 MPa to ~ 0.09 MPa, depending on the flow rate and the impeller rotational velocity. It can be concluded from these experiments that the change in emulsion droplet size is not the main parameter affecting the emulsion elasticity in lipstick emulsions.

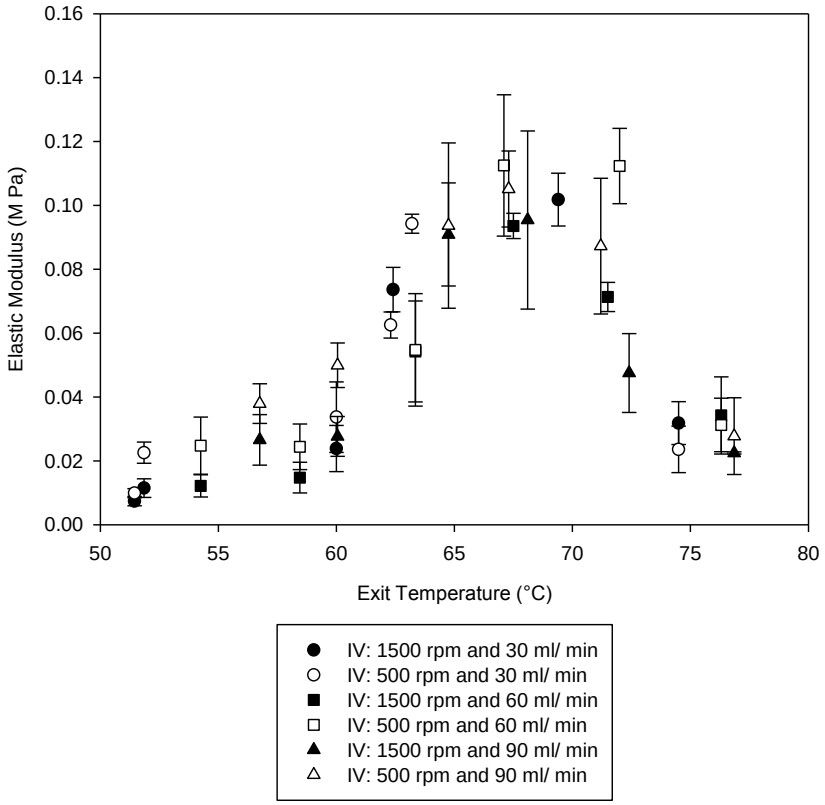

Figure 5.10 - Elastic modulus G' as a function of exit temperature for 10 % water-in-oil emulsions (where the continuous phase consisted of 5% CW and 10% MW in castor oil). All samples produced using various processing conditions (● is 30 mL/min, ■ is 60 mL/min and ▲ is 90 mL/min; shaft speed was adjusted at either 500 rpm (open symbols) or 1500 rpm (full symbols)). All samples were produced using a SSHE unit and cooled quiescently in the freezer till solid and measured *via* oscillation rheology and G' taken at a frequency of 5 Hz.

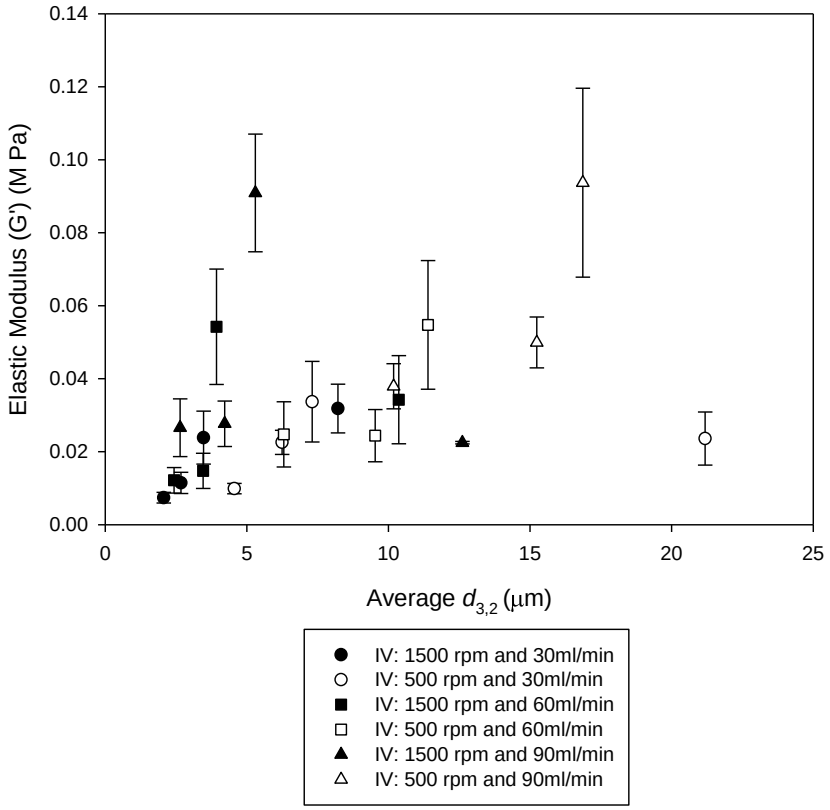

Figure 5.11 - Elastic modulus of 10 % W/O emulsions (where the continuous phase consisted of 5% CW and 10% MW in castor oil) formed at various temperatures in the SSHE unit as a function of (a) droplet diameter (● is a flow rate of 30 mL/min, ■ 60 mL/min and ▲ is 90 mL/min; shaft speed was adjusted at either 500 rpm (open symbols) or 1500 rpm (full symbols)). All samples were produced using a SSHE and cooled quiescently in the freezer till solid and measured *via* oscillation rheology and G' taken at a frequency of 5 Hz.

The other emulsion structural parameters affected by the exit temperature is the number and size of crystals present in the continuous phase. If these are to modify emulsion elasticity, it would be expected that the G' of the continuous phase only (without water droplets) which passes through the SSHE unit would react in a similar manner as the emulsion does, to exit temperature changes. However, by comparing Figure 5.12 with Figure 5.10, it becomes evident that temperature affects emulsion and continuous phase elasticity differently; the elastic modulus of the continuous phase only increases with temperature to reach a maximum of ~ 0.3 MPa at 75°C. As previously mentioned, a greater number of smaller crystals are formed in the SSHE chamber at low temperature, due to more nucleation sites being formed at lower temperatures (Campos

et al., 2002). Larger crystals are formed post production during emulsion cooling as this has a higher cooling rate (Beri *et al.*, 2013, Campos *et al.*, 2002). At high temperatures (largely above crystallisation temperature), wax crystals are only formed during post production. It is suggested here that the formation of large crystals contributes to the production of a stronger network in the continuous phase resulting in a higher continuous phase elasticity. This behavior is similar to that observed by Kim and Bush (1999) for work on nanocrystalline structures. They showed that as crystal size increased from 20 to 80 nm, the elastic modulus increased from 115 – 135 GPa (Kim and Bush, 1999). It is important to note that the G' of the emulsion is lower than that of the continuous phase only, as the inclusion of water weakens the overall network formulation. The difference in G' noticed between emulsion and continuous phase will be discussed.

At ~65°C, crystallisation occurs in the SSHE chamber and small crystals are formed. As mentioned in section 4.2.1.2.1, these small crystals have the ability to move quickly through the continuous phase, to adsorb at the oil/water interface to form Pickering water droplets (*i.e.* solid shells). It was shown by Le Révérend *et al.* that in presence of PGPR, wax crystals adsorbed at the interface, which then sinter to form a solid shell (hard shell) around the droplets (Le Révérend *et al.*, 2011a). Nonetheless, at this temperature, it is assumed that a large quantity of wax remained liquid at the exit of the SSHE unit, which crystallised in post production.

Emulsions formed at 65°C contain "hard shell like" water droplets and large crystals; this structure allows unique interaction between water droplets and the crystalline network, providing high elasticity to these emulsions. At higher temperatures, large crystals are unlikely to adsorb at the interface and the water droplet

acts as defects, lowering the emulsions elasticity. At low temperatures, the small crystals formed, can adsorb at the interface, but the reduced number of large crystals formed result in lower elasticity.

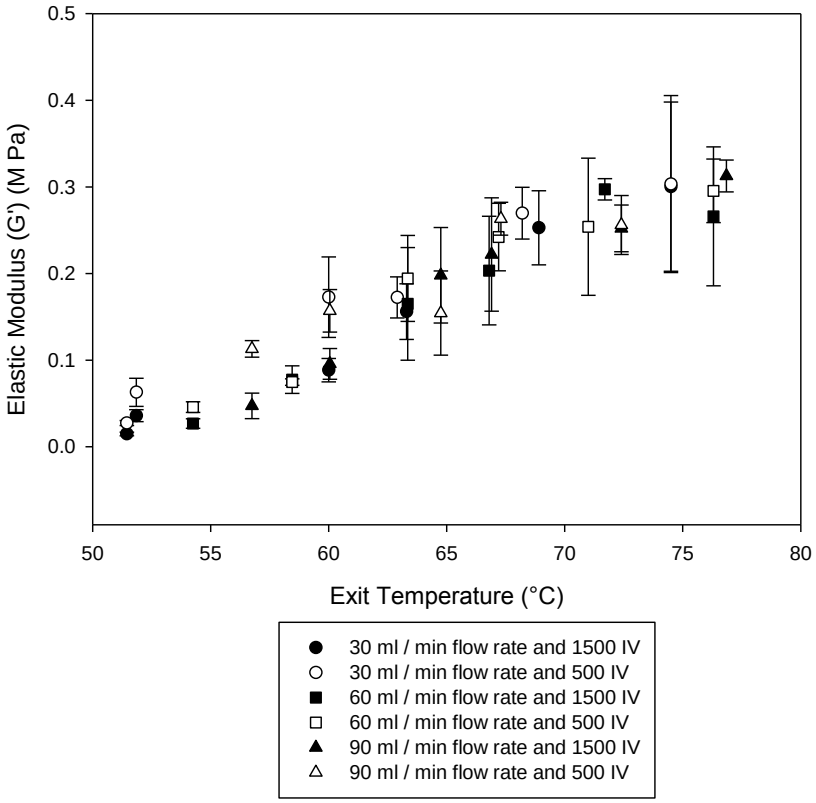

Figure 5.12 - Elastic modulus G' as a function of exit temperature for continuous phase only (consisting of 5% CW and 10% MW in castor oil). All samples produced using various processing conditions (● is 30 mL/min, ■ is 60 mL/min and ▲ is 90 mL/min; shaft speed was adjusted at either 500 rpm (open symbols) or 1500 rpm (full symbols)). All samples were produced using a SSHE unit and cooled quiescently in the freezer till solid and measured *via* oscillation rheology and G' taken at a frequency of 5 Hz.

It is hypothesised here that the interactions between "hard shelled" water droplets covered by small wax crystals and the large crystals is the mechanism by which the emulsion strength increases. This is only possible because of the adsorption and sintering of wax crystals at the interface. To test this hypothesis, glass balontini beads (~ 50 μm) were used to replace the water droplets. Glass beads play the role of "hard" water droplets, with the difference that wax crystals are unable to adsorb at the glass

surface. If the hypothesis is correct, the glass beads will not be incorporated in the crystal network, which should result in different emulsion elasticity's with changes in SSHE jacket temperature. Figure 5.13 shows that the hypothesis was correct. Glass bead "emulsions" exhibit different behavior to water-in-oil emulsions, but show similar behaviour to the continuous phase only system (Figure 5.12); with elasticity increasing to a maximum at ~ 80°C.

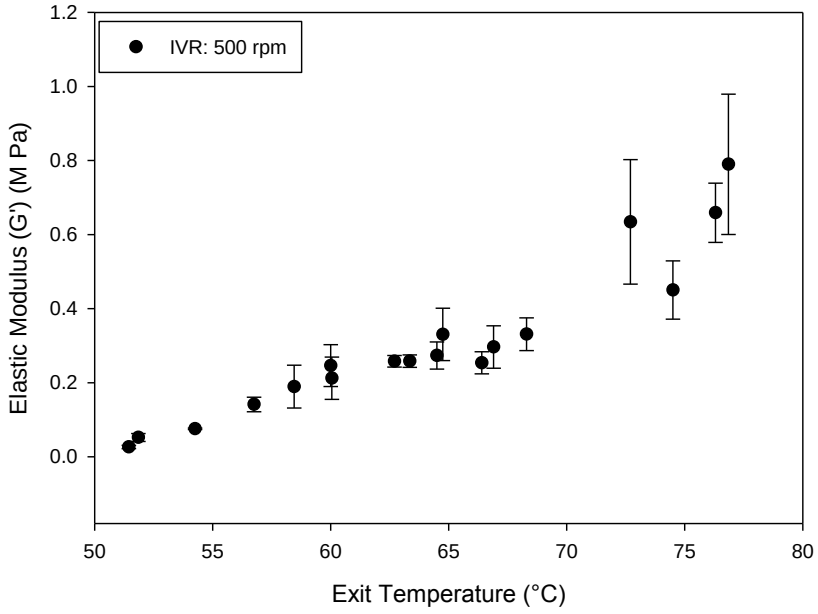

Figure 5.13 - Elastic modulus G' as a function of exit temperature for "emulsions" made with 10 % glass balontini beads instead of water. Continuous phase consisted of 5% CW and 10% MW in castor oil)All samples produced using various processing conditions (● is 30 mL/min, ■ is 60 mL/min and ▲ is 90 mL/min with a shaft speed of 500 rpm. All samples were produced using a SSHE unit and cooled quiescently in the freezer till solid and measured *via* oscillation rheology and G' taken at a frequency of 5 Hz.

It was previously stated that by modifying the temperature in the SSHE unit, the ratio between the number of crystals formed during or after emulsification changes. This was determined by measuring the elasticity of the final emulsion formed as a function of flow rate (Figure 5.14). By increasing the flow rate, emulsion G' increases for all temperatures except 80°C. This increase is due to the fact that fewer crystals are formed in the chamber, thus a greater number of large crystals are produced post

production, as the emulsion has a shorter residence time. At 80°C, all crystals are formed post production, it is then expected that the flow rate has no effect on the elasticity.

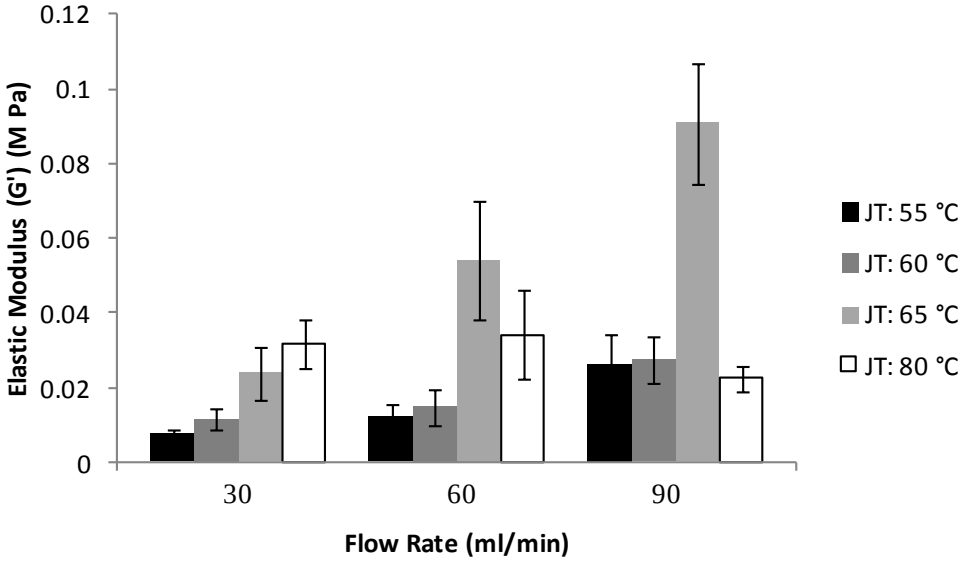

Figure 5.14 - Elastic modulus of 10 % W/O emulsions (where the continuous phase consisted of 5% CW and 10% MW in castor oil) formed at various temperatures in the SSHE unit as a function of flow rate. All samples were produced using a SSHE and cooled quiescently in the freezer till solid and measured *via* oscillation rheology and G' taken at a frequency of 5 Hz.

5.2.3.2.2 Effect of the PS on Elastic Modulus

The effect of the PS processing parameters on the elastic modulus of the formulation was investigated via oscillatory rheology. It is important to note that 5 % paraffin was added to the formulation as it was expected that the PS would disrupt a network resulting in a weaker network. Figure 5.15 shows that at exit temperatures below 65 °C the use of a PS (regardless of the IV) reduces G'. For example at an IV of 1500 rpm, G' is reduced from 0.3 – 0.05 MPa. It has previously been shown in this chapter that crystal interactions determine the G' of the network. Therefore at high IV and low temperatures

the shear of the impeller breaks connections between crystals resulting in a lower G' being measured. However, at higher temperatures G' does not seem to increase. This is due the formulation melting and re-crystallising allowing the connections between crystals to reform. Polarised microscopy was used to visualise the effect on the microstructure. When a SSHE is utilised on its own (jacket temperature of 65 °C), small droplets coated in Pickering particles in a wax network can be observed (Figure 5.16a). When the emulsion was passed through a SSHE and a PS (at an IV -500 rpm and a jacket temperature of 55 °C), the impeller destroys the wax network resulting in numerous of Pickering particles that are not connected in a strong network (Figure 5.16 b). However when a high jacket temperature is used for the PS, the bulk can melt and re-crystallise creating a stronger network (Figure 5.16c).

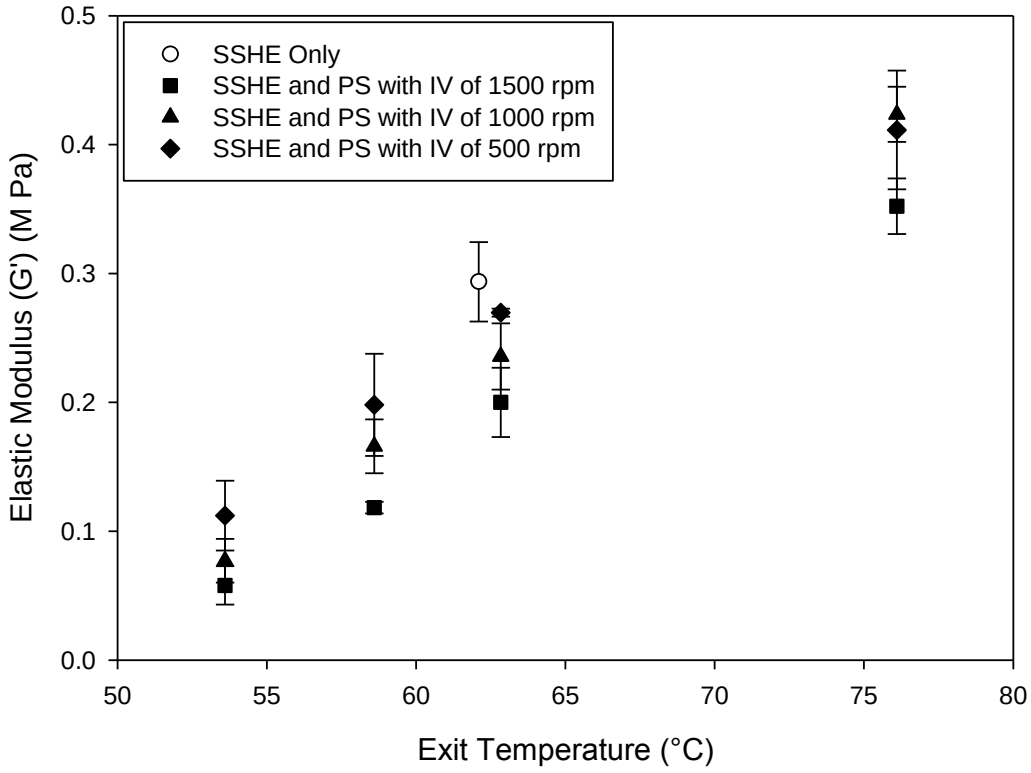

Figure 5.15 - Elastic Modulus (G') as a function of exit temperature under varying processing conditions (○ – SSHE only, ■ -SSHE and PS (impeller velocity (IV) of 1500 rpm, ▲- SSHE and PS (IV of 1000 rpm) and ◆ – SSHE and PS (IV of 500 rpm) All 10 % W/O emulsions (where the continuous phase consisted of 5% CW, 10% MW and 5% P in castor oil) passed through a SSHE at a Jacket temperature of 65 C and an IV of 500 rpm with an overall flow rate of 60 ml /min. They were then passed through a PS and cooled quiescently in the freezer until solid and measured *via* oscillatory rheology and G' taken at a frequency of 5 Hz.

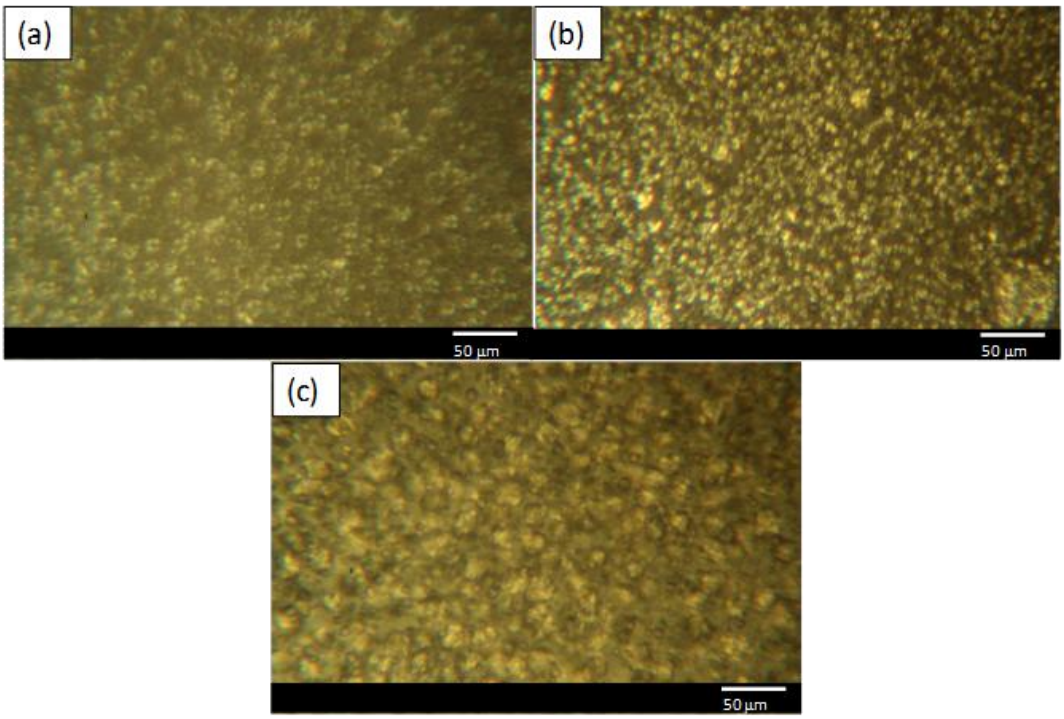

Figure 5.16 - Polarised Microscopy of W/O emulsions which have passed through; (a) SSHE only, (b) SSHE and PS (Impeller velocity (IV) – 1500 rpm and a jacket temperature (JT) of 55 °C) and (c) SSHE and PS (IV – 500 rpm and JT 80 °C). All utilise a flow rate of 60 ml/min

5.3 Concluding Remarks

In this chapter the material properties of wax based emulsion systems were investigated. These results showed that Young's modulus, point of fracture and bulk modulus increase with an increasing percentage of CW (which follows a power law dependency of 3), but decreases with an increasing percentage of MW. This suggests that the CW is part of the overall wax crystal network which is comprised of saturated components, whereas the MW forms irregular crystals that disrupt the overall wax crystal network. The Young's modulus, elastic modulus and viscous modulus all decrease with increasing aqueous phase volume. The slope of the decrease in elastic and viscous moduli is reliant on the addition of solid wax which strengthens the wax network. Although the addition of water droplets (2 – 4 μm) weakens the material

properties, the addition of either paraffin or performalene increases strength, this is more evident for the lower aqueous phase volume emulsions. In particular, the emulsions containing 30 % aqueous phase had very similar material properties to the non emulsified control system.

A lab scale scraped surface heat exchanger and pin stirrer were shown to be able to control the crystallisation of the emulsion during processing. In particular, the size of the crystals can be adjusted by controlling the temperature gradient between the emulsion and the inner walls of the SSHE chamber, as the ratio between large crystals formed in post production and small crystals formed during processing by adjusting the flow rate through the unit. Due to the greater control over wax crystallisation the emulsion microstructure and material properties can be selected. In particular, hard lipsticks can be formed while containing small water droplets coated in small wax crystals, which allows interactions to be formed with the larger wax crystals in the continuous phase.

Chapter 6. Use of a dynamic tribological technique for investigating the lubricating properties of solid wax based emulsion systems with a sensory comparison

6.1 Introduction

Designing solid wax stabilised emulsions which could provide moisture to the lips is one of the key aims of this project. When designing such emulsions it is important to consider the impact of water incorporation on the lubricating properties of an emulsion based lipstick. Tribology has been used in both the food (Malone *et al.*, 2003, Dresselhuis *et al.*, 2008, Prinz and Lucas, 2000) and cosmetic industry (Timm *et al.*, 2011) to study the lubricating properties of both W/O and O/W liquid emulsion systems which provides an insight into how samples are perceived by the consumer (de Wijk and Prinz, 2005, Mills, 2011)). For example; in the food industry Chojnicka-Paszun *et al.* (2012) compared the frictional behavior of increasing fat content in milk and related the findings to perceived creaminess (obtained using a sensory panel). They found a linear correlation between perceived creaminess and friction was obtained when the fat content was above 1 wt %. However, to the author's knowledge there has been no work done on investigating solid formulations in a tribometer. Therefore the aim of this work was investigate the possibility of using a pin-on-disk tribometer set-up to examine the lubricating properties of solid wax based emulsion systems. After which, a small sensory study was conducted to allow comparison between tribological results and sensory attributes (application and sticky tacky) in order to determine whether a tribometer could be used to indicate how a formulation will be received by the consumer.

6.2 Results and Discussion

6.2.1 Tribology

6.2.1.1 Effect of Disk Speed and Normal Force on Friction and Wear

In order to employ pin and disk tribology to investigate the lubricating properties of wax based emulsions, it is important to consider both the disk rotation speed and normal force applied to the sample. This was conducted on a wax blend formulation (containing 5 wt % carnauba wax and 10 wt % microcrystalline wax and in castor oil).

6.2.1.1.1 Disk Speed

Six different disk speeds (1, 3, 5, 10, 30, 50 mms^{-1}) were investigated over a period of 3600 seconds with a fixed applied load (0.5 N) using a pin and disk tribological setup. The different disk speeds were investigated as the speed of the elastomer disk can be 'likened' to the speed at which a lipstick is applied. However, increasing the speed could lead to greater wear occurring which would result in less wax being within the contact zones. Figure 6.1 shows the effect of varying disk speeds on both the friction (Figure 6.1a) and wear (Figure 6.1b) of a wax blend (containing 5 wt % carnauba wax and 10 wt % microcrystalline wax in castor oil). Wear is an important parameter to examine, as when a lipstick is applied it must initially wear resulting in a thin film remaining on the lips.

Figure 6.1a shows that for all disk speeds the friction coefficient decreases over a period time from ~ 0.7 to reach a plateau value at ~ 0.1. The time taken to reach the plateau value varies depending on the time taken for the solid emulsion disk to wear to a thin film. It is important to note that the data points represent a moving average of 3 points and the error bars are representative of the original data. The moving average presentation of the original data was conducted as previous work by Godfrey (1995) and

Blau (1991) showed that when working with an unlubricated system in a pin-on-disk tribometer it is unrealistic to expect a single frictional force value as a lot of noise can be generated. Therefore a moving average of 3 points was conducted to minimise the noise. It should also be noted that after the sample material goes through the contact area it wears and displaces from the elastomer disk. It then attaches to the side of the vessel.

Figure 6.1b shows the wear of the solid disk as a function of time. From this it is clear that at higher disk speeds the disk is worn away more rapidly. For example to reach a thin film on the disk at 1 and 50 mms^{-1} it took ~2000 and ~400 s respectively. This is to be expected as at greater speeds the disk will go through more revolutions and therefore experience the localized applied load at a greater frequency. Therefore one would expect that if the number of revolutions to wear the sample was plotted against disk speed, a horizontal line would be obtained. However Figure 6.2 clearly shows a linear correlation (R^2 = 0.98) between the number of revolutions required to wear the sample to a thin film and the disk speed. This can be attributed to the wax blend not experiencing the full load at higher disk speeds.

(a)

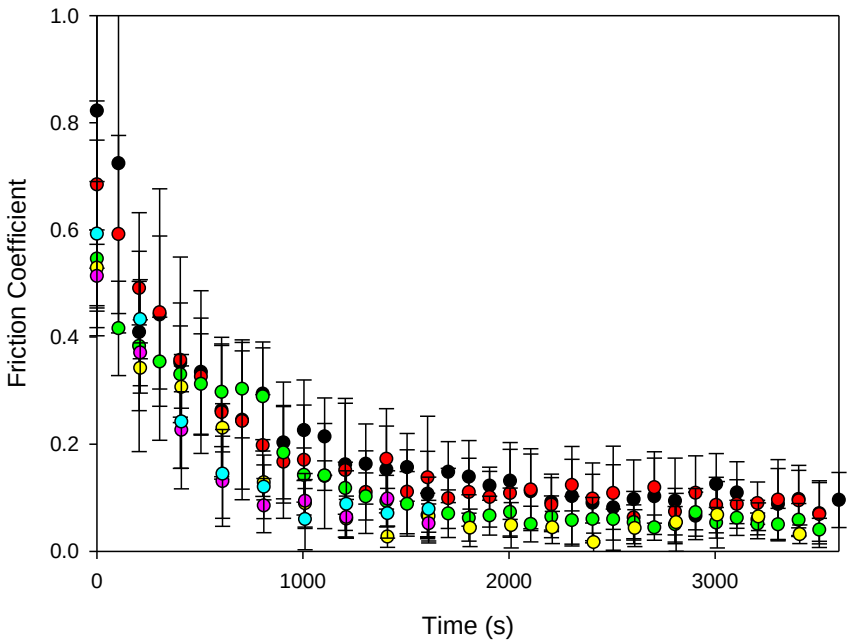

(b)

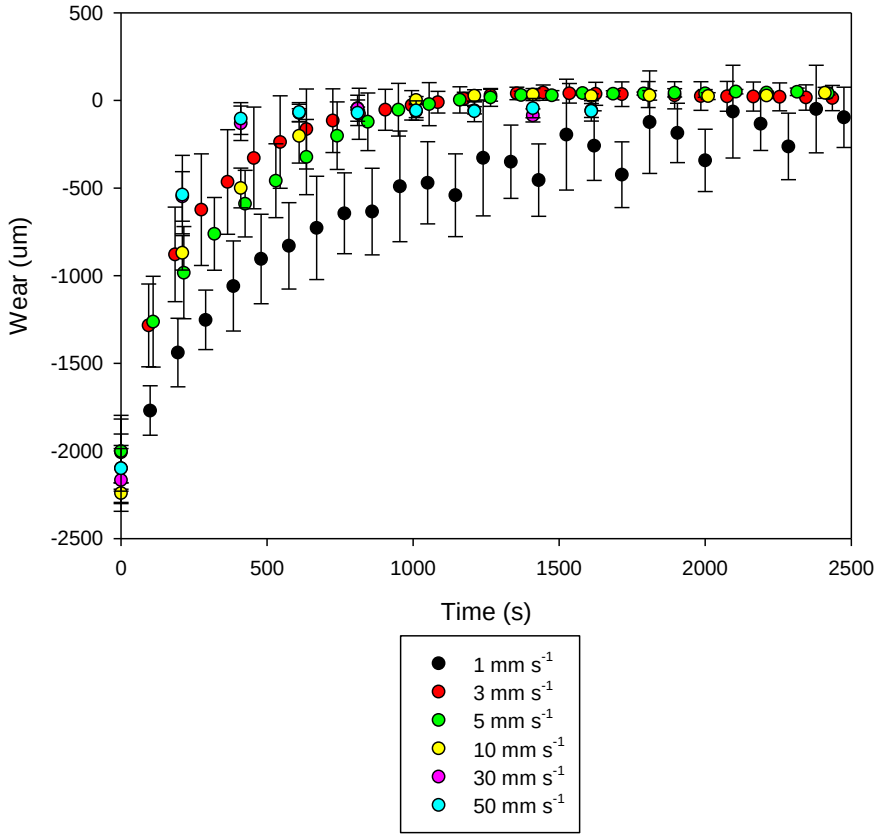

Figure 6.1 – (a)Friction coefficient and (b) wear vs time for a wax blend (5 wt % carnauba wax and 10 wt % microcrystalline wax in castor oil) at varying disk speeds. All experiments were conducted in a pin-on disk set up with a load of 0.5 N.

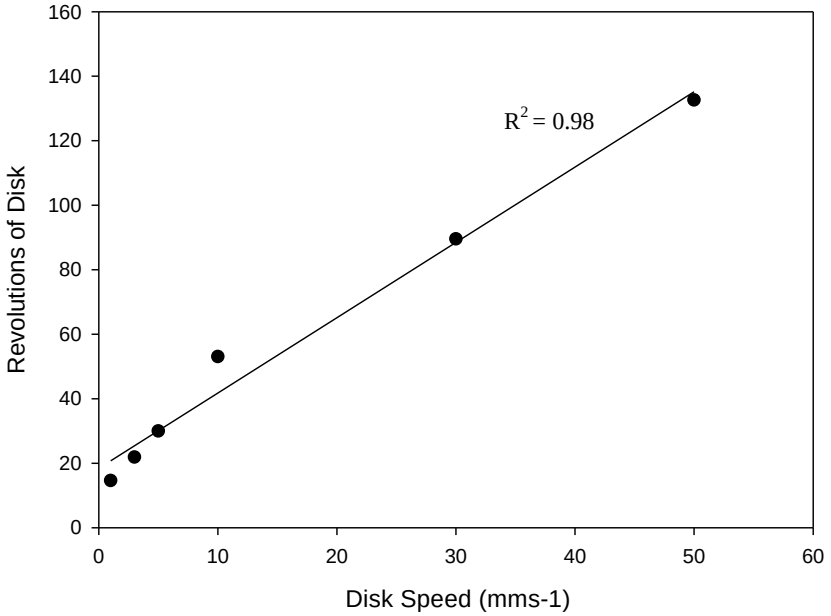

Figure 6.2 – Number of revolutions (required to produce a thin film) vs disk speed (mms^{-1}). All experiments were conducted in a pin-on disk set up with a load of 0.5 N. All experiments were conducted on a wax blend (5 wt % carnauba wax and 10 wt % microcrystalline wax in castor oil)

From these graphs, it becomes clear that a disk speed needs to be chosen that not only can be 'likened' to the speed at which a lipstick is applied but also creates enough wear to allow a thin film of wax in the contact zone. Therefore 10 mm s^{-1} will be used for the remainder of the studies.

6.2.1.1.2 Normal Force

Four different normal forces (0.3, 0.5, 1 and 3N) were investigated over a period of 3600 s with a fixed disk speed of 10 mms^{-1}. Different normal forces were investigated as it is expected that with increasing downward force an increase in wear will occur on the sample. It is important to select an appropriate normal force that will not cause the sample to fracture, as fracture results in the solid wax disk coming away from the elastomer disk. Figure 6.3 shows the effect of normal force on both friction (Figure 6.3 a) and wear (Figure 6.3 b). Figure 6.3 a shows that the final friction value is the same (~ 0.03) for all normal forces investigated. The only difference is the time taken to get to the final friction value, this is caused by the level of wear to the sample. Figure 6.3 b

shows that as normal force increases from 0.3 N to 1 N the time taken for the sample to wear to a thin film decreases from ~ 1200 s to ~ 100 s. This is due to the increased downward force which destroys the wax network thus allowing the solid wax to displace and wear away quicker. The effect of normal force on wear depth has been reported in the literature. Bhushan and Kulkarni (2001) investigated the effect of normal force on single crystal silicon and silicon oxide. Results showed that for single crystal silicon as normal force increased from 10 – 40 μN the wear depth increased from 1 – 35 nm. This was also attributed to the greater downward force (Bhushan and Kulkarni, 1996). It is important to note that when 3 N was used, it resulted in immediate fracture of the solid disk which prevented analysis.

(a)

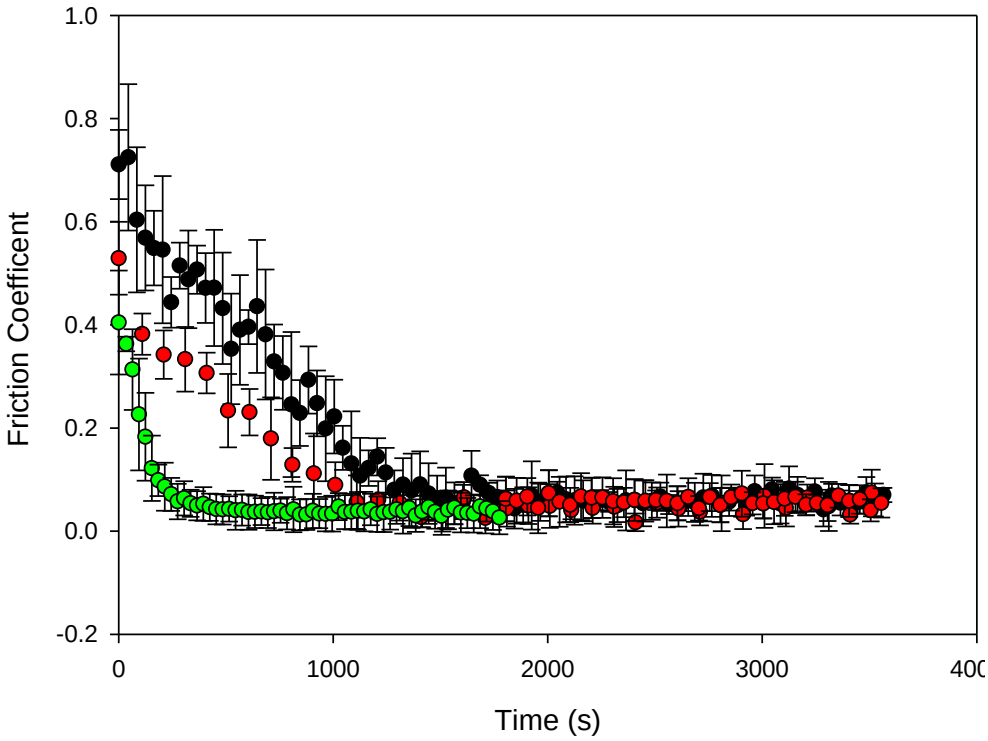

(b)

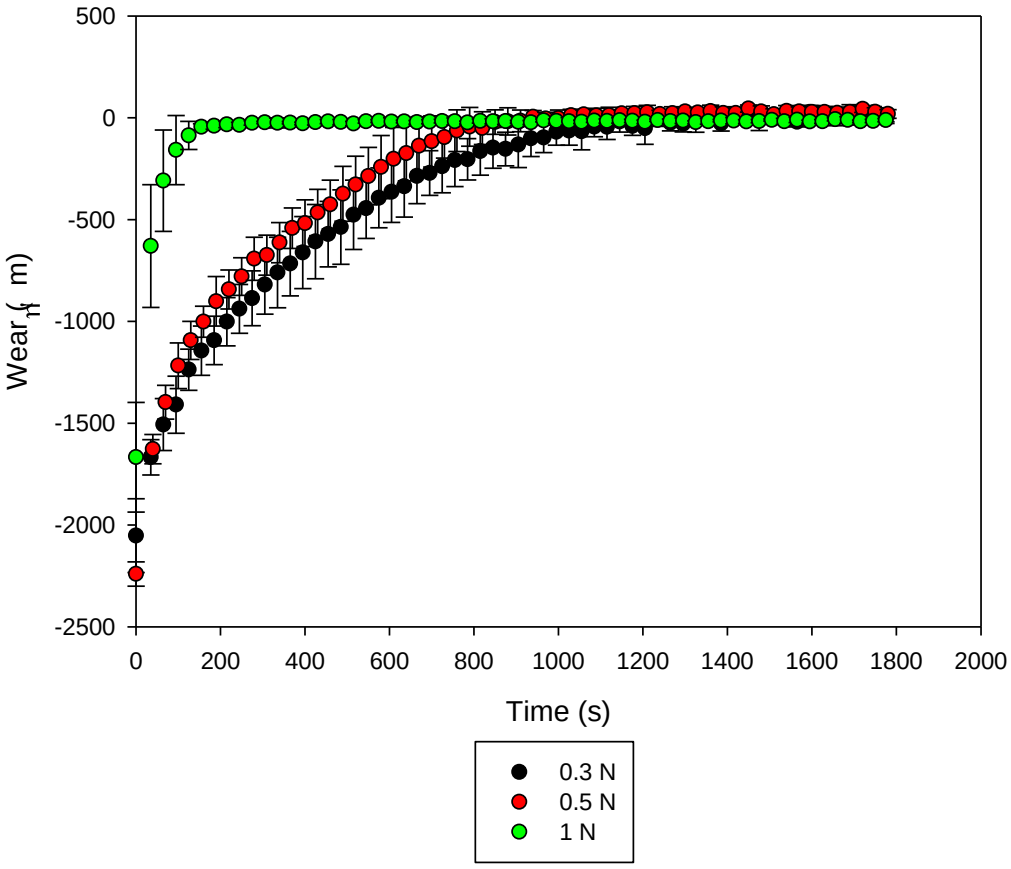

Figure 6.3 - (a) Friction coefficient and (b) wear vs time for a wax blend (5 wt % carnauba wax and 10 wt % microcrystalline wax in castor oil) at varying normal forces. All experiments were conducted in a pin-on disk set up with a disk speed of 10 mms^{-1}.

6.2.1.2 Effect of Waxes on Friction and Wear

As stated in section 1.1 lipsticks consist of a combination of different waxes. In the following section the lubricating and wear properties of both carnauba wax (CW) and microcrystalline wax (MW) were investigated. The individual waxes were investigated as this will give an insight into the moisturising abilities of the individual waxes. Six samples for each wax blend (containing castor oil (75 – 95 wt %), CW (0 – 20 wt%), and MW (0 - 20 wt %)) were anaylsed using a pin-on-disk set up with an applied load of 0.5 N and a disk speed of 10 mms^{-1}. The friction coefficient and wear were then recorded and plotted against time.

In addition, the effect of adding paraffin or performalene to the wax blend was also investigated as results in section 5.2.2.1 showed that either paraffin or performalene were required to produce an emulsion based lipstick with higher aqueous phase volume.

6.2.1.2.1 Effect of Carnauba Wax

The effect of carnauba wax (CW) concentrations on both lubrication and wear was investigated over a period of time. Initially, 10, 20, 30 and 40 wt % CW in castor oil was going to be investigated, however it was noticed visually that at 20 wt % and above the sample became brittle and fractured away from the elastomer disk. This prevents the wax from entering the contact zone thus preventing any type of analysis. Figure 6.4 shows an example of a before and after photo for CW samples (above and below 15 wt %) that have experienced a load (0.5 N) and a disk speed (10 mms^{-1}). Figure 6.4 shows that when at concentrations below 15 wt %, the sample wears and remains attached to the elastomer disk, whereas at higher concentrations (> 15 wt %) the sample fractures and detaches from the elastomer disk. This difference is indicative of a change in material properties as the concentration of CW increases above 15 wt %. Darvell (2002) stated that the shape of a stress-strain curve can give an indication of the material

properties. Therefore two different CW concentrations (10 and 15 wt % in castor oil) were compressed and the true stress was plotted against true strain (Figure 6.5). From Figure 6.5 a there is no major drop after fracture which is indicative of plastic behavior whereas the sharp drop observed after fracture in Figure 6.5 b is indicative of brittle behavior (Darvell, 2002). This behaviour has been explained in Chapter 5 which showed that as CW concentration increases the level of interaction between CW crystals increased *via* a power law relationship (~3).

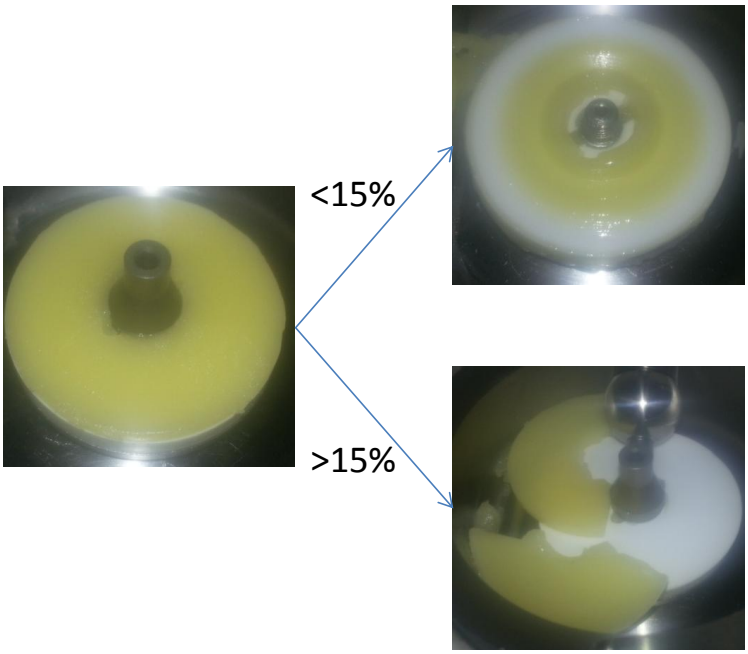

Figure 6.4 – Visual representation of before and after a sample has experienced a load (0.5 N) and a disk speed (10 mms^{-1}) for samples containing either >15 wt % or <15 wt % in castor oil.

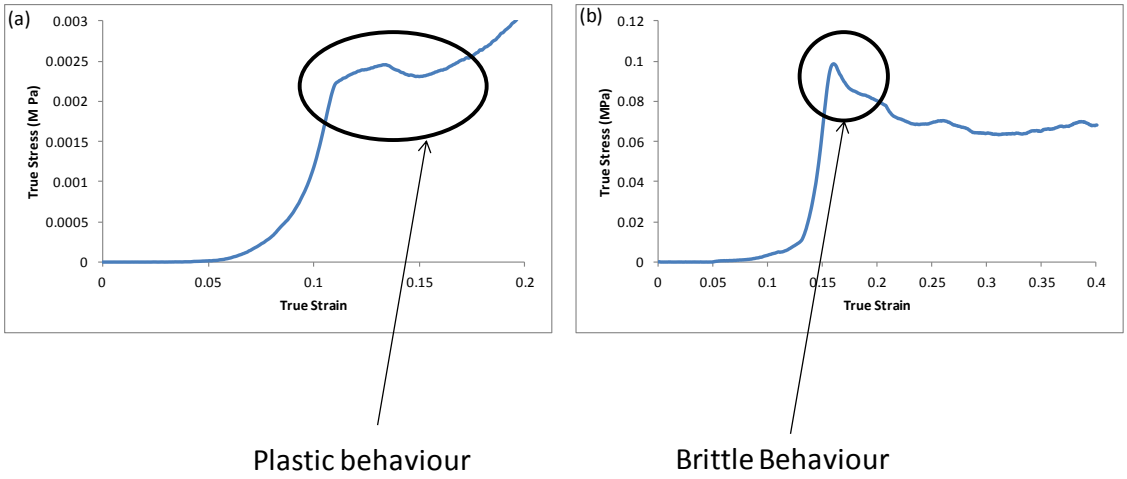

Figure 6.5 Typical True stress (MPa) vs True Strain curves for (a) 10 wt % and (b) 15 wt % carnauba wax in castor oil. All samples were melted and stirred until molten (~30 – 40 min) and cooled quiescently in the freezer until solid. They were then compressed at a rate of 1 mms^{-1} at 32 °C.

The lubricating and wear behavior of CW (5, 7, 10, 11, 12 and 13 wt %) in castor oil was investigated using a pin-on-disk setup over a period of time. The time varied depending on the time taken for the sample to wear to a thin film. It is important to consider a thin film as this is what will remain on the lip after application. Figure 6.6 shows the moving average for the friction coefficient of varying CW concentrations over time (where the error bars represent the original data). In general there is a slight increase in the final friction value between 5 wt % CW and 13 wt % from 0.04 – 0.06, however, when the error bars are taken into account there is no significant difference. This is to be expected as all samples contain carnauba wax and should therefore reduce friction in the same manner. However, the time taken to reach the final friction value increases to~3000 s at 13 wt % which is a direct result of the time taken for 100 % wear increasing. When wear was plotted against time, it becomes clear that the time taken for 100 % wear increases as CW content increases (Figure 6.7). It is suggested here that the wear could be a function of destroying the network by melting and/or load. This will be discussed in the following section.

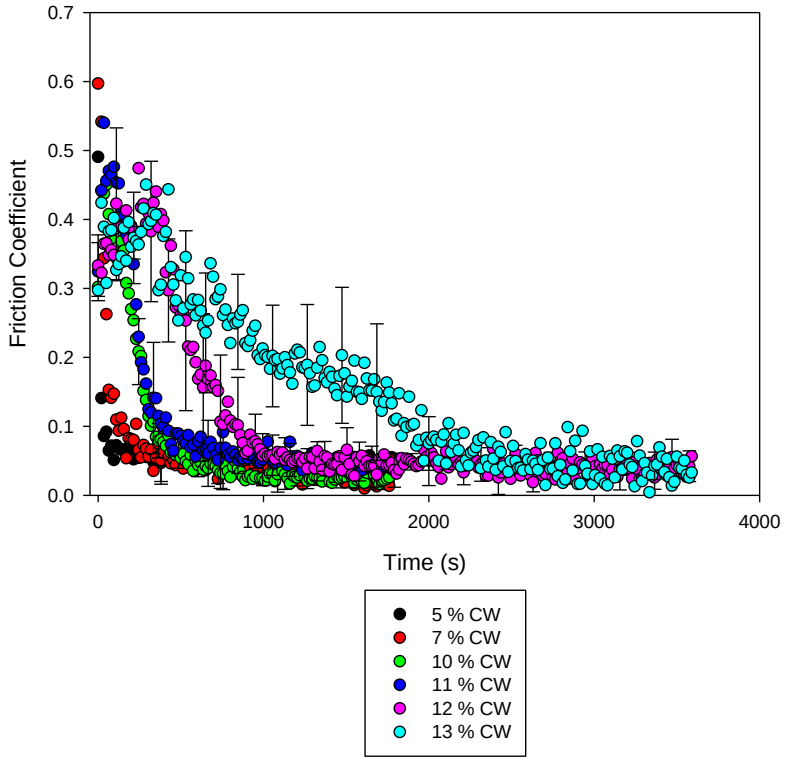

Figure 6.6 – Friction coefficient vs time for a varying carnauba wax concentrations in castor oil. All experiments were conducted in a pin-on disk set up with a load of 0.5 N and a disk speed of 10 mm^{s-1}.

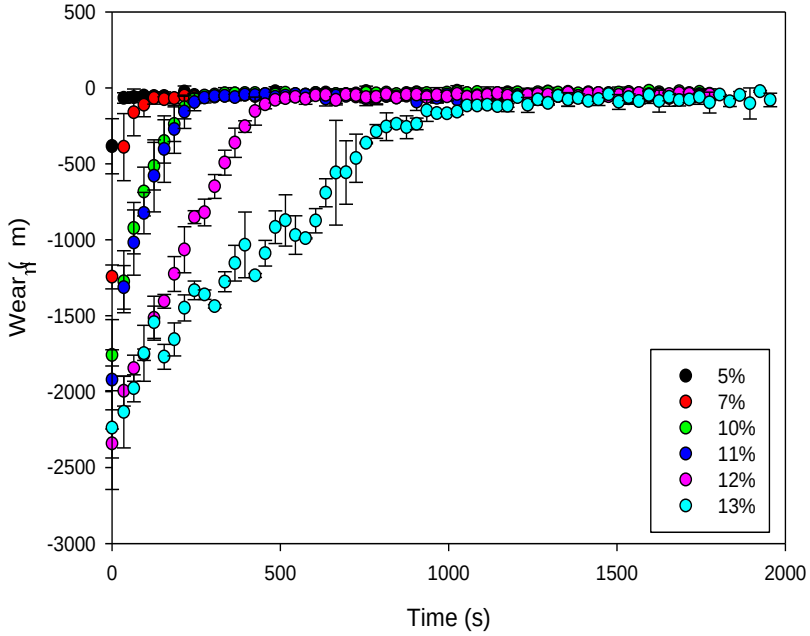

Figure 6.7 – Wear vs time for a varying carnauba wax concentrations in castor oil. All experiments were conducted in a pin-on disk set up with a load of 0.5 N and a disk speed of 10 mms^{-1}.

To investigate the effect of melting on the sample, it is important to consider the change in temperature (ΔT) within the experiment. This can be calculated by rearranging the following two equations;

$$\boldsymbol{Q = F \times V} \qquad \text{Equation 6-1}$$

$$\boldsymbol{Q = m \times Cp \times \Delta T} \qquad \text{Equation 6-2}$$

Where Q – energy dissipated, F – frictional force, V – velocity, m – mass and Cp – heat capacity.

The ΔT was calculated for both 5 and 10 % CW, as the heat capacity can be obtained from the specific heat capacity curves shown in Figure 4.9. Results show (Table 6.1) that for increasing CW concentration there is relatively no change in temperature (up to 3 °C). As there is relatively no change in temperature the time taken to wear must be a function of the strength of the wax network. Therefore the elastic modulus (G') was determined for each CW concentration using oscillatory rheology and compared to the average time taken for each sample to wear (Figure 6.8). Figure 6.8 shows there is a direct correlation between time taken to wear and the elastic modulus of the wax network. Therefore at higher concentrations (12 wt %) it takes longer (550 s) for the structure to wear to a thin film when compared to lower wax concentrations (7 wt % takes 180 s to wear).

Table 6.1 – Change in temperature within tribometer calculated from Equations 7.1 and 7.2

Carnauba Wax Concentration (wt %)	Change in Temp (ΔT) (°C)
5	1.35
10	2.9

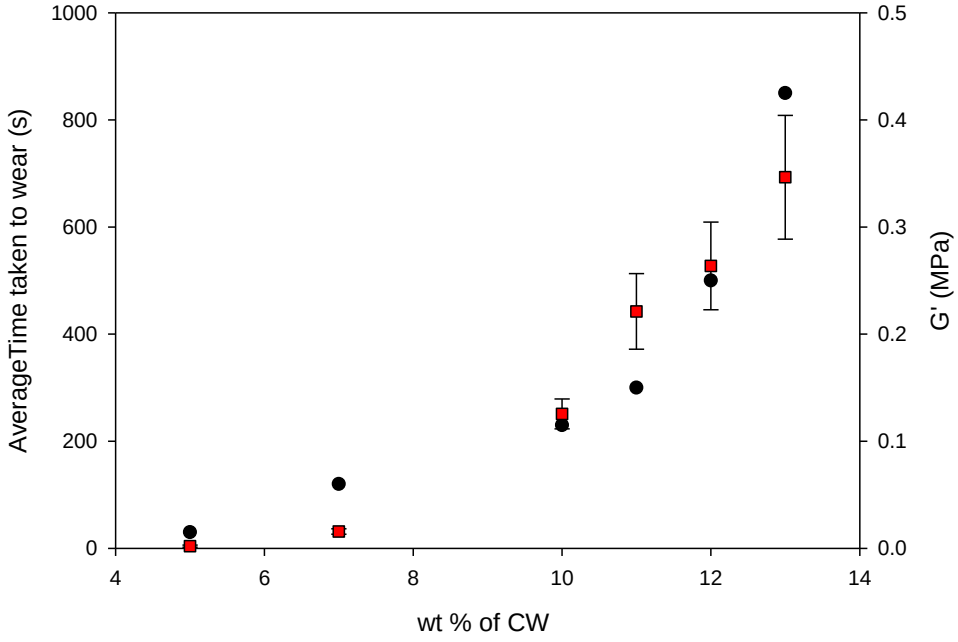

Figure 6.8 – Average time take taken to wear to a thin film (●) and elastic modulus (G') (■) vs wt % of carnauba wax. Samples produced for rheology were produced by melting and stirring until molten (~30 – 40 min) and cooled quiescently in the freezer until solid. The G' was then measured using oscillatory rheology and taken from a frequency of 5 Hz.

6.2.1.2.2 Effect of Microcrystalline Wax

During in the demoulding process, samples removed from moulds with only MW were too soft to be removed successfully, therefore it was not possible to analyse such samples. Hence 5 wt % CW was added to 5 -20 wt % MW to investigate the effect of MW on both friction and wear. It is important to note that greater than 20 wt % addition of MW results in shrinkage of the sample; this prevents the sample adhering to the elastomer thus preventing analysis (Zhang *et al.*, 2002). Figure 6.9 shows that as MW concentration increases from 5 wt % to 20 wt % the final friction value increases (~0.04 – ~0.11 respectively). It is important to note that if the error bars for the original data are taken into consideration there is relatively no difference in friction coefficient. However there is a general trend that increasing MW concentration increases friction slightly. This increase could be a result of a greater number of irregular crystals (Petersson *et al.*, 2008) being in the contact zone which could lead to a slight increase in friction.

The effect of MW concentration on the time taken to wear is shown in Figure 6.10 (original data shown in Appendix 3). Results show that the time taken to wear to a thin film is directly related to the strength of the network. As MW concentration increases (5 – 20 wt %) the time taken to wear decreases from ~400 to ~310 s as does the elastic modulus (~ 0.27 – ~ 0.23 MPa). This decrease is attributed to a weaker structure being produced as MW concentration increases which has been explained previously in section 5.2.1.2.

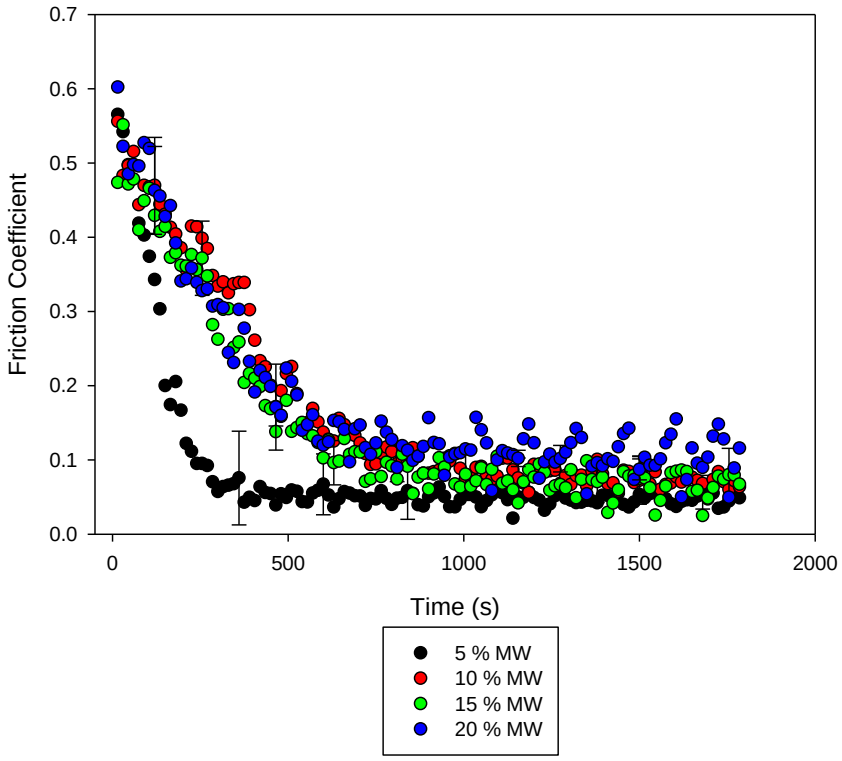

Figure 6.9 – Friction coefficient vs time for a varying microcrystalline wax (MW) concentrations in castor oil (each sample contained 5 wt % carnauba wax). All experiments were conducted in a pin-on disk set up with a load of 0.5 N and a disk speed of 10 mm^{s-1}.

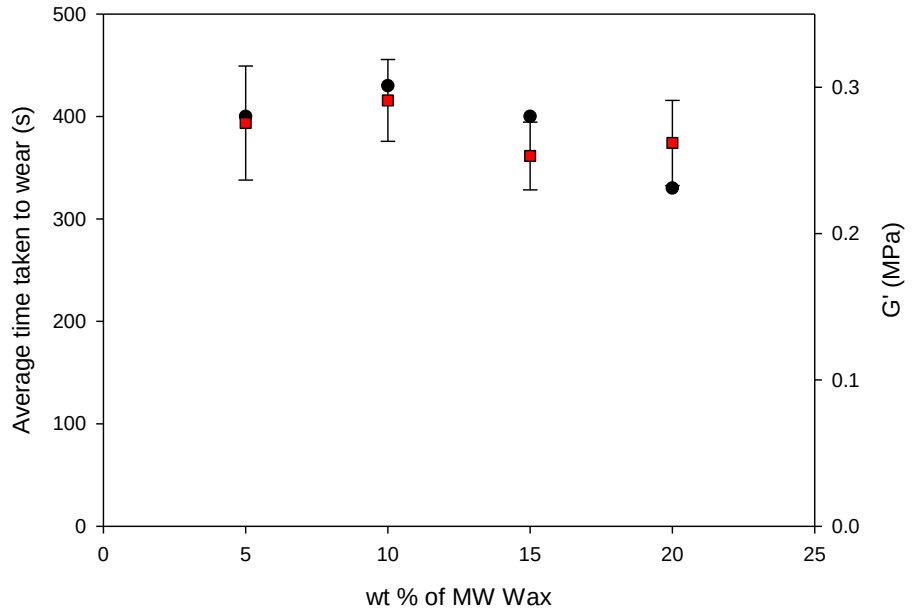

Figure 6.10 - Average time taken to wear to a thin film (●) and elastic modulus (G') (■)vs wt % of microcrystalline wax. Samples produced for rheology were produced by melting and stirring until molten (~30 – 40 min) and cooled quiescently in the freezer until solid. The G' was then measured using oscillatory rheology and taken from a frequency of 5 Hz.

6.2.1.2.3 Effect of Adding Paraffin and Performalene on friction and wear

In Chapter 5 it was shown that paraffin and performalene increases the elastic modulus of the emulsion based lipsticks. Therefore initially it is important to consider how they both affect the friction and wear properties of a wax blend. Hence the effect of adding either paraffin or performalene to a wax blend (5 wt % CW and 10 wt % MW in castor oil) on friction and wear was investigated.

Figure 6.11 shows the effect of increasing either paraffin (Figure 6.11 a) or performalene (Figure 6.11 b) concentrations on the friction coefficient. Results show that as the concentration of either paraffin or performalene increases (5 – 20 wt % and 2.5 – 10 wt % respectively) so does the final friction coefficient (0.06 – 0.12 and 0.08 – 0.14 respectively). These increases can be attributed to a greater number of crystals being present in the contact zones. This agrees with work reported for food systems

which showed that adding large starch particles to a vanilla custard dessert increased the friction coefficient from 0.6 to 0.81 (de Wijk and Prinz, 2005) due to more large starch particles present in the contact zone.

It is important to note that the major difference between adding paraffin and performalene is the time taken for the samples to reach a final friction value. The time to wear the system to a thin film is again related to the elastic modulus as shown in Figure 6.12. Results show that as the concentration of paraffin increases (5 - 20 wt %) the time taken to wear increases from 700 s to 1900 s. This is attributed to the elastic modulus of the network increasing from 0.5 to 0.6 MPa. If performalene is used instead of paraffin, the time taken to wear increases from 400 s to 10,000 s as concentration increases from 2.5 to 10 wt %. This is due to performalene forming a stronger network which is observed by G' increasing from 1 – 3 MPa (previously discussed in section 5.2.2.1).

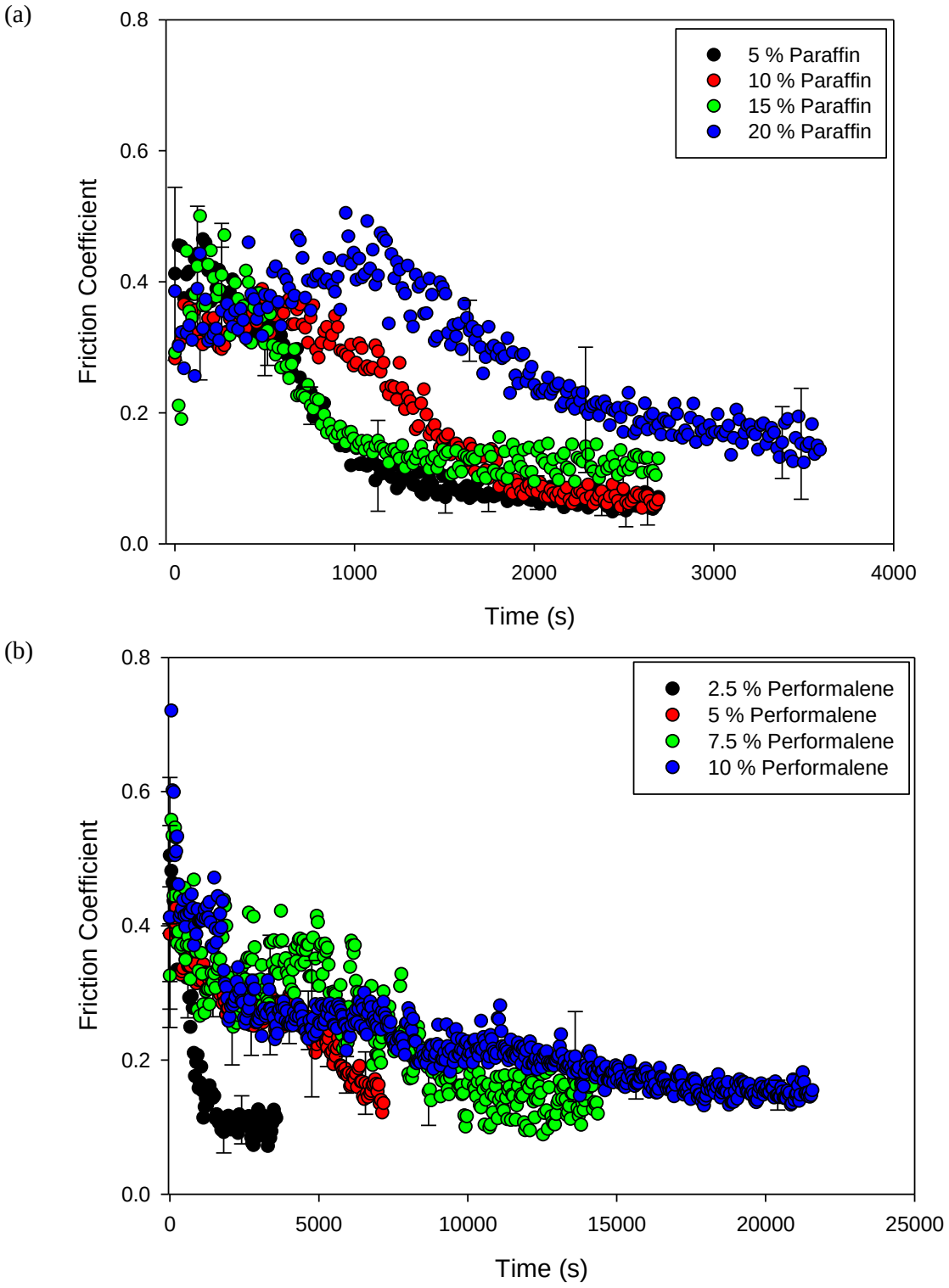

Figure 6.11 - Friction coefficient vs time for a varying (a) paraffin and (b) performalene concentrations in castor oil (each sample contained 5 wt % carnauba wax and 10 wt % microcrystalline wax). All experiments were conducted in a pin-on disk set up with a load of 0.5 N and a disk speed of 10 mms^{-1}

(a)

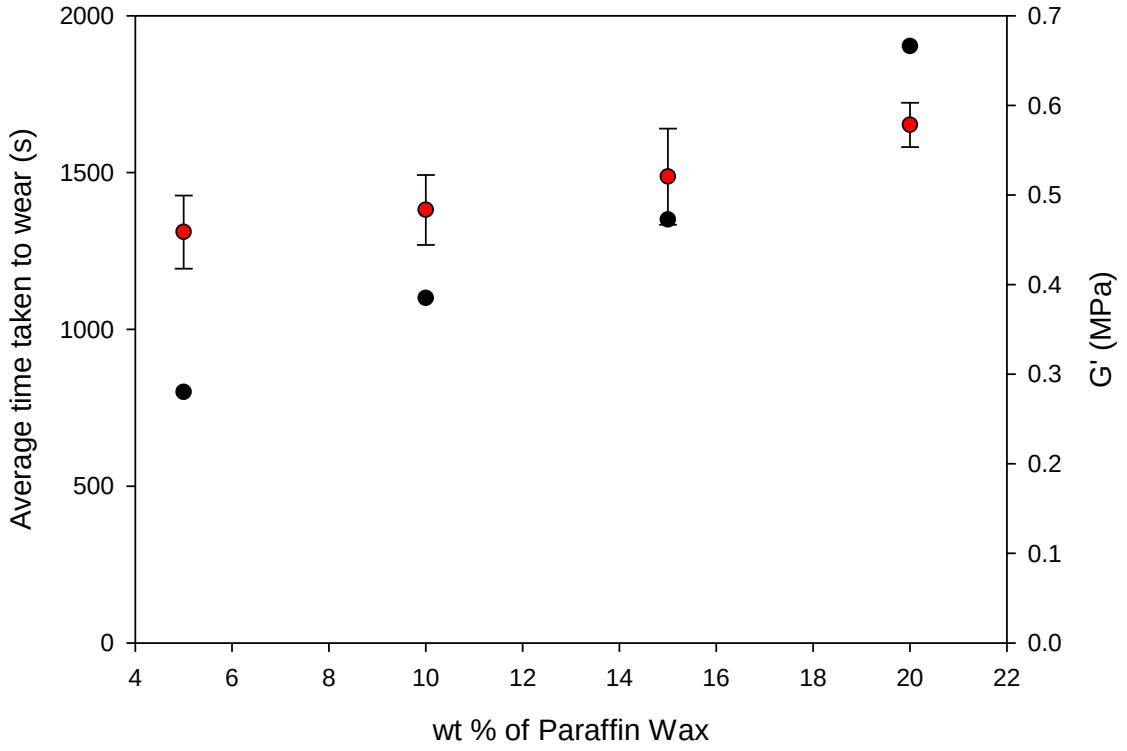

(b)

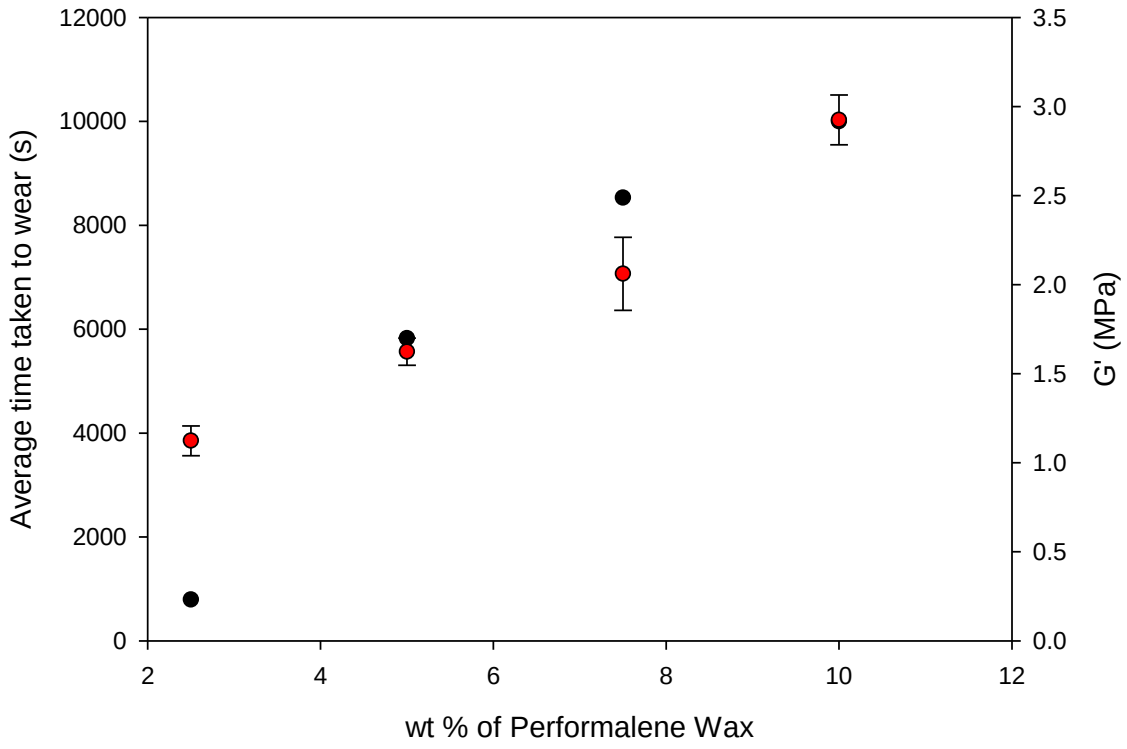

Figure 6.12 - Average time take taken to wear to a thin film (●) and elastic modulus (G') (●) vs wt % of (a) paraffin and (performalene). Samples produced for rheology were produced by melting and stirring until molten (~30 – 40 min) and cooled quiescently in the freezer until solid. The G' was then measured using oscillatory rheology and taken from a frequency of 5 Hz.

6.2.1.3 Effect of Emulsions on Friction and Wear

In the preceding work in this chapter, the effect of different waxes on lubrication and wear was investigated. However when producing emulsion based lipsticks, it is important to consider the impact incorporating water (as an emulsion) has upon the lubrication and wear.

6.2.1.3.1 Effect of Aqueous Phase Volume

In order to investigate the effect of water content on lubrication and wear, emulsions were produced containing varying amounts of aqueous phase (5, 10, 20, 30 and 40 wt %) which were analysed using a pin-on-disk set up. It is important to note that the continuous phase (58 – 93 wt %) comprised of 5 wt % CW, 10 wt % MW and 5 wt % paraffin in castor oil with each emulsion containing an overall 2 wt % polyglycerol polyricinoleate (PGPR). Figure 6.13 and Table 6.2 show the effect of incorporating an increasing aqueous phase volume. In general, increasing the aqueous phase volume increases the final friction value (0.056 – 0.143, shown in Table 6.2). It is suggested here that this increase is due to water droplets being in the contact zones which increases the friction coefficient. Dresselhuis *et al* (2007) investigated the tribology of O/W emulsion under mouth-like conditions. They found that breakdown of the O/W emulsion resulted in surface induced coalescence of the oil droplets which lowered the overall friction (Dresselhuis *et al.*, 2007, Dresselhuis *et al.*, 2008). Therefore in the system examined in this research, structural breakdown of the emulsion will lead to water droplets in the contact zone resulting in the observed (Table 6.2) increase in friction coefficient.

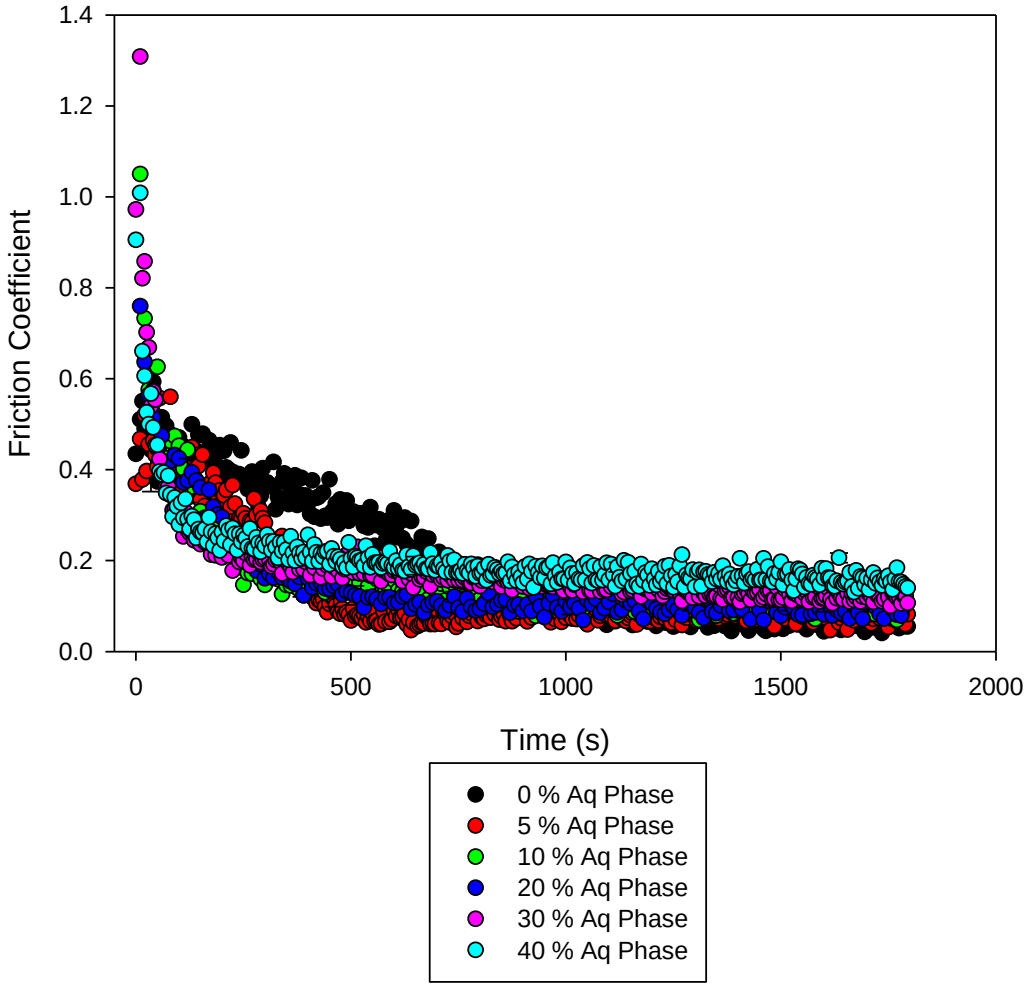

Figure 6.13 - Friction coefficient vs time for a varying aqueous phase volumes with 58 – 93 wt % continuous phase (containing 5 wt % carnauba wax, 10 wt % microcrystalline wax and 5 wt % performalene in castor oil) and 2 wt % polyglycerol polyrinceoleate. All emulsions were produced using a silverson high shear mixer (10,000 rpm for 5 minutes). All experiments were conducted in a pin-on disk set up with a load of 0.5 N and a disk speed of 10 mms^{-1}

Table 6.2 – Final friction values (taken from Figure 6.13) vs aqueous phase volume.

Aqueous Phase (%)	Final Friction Coefficient Value
0	0.056
5	0.082
10	0.086
20	0.093
30	0.117
40	0.143

The effect of aqueous phase volume on wear is shown in Figure 6.14. The time taken to reach a thin film decreases from ~800 to ~100 s as the aqueous phase volume increase from 0 to 40 wt %. This is directly related to water droplets acting as defects resulting in G' decreasing from~0.5 to ~0.1 with increasing aqueous phase volume (0 – 40 wt % (explained section 5.2.2).

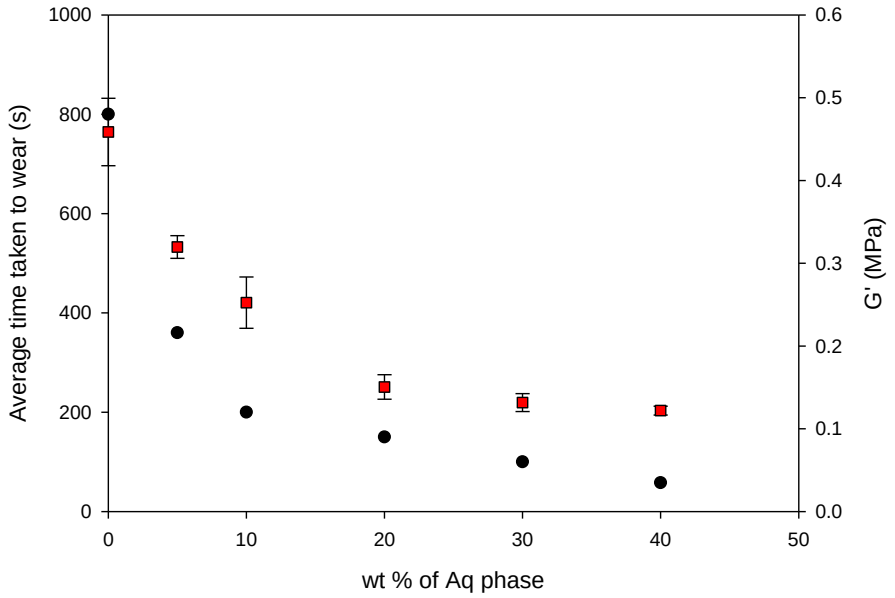

Figure 6.14 - Average time take taken to wear to a thin film (●) and elastic modulus (G') (■) vs wt % Aq phase with 58 – 93 wt % continuous phase (containing 5 wt % carnauba wax, 10 wt % microcrystalline wax and 5 wt % performalene in castor oil) and 2 wt % polyglycerol polyrinceoleate. Samples produced for rheology were produced by melting and stirring until molten (~30 – 40 min) and cooled quiescently in the freezer until solid. The G' was then measured using oscillatory rheology and taken from a frequency of 5 Hz.

6.2.1.3.2 Effect of Droplet Size

It has been reported in the literature that droplet size can have an effect on the lubricating properties of a material. De Wijk and Prinz (2005) investigated the effect of fat droplets on the coefficient of friction in an O/W emulsion system. Their results showed that as the fat droplet size increased (2 – 6 μm), the coefficient of friction increased from 0.59 – 0.75. However to the author's knowledge there is no evidence of the droplet size of the dispersed phase in W/O emulsions being investigated. Therefore

this section looks at the effect of varying the dispersed phase droplet size. As shown in Table 4.2, varying the amount of PGPR (0.2 – 2 wt %) in the emulsion system can control the droplet size (100 – 2.8 μm).

Four different droplet sizes (100, 5.8, 3.4 and 2.8 μm) were produced using a Silverson high shear mixer and these were analysed using a pin-on-disk set-up in a tribometer. Figure 6.15 shows the effect of droplet size on friction coefficient. There is a general trend that friction coefficient increases (0.12 – 0.19) as droplet size increases (2.8 - 100 μm). It is suggested here that this increase is either due to larger water droplets being in the contact zone or a result of increasing the amount of emulsifier in the formulation. It has been reported by Cambiella *et al.* (2006) that emulsifier concentration can impact the lubricating properties of an emulsion. They investigated the effect of emulsifiers (anionic, nonionic and cationic) in O/W emulsions on metal lubrication. Results showed that the mechanism of lubrication between the metal surface and oil droplets was controlled by the emulsifier concentration, as this dictated the stability, droplet size distribution and surface/interfacial tension of the droplets. In order to investigate if PGPR effected the lubricating properties, a control experiment was conducted to investigate the effect of low (0.5 wt %) and high (2 wt %) PGPR concentrations on the friction coefficient. Figure 6.16 shows that that friction coefficient value does not change as the concentration of PGPR increases, therefore the change in friction coefficient observed in Figure 6.15 is a result of larger water droplets being present in the contact zone causing an increase in friction. Similar behaviour was observed by Timm *et al.* (2011) who investigated the effect of different cosmetic particle sizes (11.5 – 63.2 μm) on friction coefficient. They found that the friction coefficient increased from 0.075 – 0.4 as particle size increased from 11.5 – 63.2 μm. They concluded that this was due to larger particles concentrating around the contact

region of the ball which increases the friction coefficient (Timm *et al.*, 2011, Johnson and Kauzlarich, 2004).

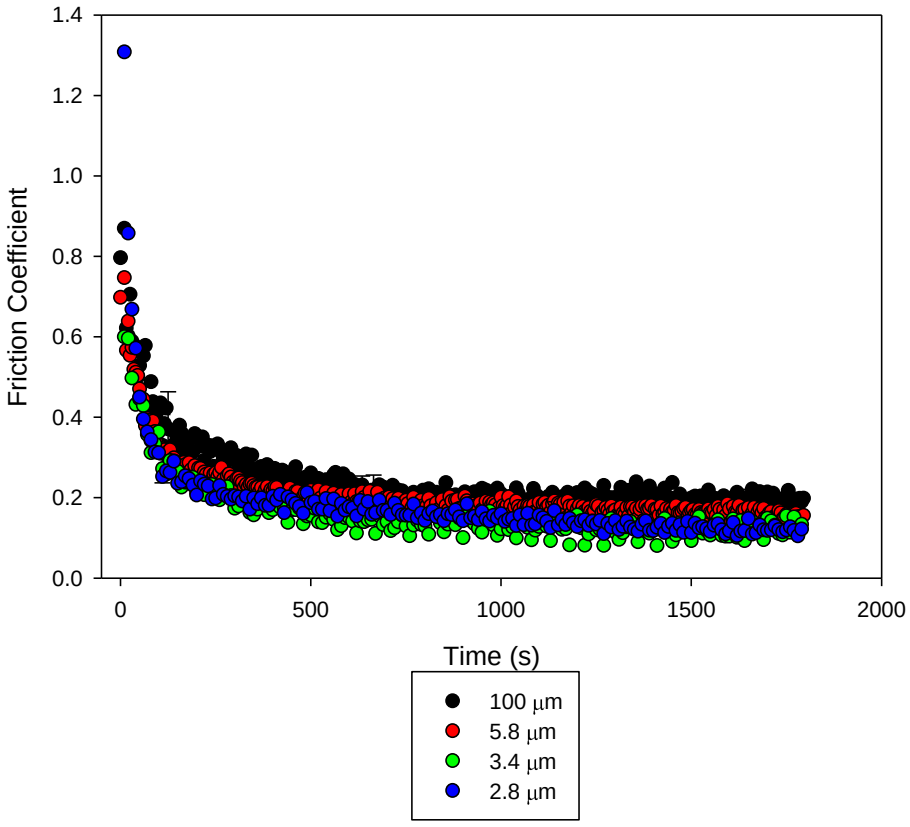

Figure 6.15 - Friction coefficient vs time for a varying droplet sizes. All samples were produced using a Silverson high shear mixer (10,000 rpm for 5 minutes) and consist of 20 wt % Aqueous phase, 78 – 79.8 wt % continuous phase (containing 5 wt % carnauba wax, 10 wt % microcrystalline wax and 5 wt % performalene in castor oil) and 0.2 – 2 wt % polyglycerol polyrinceoleate. All experiments were conducted in a pin-on disk set up with a load of 0.5 N and a disk speed of 10 mms^{-1}

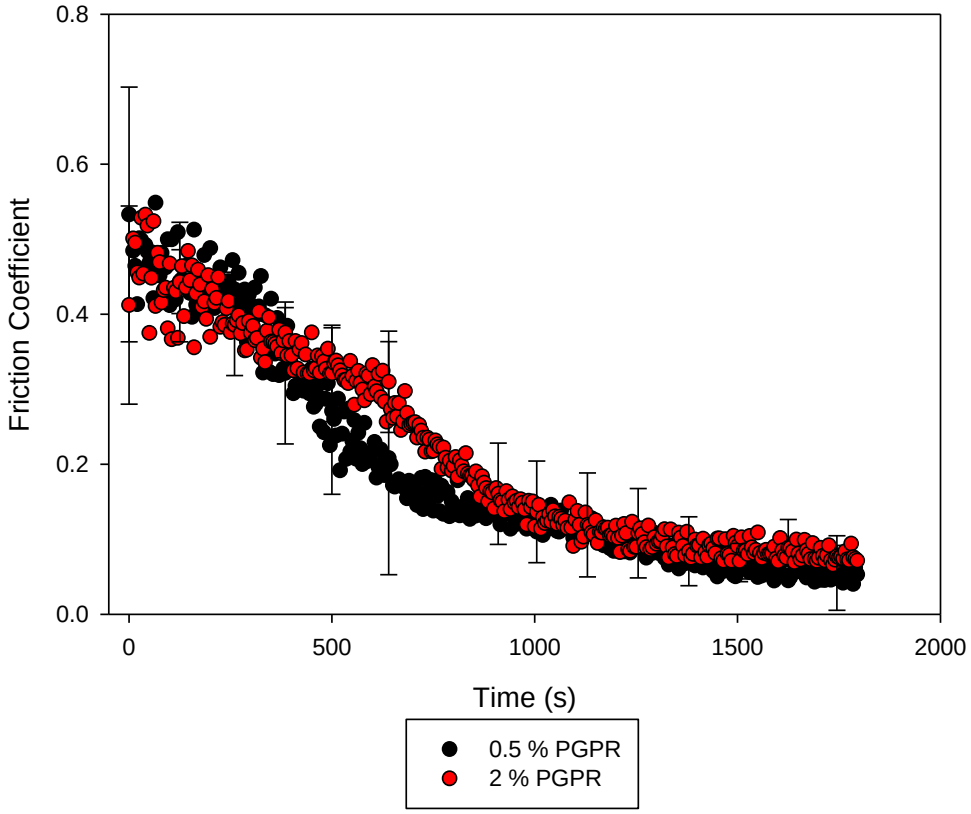

Figure 6.16 - Friction coefficient vs time for a varying polyglycerol polyrinceoleate (PGPR) concentrations. All samples were produced using a silverson high shear mixer (10,000 rpm for 5 minutes) and consist of 20 wt % Aqueous phase, 78 – 79.5 wt % continuous phase (containing 5 wt % carnauba wax, 10 wt % microcrystalline wax and 5 wt % performalene in castor oil) and 0.5 – 2 wt % PGPR. All experiments were conducted in a pin-on disk set up with a load of 0.5 N and a disk speed of 10 mms^{-1}

6.2.1.3.3 Effect of Dispersed Phase Viscosity

In the food industry, it has been reported that the high viscosity dispersed phases in O/W emulsions lowered the perceived oral friction thus improving the perception of creaminess (Dresselhuis *et al.*, 2008). Therefore varying the dispersed phase viscosity of a W/O emulsion may affect the frictional properties of a material which could enhance its sensory perceptions. In order to vary the dispersed phase viscosity, glycerol was added in varying quantities (20- 50 wt % of aqueous phase) to distilled water. Glycerol was chosen for two reasons: (1) it has been shown to improve moisturising ability (Blichmann *et al.*, 1989) and revive clinical signs of dryness (Serban *et al.*,

1983). (2) Stamatoudis and Tavlavides (1985) have shown that glycerol can be added to a formulation to alter the viscosity.

The viscosity of the dispersed phases was measured at a fixed shear rate (100 s^{-1}) using a Bohlin rheometer and is shown in Figure 6.17. As the amount of glycerol increases (0 – 50 wt %) the effective viscosity increases. This is to be expected as glycerol has a higher viscosity and the overall viscosity of a mixture of liquid is governed by the viscosity of the individual liquids (Reid *et al.*, 1987).

Emulsions with different dispersed phase viscosities were produced using a Silverson high shear mixer (all emulsions contained 20 wt % Aqueous phase, 78 wt % continuous phase (containing 5 wt % CW, 10 wt % MW and 5 wt % paraffin in 80 wt % castor oil) and 2 wt % PGPR). Emulsions were then analysed using a pin-on-disk setup in a tribometer. Figure 6.18 shows the effect of increasing dispersed phase viscosities on the friction coefficient over time. It can be observed that there are no distinct differences between the frictions values as all the results overlap. It is also important to note that there is no general trend of increasing/decreasing friction coefficient as dispersed viscosity increases. Therefore it can be concluded that the dispersed viscosity does not affect the frictional coefficient in these systems. This is a result of the high wax/oil content that has a greater impact on the friction coefficient than the dispersed phase.

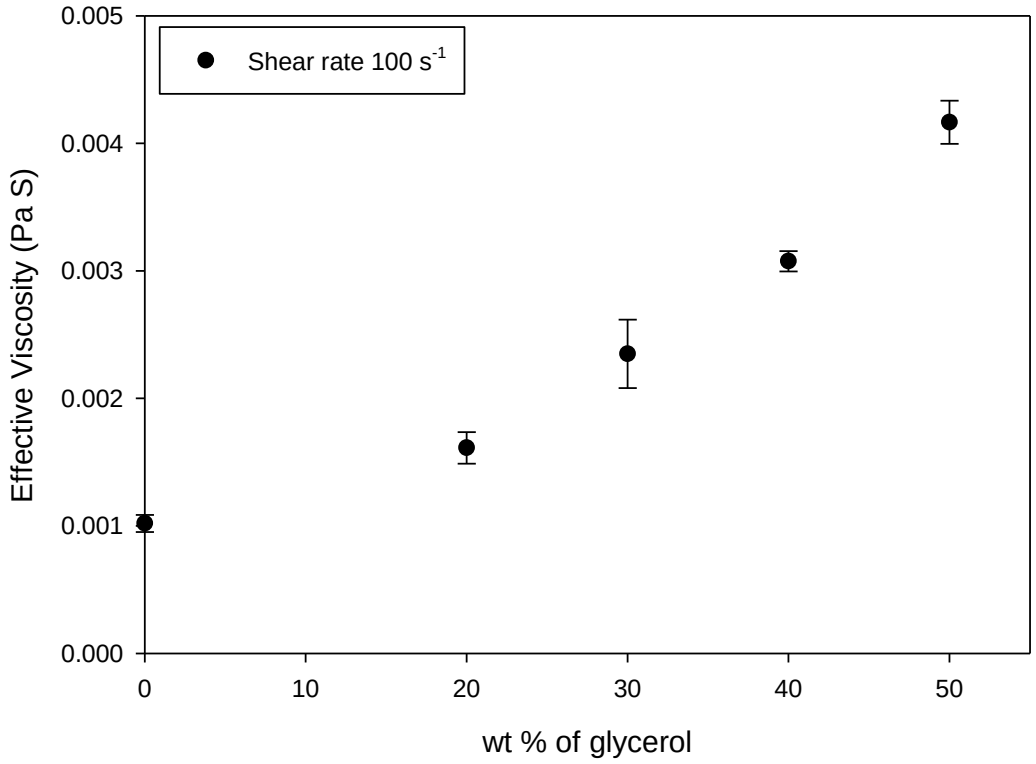

Figure 6.17 – Effective viscosity of the dispersed phase with varying wt % of glycerol in distilled water. All samples were measured at a constant shear rate (100 s^{-1}) using a 40 mm acrylic cone and plate geometry (0.15 mm gap width) at a temperature of 32 °C

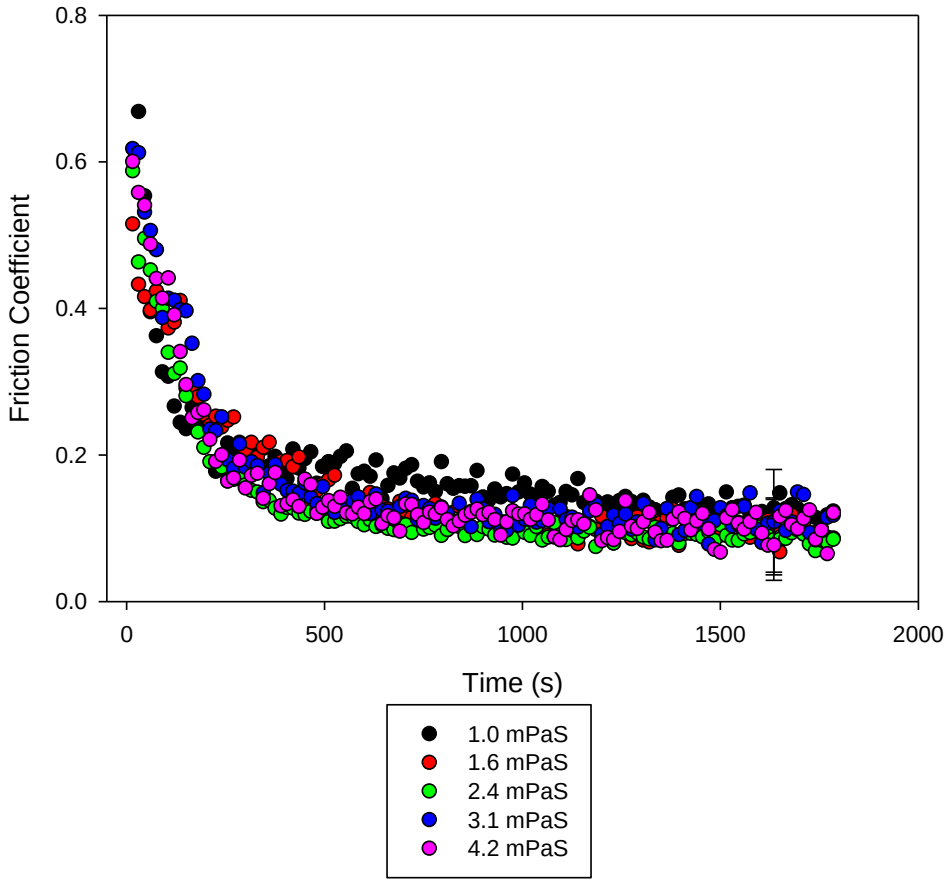

Figure 6.18 - Friction coefficient vs time for a varying dispersed phase viscosities. All samples were produced using a silverson high shear mixer (10,000 rpm for 5 minutes) and consist of 20 wt % Aqueous phase (0- 50 wt % glycerol in water), 78 – 79.5 wt % continuous phase (containing 5 wt % carnauba wax, 10 wt % microcrystalline wax and 5 wt % performalene in castor oil) and 2 wt % PGPR. All experiments were conducted in a pin-on disk set up with a load of 0.5 N and a disk speed of 10 mms^{-1}

6.2.2 Sensory

In order to investigate the effect of emulsion structure on consumer perception, four samples (bench mark (base formulation with no water), 5 % wt Aqueous phase, 20 % wt Aqueous phase and 20 % wt Aqueous phase with a larger droplet size) were analysed by a trained sensory panel using compusense software. These four samples were chosen as they showed differences in friction coefficient and therefore could be used to directly compare sensory data to tribology data.

The sensory panel used quantitative descriptive analysis to identify perceived differences between emulsions and the bench mark. The panel investigated two distinct attributes; application (drag) and sticky/tacky. These were assessed on both the hand and lip. The trained panel was also asked to give their opinion verbally (in the language generation session) regarding the moisturising ability of the samples. Initially, it is important to check that the panel is performing well and any differences observed between samples are due to the samples and nothing else. There are two main factors that influence the sensory score; the samples and the panelists. The Compusense software utilised analysis of variance (ANOVA) to calculate how significant these effects were for a 95 % confidence level.

There was a significant panelist effect on both hand and lip for application and sticky/tacky ($p < 0.05$ at 95 % confidence interval). This indicates that the panelists are scoring differently across all the samples, but they are consistently doing so across all samples (*e.g.* a panelist is scoring all samples 2 points higher than other panelists). There was also a significant sample effect on both hand and lip for application ($p < 0.05$ at 95 % confidence interval) whereas for sticky/tacky the results did not prove to be significant ($p > 0.05$ at a 95 % confidence interval) for either hand or lip. This suggests that there is a significant difference between samples when the application attribute is being investigated. Before this difference may be examined, it is important to consider the impact of the interaction effect between the panel effect and sample effect as this could affect the results of the sensory study. ANOVA results (Table 6.3) generated a p-value ranging from 0.16 – 0.83 (at a 95 % confidence interval) for the interaction effect between sample and panelist for all attributes. Thus showing there is no significant interaction which means the panelists rankings for the samples can be considered for post hoc analysis.

ANOVA analysis has shown a significant difference in application (drag) for both hand and lip. Post-hoc analysis was then conducted to analyse the difference between the four samples (bench mark, 5 % wt aqueous phase, 5 % wt aqueous phase and 5 % wt aqueous phase with a larger droplet size). Each of the emulsions was compared to the benchmark sample by a trained professional panel of 21 subjects (average age 56.3, 35 – 73 yrs old). It is important to note that the panelists were trained to position the benchmark between 0 – 10 for both attributes, this position was then agreed and between the panelists and set as a standard. They then assessed how different each of the emulsions were and rated them with regards to a difference from the benchmark sample. Figure 6.19 shows the sensory scores for the effect of different emulsion structures on both drag and sticky/tacky feel when applied to either the hand or lip. Results show that introducing water to the structure (5 wt % aqueous phase sample) lowers the drag score from 5.5 to 4.1 ± 1.1 (on the hand) and 6 to 4.5 ± 1.0 on the (on the lips). When the water content is increased from 0 – 20 wt % the drag score decreased from 5.5 to 4.5 ± 1.5 (on the hand) and 6 to 4.7 ± 1.3 (on the lips). Finally when the emulsion had larger droplets the drag score decreased from 5.5 to 3.5 ± 1.0 (on the hand) and 6.0 to 3.6 ± 1.3 (on the lips).

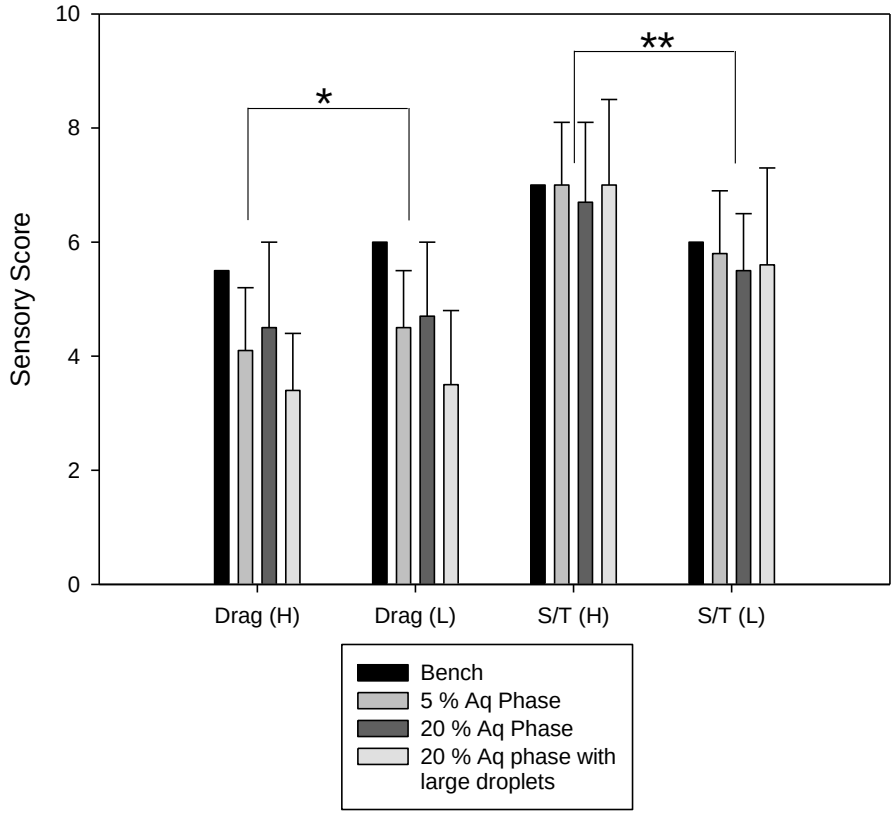

Figure 6.19 – The sensory score at different attributes (where H – on hand and L – on lip) for bench formulation (5, 10, 5 wt % of carnauba wax, microcrystalline wax and paraffin wax in castor oil) and emulsions varying in aqueous phase volume (5 – 20 wt %) and PGPR concentrations (0.2 + 2 wt %). Error bars indicate standard deviation. * indicates a significant result (P < 0.05) and ** indicates a non significant result (P>0.05) at a 95 % confidence interval.

The differences from the benchmark (D.F.B) sample observed for drag (on either hand or lips) are shown to be significantly different using the least significant difference (L.S.D) method (shown inTable 6.3) as the difference from the bench (D.F.B) (1.4 for hand and 1.5 for lips) is greater than the L.S.D (0.5 for hand and 0.6 for lips).Thus suggesting that increasing the water content reduces the perception of drag for the consumers (This will be explained in section 6.2.3 by comparing the sensory data to the tribology data).

It is important to note that there is no significant difference observed for sticky/tacky feel for either the hand or the lips which is observed in Table 6.3 as the D.F.B (0 for hand and 0.3 for lip) is lower than the L.S.D (0.5 for hand and 0.6 for lip).

Even though there is not a significant difference observed for the sticky/tacky attribute, it should be noted that samples on the lip behaved less sticky than on the hand. This finding is extremely important to industry as a consumer will always test a lipstick on their hand before purchasing and even though a lipstick may behave less sticky on the lip a consumer may decline to purchase based on the stickiness observed on the hand.

Table 6.3 - The sensory score at different attributes (where H – on hand and L – on lip) for bench formulation (5, 10, 5 wt % of carnauba wax, microcrystalline wax and paraffin wax in 80 wt % castor oil) and emulsions varying in aqueous phase volume (5 and 20 wt %) and PGPR concentrations (0.2 and 2 wt %). Error indicates standard deviation. Results represent least significant difference (L.S.D) data with differences from the bench (D.F.B)

Attribute	Bench	5% Aq	D.F.B	20% Aq	D.F.B	20% Aq with large droplets	D.F.B	L.S.D @ 95% confidence interval
Drag (H)	5.5	4.1 ± 1.1	1.4	4.5 ± 1.5	1	3.5 ± 1.0	2	0.5
Drag (L)	6.0	4.5 ± 1.0	1.5	4.7 ± 1.3	1.3	3.6 ± 1.3	2.4	0.6
S/T (H)	7.0	7.0 ± 1.1	0	6.7 ± 1.4	0.3	7.0 ± 1.5	0	0.5
S/T (L)	6.0	5.7 ± 1.1	0.3	5.5 ± 1.0	0.5	5.6 ± 1.7	0.4	0.6

In order to compare the effect of droplet size on both drag and sticky/tacky, L.S.D analysis was used to check if there was a significant difference between emulsions made with 20 wt % aqueous phase and 20 wt % aqueous phase (with larger droplets). Results show (Table 6.4) the differences observed for drag (on either hand or lip) are shown to be significant as the difference (1.0 for hand or 1.1 for lip) is greater than the L.S.D value (0.5 and 0.6 respectively). Thus, suggesting that increasing the droplet size from 2.8 to 100 μm results in the panelists perceiving a reduction in drag (This will be explained in section 6.2.3 by comparing the sensory data to the tribology data).

Table 6.4 - The sensory score at different attributes (where H – on hand and L – on lip) for comparison between large droplets (>100 µm) and small droplets (~3 µm). Emulsions were comprised of an aqueous phase volume (20 wt %), PGPR concentrations (0.2 and 2 wt %) and continuous phase (78 – 79.8 wt % which contained 5, 10, 5 wt % carnauba wax, paraffin and microcrystalline wax in 80 wt % castor oil). Error indicates standard deviation. Results represent least significant difference (L.S.D) data with differences between large and small droplets

Attribute	20% Aq	20% Aq with large droplets	Difference	L.S.D @ 95% confidence interval
Drag (H)	4.5 ± 1.5	3.5 ± 1.0	1.0	0.5
Drag (L)	4.7 ± 1.3	3.6 ± 1.3	1.1	0.6
S/T (H)	6.7 ± 1.4	7.0 ± 1.5	0.3	0.5
S/T (L)	5.5 ± 1.0	5.6 ± 1.7	0.1	0.6

In the qualitative analysis (language generation session) (an overview of language session is shown in Appendix 4), panelists commented that all three emulsion products performed well regarding moisturisation. Panelists identified that both emulsions with 20 wt % aq phase (regardless of droplet size) were thought to leave the lips feeling moisturised, supple and conditioned. Panelists also commented that it felt like the lipstick was melting and moisture was being absorbed leaving a more natural less coated feel to the lips.

6.2.3 Comparison between Tribology and Sensory

Friction coefficients obtained in section 6.2.1 *via* pin on disk tribology were compared to the sensory data (section 6.2.2) (Figure 6.20), in order to determine whether tribology was a suitable technique to predict consumer perceptions to new formulations. It was expected that as the friction of the formulation increased, the drag would also increase. However Figure 6.20 shows the exact opposite trend, where drag score decreases (6 – 3.6 (on lip) and 5.5 – 3.5 (on hand)) as friction increases from 0.06 – 0.2. It is hypothesised here that the perception of drag can be related to the attribute used in the food industry to describe smoothness (Chen and Stokes, 2012). Chen and

Stokes (2012) used the Kokini model (1987) to describe that the smoothness is inversely proportional to the friction (multiplied by the load). Figure 6.21 shows that when the Kokini model is applied, a linear relationship is observed for both hand and lip (R^2 = 0.9) testing, thus indicating that a tribometer can be used to relate frictional coefficient to the drag score obtained from a sensory panel. From an industrial point of view this is an important finding as the use of trained sensory panel is both time consuming and very expensive. A tribometer could be used to link the formulation design to sensory perception. However more data points would be required before this could be proved conclusively.

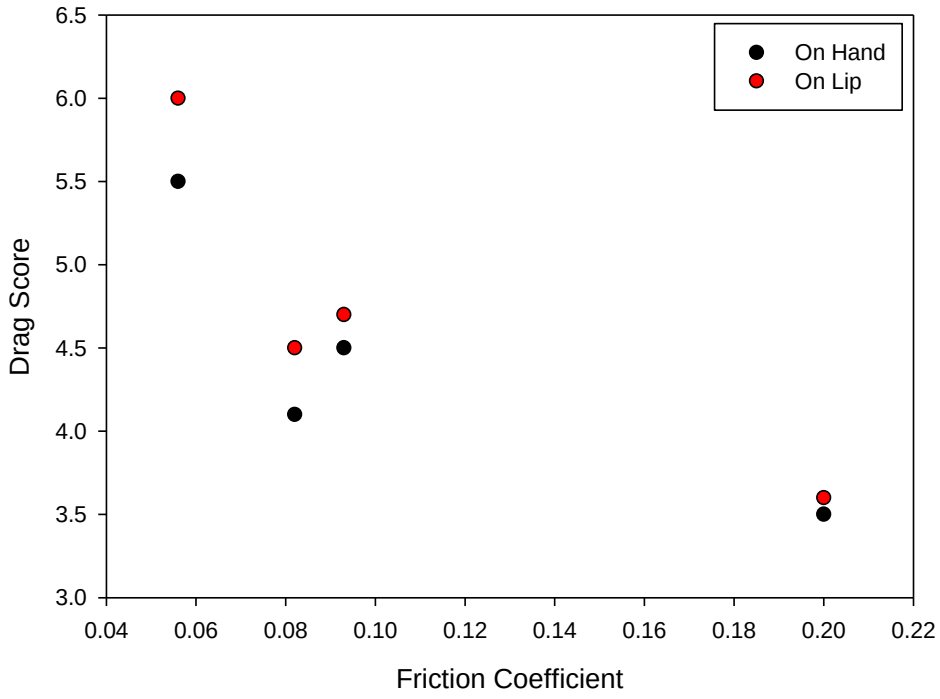

Figure 6.20 – Comparison of average drag score vs final friction final. Results taken from data presented throughout this chapter.

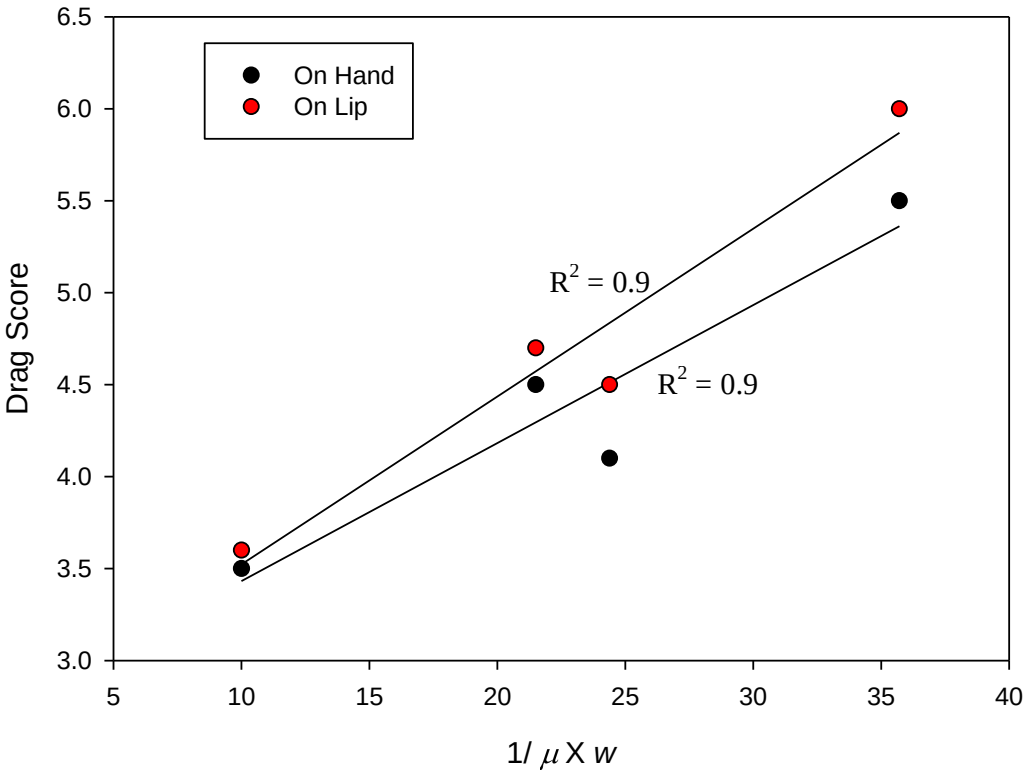

Figure 6.21 – Comparison of drag score vs 1/ friction coefficient multiplied by applied load (0.5N).

6.3 Concluding Remarks

In this chapter a pin-on-disk setup in a tribometer was used to examine the lubricating properties of a solid wax based system. These results showed that an applied load of greater than 1 N resulted in the solid wax disks fracturing thus preventing analysis. The disk rotational speed was also important in controlling the time taken for the disk to wear to a thin film.

In general, the friction coefficient slightly increased as the varying wax concentration increased (microcrystalline wax, paraffin and performalene). It was suggested here that this was a result of a greater amount of solid crystals being present in the contact zones. The friction coefficient also increased as aqueous phase volume and droplet size increased. This was due to a greater amount of water and larger droplets being present in the contact zone. It was also shown that the wear was directly linked to elastic modulus of the samples.

Sensory analysis showed that there was a significant difference when analysing drag scores. This suggests that panelists were able to distinguish a difference in this attribute. Post hoc analysis showed that panelists perceived emulsion samples, increasing in aqueous phase volume and water droplets to drag less than a wax blend formulation. On comparing the sensory panel drag results with tribological data it was shown that the drag perception followed the Kokani model. Thus showing that panelist related the drag to how smooth a formulation felt. These results are a promising start to predict how consumers will asses new formulations. However, further work is required to establish tribology as a suitable technique to model consumer expectations from formulations.

Chapter 7. Release of Glycerol from Wax Based Emulsion Systems for possible use in a Lipstick Application

7.1 Introduction

Addition of a water phase to lipstick formulations allows the introduction of hydrophilic ingredients (glycerol) that could deliver moisture directly to the lips. Glycerol has been widely used in the pharmaceutical and cosmetic industry, due to its humectant and protecting properties (Lodén and Wessman, 2001). Glycerol has been shown to diffuse into the stratum corneum (Batt and Fairhurst, 1986) which increases skin hydration (Lodén, 1996, Blichmann *et al.*, 1989, Serban *et al.*, 1983) and relieves clinical signs of dryness (Batt *et al.*, 1988, Dunlap, 1984).

Thus, the aim of this chapter was to develop a system for measuring the release of glycerol from wax based structures, which can be related to the release of glycerol from a lipstick system. Initially the release of glycerol was examined in a model formulation (without wax) and lipstick formulations (with wax), during quiescent conditions at three different temperatures (20 °C and 32 °C were chosen as they represent storage temperature and lip temperature respectively; whereas 80 °C was chosen as it is the point where all wax crystals are molten (shown in Figure 4.11). The phenomenon which governs release was modelled using COMSOL with MATLAB, and was related to temperature. Finally, the effect of compression on release was investigated in order to monitor the effect of disrupting a wax network.

7.2 Results and Discussion

In this section, the release of a moisturising agent (glycerol) from an emulsion based lipstick using two different experimental set ups (quiescent and compression (schematic shown in Figure 3.3)) was investigated.

7.2.1 Release under Quiescent conditions

Release was initially examined in a model system in order to understand the release behaviour of glycerol prior to encapsulation. Following this, wax was added to the system to create a shell that encapsulated the water/glycerol mix.

7.2.1.1 Model System

Figure 7.1 shows the release of glycerol from an emulsion structure as a function of time for 20, 32 and 80 °C. It should be noted that for all temperatures the shape of the curve has two distinct sections. Initially there is a fast release which slows as the majority of the glycerol is released.

Experiments conducted at 20 °C had the lowest release rates, releasing approximately 0.05 % of glycerol per minute. It is important to note that only 40 % of glycerol could be released before the emulsion phase separated (observed visually) into its two component phases (aqueous and oil) (process known as phase separation), which allowed the glycerol to diffuse freely into the surrounding body of water. At higher temperatures (80 °C), the highest release rate was observed, resulting in approximately 2.1 % of glycerol per minute being released. At this temperature 80 % of the encapsulated glycerol was released before phase separation occurred. The Stokes Einstein equation has been used in the literature to explain temperature based release. (Young *et al.*, 1980);

$$\boldsymbol{D} = \frac{\boldsymbol{R\,T}}{\boldsymbol{N}} \times \frac{\mathbf{1}}{\mathbf{6\,\pi\,k\,r}} \qquad \textbf{Equation 7.1}$$

Where, D is the diffusion coefficient, R is the gas constant, N is Avogadro's number, T is the absolute temperature of the system, k is the viscosity and r is the radius of the droplet.

From this equation it is clear that as temperature increases so does the diffusion coefficient assuming the other parameters remain constant (it is important to note the particle size will increase as phase separation occurs). This temperature dependence on the diffusion coefficient has been seen by both Türker and Erdoğdu (2006) and Mills (2011). Türker and Erdoğdu investigated the effective diffusivity of anthocyanin pigments from black carrot samples at varying temperatures (25 – 50 °C). Results showed that the effective diffusivity increased from 3.73 – 7.37 m^2/s at pH 2 as temperature increased from 25 - 50 °C. This was explained using Einstein's equation (Cacace and Mazza, 2003) for diffusion which states that the diffusion coefficient is proportional to the temperature and dynamic viscosity^{-1} (Türker and Erdog˘du, 2006). Therefore one would expect the effective diffusivities of glycerol to increase in a proportional manner if the release was governed solely by temperature.

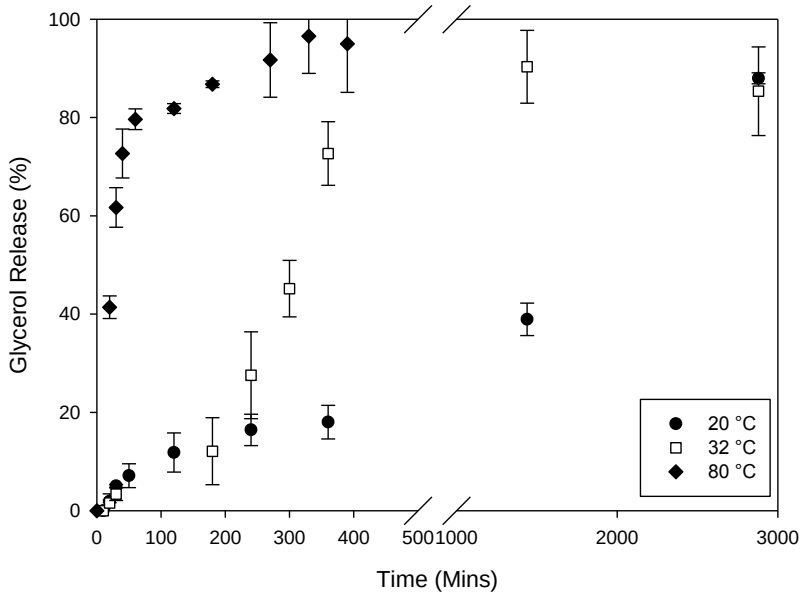

Figure 7.1 - Glycerol release over a period of time into 200 ml of water from 30 g of emulsion at 3 different temperatures under quiescent conditions. Release was measured using FT-IR. All emulsions contained 30 wt % aq phase (50:50 glycerol:water), 68 wt % castor oil and 2 wt % PGPR.

7.2.1.2 Mathematical Modelling

The effective diffusivities were calculated using a method developed in COMSOL (a similar model was used by Mills *et al.* (2011)). A system was set up which assumed pure Fickian diffusion, which is defined as diffusion that follows a concentration gradient over time (Bergman *et al.*, 2011). The model was run as a script linked with MATLAB. The effective diffusivity was altered to reduce the sum of squares between the calculated and actual values. Figure 7.2 shows a comparison of calculated and experimental data for 20, 32 and 80 °C. For all temperatures, the initial predicted glycerol release is faster than the experimentally measured release. This difference can be attributed to a lag in recording as the system was under quiescent conditions and instantaneous mixing would not have occurred. After the initial lag there was close agreement with both the experimental and calculated data for all temperatures until ~1450 minutes (for 20 °C), ~180 minutes (for 32 °C) and ~40 minutes (for 80 °C). After these points phase separation of the emulsion occurs, which results in the experimental

data deviating from the model results. This causes the trapped glycerol to be released into the surrounding body of water. Therefore the effective diffusivities were calculated before phase separation. The results observed (Figure 7.2) before the phase separation point are similar to that shown by Mills *et al.* (2011), who investigated the release of salt from gel structures. Mills *et al.* showed that there was close agreement between model and experimental data when analysing gel structures made from 0.5 % gellan at 25 °C, which showed an 80 % release of salt after ~60 minutes. They concluded that this release was governed by a simple diffusion mechanism (Mills *et al.*, 2011).

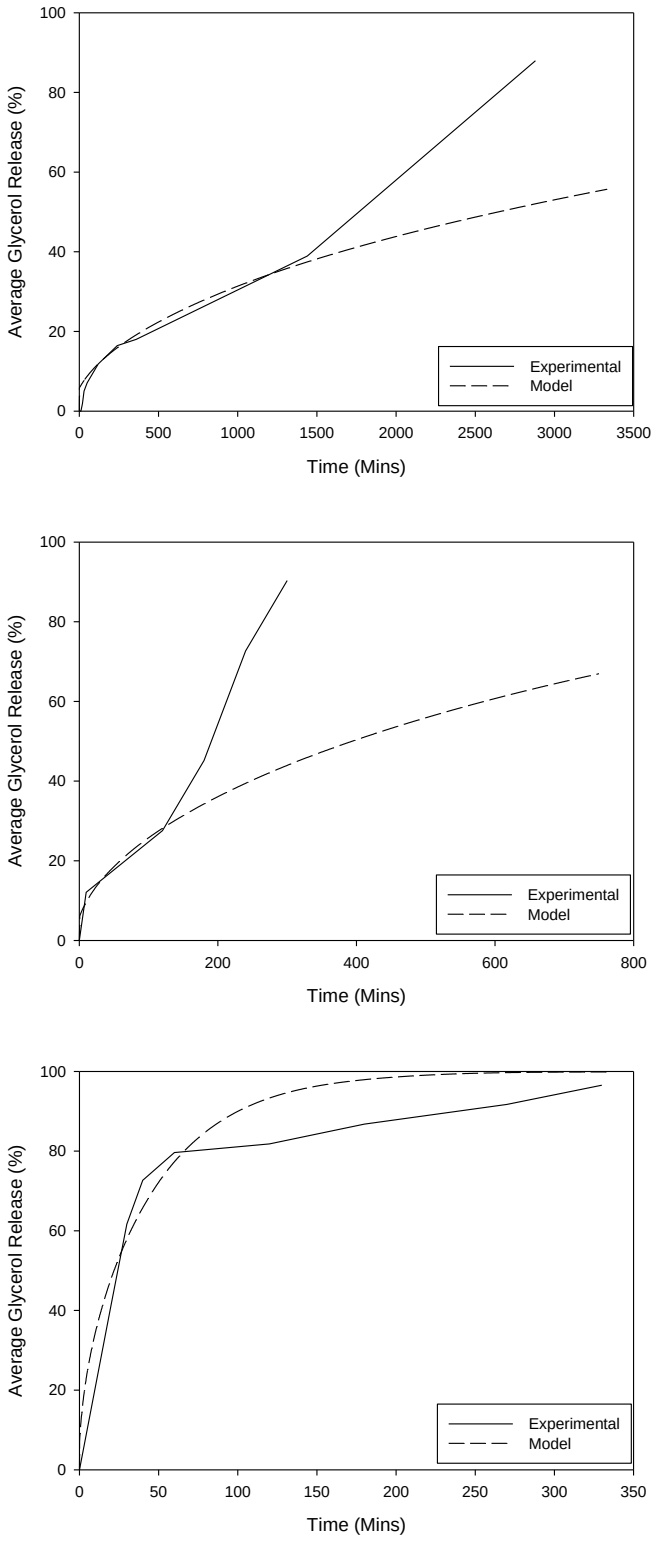

Figure 7.2 - Comparison of model output and experimental data for glycerol release over time from 30 g emulsion samples at (a) 20 °C, (b) 32 °C and (c) 80 °C. All emulsions contained 30 wt % aq phase (50:50 glycerol:water), 68 wt % castor oil and 2 wt % PGPR.

Table 7.1 shows the effective diffusivities calculated using the COMSOL model at three different temperatures (20, 32 and 80 °C). Results show that as temperature increases from 20 to 80 °C the effective diffusivity increases from 0.013 – 1.36 x 10^{-8} m^2/s respectively. These values are very similar to that obtained by Henin *et al.* (2008) who investigated the diffusion of glycerol through Escherichia coli Aquaglyceroporin GlpF. They utilised a NAMD simulation package to calculate the effective diffusivity which was compared to experimental data. They found that their simulations generated similar effective diffusivities (0.21 x 10^{-8}) m^2/s) when compared to the experimental data (0.11 x 10^{-8}) m^2/s) at 25 °C (Hénin *et al.*, 2008). The values obtained by Henin *et al.* are similar to those observed in this study 0.3 x 10^{-8}) m^2/s at 32 °C. Thus indicating that the water/glycerol droplets are free to move through the continuous phase (without being trapped) *via* simple diffusion.

Table 7.1 - Effective Diffusivities of glycerol at different temperatures in quiescent conditions. Calculated assuming Fickian diffusion using a model from COMSOL linked to MATLAB.

Temperature (°C)	Effective diffusivity (m^2/s)(10^{-8})
20	0.013
32	0.30
80	1.36

7.2.1.3 Effect of Wax Addition

It the previous section it was shown that glycerol can move through the continuous phase *via* simple diffusion. However, when producing an emulsion suitable for use in lipstick application, wax needs to be considered as part of the formulation. Therefore the effect of wax addition on glycerol release in quiescent conditions was investigated at

three different temperatures. Le Reverend *et al. (2011b)* have shown that in water-in-oil emulsions, waxes adsorb at the interface which stabilises the emulsion, thus preventing coalescence of the water droplets. This is achieved by producing shells around the aqueous droplets which prevents water migration. Therefore it is hypothesised here that wax addition will inhibit the release of glycerol by producing shells around the aqueous droplets resulting in encapsulation of the water/glycerol mix. Thus changing the diffusion mechanism from simple diffusion to barrier controlled diffusion. Barrier controlled mechanisms have been shown in the food industry (Pothakamury and Barbosa-Cánovas, 1995) and are described as reservoir systems, whereby an active ingredient is trapped in a droplet by a barrier which is either: micro porous, macro porous or non-porous (Langer and Peppas, 1983a). This barrier then either slows down the rate of release or inhibits release completely depending on the thickness and permeability of the barrier (Baker and Lonsdale, 1974).

Figure 7.3 shows the effect of adding wax (barrier) (15 wt % of the continuous phase (5 wt % carnauba wax and 10 wt % microcrystalline wax in castor oil)) on release at three different temperatures. At 20 °C (Figure 7.3a) and 32 °C (Figure 7.3b), the addition of wax prevents the release of glycerol. However at 80 °C (Figure 7.3c), there is a slow release observed up to 400 minutes. At this point the emulsion phase separates resulting in full release. The initial slow release is caused as the shells around the droplets begin to melt allowing glycerol to diffuse through the continuous phase. The effect of temperature on release has also been observed in the food industry by Frasch-Melik *et al.* (2010). In that study they investigated the release of salt from sintered shells. Results showed that as temperature increases from 5 – 50 °C (allowing crystals to melt) the time taken for release to occur decreases from > 100 days to 20 seconds respectively.

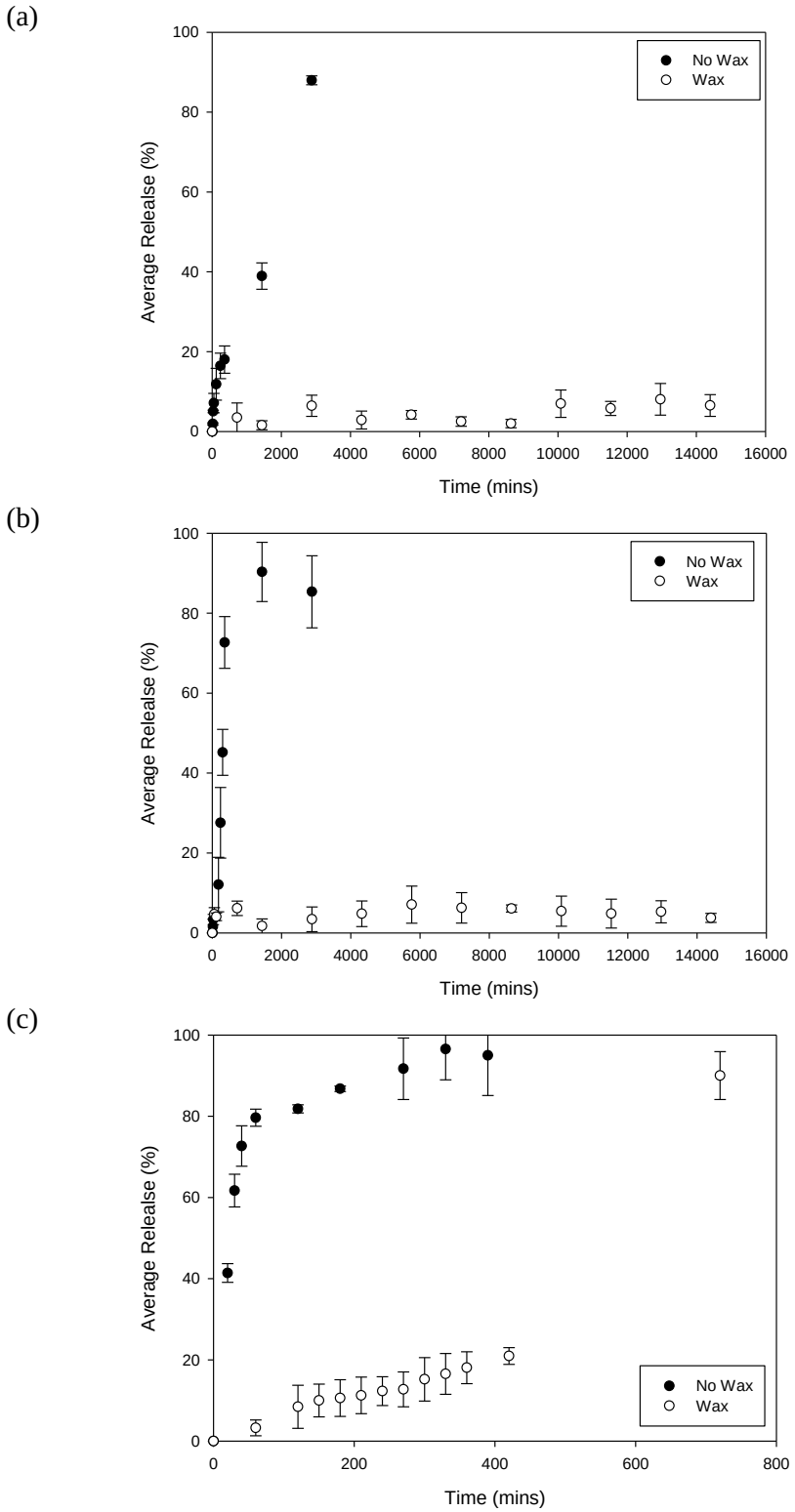

Figure 7.3 - Comparison of glycerol release of systems containing wax and no wax over time (12 days) into 200 ml of water from a 30 g emulsion at three different temperatures: (a) 20 °C, (b) 32 °C and (c) 80 °C under quiescent conditions. Release was measured using FT-IR. Emulsions contained 30 wt % aq phase (50:50 glycerol:water), 68 wt % continuous phase (either castor oil or 5 wt % carnauba wax and 10 wt % microcrystalline wax in castor oil) and 2 wt % PGPR.

Figure 7.3 clearly shows that the addition of 15 % wax (5 wt % carnauba wax and 10 wt % microcrystalline wax in castor oil) to the continuous phase inhibits the release of glycerol. However it is unclear whether this is the critical concentration required to induce barrier controlled release. Therefore the amount of wax added to the continuous phase was reduced in increments from 15 % to 3.75 % in order to determine the effect of varying the total wax concentration on barrier controlled release. Figure 7.4 shows that when no wax is present 80 % of glycerol is released within ~45 hours. The addition of 3.75 – 15 % wax results in a reduction in the amount of glycerol released, with only ~10 % released over a period of 12 days. The release of glycerol (or lack of release) from these structures seems to be governed by the presence of wax crystals at the interface. To visualise these shell like structures Cryo-SEM was utilised. Figure 7.5 shows droplets embedded into a network which are coated with wax crystals that sit either at or in the interface. These images are similar to those previously published in the literature by Norton *et al.* (2009) for chocolates.

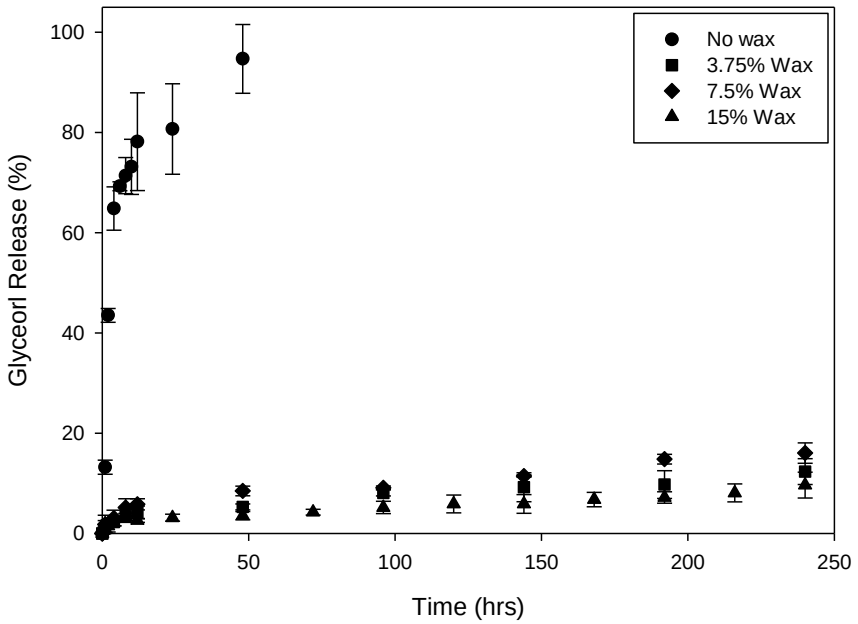

Figure 7.4 - Comparison of glycerol release from systems with varying wax content over time (10 days) into 200 ml of water from a 30 g emulsion at 32 °C. Release was measured using FT-IR.

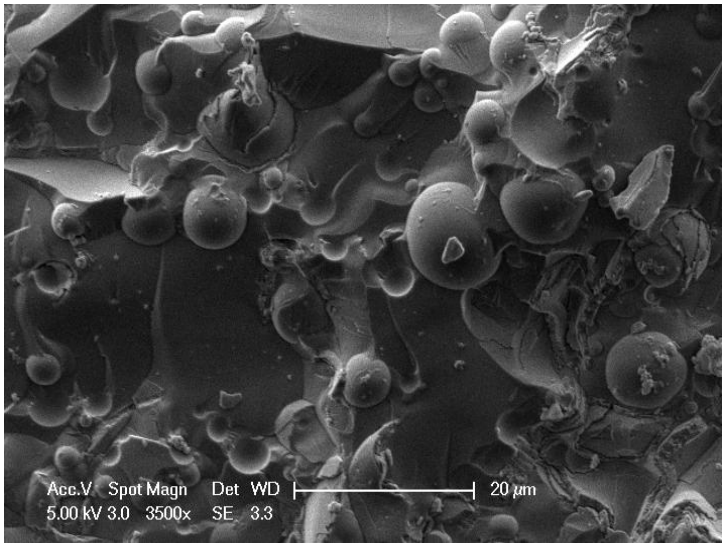

Figure 7.5 - Cyro-SEM micrograph of water/glycerol droplets trapped in a wax shell surrounded by a hydrophobic continuous phase. Emulsion contained 30 % aquoues phase (50:50 mix of water and glycerol), 68 % continuous phase (5 % carnauba wax, 10 % microcrystalline wax and 85 % castor oil) and 2 % polyglycerol polyricinoleate.

7.2.2 Release under compression

In order to relate the release of glycerol from solid emulsions to application on lips, it is important to consider the effect of structural breakdown on glycerol release. Samples were tested using the compression set up described in the materials and method section (Figure 3.3). A texture analyser was then used to provide compressions. The use of a texture analyser allows the sample to experience different degrees of disruption by varying the strain. Samples containing glycerol were then tested using 7, 20 and 90 % strain, and release was calculated using FT-IR (Further details are available in section 3.3.4.3). Cyclic compressions (every 3 minutes) were used at 7 and 20 % each strain to highlight the effect of multiple compressions on structural breakdown, whereas only one compression occurred at 90 % strain.

Figure 7.6 shows the release of glycerol from emulsions being compressed every 3 minutes. It clearly shows that there is no difference in release when being compressed at different strains. For all strains, a release of approximately 10 % is observed. This is independent of the destruction caused to the structure. It is hypothesised here, that the 10 % release is a result of having an emulsion with varying droplet sizes. Whereby large droplets (coated in a wax shell) can be fractured under compression and small droplets (coated in wax shells) interact with the deforming continuous phase allowing them to flow (un-fractured) under compression. To test this theory; the droplet size of emulsions was initially calculated using restricted NMR (Table 7.2). This showed that when 2 % PGPR was used, approximately 90 % of the emulsion resulted in small droplets ($d_{3,2}$ ~12 μm) and ~10 % of the emulsion contained large droplets ($d_{3,2}$ > 100 μm). These findings agreed with the initial hypothesis and to test this further, the amount of PGPR was reduced to increase the amount of larger droplets in the emulsion. When 1 wt % PGPR was utilised in the formulation the larger droplets increased to ~ 34 %. Therefore

it is expected that when the 1 % PGPR emulsions are compressed the glycerol release should increase.

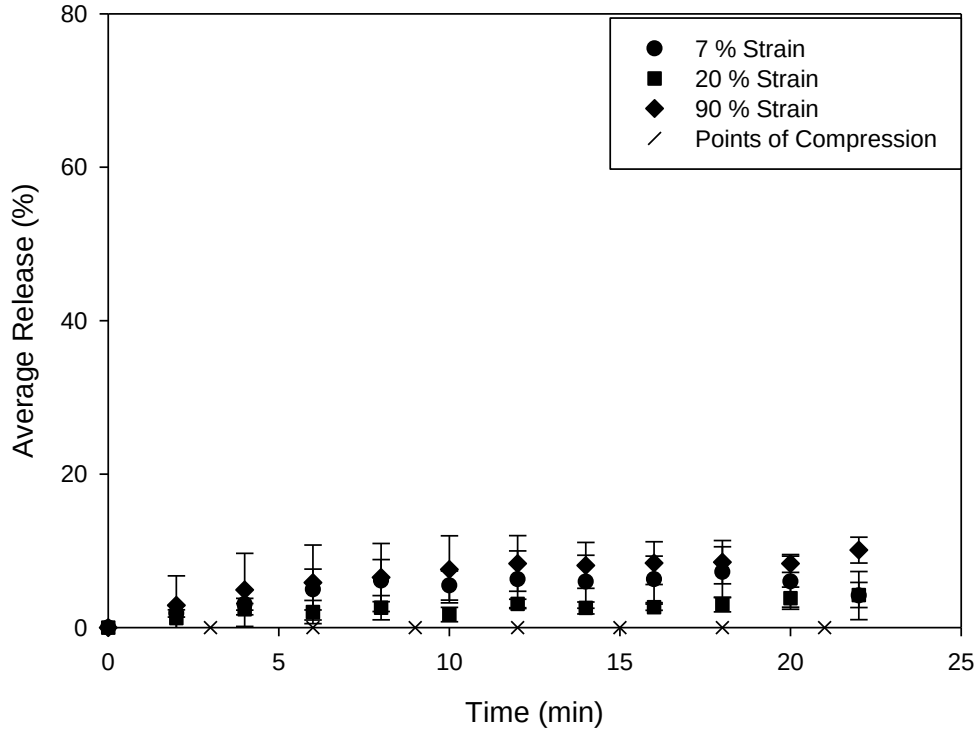

Figure 7.6 - Glycerol release over time (into 200ml of water) from 30g emulsions. Emulsions were compressed at varying strains (7, 20 and 90 %) every 3 minutes over 21 minutes. Emulsions contained 2 % PGPR. Release was measured using FT-IR.

Table 7.2 - Mean droplet diameter ($d_{3,2}$, µm) measured by NMR restricted diffusion on day of formation as a function of PGPR concentration. Standard deviation is of triplicate measurements.

Amount of Emulsifier	Mean Droplet Size ($d_{3,2}$)	Standard deviation	Droplets(≥ 100 µm)
2 % PGPR	12	0.4	~ 10 %
1 % PGPR	17	4.5	~ 34 %
2% PGPR (only Paraffin)	8.4	0.9	~ 7 %

Figure 7.7 shows the effect of compression on a 1 wt % PGPR emulsion. Results show there is still minimal release when the sample is compressed under elastic deformation (7 % strain). It is suggested that there is no destruction of the sample during elastic compression which results in minimal glycerol release. Figure 7.8 shows seven repeat force/distance curves for a single 1 wt % PGPR emulsion. The structure is shown to be elastic under small strains where the curves overlap for each compression. These findings are similar to those shown by Mills (2011), who showed that gelatine structures exhibited elastic behaviour under low strain (30 %).

When the structure is fractured (20 % and 90 % strain) approximately 35 % of glycerol is released after 24 minutes. To confirm that this was due to larger droplets being fractured, the droplet size of emulsions containing 1 % PGPR was calculated using a restricted NMR diffusion technique (Table 7.2). Results show that when 1 % PGPR is utilised then approximately 35 % of droplets are greater than 100 μm. Thus, confirming the hypothesis that release occurs from larger droplets.

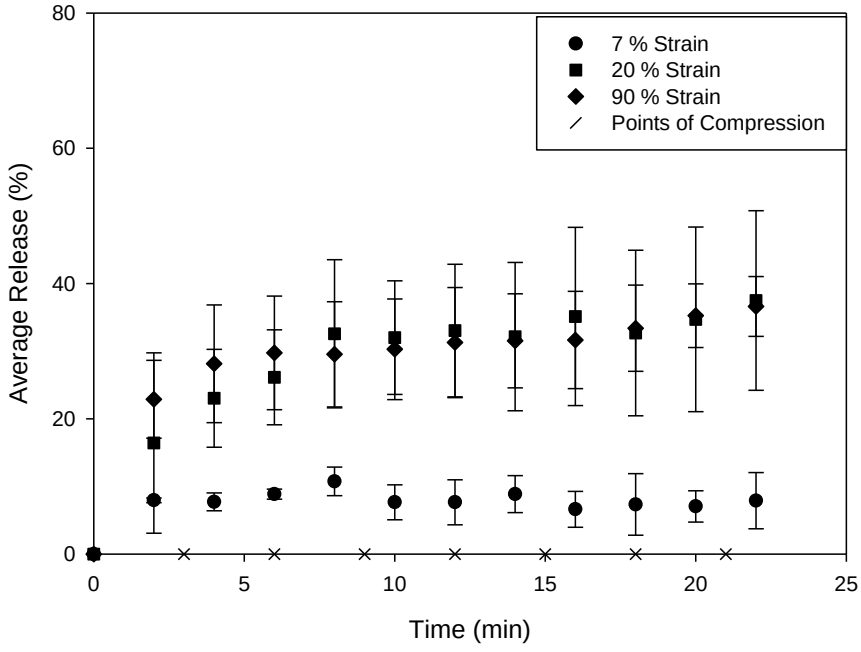

Figure 7.7 - Glycerol release over time (into 200ml of water) from 30g emulsions. Emulsions were compressed at varying strains (7, 20 and 90 %) every 3 minutes over 21 minutes. Emulsions contained 1 % PGPR. Release was measured using FT-IR.

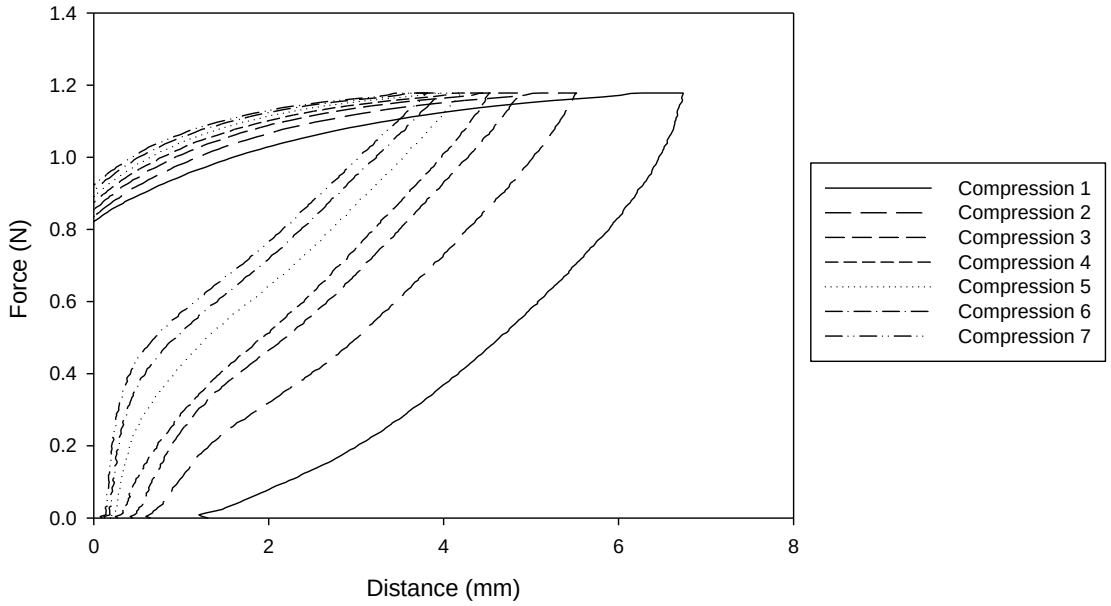

Figure 7.8 – Force Distance curves for emulsions at 7 % strain, using 1% polyglycerol polyricinoleate samples. 30g cylindrical segments were compressed at 1 mm/s, to 7 % of the original height, 7 times with 3 minute intervals.

To further confirm that release is governed by wax forming at the interface (resulting in a shell), an alternative wax (paraffin) which is known not to migrate to this surface was used (Le Révérend *et al.*, 2011b). Paraffin wax is known to form large crystals that are not surface active, but crystallise in the continuous phase (Le Révérend *et al.*, 2011b). It is important to note that when paraffin wax was used as the wax component, the average droplet size did not drastically change (8.4 μm) and neither did the amount of droplets greater than 100 μm (~7 %). Samples containing paraffin wax were then compressed to 90 % strain and the release was monitored over a period of 12 days. When wax crystals are not at the interface, release increases from 0.5 to 31 % over 12 days (Table 7.3), whereas when wax crystals are at the interface, release remains constant from day 1 to day 12 (~18.5 %). This is due to the wax crystals acting as a barrier which inhibits the release of glycerol.

Table 7.3 - Glycerol release over time (into 200 ml of water) from 30 g emulsions. Emulsions were compressed (90% strain) and stored at 32 C for 12 days. Release was measured using FT-IR. All emulsions contained 2 % PGPR and a continuous phase of 68 % (either: 5 % carnauba wax and 10 % microcrystalline wax in castor oil or 15 % paraffin in castor oil).

Continuous Phase	Average Released (%)		
	After 20 min	Day 1	Day 12
Wax Phase (no paraffin)	10.1 ± 1.7 %	19.2 ± 5.9 %	18.5 ± 1.3 %
Wax Phase (only paraffin)	0.5 ± 0.3 %	10.3 ± 2.3 %	31 ± 6.9 %

In an attempt to visualise the differences between wax crystals being at either the interface or Figure 7.9 shows SEM micrographs of emulsions with varying continuous formulations (either 15 wt % paraffin wax in castor oil (Figure 7.9 a,b and c) or 5 wt % carnauba wax and 10 wt % microcrystalline wax in castor oil (Figure 7.9d, e and f)) at varying etching times. When emulsions with paraffin in the continuous phase were etched, visible craters are observed in the microstructure. This suggests that the droplets were not trapped in a shell structure and there the liquid evaporated off during etching. Whereas when the emulsions containing both carnauba wax and microcrystalline wax in the continuous phase were etched, no craters were physically visible. Instead coated shell like droplets were observed, thus confirming that emulsions with wax at the interface prevent glycerol from freely moving through a structure which inhibits release.

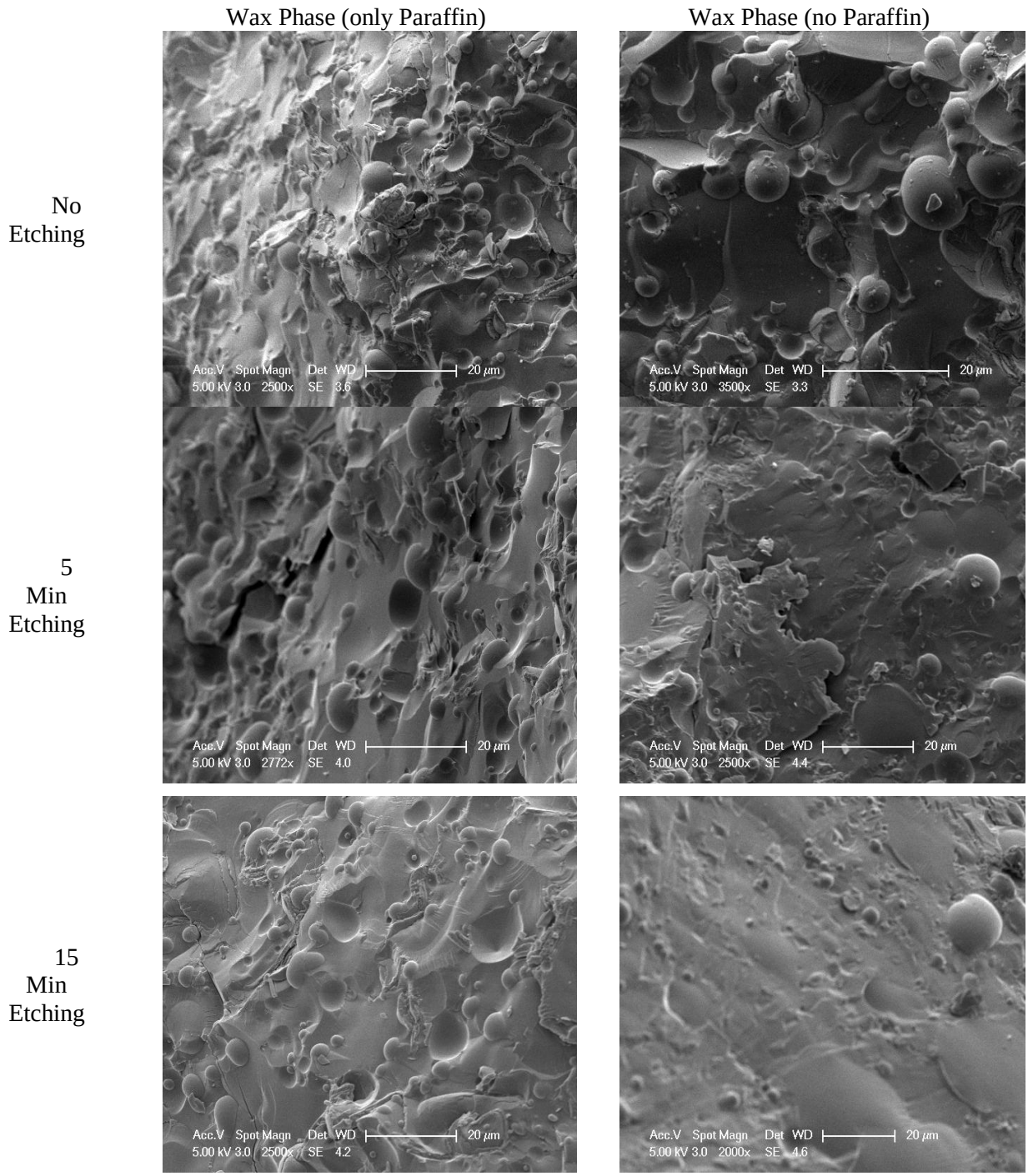

Figure 7.9 – Cyro-SEM micrographs of water/glycerol droplets surrounded by a hydrophobic continuous phase where (a), (b) and (c) consist of 15 % paraffin wax in castor oil and (d), (e) and (f) consist of 5 % carnauba wax and 10 % microcrystalline wax in castor oil. All samples were treated with 0, 5 or 15 minute etching times.

7.3 Concluding Remarks

It can be concluded from this work that the release curves obtained under quiescent conditions show that there is very little to impede the diffusion of glycerol in systems containing no wax. Modelling of quiescent conditions has allowed effective diffusivities to be calculated and these showed the release rate is controlled by temperature. The addition of wax changes the release mechanism from simple diffusion to a barrier controlled mechanism by producing shells that inhibit release.

Compression was then shown to affect the release of glycerol, depending on the size of the droplets and the disruption caused to the structure. Small shell coated droplets inhibited release, as the droplets do not fracture under compression. When larger droplets are produced: release is governed by the amount of strain applied to the structure. If low strain is used (7 %), there is only elastic deformation which does not cause release whereas any strain greater than the point of fracture (>20 %) resulted in glycerol release.

It was shown that the release of glycerol is controlled by a barrier controlled diffusion when a wax shell is present. This allows these structures to be suitable for use in lipstick application, as release will not occur in storage but in application. Future work should consider controlling the release rate of glycerol under compression.

Chapter 8. Conclusions and Future Recommendation

This thesis examined the production of wax based emulsion systems suitable for application in lipsticks. Specifically, this work consisted of

- Designing emulsion structures using either a batch (in particular the effect of emulsifiers and aqueous phase volumes) or continuous process (in particular processing parameters). This included investigating the melting behaviour of wax based emulsions. Emulsion structure was assessed using a variety of techniques.
- Manipulating the material properties of wax based emulsion systems. This included investigating different waxes and wax blends and the effect of water inclusion and water content. The material properties were then manipulated using a continuous process which allowed the control of crystallisation in the process. The material properties were assessed using either uni-axial compression and/or oscillatory rheology.
- Using a pin-on-disk tribometer to monitor the lubricating properties of solid wax based emulsion systems. This included investigating the role of different waxes, water content, dispersed phased viscosities and droplet size on friction coefficient and wear. Following this, a trained sensory panel was used to compare to identify links between tribological data with sensory attributes.
- Monitoring release of glycerol from wax based structure. This included investigating a technique to monitor the release of glycerol. Followed by monitoring the release of glycerol from wax based structure, in both quiescent conditions and during structural breakdown.

8.1 Designing Emulsion Structures

Water-in-oil (W/O) emulsions were prepared using either a batch process or a continuous process. Emulsions were initially assessed in terms of droplet size, after which the melting behaviour of wax based emulsions was investigated.

- Batch Process

Emulsions were stabilised using a variety of emulsifiers (monoolein, monostearate, sorbitan olivate and polyglycerol polyricinoleate (PGPR) Results showed that droplet size was not affected by the saturated nature of the monoglycerides or by increasing the head group size (sorbitan olivate) ($d_{3,2}$ ~ 18 – 25 μm), PGPR stabilised emulsions, resulted in the smallest droplets (~ 2 – 4 μm) due to its ability to form a thick elastic interface (Le Révérend *et al.*, 2011b).

- Continuous Process

A lab scale scraped surface heat exchanger (SSHE) and pin stirrer (PS) were shown to be able to (1) produce emulsion based lipsticks and (2) control emulsion properties (*e.g* droplet size). Results showed that when the SSHE was utilised with higher impeller rotational velocities (IV) (1500 rpm) there were greater disruptive forces which produced smaller droplets (~ 3 μm). The addition of PS to the process only affected the droplet size when the SSHE had a low IV (500 rpm).

- Melting Behaviour

The melting behaviour of different waxes, wax blends was assessed using DSC. Results showed that a wax blend (5 wt % carnauba wax (CW) and 10 wt % microcrystalline wax (MW) in castor oil) provided a melting range (30 – 80 °C) similar

to a commercially available lipstick (30 – 90 °C). It was also concluded that the melting profile is not affected by incorporation of water or by increasing aqueous phase volume.

8.2 Manipulating Material Properties

Material properties of wax based emulsion systems were assessed using either uni axial compression or oscillatory rheology. Initially individual waxes and wax blends were investigated. This was followed by the assessment of incorporating water, increasing aqueous phase volume and controlling crystallisation (in the process) on the material properties.

- Waxes/Wax blends

Results showed that Young's modulus, bulk modulus and point of fracture increase with increasing percentage of CW (which follows a power law dependency of 3), but decreases with an increasing percentage of MW. It was concluded that CW is part of the overall wax crystal network (comprised of saturated components), whereas the MW forms irregular crystals that disrupt the overall wax crystal network.

- Incorporating an aqueous phase

Increasing aqueous phase volume (droplets with a $d_{3,2}$ of 2 – 4 μm) resulted in a decrease of Young's modulus, elastic modulus and viscous modulus. The slope of the decrease (for elastic and viscous moduli) is dependent on the addition of paraffin or performalene (which both strengthen the network). It was concluded that emulsions containing 30 wt % aqueous phase (with either paraffin or performalene) had very similar material properties to a non emulsified control system.

- Controlling Crystallisation

Controlling crystallisation in the process was achieved using a scraped surface heat exchanger (SSHE) and pin stirrer. In particular, crystal size was adjusted by altering the temperature gradient between the inner walls of the chamber and the emulsions. This allowed the ratio of small crystals formed in the SSHE chamber and large crystals formed in post production to be altered by varying the flow rate through the unit. Results showed that emulsions formed where crystallisation occurred in both the chamber and post production produced water droplets coated in a wax shell, which allowed the wax coated droplets to interact with the larger wax crystals in the continuous phase. This resulted in an increase in the strength of the emulsion.

8.3 Tribology of Wax Based Systems

Lubricating properties of solid wax based systems were assessed using a pin on disk setup in a tribometer. Initially individual waxes and wax blends were investigated. This was followed by the assessment of incorporating water, increasing aqueous phase volume and varying dispersed phase droplet size on both the friction coefficient and the wear. Finally these results were compared to degree of difference scores obtained from a trained sensory panel.

- Waxes/Wax Blends

Results showed that the friction coefficient slightly increased as the wax concentration increased. This was due to a greater amount of solid wax crystals within the contact zones. It was also shown that the wear was directly linked to elastic modulus of the wax samples. This is also true for all emulsion samples.

- Increasing Aqueous Phase Volume/ varying droplet size

Results showed that as both aqueous phase volumes increased and droplet size increased so did the friction coefficient. This was shown to be due to either a greater volume of water or larger droplets being present in the contact zone.

- Sensory Analysis

Results showed that trained panelists were able to distinguish a difference in drag when investigating increasing aqueous phase volume and droplet size. It was shown that the drag scores followed the Kokani model, therefore indicating that tribology could be used to predict how smooth a formulation may feel.

8.4 Release Behaviour of Glycerol

Release of glycerol under quiescent and uni axial compression was assessed using FT-IR. Initially the release of glycerol was assessed in a model system (no wax) in order to understand glycerol's release behaviour. The glycerol was then encapsulated in a wax shell and the release was assessed in quiescent conditions. Following this the encapsulated glycerol was compressed to assess the release under structural breakdown.

- Quiescent Conditions

Results showed that in a model system, release was a function of temperature, where the effective diffusivities increased as the temperature increased. This showed that in a model system, diffusion was controlled by simple Fickian diffusion.

Results also show that the release mechanism changes from simple diffusion to barrier controlled diffusion upon the addition of wax to the formulation. This is a result of the wax producing a shell around the glycerol which inhibits release.

- Uni Axial Compression

Results show that release under compression is dependent on the size of the droplets and the disruption caused to the structure. When small encapsulated droplets are produced, glycerol release is inhibited as the droplets do not fracture. However, when large encapsulated droplets are produced, release is controlled by the amount of strain applied to the system. Results showed that a strain of greater than 20% is required to cause glycerol release.

8.5 Future Work

This section is designed to highlight possible areas of future research based on the conclusions made throughout this thesis.

- Incorporation of pigments into the continuous phase of the formulation.

Throughout this thesis, a model system has been utilised to investigate the use of an emulsion in lipstick application. In order for this to be considered as a product, one must consider the impact of pigments on the formulation. Pigments come in various forms (Eoisin Y and Eoisin B), traditionally in Boots formulations, they are hydrophobic in nature. In conventional formulations (*i.e.* completely hydrophobic), pigments are added to the castor to be dispersed. Therefore one should investigate the effect of adding pigments to the continuous phase of the emulsions and thus the effect this has on both the droplet size and material properties of the final emulsion. It is suggested here that the addition of a solid pigment will increase the G' of the formulation, this is based on the results shown in Chapter 5 which showed that the addition of solid material increased the G'.

The way in which the pigment is added to the emulsion can be investigated. The pigment could be dispersed through the continuous phase using the SSHE and PS process or alternatively it could be added to the continuous phase using a Silverson high shear mixer.

Long term work in this area could include investigating the effect of multi pigment systems whereby both a hydrophobic pigment and a hydrophilic pigment could be added in order to produce a lipstick with multiple colors.

- Investigate different crystal sizes

Chapter 5 shows the effect of different crystal sizes on material properties. It order further this work the crystals could be visualised. This can be achieved by using a hot stage microscope thus allowing the visualisation of crystals to occur as they grow at varying cooling rates.

The hot stage microscope has been utilised in the pharmaceutical industry. Araya-Sibaja *et al.* (2014) used this technology to visualise the polymorphic changes in progesterone from form 1 to form 2.

- Extensive comparison between tribological and sensory data.

Chapter 6 showed a link between drag scores obtained from a sensory panel and 1/friction coefficient obtained from tribological data. This link highlighted that the drag corresponded to how smooth a formulation behaved based on the Kokani model. To validate these findings further, more data points are required with varying drag scores. This can be achieved by producing emulsions with varying aqueous phase volumes (5 – 50 %, at iterations of 5 %). These can then be the analysed by a pin-on-disk tribometer and assessed by a trained sensory panel. It should be noted that initially this process will be extremely expensive as a trained sensory panel is an expensive investment. However once complete, formulations could be assessed using a tribometer to predict how smooth said formulation would be perceived.

- Controlling release of glycerol

The aqueous phase of the emulsion could be turned into a quiescent gel in order to slow the release of glycerol upon destruction of the network. This would require a comprehensive investigation into varying hydrocolloids (*i.e.* xanthan gum, guar gum, carrageenan etc) to produce a quiescent gel.

Garrec and Norton (2012) produced gels using a SSHE and PS with a selection of hydrocolloids. These included guar gum, locust bean gum, λ-carrageenan and scleroglucan. Emulsion based lipsticks have been produced using a SSHE and PS throughout this thesis, therefore quiescent gels could be produced in the same process.

Following production of a gelled emulsion lipstick, release would have to be investigated under compression (as results in this thesis have shown no release occurs from a wax based emulsion unless the network is destroyed). The release rates can then be compared to deliver varying levels of moisture to the lips.

Appendices

Appendix 1

Droplet size vs PGRP concentration over time with varying aqueous phase volumes

Table 0.1 Mean droplet diameter ($d_{3,2}$, µm) measured by NMR restricted diffusion from day 0 to day 180 for emulsions produced with varying PGPR concentrations (0.5, 1, 2 and 5wt%). All emulsions contain 10 % (Top), 20 % (Middle) and 40 % (Bottom) water.

	Day 0		Day 1		Day 7		Day 10		D ay 180	
PGPR Concentration (%)	d3,2 (µm)	SD (σ)	d3,2 (µm)	SD (σ)	d3,2 (µm)	SD (σ)	d3,2 (µm)	SD (σ)	d3,2 (µm)	SD (σ)
0.5	4.6	1.1	4.2	0.5	4.1	0.5	4.2	0.5	4.1	0.4
1	4.4	0.8	4.2	0.6	4.3	0.8	4.4	0.8	4.3	0.7
2	2.4	0.2	2.1	0.5	2.1	0.4	2.5	0.3	2.1	0.3
5	2.5	0.1	2.5	0.1	2.3	0.3	2.5	0.1	2.0	0.1

	Day 0		Day 1		Day 7		Day 10		D ay 180	
PGPR Concentration (%)	d3,2 (µm)	SD (σ)	d3,2 (µm)	SD (σ)	d3,2 (µm)	SD (σ)	d3,2 (µm)	SD (σ)	d3,2 (µm)	SD (σ)
0.5	5.8	1.8	5.8	1.8	5.8	1.8	5.8	2.0	5.9	1.9
1	3.4	0.2	3.4	0.2	3.4	0.2	3.3	0.2	3.3	0.2
2	2.8	0.1	2.5	0.4	2.7	0.1	2.6	0.1	2.8	0.1
5	2.3	0.1	2.3	0.5	2.0	0.1	2.0	0.2	2.0	0.2

	Day 0		Day 1		Day 7		Day 10		D ay 180	
PGPR Concentration (%)	d3,2 (µm)	SD (σ)	d3,2 (µm)	SD (σ)	d3,2 (µm)	SD (σ)	d3,2 (µm)	SD (σ)	d3,2 (µm)	SD (σ)
0.5	n/a	n/a	n/a	n/a	n/a	n/a	n/a	n/a	n/a	n/a
1	3.4	0.1	3.4	0.1	3.5	0.1	3.4	0.1	3.4	0.1
2	2.7	0.4	2.6	0.4	2.7	0.4	2.7	0.5	2.6	0.4
5	2.8	0.1	2.7	0.1	2.8	0.1	2.8	0.1	2.9	0.1

Appendix 2

Bulk modulus and Point of fracture of an emulsion which passes through both SSHE and PS

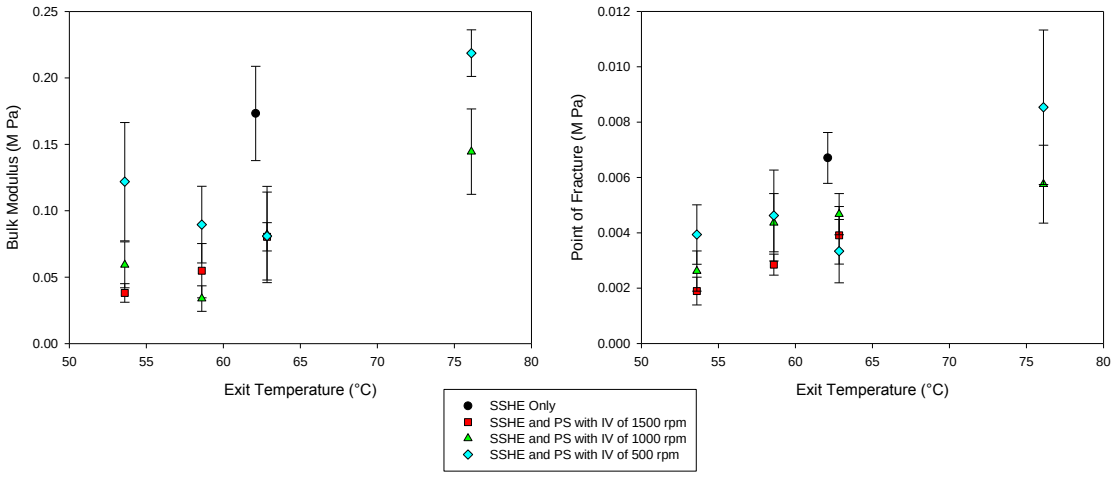

Figure 0.1 - Bulk modulus (left) and point of fracture (right) as a function of exit temperature for W/O emulsions passed both the SSHE (IV = 1500 rpm) and PS, at various shaft speeds. Flow rate was fixed at 60 mL/min. All samples were cooled quiescently in a freezer until solid then tested with a compression rate of 1 mm/s at 32°C.

Appendix 3

Effect of MW concentration on the time taken to wear

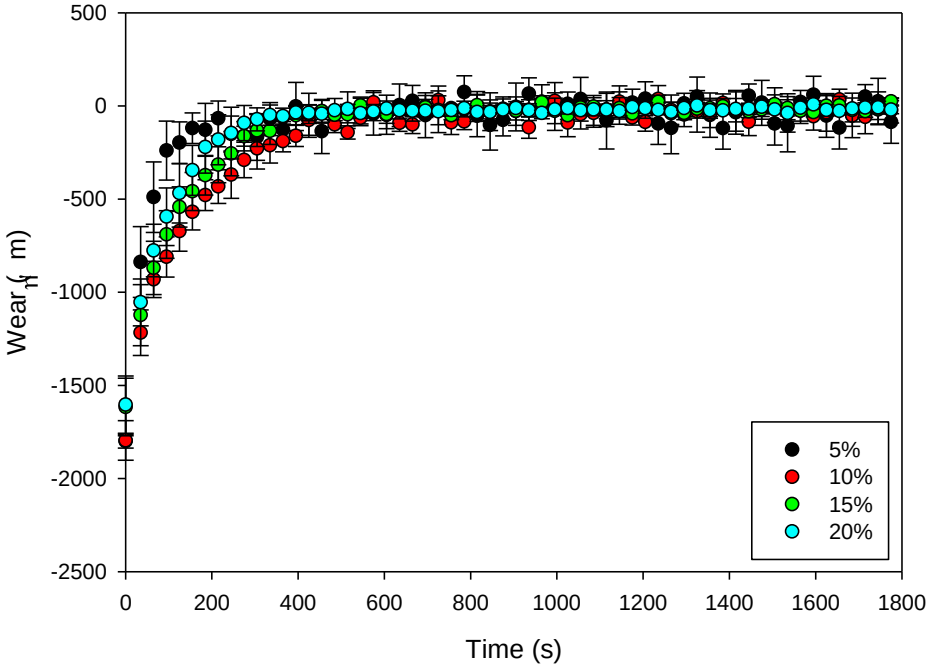

Figure 0.2 Wear vs time for a varying microcrystalline wax concentrations in castor oil. All experiments were conducted in a pin-on disk set up with a load of 0.5 N and a disk speed of 10 mms^{-1}.

Appendix 4

Overview of Language Session

Table 0.2 – Outline of comments made during in the language generation session

Bench Mark – Standard Base Lipstick	5% Aqueous phase
• Feels thicker than a normal lipstick • Thick to apply • Drags/pulls on application • Feels unnatural, heavy feel, sits on the lips • Waxy coated feel on hands, less so on lips, but leaves a coated film on lips which feels like a protective barrier • Product moves on the lips and question whether product would last (58%), others felt coating would make it last (42%) • Tacky, although not really sticky. Less tacky on the lips vs hand • Lips feel moisturised and more moisturised than side with no product • Not greasy, but feels more like a lip balm rather than lipstick • Lips feel smooth • Lips feel supple and conditioned • Shiny on hand and lips	• Most similar to BM, but feels lighter • Glides more than the BM, but less than Ref 233 • Slightly tackier than BM (58%) / less tacky (42%) • Smoothes lips, but feels more like a lip balm than a lipstick • Leaves protective film on lips, less than BM but more than Ref 233. Perception it offers more protection than Ref 233 would. • Film is more oily/Vaseline like, rather than sticky like film felt with BM • Greasy • Feel more product than with Ref 233, but not as drying as Ref 233 or BM • More moisturising than BM and product moves on lips more than BM • Slip, but lips feel nourished/hydrated

20% Aqueous phase	20% Aqueous phase (larger water droplet size)
• Looks and feels more solid than BM • Glides smoothly, much more than BM • Feels less heavy than BM when on the lips, although still aware it is on • More natural feel, lips feel less coated, but less film suggests product offering less protection • Feels like a lipstick • Thinner, lighter than BM, perception you might lick it off • Less sticky on hand and lips vs BM. BM sticky like a lipgloss • Product feels like it is melting, slightly more oily than BM – like licking butter (58%) • Product breaks down quicker than BM, feels like it has absorbed • Lips feel moisturised, supple and conditioned, similar to BM • Smoothes out ridges • Lips feel like stroking velvet • Similar tacky feel to BM initially, but tackier after time (5-10 mins) (58%) / slightly tacky/sticky (42%) • Perception you would need to reapply more often than others. Product melts/absorbs and feels dry giving the impression you need to reapply to add moisture to the lips • Seen as a perfect base coat, under your normal lipstick, to condition lips	• Soft bullet • Looks denser than BM • Cold and wet on lips when applied (58%) • Lighter, thinner feel to BM • Feels more like a lipstick than a lip balm (58%) / feels like a lip balm (42%) • Less cushioned feel than BM and less greasy, product feels more like a lipstick • Glides really well • Gritty, powdery feel, particularly if you lick your lips. Feels as though water evaporates and leaves powder • More mobile for longer than other products. Moves more on the lips, but not in a bad way • Slips, melts the most and feels oily, watery. For some this felt slippery • Fat droplets deposited on hand when applied • Softens, smoothes lips • More moisturising than BM, not as coated • Perceived to offer same protection as BM, but not as heavy/sticky. Same protection, but lighter feel • Lips feel conditioned • Perceived to be long lasting and wouldn't need to be reapplied as often

without giving colour	as the BM • Feels tackier than the BM on the hand but not on the lips, least tacky on the lips • Shinier than BM

References

ADAMS, N. & LODGE, A. S. 1964. Rheological Properties of Concentrated Polymer Solutions II. A Cone-And-Plate and Parallel-Plate Pressure Distribution Apparatus for Determining Normal Stress Differences in Steady Shear Flow. *Philosophical Transactions of the Royal Society of London. Series A, Mathematical and Physical Sciences,* 256**,** 149-184.

ALLISON, D. B., PAULTRE, F., MAGGIO, C., MEZZITIS, N. & PI-SUNYER, F. X. 1995. The Use of Areas Under Curves in Diabetes Research. *Diabetes Care,* 18**,** 245-250.

ARAYA-SIBAJA, A. M., PAULINO, A. S., RAUBER, G. S., CAMPOS, C. E. M., CARDOSO, S. G., MONTI, G. A., HEREDIA, V., BIANCO, I., BELTRANO, D. & CUFFINI, S. L. 2014. Dissolution properties, solid-state transformation and polymorphic crystallization: progesterone case study. *Pharmaceutical Development and Technology,* 19**,** 779-788.

BAKER, R. W. 1987. *Controlled release of biologically active agents*, John Wiley & Sons.

BAKER, R. W. & LONSDALE, H. K. 1974. Controlled Release: Mechanisms and Rates. *In:* TANQUARY, A. C. & LACEY, R. E. (eds.) *Controlled Release of Biologically Active Agents.* Springer US.

BARWELL, F. 1974. The tribology of wheel on rail. *Tribology,* 7**,** 146-150.

BATT, M. D., DAVIS, W. B., FAIRHURST, E., GERRARD, W. A. & RIDGE, B. D. 1988. CHANGES IN THE PHYSICAL-PROPERTIES OF THE STRATUM-CORNEUM FOLLOWING TREATMENT WITH GLYCEROL. *Journal of the Society of Cosmetic Chemists,* 39**,** 367-381.

BATT, M. D. & FAIRHURST, E. 1986. Hydration of the stratum corneum. *International Journal of Cosmetic Science,* 8**,** 253-264.

BERGMAN, T. L., LAVINE, A. S., INCROPERA, F. & DEWITT, D. P. 2011. *Fundamentals of heat and mass transfer*, John Wiley & Sons.

BERI, A., NORTON, J. E. & NORTON, I. T. 2013a. Effect of emulsifier type and concentration, aqueous phase volume and wax ratio on physical, material and mechanical properties of water in oil lipsticks. *International Journal of Cosmetic Science***,** n/a-n/a.

BERI, A., PICHOT, R. & NORTON, I. T. 2013b. Physical and material properties of an emulsion-based lipstick produced via a continuous process. *International Journal of Cosmetic Science***,** n/a-n/a.

BETTINA VOUTOU & STEFANAKI, E.-C. (eds.) 2008. *Electon Microscopy: The Basics*.

BEYDOUN, D., GUANG, D., CHHABRA, R. P. & RAPER, J. A. 1998. Particle settling in oil-in-water emulsions. *Powder Technology,* 97**,** 72-76.

BHUSHAN, B. & HSU, S. M. (eds.) 2001. *Section IV: Triobology of industrial components and systems* CRC.

BHUSHAN, B. & KULKARNI, A. V. 1996. Effect of normal load on microscale friction measurements. *Thin Solid Films,* 278**,** 49-56.

BLAU, P. 1991. Scale effects in steady-state friction. *Tribology transactions,* 34**,** 335-342.

BLICHMANN, C. W., SERUP, J. & WINTHER, A. 1989. EFFECTS OF SINGLE APPLICATION OF A MOISTURIZER - EVAPORATION OF EMULSION WATER, SKIN SURFACE-TEMPERATURE, ELECTRICAL CONDUCTANCE, ELECTRICAL CAPACITANCE, AND SKIN SURFACE (EMULSION) LIPIDS. *Acta Dermato-Venereologica,* 69**,** 327-330.

BOHLIN-INSTRUMENTS 1994. *A Basic Introduction to Rheology* Bohlin Instruments Ltd

BOLAND, A. B., DELAHUNTY, C. M. & VAN RUTH, S. M. 2006. Influence of the texture of gelatin gels and pectin gels on strawberry flavour release and perception. *Food Chemistry,* 96**,** 452-460.

BRAISCH, B., KÖHLER, K., SCHUCHMANN, H. P. & WOLF, B. 2009. Preparation and Flow Behaviour of Oil-In-Water Emulsions Stabilised by Hydrophilic Silica Particles. *Chemical Engineering & Technology,* 32**,** 1107-1112.

BROWN, W. & BALL, R. 1985. Computer simulation of chemically limited aggregation. *Journal of Physics A: Mathematical and General,* 18**,** L517.

BRUKER 2001. mq Series Oil / Water Droplet Size Applications. Bruker Optik GmbH.

CACACE, J. E. & MAZZA, G. 2003. Mass transfer process during extraction of phenolic compounds from milled berries. *Journal of Food Engineering,* 59**,** 379-389.

CAMBIELLA, A., BENITO, J. M., PAZOS, C., COCA, J., RATOI, M. & SPIKES, H. A. 2006. The effect of emulsifier concentration on the lubricating properties of oil-in-water emulsions. *Tribology Letters,* 22**,** 53-65.

CAMPBELL, S. D., GOFF, H. D. & ROUSSEAU, D. 2002. Comparison of crystallization properties of a palm stearin/canola oil blend and lard in bulk and emulsified form. *Food Research International,* 35**,** 935-944.

CAMPOS, R., NARINE, S. S. & MARANGONI, A. G. 2002. Effect of cooling rate on the structure and mechanical properties of milk fat and lard. *Food Research International,* 35**,** 971-981.

CHANAMAI, R. & MCCLEMENTS, D. J. 2002. Comparison of gum arabic, modified starch, and whey protein isolate as emulsifiers: Influence of pH, CaCl(2) and temperature. *Journal of Food Science,* 67**,** 120-125.

CHEN, J. & STOKES, J. R. 2012. Rheology and tribology: Two distinctive regimes of food texture sensation. *Trends in Food Science & Technology,* 25**,** 4-12.

CHOI, J. H., LEE, H. Y., KIM, J.-C. & KIM, Y. C. 2007. Monoolein Cubic Phases Containing Hydrophobically Modified

Poly(N-isopropylacrylamide) *J. Ind. Eng. Chem,* 13**,** 380-386.

CHOJNICKA-PASZUN, A., DE JONGH, H. H. J. & DE KRUIF, C. G. 2012. Sensory perception and lubrication properties of milk: Influence of fat content. *International Dairy Journal,* 26**,** 15-22.

COUPLAND, J. N. & MCCLEMENTS, D. J. 1996. Lipid Oxidation in food emulsions *Trends in Food Science and Technology* 7**,** 83-91.

DALEY, P. D. W. 1968. Modern lipstick base manufacture. *J. Soc. Cosmetic Chemists,* 19**,** 521-530.

DARVELL, B. W. 2002. *Material Science for Dentistry,* Woodhead Publishing.

DE GENNES, P.-G. 1979. *Scaling concepts in polymer physics*, Cornell university press.

DE WIJK, R. A. & PRINZ, J. F. 2005. The role of friction in perceived oral texture. *Food Quality and Preference,* 16**,** 121-129.

DECKER, G. E., HUNTER, S., TURNER, C. & WATTS-MCMILLAN, K. 1997. *Moisturizing lipstick compositions*. United States of America patent application.

DESTEVOU, P. O., MONTENAT, C., LADURE, F. & DAUTREY, L. P. 1998. Tectonic-sedimentary evolution of the eastern Prebetic domain (Spain) during the Miocene. *Comptes rendus des séances de l'Academie des sciences. Série II, Mécanique, physique, chimie, sciences de l'univers, sciences de la terre,* 87**,** 111-123.

DICKINSON, E. 2010. Food emulsions and foams: Stabilization by particles. *Current Opinion in Colloid & Interface Science,* 15**,** 40-49.

DICKINSON, E., RITZOULIS, C., YAMAMOTO, Y. & LOGAN, H. 1999. Ostwald ripening of protein-stabilized emulsions: effect of transglutaminase crosslinking. *Colloids and Surfaces B-Biointerfaces,* 12**,** 139-146.

DICKINSON, E. & STAINSBY, G. 1982. *Colloids in Foods*.

DRESSELHUIS, D., KLOK, H. J., STUART, M. C., VRIES, R., AKEN, G. & HOOG, E. A. 2007. Tribology of o/w Emulsions Under Mouth-like Conditions: Determinants of Friction. *Food Biophysics,* 2**,** 158-171.

DRESSELHUIS, D. M., DE HOOG, E. H. A., COHEN STUART, M. A., VINGERHOEDS, M. H. & VAN AKEN, G. A. 2008. The occurrence of in-mouth coalescence of emulsion droplets in relation to perception of fat. *Food hydrocolloids.,* 22**,** 1170-1183.

DUNLAP, F. E. 1984. CLINICAL-EVALUATION OF A HIGHLY EFFECTIVE HAND AND BODY LOTION. *Current Therapeutic Research-Clinical and Experimental,* 35**,** 72-77.

DUNPHY, P. J., MEYERS, A. J. & RIGG, R. T. 1992 *Cosmetic Water-in-oil emulsion lipstick comprising a phospholipid and glycerol fatty acid esters emulsifiying systems*. United States of America patent application.

DWECK, A. C. & BURNHAM, C. A. M. 1980. Moulding techniques in lipstick manufacture: a comparative evaluation. *International Journal of Cosmetic Science,* 2**,** 143-173.

EDWARDS, S. & OAKESHOTT, R. 1989. The transmission of stress in an aggregate. *Physica D: Nonlinear Phenomena,* 38**,** 88-92.

FAVA, R. A. 1968. DIFFERENTIAL SCANNING CALORIMETRY OF EPOXY RESINS. *Polymer,* 9**,** 137-&.

FOLEY, J. & BRADY, J. P. 1984. Temperature-induced effects on crystallization behaviour, solid fat content and the firmness values of milk fat. *Journal of Dairy Research,* 51**,** 579-589.

FRASCH-MELNIK, S., NORTON, I. T. & SPYROPOULOS, F. 2010. Fat-crystal stabilised w/o emulsions for controlled salt release. *Journal of Food Engineering,* 98**,** 437-442.

GARREC, D. A. & NORTON, I. T. 2013. Kappa carrageenan fluid gel material properties. Part 2: Tribology. *Food Hydrocolloids*.

GE, H. Y., ZHAO, C. L., PORZIO, S., ZHUO, L., DAVIS, H. T. & SCRIVEN, L. E. 2006. Fracture behavior of colloidal polymer particles in fast-frozen suspensions viewed by cryo-SEM. *Macromolecules,* 39**,** 5531-5539.

GHOSH, S. & ROUSSEAU, D. 2011. Fat crystals and water-in-oil emulsion stability. *Current Opinion in Colloid & Interface Science,* 16**,** 421-431.

GODFREY, D. 1995. Friction oscillations with a pin-on-disc tribometer. *Tribology International,* 28**,** 119-126.

GOUDAPPEL, G. J. W., VAN DUYNHOVEN, J. P. M. & MOOREN, M. M. W. 2001. Measurement of Oil Droplet Size Distributions in Food Oil/Water Emulsions by Time Domain Pulsed Field Gradient NMR. *Journal of Colloid and Interface Science,* 239**,** 535-542.

GUNES, D. Z., CLAIN, X., BRETON, O., MAYOR, G. & BURBIDGE, A. S. 2010. Avalanches of coalescence events and local extensional flows – Stabilisation or destabilisation due to surfactant. *Journal of Colloid and Interface Science,* 343**,** 79-86.

HAIGHTON, A. J. 1976. Blending, chilling, and tempering of margarines and shortenings. *Journal of the American Oil Chemists' Society,* 53**,** 397-399.

HARRIS, J. & BUTTERWORTH, D. K. 2013. *Skin conditioning and lubricating creme, and method of making and using same cross-reference to related applications*. United States of America patent application PCT/US2013/025391.

HARRY, R. G. T. 1973. *Harry's Cosmetiology*, Hill.

HEIDENREICH, R. D. 1964. *Fundamentals of Transmission Electon Microscopy*

HÉNIN, J., TAJKHORSHID, E., SCHULTEN, K. & CHIPOT, C. 2008. Diffusion of Glycerol through Escherichia coli Aquaglyceroporin GlpF. *Biophysical Journal,* 94**,** 832-839.

HIGSON, S. & AMUS 2004. Analytical Chemistry. Oxford University Press.

HIMMELSTEN, K. J. 1991. Controlled release: A quantitative treatment. Edited by L. T. Fan and S. K. Singh. Springer-Verlag: New York. 1989. × + 233 pp. 25 × 17 cm. ISBN 3-540-50823-6. Price not given. *Journal of Pharmaceutical Sciences,* 80**,** 304-304.

HINDMARSH, J. P., SU, J. H., FLANAGAN, J. & SINGH, H. 2005. PFG-NMR analysis of intercompartment exchange and inner droplet size distribution of W/O/W emulsions. *Langmuir,* 21**,** 9076-9084.

HODGE, S. M. & ROUSSEAU, D. 2003. Flocculation and coalescence in water-in-oil emulsions stabilized by paraffin wax crystals. *Food Research International,* 36**,** 695-702.

IVANOV, I. B., DANOV, K. D. & KRALCHEVSKY, P. A. 1999. Flocculation and coalescence of micron-size emulsion droplets. *Colloids and Surfaces A: Physicochemical and Engineering Aspects,* 152**,** 161-182.

JENNING, V. & GOHLA, S. 2000. Comparison of wax and glyceride solid lipid nanoparticles (SLN®). *International journal of pharmaceutics,* 196**,** 219-222.

JENSEN, L. H. & MABIS, A. J. 1966. Refinement of the structure of [beta]-tricaprin. *Acta Crystallographica,* 21**,** 770-781.

JOHNSON, K. L. & KAUZLARICH, J. J. 2004. Transfer of material between rolling and sliding surfaces. *International Journal of Mechanical Sciences,* 46**,** 343-357.

JULLIEN, R. & BOTET, R. 1987. *Aggregation and fractal aggregates,* World scientific Singapore.

JUTEAU, A., CAYOT, N., CHABANET, C., DOUBLIER, J. L. & GUICHARD, E. 2004. Flavour release from polysaccharide gels: different approaches for the determination of kinetic parameters. *Trends in Food Science & Technology,* 15**,** 394-402.

KABALNOV, A. 1998. Thermodynamic and theoretical aspects of emulsions and their stability. *Current Opinion in Colloid & Interface Science,* 3**,** 270-275.

KIM, H. S. & BUSH, M. B. 1999. The effects of grain size and porosity on the elastic modulus of nanocrystalline materials. *Nanostructured Materials,* 11**,** 361-367.

KLOEK, W., WALSTRA, P. & VLIET, T. 2000. Crystallization kinetics of fully hydrogenated palm oil in sunflower oil mixtures. *Journal of the American Oil Chemists' Society,* 77**,** 389-398.

KOKINI, J. L. 1987. The physical basis of liquid food texture and texture-taste interactions. *Journal of Food Engineering,* 6**,** 51-81.

KOLIANDRIS, A., LEE, A., FERRY, A.-L., HILL, S. & MITCHELL, J. 2008. Relationship between structure of hydrocolloid gels and solutions and flavour release. *Food Hydrocolloids,* 22**,** 623-630.

KULISIEWICZ, L. & DELGADO, A. 2010. HIGH-PRESSURE RHEOLOGICAL MEASUREMENT METHODS: A REVIEW. *Applied Rheology,* 20.

KULKARNI, C. V., WACHTER, W., IGLESIAS-SALTO, G., ENGELSKIRCHEN, S. & AHUALLI, S. 2011. Monoolein: a magic lipid? *Physical Chemistry Chemical Physics,* 13**,** 3004-3021.

KUSAKARI, K., YOSHIDA, M., MATSUZAKI, F., YANAKI, T., FUKUI, H. & DATE, M. 2003. Evaluation of post-application rheological changes in cosmetics using a novel measuring device: Relationship to sensory evaluation. *Journal of cosmetic science,* 54**,** 321-334.

LACERDA, S. P., CERIZE, N. N. P. & RE, M. I. 2011. Preparation and characterization of carnauba wax nanostructured lipid carriers containing benzophenone-3. *International Journal of Cosmetic Science,* 33**,** 312-321.

LANGER, R. & PEPPAS, N. 1983a. Chemical and Physical Structure of Polymers as Carriers for Controlled Release of Bioactive Agents: A Review. *Journal of Macromolecular Science, Part C,* 23**,** 61-126.

LANGER, R. & PEPPAS, N. 1983b. CHEMICAL AND PHYSICAL STRUCTURE OF POLYMERS AS CARRIERS FOR CONTROLLED RELEASE OF BIOACTIVE AGENTS: A REVIEW. *Journal of Macromolecular Science - Reviews in Macromolecular Chemistry and Physics,* C23**,** 61-126.

LARSSON, K. 1966. Classification of Glyceride Crystal Forms *Acta Chemica Scandinavica* 20**,** 2255 - 2260.

LE RÉVÉREND, B. J. D., TAYLOR, M. S. & NORTON, I. T. 2011a. Design and application of water-in-oil emulsions for use in lipstick formulations. *International Journal of Cosmetic Science***,** no-no.

LE RÉVÉREND, B. J. D., TAYLOR, M. S. & NORTON, I. T. 2011b. Design and application of water-in-oil emulsions for use in lipstick formulations. *International Journal of Cosmetic Science,* 33**,** 263-268.

LI, L. 2002. Thermal Gelation of Methylcellulose in Water: Scaling and Thermoreversibility. *Macromolecules,* 35**,** 5990-5998.

LODÉN, M. 1996. Urea-containing moisturizers influence barrier properties of normal skin. *Archives of Dermatological Research,* 288**,** 103-107.

LODÉN, M. & WESSMAN, W. 2001. The influence of a cream containing 20% glycerin and its vehicle on skin barrier properties. *International Journal of Cosmetic Science,* 23**,** 115-119.

LOMBARDI, M. H. & VACCARO, J. 1993. *Lipstick Article*. United States of America patent application.

LUENGO, G., TSUCHIYA, M., HEUBERGER, M. & ISRAELACHVILI, J. 1997. Thin film rheology and tribology of chocolate. *Journal of Food Science,* 62**,** 767-812.

MACKLES, L. 1987. *Aerosol Foam*. USA patent application 778026. 27/01/1987.

MALONE, M., APPELQVIST, I. & NORTON, I. 2003. Oral behaviour of food hydrocolloids and emulsions. Part 1. Lubrication and deposition considerations. *Food Hydrocolloids,* 17**,** 763-773.

MARANGONI, A. G. & WESDORP, L. H. 2012. *Structure and Properties of Fat Crystal Networks, Second Edition*, Taylor & Francis.

MCCABE, J. & WALLIS, A. 2008. *Applied dental materials*, Wiley-Blackwell

MCCLEMENTS, D. J. (ed.) 2002. *Food Lipids*

Chemistry, Nutrition and Biotechnology CRC Press 2008

MCCLEMENTS, D. J. 2005. *Food Emulsions - Principles, Practices, and Techniques*.

MCKETTA, J. J. 1993. Cosmetics *Encyclopedia of chemical processing and design* New York: Marcel Dekker INC.

MILLS, T., SPYROPOULOS, F., NORTON, I. T. & BAKALIS, S. 2011. Development of an in-vitro mouth model to quantify salt release from gels. *Food Hydrocolloids,* 25**,** 107-113.

MILLS, T. B. 2011. *Development of In-Vitro Mouth Models.* Ph. D., University of Birmingham

MINTEL 2012. Colour Cosmetics - UK. *Report supplied by Alliance Boots*.

MORESI, M. & BRUNO, M. 2007. Characterisation of alginate gels using quasi-static and dynamic methods. *Journal of Food Engineering,* 82**,** 298-309.

MÜLLER, C. M. O., LAURINDO, J. B. & YAMASHITA, F. 2009. Effect of cellulose fibers addition on the mechanical properties and water vapor barrier of starch-based films. *Food Hydrocolloids,* 23**,** 1328-1333.

NAKADA, M. 1994. Trends in engine technology and tribology. *Tribology International,* 27**,** 3-8.

NAKAYAMA, A., KAKUGO, A., GONG, J. P., OSADA, Y., TAKAI, M., ERATA, T. & KAWANO, S. 2004. High mechanical strength double-network hydrogel with bacterial cellulose. *Advanced Functional Materials,* 14**,** 1124-1128.

NAPPER, D. H. 1983. *Polymeric Stabilization of Colloidal Dispersions* London.

NARINE, S. S. & MARANGONI, A. G. 1999a. Fractal nature of fat crystal networks. *Physical Review E,* 59**,** 1908-1920.

NARINE, S. S. & MARANGONI, A. G. 1999b. Relating structure of fat crystal networks to mechanical properties: a review. *Food Research International,* 32**,** 227-248.

NEDERVEEN, C. 1963. Dynamic mechanical behavior of suspensions of fat particles in oil. *Journal of Colloid Science,* 18**,** 276-291.

NORTON, A. B., COX, P. W. & SPYROPOULOS, F. 2011. Acid gelation of low acyl gellan gum relevant to self-structuring in the human stomach. *Food Hydrocolloids,* 25**,** 1105-1111.

NORTON, I. T., LEE-TUFFNELL, C. D., ABLETT, S. & BOCIEK, S. M. 1985. A Calorimetric, NMR and X ray Diffraction Study of the Melting Behaviour of Tripalmitin and Tristearin and their Mxing Behaviour with Trioloein. *Journal of the American Oil Chemists' Society,* 62**,** 1237 - 1244.

NORTON, J. & NORTON, I. 2010. Designer colloids—towards healthy everyday foods? *Soft Matter,* 6**,** 3735-3742.

NORTON, J. E. & FRYER, P. J. 2012. Investigation of changes in formulation and processing parameters on the physical properties of cocoa butter emulsions. *Journal of Food Engineering,* 113**,** 329-336.

NORTON, J. E., FRYER, P. J., PARKINSON, J. & COX, P. W. 2009. Development and characterisation of tempered cocoa butter emulsions containing up to 60% water. *Journal of Food Engineering,* 95**,** 172-178.

OH, S. G., JOBALIA, M. & SHAH, D. O. 1993. The Effect of Micellar Lifetime on the Droplet Size in Emulsions. *Journal of Colloid and Interface Science,* 156**,** 511-514.

PACKER, K. J. & REES, C. 1971. Pulsed NMR studies of Restricted Diffusion. *Journal of Colloid and Interface Science,* 40**,** 206 - 218.

PAL, R. 1996. Effect of droplet size on the rheology of emulsions. *AIChE Journal,* 42**,** 3181-3190.

PAL, R. 2000. Slippage during the flow of emulsions in rheometers. *Colloids and Surfaces A: Physicochemical and Engineering Aspects,* 162**,** 55-66.

PAPENHUIJZEN, J. 1971. Superimposed steady and oscillatory shear in dispersed systems. *Rheol. Acta,* 10**,** 493-502.

PETERSSON, M., GUSTAFSON, I. & STADING, M. 2008. Comparison of microstructural and physical properties of two petroleum waxes. *Journal of Materials Science,* 43**,** 1869-1879.

PICKERING, S. U. 1907. Emulsions. *Journal of the Chemical Society,* 91**,** 2001-2021.

POTHAKAMURY, U. R. & BARBOSA-CÁNOVAS, G. V. 1995. Fundamental aspects of controlled release in foods. *Trends in Food Science & Technology,* 6**,** 397-406.

PRINZ, J. F. & LUCAS, P. W. 2000. Saliva tannin interactions. *Journal of Oral Rehabilitation,* 27**,** 991-994.

REID, R. C., PRAUSNITZ, J. M. & POLLING, B. 1987. *The properties of Gases and Liquids,* McGraw-Hill Book Company.

ROSEN, M. 1988. *Surfactants and Interfacial Phenomena,* John Wiley & Sons.

ROUSSEAU, D. 2000. Fat crystals and emulsion stability - a review. *Food Research International,* 33**,** 3-14.

ROUSSEAU, D. & HODGE, S. M. 2005. Stabilization of water-in-oil emulsions with continuous phase crystals. *Colloids and Surfaces a-Physicochemical and Engineering Aspects,* 260**,** 229-237.

ROUSSEAU, D., MARANGONI, A. G. & JEFFREY, K. R. 1998. The influence of chemical interesterification on the physicochemical properties of complex fat systems. 2. Morphology and polymorphism. *Journal of the American Oil Chemists' Society,* 75**,** 1833-1839.

SATO, K. 2001. Crystallization behaviour of fats and lipids — a review. *Chemical Engineering Science,* 56**,** 2255-2265.

SERBAN, G. P., HENRY, S. M., COTTY, V. F., COHEN, G. L. & RIVELEY, J. A. 1983. ELECTROMETRIC TECHNIQUE FOR THE INVIVO ASSESSMENT OF SKIN DRYNESS AND THE EFFECT OF CHRONIC TREATMENT WITH A LOTION ON THE WATER BARRIER FUNCTION OF DRY SKIN. *Journal of the Society of Cosmetic Chemists,* 34**,** 383-393.

SHIH, W.-H., SHIH, W. Y., KIM, S.-I., LIU, J. & AKSAY, I. A. 1990. Scaling behavior of the elastic properties of colloidal gels. *Physical Review A,* 42**,** 4772.

SHRINIVAS, P., KASAPIS, S. & TONGDANG, T. 2009. Morphology and Mechanical Properties of Bicontinuous Gels of Agarose and Gelatin and the Effect of Added Lipid Phase. *Langmuir,* 25**,** 8763-8773.

STAMATOUDIS, M. & TAVLARIDES, L. L. 1985. Effect of continuous-phase viscosity on the drop sizes of liquid-liquid dispersions in agitated vessels. *Industrial & Engineering Chemistry Process Design and Development,* 24**,** 1175-1181.

STONE, H. A. 1994. Dynamics of drop deformation and breakup in viscous fluids. *Annual Review of Fluid Mechanics,* 26**,** 65-102.

TABILO-MUNIZAGA, G. & BARBOSA-CÁNOVAS, G. V. 2005. Rheology for the food industry. *Journal of Food Engineering,* 67**,** 147-156.

TAYLOR, M. S. 2011. *Stabilisation of water-in-oil emulsions to improve the emollient properties Lipsticks.* Mres, University of Birmingham.

TIMM, K., MYANT, C., SPIKES, H. A. & GRUNZE, M. 2011. Particulate lubricants in cosmetic applications. *Tribology International,* 44**,** 1695-1703.

TRAN, T. & ROUSSEAU, D. 2013. Stabilization of acidic soy protein-based dispersions and emulsions by soy soluble polysaccharides. *Food Hydrocolloids,* 30**,** 382-392.

TÜRKER, N. & ERDOĞDU, F. 2006. Effects of pH and temperature of extraction medium on effective diffusion coefficient of anthocynanin pigments of black carrot (Daucus carota var. L.). *Journal of Food Engineering,* 76**,** 579-583.

VAN AKEN, G. A. 2004. Coalescence mechanisms in protein-stabilized emulsions. *Food emulsions***,** 299-324.

VAN DEN ENDEN, J. C., WADDINGTON, D., VAN AALST, H., VAN KRALINGEN, C. G. & PACKER, K. J. 1990. Rapid determination of water droplet size distributions by PFG-NMR. *Journal of Colloid and Interface Science,* 140**,** 105-113.

VAN DEN TEMPEL, M. 1961. Mechanical properties of plastic-disperse systems at very small deformations. *Journal of Colloid Science,* 16**,** 284-296.

VAN DUYNHOVEN, J. P. M., GOUDAPPEL, G. J. W., VAN DALEN, G., VAN BRUGGEN, P. C., BLONK, J. C. G. & EIJKELENBOOM, A. 2002a. Scope of droplet size measurements in food emulsions by pulsed field gradient NMR at low field. *Magnetic Resonance in Chemistry,* 40**,** S51-S59.

VAN DUYNHOVEN, J. P. M., GOUDAPPEL, G. J. W., VAN DALEN, G., VAN BRUGGEN, P. C., BLONK, J. C. G. & EIJKELENBOOM, A. P. A. M. 2002b. Scope of droplet size measurements in food emulsions by pulsed field gradient NMR at low field. *Magnetic Resonance in Chemistry,* 40**,** S51-S59.

VAN DUYNHOVEN, J. P. M., MAILLET, B., SCHELL, J., TRONQUET, M., GOUDAPPEL, G.-J. W., TREZZA, E., BULBARELLO, A. & VAN DUSSCHOTEN, D. 2007. A rapid benchtop NMR method for determination of droplet size distributions in food emulsions. *European Journal of Lipid Science and Technology,* 109**,** 1095-1103.

VEREECKEN, J., MEEUSSEN, W., LESAFFER, A. & DEWETTINCK, K. 2010. Effect of water and monoglyceride concentration on the behaviour of monoglyceride containing fat systems. *Food Research International,* 43**,** 872-881.

VERHAGEN, J. V. & ENGELEN, L. 2006. The neurocognitive bases of human multimodal food perception: sensory integration. *Neuroscience & Biobehavioral Reviews,* 30**,** 613-650.

WALSTRA, P. (ed.) 1983a. *Formation of emulsions,* New York: Marcel Dekker.

WALSTRA, P. 1983b. *Formation of Emulsions in Encyclopedia of Emulsion Technology* New York, Marcel Decker

WALSTRA, P. 1993. Principles of emulsion formation. *Chemical Engineering Science,* 48**,** 333-349.

WALSTRA, P. 1998. Secondary nucleation in triglyceride crystallization. *In:* LINDMAN, B. & NINHAM, B. W. (eds.) *Colloid Science of Lipids: New Paradigms for Self-Assembly in Science and Technology.* Berlin 33: Steinkopff Darmstadt.

WANG, J., YANG, F., TAN, J. J., LIU, G. P., XU, J. & SUN, D. J. 2010. Pickering Emulsions Stabilized by a Lipophilic Surfactant and Hydrophilic Platelike Particles. *Langmuir,* 26**,** 5397-5404.

WANG, J. F., CALHOUN, M. D. & SEVERTSON, S. J. 2008. Dynamic rheological study of paraffin wax and its organoclay nanocomposites. *Journal of Applied Polymer Science,* 108**,** 2564-2570.

WANG, Q., ROJAS, E. C. & PAPADOPOULOS, K. D. 2012. Cationic liposomes in double emulsions for controlled release. *Journal of Colloid and Interface Science,* 383**,** 89-95.

WANG, T. S. & LEE, G. 1997. The effect of formulation on the hardness and crystallization of emulsion lipsticks. *Journal of the Society of Cosmetic Chemists,* 48**,** 41-50.

YILDIZ, O. & UNLUTURK, S. 2009. Differential scanning calorimetry as a tool to detect antibiotic residues in ultra high temperature whole milk. *International Journal of Food Science and Technology,* 44**,** 2577-2582.

YOUNG, M. E., CARROAD, P. A. & BELL, R. L. 1980. Estimation of diffusion coefficients of proteins. *Biotechnology and Bioengineering,* 22**,** 947-955.

ZHANG, H., JACOBSEN, C. & ADLER-NISSEN, J. 2005. Storage stability study of margarines produced from enzymatically interesterified fats compared to margarines produced by conventional methods. I. Physical properties. *European Journal of Lipid Science and Technology,* 107**,** 530-539.

ZHANG, J., HUANG, B., LI, Y. & LI, S.-L. 2002. Influence of Microcrystalline Wax on Properties of MIM Multi-Component Wax Matrix Binder. *Trans. Nonferrous Met. Soc. China,* 12**,** 918 - 921.